STUDY OF PHYSICAL, MECHANICAL AND SLIDING WEAR CHARACTERIZATION OF FEMORAL HEAD MATERIAL FOR HIP JOINT REPLACEMENT

A THESIS SUBMITTED IN PARTIAL FULFILEMNT OF THE REQUIREMENT
FORTHE AWARD OF THE DEGREE OF

Doctor of Philosophy
In
Mechanical Engineering

Submitted to

Malaviya National Institute of Technology, Jaipur, Rajasthan

By

Amit Aherwar

(Student ID: 2012RME9548)

Department of Mechanical Engineering
Malaviya National Institute of Technology
Jaipur Rajasthan - 302017, INDIA
Jan, 2017

STUDY OF PHYSICAL, MECHANICAL AND SLIDING WEAR CHARACTERIZATION OF FEMORAL HEAD MATERIAL FOR HIP JOINT REPLACEMENT

A THESIS SUBMITTED IN PARTIAL FULFILEMNT OF THE REQUIREMENT FORTHE AWARD OF THE DEGREE OF

Doctor of Philosophy

In

Mechanical Engineering

Submitted to

Malaviya National Institute of Technology, Jaipur, Rajasthan

By

Amit Aherwar

(Student ID: 2012RME9548)

Under the supervision of

Dr.Amit Singh
and
Dr. Amar Patnaik

Department of Mechanical Engineering
Malaviya National Institute of Technology
Jaipur Rajasthan - 302017, INDIA
Jan, 2017

Dedicated to

My Parents

And

Family Members

CANDIDATE'S DECLARATION

I hereby certify that the thesis entitled "**Study of Physical, Mechanical and Sliding Wear Characterization of Femoral Head Material for Hip Joint Replacement**" submitted by **Amit Aherwar (Roll No: 2012RME9548)** in partial fulfilment of the requirements for the award of **Doctor of Philosophy** in **Mechanical Engineering** to the **Malaviya National Institute of Technology**, **Jaipur** is an authentic record of research work carried out by me under my supervision and guidance. The work incorporated in this thesis has not been submitted elsewhere for the award of any degree.

Amit Aherwar

Date: ID No.: 2012RME9548

This is to certify that the above statement made by the candidate is correct to the best of my knowledge and belief.

Dr.Amit Singh   **Dr. Amar Patnaik**

(Supervisor)   (Co-Supervisor)

Asst. Professor   Asst. Professor

Mechanical Engineering Department   Mechanical Engineering Department

MNIT, Jaipur-302017 (Rajasthan), India   MNIT, Jaipur-302017 (Rajasthan), India

Malaviya National Institute of Technology, Jaipur
Mechanical Engineering Department

CERTIFICATE

This is certify that the thesis entitled "**Study of Physical, Mechanical and Sliding Wear Characterization of Femoral Head Material for Hip Joint Replacement**" submitted by **Amit Aherwar (Roll No: 2012RME9548)** in partial fulfilment of the requirements for the award of **Doctor of Philosophy** in **Mechanical Engineering** to the **Malaviya National Institute of Technology**, **Jaipur** is an authentic record of research work carried out by him under my supervision and guidance. To the best my knowledge, the work incorporated in this thesis has not been submitted elsewhere for the award of any degree.

Dr.Amit Singh	**Dr. Amar Patnaik**
(Supervisor)	(Co-Supervisor)
Assistant Professor	Assistance Professor
Mechanical Engineering Department	Mechanical Engineering Department
MNIT, Jaipur	MNIT, Jaipur

The Ph.D. viva voce examination of Mr **Amit Aherwar** has been conducted by the Oral Defense Committee (ODC) constituted by the Dean (Academic Affairs), on Saturday, 28th Jan, 2017. The ODC declares that the student has successfully defended the thesis in the viva-voce examination.

External Examiner

Acknowledgement

A journey is easier when you travel together. This thesis is the results of years of work whereby I have been guided and supported by many people. Hence, this would be worthwhile and pleasing to express sense of gratitude for all of them.

I would like to express my deep sense of gratitude to my supervisor's **Dr. Amit Singh** and **Dr. Amar Patnaik**, Assistant Professor, MNIT, Jaipur, for their invaluable guidance, motivation, untiring efforts, meticulous attention and support throughout my research work.

I am also grateful to Professor **G. S. Dangayach** Head of the Mechanical Engineering Department for his help and cooperation. I appreciate the encouragement from faculty members of the Mechanical Engineering Department, Malaviya National Institute of Technology Jaipur.

I would also like to extend my appreciation to my PhD committee members, **Prof. G.S. Dangayach**, Dr. **Amar Patnaik,** Dr.**Harlal Singh Mali** and Dr. **M.L. Meena** for giving me valuable suggestion time-by-time and serving on my committee.

I am grateful to **Dr. S.C. Pant**, Scientist 'G', DRDE, Ministry of Defence, Gwalior for being helpful and generous during the course of this work and my hearty thanks to Dr. **R.K. Pandit**, Director MITS Gwalior for permitting and timely help during the course of this work.

It is a great pleasure for me to acknowledge and express my sincere thanks to my parents, family members and relatives for their understanding, support and encouragement that enabled me to complete this work. I am also thankful to all those who have directly or indirectly helped during my research period. Finally, but most importantly, I am thankful to Almighty, my Lord for giving me the will power and strength to make it this far.

Date:

MNIT, Jaipur   **Amit Aherwar**

Abstract

The field of biomaterials has turned into an electrifying area because these materials improve the quality and longevity of human life. These biomaterials are used to make devices to replace a part or a function of the body in safe, reliably economically, and physiologically acceptable manner. But, the first and foremost necessity for the selection of the biomaterial is the acceptability by human body. The most common classes of metal materials used as biomedical materials are stainless steel, Cobalt chromium alloy, Titanium and Ti-6Al-4V. Cobalt based alloys have been used for biomedical implants for a number of years. They are now frequently used for the metal-on-metal hip resurfacing joints due to their high corrosion and wear performance. Biomaterials in the form of implants (joint replacements) are also widely used to restore the function of traumatized or degenerated tissues or organs, and thus improve the quality of life of the patients.

The research reported in this thesis consists of three parts: The first part has provided the descriptions of the experimental program and has presented the physico-mechanical and wear characteristics of the fabricated alloy composites under this study; the second part has reported to predict the wear volume of the fabricated alloy composites under different operating conditions and compared with experimental results by using neural network and the third part discusses the results of corrosion behavior and to analyze the biocompatibility of the fabricated alloy composites according to the formulations. Three particulates i.e. molybdenum, nickel and tungsten in the form of powder as the filler materials and cobalt-chromium have been used as the base materials. The presence of particulate fillers in these alloy composites improves their wear resistance and this improvement depends on the type and content of the fillers.

The effect of varying wt.% loading of the ingredients is reported on physical, mechanical and tribological properties of these alloy composites. The physical and mechanical characterizations are analyzed experimentally via micro hardness tester and compression testing machine. The wear tests are performed on a pin-on-disk tribometer against a hardened alloy steel (EN-31) disk under different operating conditions at room temperature.For this purpose, an experiment schedule is prepared following design of experiments approach using Taguchi's orthogonal arrays in order to reduce the number of experiments without sacrificing the information to be extracted. In addition the corrosion behaviour and biocompatibility nature of the fabricated alloy composites are also analysed.

The cross-sectional microstructure of the fabricated alloy composites are examined by X-ray diffraction (XRD) and the worn out surface morphology have been investigated by scanning electron microscopy (SEM). Comprehensively, it is found that incorporation of fillers (i.e. Mo, Ni and W)in the matrix material provides better wear resistance.The 3D surface topographies and wear profiles of the worn surfaces were obtained by atomic force microscope (AFM). For this, a contact mode hard silicon commercial tip is used.

The corrosion resistance is determined by electrochemical test. The electrochemical corrosion behaviors of fabricated implant alloy composites under NaCl solution by using potentiodynamic scan method. The corrosion characteristic properties of the fabricated implant alloy composites are investigated in terms of corrosion potential (E_{corr}) and corrosion current density (i_{corr}).All these tests have been carried out as per ASTM standard. The fabricated alloy composites used as implant are expected to be highly nontoxic and should not cause any inflammatory or allergic reactions in the human tissues and cells. However, the success of the biomaterials is mainly dependent on the reaction of the human tissues with implant, and this also measures the biocompatibility of a material. For this, Irritability tests in subcutaneous tissue were performed in rats (*Rattus norvegicus*) according to the standard ISO10993 to determine the biocompatibility of the fabricated alloy composites.

Wear characteristics of these alloy composites have been successfully analyzed using Taguchi experimental design scheme. Significant control factors affecting the wear rate have been identified through successful implementation of analysis of variance (ANOVA). One predictive model i.e. artificial neural network (ANN) is proposed to predict the wear volume of the fabricated alloy composites under different operating conditions and compared with experimental results. This study will give an idea for femoral head material of hip implant application but not direct replacement of human joints. In future this study may be extended more detail for biomedical applications for replacement of either human hip implant or animal implant respectively.

TABLE OF CONTENTS

Chapter summary

Chapter summary

＊＊＊＊＊

LIST OF FIGURES

✵✵✵✵✵

LIST OF TABLES

✱✱✱✱✱

LIST OF ABBREVIATION

S/N   :   Signal-to-Noise

ANOVA   :   Analysis of Variance

FESEM   :   Field Emission Scanning Electron Microscopy

AFM   :   Atomic Force Microscopy

EDAX   :   Energy Dispersive X-Ray

XRD   :   X-ray Diffraction

ANN   :   Artificial Neural Network

OCP   :   Open Circuit Potential

MCDM   :   Multi-criteria decision making

PROMETHEE   :   Preference Ranking Organization Method for Enrichment Evaluations

CHAPTER 1
INTRODUCTION

1.1 Background and Motivation

Before the arrival of artificial hip joints, patients with severe arthritis and/or injured joints often suffered from continuous pain and decreased functional capacity of their joints. At present, the prosthetic joint replacement i.e. Hip joint has radically enhanced the life-quality of millions of patients globally. For more patients, end-stage arthritis occurs in the inferior extremities such as the hip joint. Therefore, hip joint replacements have taken a substantial share of the artificial joint market. For example, more than 1, 93,000 complete hip replacements and 1, 40,000 partial and revision hip replacements are accomplished every year in the United States [1] according to the American Academy of Orthopedic Surgeons. The design and development of hip joint replacements are receiving constant attention in terms of enhancement in wear, corrosion and biocompatibility performance. A number of doctors, scientists and metallurgical and material engineers globally have been trying to solve the problem of bone, especially in the hip joint area. No researcher has attained this challenging goal with complete success as far as literature is concerned. Therefore, developing an appropriate hip implant material and design for this painful problem is a great challenge to the researcher. For developing successful implant materials, there is a need for mutual effort for medical and engineering researchers. The general criteria for materials selection for hip implant materials are; highly biocompatible; good mechanical properties, closest to the bone and manufacturing and processing methods are economically viable [4-8].

In 1938, Philip Wiles [9] build the first hip joint replacement that comprised of a chrome steel cup and head. The cup was affixed by screws and the head was affixed by a stem that was attached to the femur neck by using a bolt. Clinical outcomes of this development were not known due to the mediation of Second World War. Years later, metal-on-metal (MoM) arrangements were commenced by McKee [10] and Haboush [11], Urist [12] and McBride [13]. The outcomes from such implants were not acceptable because of loosening and massive wear loss of the components, thus raise frictional torque [14].These metal-on-metal (MoM) prostheses were made to provide a matching femoral head and acetabular cup without clearance (minute gap between the head and the cup). It was shown that introducing a minute clearance between the

two components i.e. head and cup could reduce friction between the components by creating a polar bearing [14]. It was not until 1958 when John Charnley [15] implanted the first metal-on-polymer total hip replacement. The first polymer Charnley chose was Polytetrafluoroethylene (PTFE) articulating against a stainless steel head, which only survived two years due to the rapid wear of PTFE. In 1961, he adopted ultra-high molecular weight polyethylene (UHMWPE) which provided a low interfacial friction against a metal head. This prosthesis was called the 'Low Friction Arthroplasty' (LFA). Clinical outcomes have encouraged the use of the Charnley prosthesis. Its concept is still being used to date in less active elderly patients [16]. MoM bearings were of great interest in the late 1980s after the long-term survivorship and the low wear of such prosthesis. It was thought that the improved tolerances and superior surface finishes that could be attained by better manufacturing technologies, would improve the results of MoM prostheses [17-23].

In the early 1970s, Boutin, build the first ceramic-on-ceramic (CoC) total hip replacement [24]. It was commonly used in Europe after the promise of ceramics as a highly inert material and due to the good surface finish and excellent resistance to wear in vivo [25]. Although CoC have shown enhanced wear performance, there are still concerns about the incidental fracture of the ceramic material [26]. The success of a biomaterial in the body depends on factors such as the material properties, design and biocompatibility of the material used, as well as other factors, including the surgeon's technique used, health and condition of the patient, and the activities of the patient. Materials utilized as biomaterials within the body include metals, polymers, ceramics and composites, but the particular metallic biomaterials used in total joint replacement (TJR) applications are discussed here in details. The success of a joint replacement lies with the orthopaedic surgeon, not only to perform the surgery, but also to select the replacement that is best suited for the patient. The selection process can be influenced by the age and weight, along with the activity level of the patient post surgery [27, 28]. It is therefore important to have a complete understanding of the joint replacement and the behavior of materials utilized in total joint applications. All the required biomaterials used in total hip joint replacement are summarized in Table 1.1 [29-33].

Historically, a total hip replacement, the articulation of a human hip is simulated with the use of two components, a cup type and a long femoral type element. A typical hip implant fabricated from titanium is shown in Figure 1.1. The head of the femoral element fits inside the cup to enable the articulation of human joint. These two parts of the hip implant have been made

using a variety of materials such as metals, ceramics, polymers and composites. Typically polymeric materials alone tend to be too weak to be suitable for meeting the requirement of stress deformation responses in the THR components. Metals typically have good mechanical properties but shows poor biocompatibility, cause stress shielding and release of dangerous metal ions causing eventual failure and removal of implant. Ceramics generally have good biocompatibility but poor fracture toughness and tend to be brittle. Composite materials with engineered interfaces resulting in combination of biocompatibility, mechanical strength and toughness, is the focus of many current studies [34-42].
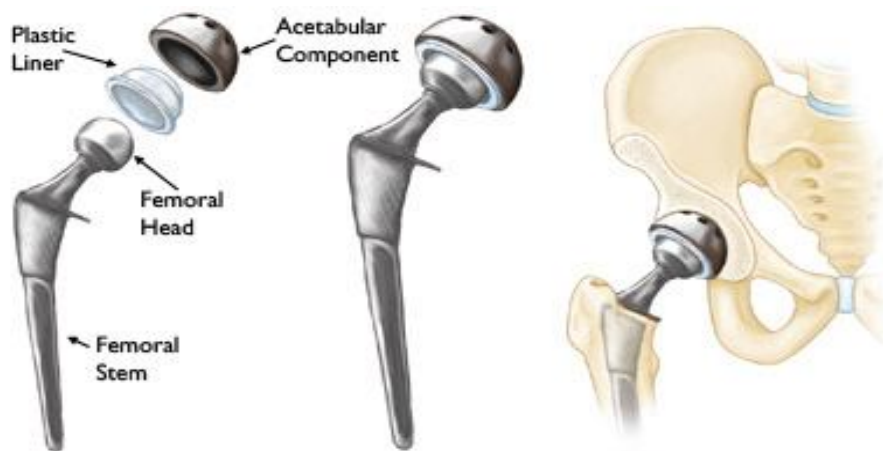
Figure 1.1: (Left) Components of a total hip replacement. (Center) The components merged into an implant. (Right) The implant as it fits into the hip [43].

Table 1.1 Biomaterials utilized in total hip joint replacement

Materials		Application
Metals	Stainless steels 316L	Femoral stems, heads
	Co based alloys	Femoral heads, stems, porous coatings and femoral components and tibial
	Cast Co-Cr-Mo	
	Wrought Co-Ni-Cr-Mo	
	Wrought Co-Cr-W-Ni	
Titanium-based materials	CP Ti	Porous coatings second phase in ceramic and PMMA composites
	Ti-6Al-4V	Femoral heads, stems, femoral components and tibial, porous coatings
	Ti-5Al-2.5Fe	Stems, Femoral heads

	Ti-Al-Nb	Stems, Femoral heads
Ceramics	Bioinert	
	Carbon	Coatings on metallic femoral stems, second phase in composites and bone cement
	Alumina	Femoral heads, Femoral stems and acetabular cups
	Zirconia	Femoral stems and acetabular cups
	Bioactive	
	Calcium Phosphates	Coatings on ceramic and metallic femoral stems, scaffold materials, second phase in PMMA and UHMWPE composites
	Bioglasses	Coatings on ceramic and metallic femoral stems
Polymers	PMMA	Acetabular cups, tibial and patellar components, porous coatings
	UHMWPE/HDPE	Ceramic and metallic femoral stems
	Polysuffolene	Porous coatings on metallic femoral stems and femoral stems
	PTFE	Porous coatings on metallic femoral stems and femoral stems
Composites	Polymer-based	Femoral stems
	Polysulflone-carbon	
	Polycarbonate-carbon	
	Polysulfone-Kevlar	
	Polycarbonate-Kevlar	

The materials utilized for orthopedic implants especially for load bearing applications should possess superior corrosion resistance in body environment, excellent biocompatibility, and excellent combination of high strength and low modulus, high fatigue and wear resistance, high ductility and without cytotoxicity [44-46]. Table 1.2 listed the various possible material combinations of total hip joint replacement prostheses [29-33]. The development of novel materials for biomedical application is an interdisciplinary research and often requires an incorporating effort of material experts, biomedical specialists, pathologists and clinicians. To be able to serve for a longer time without rejection an implant should have the following qualities.

- *Biomechanical compatibility*

The mechanical properties that designate the type of material will be nominated for a precise application. The response of biomaterial to the repeated cyclic load is determined by the fatigue strength of the material which determines the long-term success of the implant. The

biomechanical incompatibility is defined as the fracture produced in an implant due to the inadequate strength or mismatch in mechanical property (known as modulus) between the bone and implant. Hence, the biomaterial used for an implant should be biomechanical compatible and expected to have a modulus equivalent to that of bone for the success. Moreover, the biomechanical incompatibility leads to death of the bone cells known as 'stress shielding'. The bone modulus varies in the magnitude from 4 to 30 GPa depending on the type of the bone and the direction of measurement [47, 48]. If the implant material has higher stiffness than the bone, prevents the required stress being transferred to adjacent bone, leads to bone resorption around the implant, and subsequently leads implant loosening. Thus, a material with excellent combination of high strength and low modulus closer to bone has to be used for implant to avoid loosening of implants and higher service period for avoiding repeated surgery.

- *Biocompatibility*

The materials used as implant are expected to be highly nontoxic and should not cause any inflammatory or allergic reactions in the human tissues and cells. However, the success of the biomaterials is mainly dependent on the reaction of the human tissues with implant, and this also measures the biocompatibility of a material [43]. The two main factors that influence the biocompatibility of a material are the host response induced by the material and the materials degradation in body. Geetha et al. [49] classified various biomaterials for hip prosthesis based on the response in human body (see Table 1.3). Bioactive materials are highly preferred as they give rise to high integration with surrounding bone; however, bio-tolerant implants are also accepted for implant manufacturing. When implants are exposed to human tissues and fluids, several reactions take place between the host and the implant material and these reactions also dictate the bio-acceptability of these materials. The issues related to biocompatibility are (1) thrombosis - which involves blood coagulation and adhesion of blood platelets to biomaterial surface, and (2) the fibrous tissue encapsulation of biomaterials that are implanted in soft tissues.

- *High corrosion and wear resistance*

The low wear and corrosion resistance of the implants in the body fluid results in the release of non-compatible metal ions. These released ions are found to cause allergic and toxic reactions [50]. The service period of the material is mainly determined by its abrasion and wear resistance. However, the low wear resistance also results in implant loosening and wear debris

deposited in tissue causes several adverse reactions [29]. Thus, the development of implants with high corrosion and wear resistance material is of prime importance for the longevity in the human system.

- *Osseointegration*

The inability of an implant surface to amalgamate with the contiguous bone or the other tissues due to micromotion, results in implant loosening. A fibrous tissue is developed between the bone and the implant, if the implant is not healthy joined to the bone. Thus, materials with a proper surface are vital for the implant to amalgamate well with the adjacent bone [51]. The surface roughness, surface chemistry and topography play a key role in the evolution of good osseointegration. The common necessities of biomaterials and the problems occurring due to non-compliance is presented in table 1.4 [30].

Table 1.2 Materials amalgamations in hip joint replacement (THR) prosthesis

Femoral component	Socket component	Results
Co-Cr-Mo	Co-Cr-Mo	Early high loosening rate and restricted use; new evolution show lowest wear loss
Co-Cr-Mo	UHMWPE	Commonly employed; minimum wear
Alumina/zirconia	UHMWPE	Extremely low wear rate; zirconia more impact resistant
Alumina	Alumina	Minimum wear rate; pain—not in clinical use in the United States
Ti-6Al-4V	UHMWPE	Reports of high UHMWPE wear due to breakdown of titanium surface
Surface-coated Ti-6Al-4V	UHMWPE	Improved wear resistance to abrasion; only thin treated layer attained

Table 1.3 Arrangements of biomaterials based on its interaction with its surrounding tissue

Categories	Examples	Response	Effect
Biotolerant materials	Polymer-polytetra-fluo-rethylene (PTFE), poly-methylmethaacralyte (PMMA), Ti, Co–Cr, etc.	Formation of slim connective tissue capsules and the capsule does not adhere to the implant surface	Rejection of the implant leading to failure of the implant
Bioactive Materials	Bioglass, synthetic calcium phosphate with hydroxyl apatite (HAP)	development of bony tissue around the implant material and muscularly amalgamates with the implant surface	Consent of the implant leading to accomplishment of implantation
Bioreabsorbable Materials	Polylactic acid and polyglycolic polymers and processed bone grafts, composites of all tissue extracts or proteins and structural support system	changed by autologous tissue	Consent of the implant leading to accomplishment of implantation

Table 1.4 Necessities of biomaterials and problems resulting from not enough requirements

Significant necessities	Consequences of not fulfilling the requirements
Long fatigue life	Implant mechanical failure and revision surgery
Sufficient strength	Implant failure, pain to patient and revision surgery
Modulus alike to that of bone	Stress shielding effect, loosening, failure, revision surgery
High wear resistance	Loosening of implant, austere inflammatory response, and annihilation of the healthy bone and producing wear debris which can go to blood.
High corrosion resistance	Discharging non adaptable metallic ions and allergic reactions
Biocompatibility	Body reaction and unfavourable effects in the organic system
Osseointegration	Fibrous tissue between the bone and the implant, not healthy assimilation of the bone and implant and at last implant loosening

Wear particles detachment is one of the prime problems allied to total hip replacements. Wear debris, specifically UHMWPE particulates from Metal-on-Polymer (MoP) joints, may cause aseptic loosening [52]. In order to conquer or minimize this problem alternative bearings such as Metal-on-Metal (MoM) prostheses, including CoCr components, have been developed. CoCr alloys, or more especially CoCrMo, were firstly used in metal on metal implants over 50 years ago [53, 54]. The most commercially used alloy for clinical application is the cast version of Co28Cr6Mo (ASTM F75) and the wrought versions ASTM F1537 and ASTM F799 [55–59]. These alloys are the harmless biomaterials for orthopedic hip implant than stainless steel and have been used extensively due to their excellent mechanical, corrosion and especially wear resistance properties [60, 61]. The main trait of Co-based alloys is its corrosion resistance in chloride ambiance, which is due to alloying additions and the formation of the chromium oxide Cr_2O_3 passive layer [62].

The typical microstructure of cobalt-based alloys consists of a cobalt-rich solid-solution matrix containing carbides (i.e., Cr_7C_3, and $M_{23}C_6$) within the grains and at grain boundaries, where chromium, tungsten, tantalum, silicon, zirconium, nickel, and cobalt, may be present in a single carbide particle [62, 63]. Co-based alloys have two feasible crystal structures: first is close packed hexagonal (CPH) at low temperature ($> 417ºC$) and second is face centered cubic (FCC) at high temperatures ($< 417ºC$). Maximum Co-based alloys will display a metastable FCC matrix structured because the thermal treatments with which these alloys are produced involve quite rapid cooling, inhibiting the development of a CPH structure [64, 65]. Due to its material

properties Cobalt Chrome can be utilized to develop very thin metallic devices with no risk of fracture. This makes it alluring for utilize in hip arthroplasty for lively patients to produce bone conserving implants while maximizing the size of bearing diameter to lessen the threat of dislocation. With the present technology, further materials utilized in total hip arthroplasty, such as ceramics and polyethylene, can't basically be made in anatomically applicable implant sizes without sacrificing acetabular bone stock or increasing their risk of fracture. Well execution MoM hip replacements also have the potential to produce extremely low quantity of wear compared to MoP implants. Cobalt chrome implants are known to discharge metal ions in the body. Although MoM hip replacements have been utilized for more than 40 years investigations are being done into any long term clinical implications. Metal-on-metal hip implants, however, are not immune to wear debris and biocompatibility issues. The wear debris produced by metal-on-metal devices ranges from particles several nanometers to submicron in size. In this manner, in spite of a low wear rate, the amount of wear particles is significant.

Actually wear refers to the progressive expulsion of material from a surface and plastic deformation of material on a surface because of the mechanical activity of the other surface [66]. The necessity for relative movement between the working surfaces and preliminary mechanical contact between asperities lead a significant role between mechanical wear compared to different processes with similar outcomes [67]. The sliding wear behavior of various Cobalt based alloys is a boundless subject which has received much attention in recent years. The tribological behavior of metals which are in sliding contact relies on the numerous variables such as a normal load applied to the material, sliding velocity, sliding distance, surface hardness, working environment, etc., which influence the wear mechanism and results in change of wear rate [68]. Modified CoCr alloy with different particulates (i.e. molybdenum, nickel and tungsten) are widely used as the femoral head material for hip implant application experiences sliding wear. The contacting materials experience micro scale sliding between each other which can also tend towards fatigue-induced wear [69]. Hence, the study of sliding wear is one of the essential criteria to determine the life of artificial hip implant which are made of adding three different particulates (i.e. molybdenum, nickel and tungsten) with Co30Cr metal matrix. The diminution of wear and subsequent extension of life of a hip joint replacement would bring both economic benefits and a better quality of life to the patients who have to undergo replacement surgery. Diminution of wear can be attained by modifying the materials used for the replacement. Addition of fillers (i.e. molybdenum, nickel, and tungsten) affects grain size, morphology, and

texture and phase composition so as to enhance the wear resistance of fabricated alloy composite. Molybdenum basically reduces the grain size, yielding improved mechanical properties and gives solid solution strengthening and good localized corrosion resistance in the fabricated alloy composite [9-11]. Nickel is a hard and ductile transition metal that is treated corrosion-resistant due to its slow rate of oxidation. The addition of nickel stabilizes the fcc matrix, contributes to solid-solution strengthening, improves corrosion resistance and enhances ductility during services. Typically, the inclusion of tungsten content in the fabricated metal alloy composite provides additional strength to the matrix, owing to the virtue of their large atomic size, fine grain structure and is excellent for resisting heat [12, 13]. Tungsten is a light gray or whitish metal that is soft and ductile enough to be extruded into various shapes.

Statistical techniques have normally been utilized for investigation, prediction and/or optimization of countless engineering processes. Such techniques ease the user to define and study the effect of each single condition feasible in an experiment where several factors are included. Sliding wear is an intricate wear phenomenon in which numerous control factors collectively find out the performance output (i.e. wear volume) and there is immense scope in it for implementation of apposite statistical techniques for process optimization. But unluckily, such studies have not been passably reported in this way. The present work addresses to this aspect by adopting a systematic Design of experiment (DOE) or statistical technique called Taguchi method to optimize the process parameters leading to minimum sliding wear of the alloy composites under study. But when we necessitate characterizing all the likely combinations of the metal matrix and particulate, a prediction model based on Artificial Neural Network (ANN) can be formed. A well trained or designed prediction model can be used to predict the output (wear volume) for any combinations of the input variables (normal load, sliding velocity, sliding distance and filler content).

Against this background, the present research work has been undertaken to study the performance evaluation and optimization of biomedical composite alloy for femoral head material of hip joint replacement. For this, firstly develop a high strength biomedical alloy composites and afterwards evaluation of their physical, mechanical and assessment for their relative sliding wear performance, nature of corrosion resistance, biocompatibility action and on statistical interpretation of the various test results.

1.2 Thesis outline

To attain the stated objective, the study is arranged in eight chapters. A general outline of the research, motivation, and significance is presented in this chapter. A brief explanation of each chapter is as follow.

Chapter Two: Literature Review

In this chapter includes a literature review designed to give a summary of the base knowledge already available including the issues of interest. It presents the research works carried out on the physical, mechanical; sliding wear; corrosion; biocompatibility and optimization properties of various types of particulate filled metal composite alloys, by various investigators earlier.

Chapter Three: Material and Methods

This chapter discusses the detailed description of the formulation of composite materials and fabrication technique of composite alloys. It also discusses characterization methodology like physical, mechanical, corrosive, biocompatibility, sliding wear etc. It also presents Taguchi experimental design methods and PROMETHEE multi-criteria-decision-making approach for formulation ranking.

Chapter Four: Experimental Results

This chapter presents discussion on results of physical, mechanical and sliding wear characterization of the fabricated composite alloys under investigation. It includes a detailed study on the effect of particulate fillers on the physical, mechanical and sliding wear behavior of the fabricated Co-30Cr base metal alloy composite, micro-structural examination by XRD, FE-SEM/EDAX and AFM techniques. Finally, the outcomes of sliding wear behavior optimized by Taguchi experimental design and the most significant factor is determined by ANOVA.

Chapter Five: Neural Network Analysis

This chapter includes, predicting the wear volume under different operating conditions using artificial neural networks (ANN) technique and compared with experimental results.

Chapter Six: Corrosion and Biocompatibility Analysis

This chapter presents results on corrosive nature and biocompatibility behavior of the fabricated alloy composites under investigation.

Chapter Seven: Ranking of the material

This chapter presents ranking of the formulations under investigation using multi criteria-decision making techniques tool like ENTROPY-PROMETHEE.

Chapter Eight: Summary and future scope

This chapter presents the specific conclusions drawn from the experimental efforts and recommendations for future research.

<p align="center">*****</p>

Introduction

This chapter presents an extensive literature review of the main research topics for the present investigation. This is a multidisciplinary research covering a wide range of subjects including biomaterials (specifically bio-metallic materials) and their mechanical properties, wear performance, corrosion resistance and biocompatibility response. The focus of this literature review has been on the wear analysis of metal-on-metal hip replacement under body environment.

2.1 Hip replacements

2.1.1 An overview

The human hip joint is a complicated bearing system with low friction. It provides stability owing to the ball-and-socket joint configuration while at the same time, allowing a moderate range of motion [70]. The joint may lose its function owing to trauma, disease or by aberrant usage. Every year, more than thousands of people who endure from joint failure undergo hip replacement surgery, where the malfunctioned hip joint is replaced with an artificial hip implant. The hip replacement is a very common solution for osteoarthritis, rheumatoid arthritis, avascular necrosis, and traumatic arthritis. As discussed earlier in chapter 1, the possible materials usually used for modern hip replacements are metal-on-polymer (MoP), metal-on-metal (MoM), ceramic-on-ceramic (CoC) and ceramic-on-polymer (CoP). Historically, MoP bearings have been the dominating configuration in the total hip replacement field [71] and this type of hip prostheses is still the subject of considerable development at present. A major disadvantage of MoP bearings is the potential for high level of polymer (normally ultra-high-molecular-weight-polyethylene, UHMWPE) particle production. The natural biological response to these particles, i.e. immune system of the host, can alter the local pH around the implant and subsequently influence the balance between bone formation and resorption, and hence resulting in accelerated osteolysis (bone loss) [72]. In recent years, MoM hip replacement based on CoCrMo alloys have increasingly become the favored choice owing to their better wear resistance, longevity and reduced inflammatory osteolysis resulting from such devices. MoM hip replacement is one of the favored options for younger and/or more active patients, as it replaces only the femoral head and acetabular surface and is less invasive. This chapter contains review of existing research reports:

— On the basis of joint replacement implant materials and its mechanical properties

— On the basis of tribological conditions

— On the basis of corrosion resistance and biocompatibility

— On implementation of Design of Experiment (DOE) and optimization techniques

— On the basis of multi criteria decision making (MCDM) methods

2.2 On the basis of joint replacement implant materials and its mechanical properties

2.2.1 Metallic Biomaterial

Metallic implants are the chief biomaterials used for joint replacement and become gradually important. The metallic implants usually used for orthopedic applications can be fabricated from stainless steel, CoCr alloys, Ti and Ti alloys. These metallic materials have numerous promising properties, such as excellent thermal conductivity, high strength, high fracture toughness, hardness, corrosion resistance and biocompatibility, which make them an excellent choice for total joint replacement [73]. However, the disadvantage with metallic implants is their high elastic modulus, which causes stress shielding and corrosive nature. The consequence of corrosion is loss of material, which will weaken the implant, and probably the most importantly, the corrosion products and metal ions released into the tissue resulting in undesirable side effects [74]. They also have other drawbacks such as low bio-compatibility, too high stiffness compared to tissues and high density. The foremost reasons in selection of metal-based materials for biomedical applications are their excellent biocompatibility, convenient mechanical properties, good corrosion resistance and low cost [74]. The mechanical properties of various metallic biomaterials used in total hip replacement are shown in table 2.1 [29-33, 75-81].

Table 2.1 Mechanical properties of metallic biomaterials used in THR

Material	Young's Modulus E (GPa)	Fatigue Limit s_{end} (MPa)	Tensile Strength s_{UTS} (MPa)	Yield Strength s_y (MPa)
Stainless steel	190	240–820	586	222–1212
Co-Cr alloys	280	208–950	656–1896	449–1605
Titanium (Ti)	110	300	760	485
Ti-6Al-4V	116	620	965	897–1033
Cortical bone	14–30	--	71–150	30–70

2.2.1.1 Stainless Steel

Stainless steel (316 and 316L) is the first material used to engender artificial bone and facilely cast into dissimilar shapes. 316L has a superior corrosion resistance as compared to 316 with its

inferior carbon content. However it may corrode inside the body under certain circumstances such as in a highly stressed oxygen-depleted region. Both 316 and 316L are congruous to utilize in ephemeral contrivances such as fracture plates, screws, and hip nails. They are more frugal and facilely cast into different shapes but not durable [27]. Devaraju and Elayaperumal [68] depicted the stainless steel is an alloy that has perpetuated to facilitate the applications with large numbers of fields. Largely because of its simplicity of fabrication and enviable assortment of mechanical and corrosion behavior, stainless steel is one of the predominant implant alloys. The chemical compositions of austenitic stainless steel grades, as indicated by the American Iron and Steel Institute (AISI), are exhibited in Table 2.2 [29] [82, 83]. The sizeable corrosion resistance requisite by joint replacement constituents can be found within the 300-series [84]. To be contemplated "stainless" steel requires the addition of Cr to upgrade corrosion resistance by devising a CrO_2 passive layer on the surface of the steel. The lesser the carbon content in the stainless steel, the more corrosion resistant the alloy is to the physiological saline in the human body [84]. With this reasoning, it has been suggested by the ASTM that 316L ought to be the principal alloy for implant fabrication in comparison with other Stainless Steel grades [83]. Additional alloying elements include nickel, which is utilized to increment corrosion resistance in more truculent environments and molybdenum, which ameliorates localized corrosion resistance against fretting, pitting and crevice corrosion reported by Viceconti et al, [51]. The nickel balances out the austenitic phase, at room temperature and enhances corrosion resistance. The austenitic phase formation can be affected by both the Ni and Cr contents for 0.10% carbon stainless steels. The least amount of nickel for keeping austenitic phase is approximately 10%.

Table 2.2 Composition of austenitic stainless steels (balance % iron)

AISI %	%C	%Cr	%Mn	%Ni	% other elements
301	0.15	16-18	2	6-8	1.0 Si
304	0.07	17-19	2	8-11	1-Si
316, 18-8sMo	0.07	16-18	2	10-14	2-3 Mo, 1.0 Si
316L	0.03	16-18	2	10-14	2-3 Mo, 0.75 Si
430 F	0.08	16-18	1.5	1-1.5	1.0 Si, 0-6 Mo

In the UK, stemmed austenitic stainless steel (or one piece femoral components) are probably the most popular found designs of THR, and the early Charnley THR utilized a stemmed femoral component based on 18-10 austenitic stainless steel [85]. Thackrays (*now DePuy Johnson & Johnson)* of Leeds introduced 316LVM a double-vacuum remelted 18Cr-10Ni

stainless steel with superior corrosion resistance compared to the EN58J, and subsequently introduced an incipient stainless steel alloy based on Rex 734 in 1980 which remains in utilization to the present day and is kenned as Ortron 90 [85]. It is a high nitrogen 21Cr-10Ni-2.5Mo austenitic stainless steel with superior fatigue strength, corrosion and corrosion fatigue resistance, than the types EN58J or 316LVM.

Mechanical properties of biomaterials occasionally necessitate supplemental attributes to completely duplicate the structure deliberate for replacement. In some cases where the original cast, wrought, or forged alloy necessitates a physical or chemical alteration, heat treatments, for example, annealing, cold working, and hot forging, can be of service reported by Mirhosseini et al. [86]. As 316 and 316L SS are the most extensively used stainless steel alloys in surgical implant fabrication. For such heat treated alloys the mechanical properties such as ultimate tensile strengths, yield strengths, and elongations are listed in Table 2.3 [82-88]. The benefits of SS include fine hot-and cold-working mechanical properties, superior machinability and low cost [89]. Despite the fact that Stainless Steel keeps satisfactory biocompatibility and properties, there is a proclivity to fall short in the viewpoint of fatigue resistance as a result of low proportional limits that lead to start and engendering of fatigue cracks [84].

Table 2.3 Mechanical properties of stainless steels in surgical implants

Material	Condition	Ultimate Tensile Strength (MPa)	Yield Strength (MPa)	Elongation in 2 in., min. %
316	Annealed	515	203	40
	Cold finished	619	310	35
	Cold worked	860	685	12
316L	Annealed	503	195	40
	Cold finished	603	294	35
	Cold worked	858	688	12

Biomaterials with improved fatigue resistances are Ti and Ti-alloys, Co-alloys, and the stainless steel 400-series [84]. To the extent corrosion is concerned, research has disclosed that the fretting corrosion product of austenitic steel can cause inadmissible reactions in both the implant and the body [90]. From these corrosion products, Xulin et al. [90] found nickel concentrations up to 2% in tissues around recovered SS orthopaedic implants by histological examination. Apart from implanting failures owing to fabrication and manufacture, a healthy and none-too-arduous lifestyle is the optimal setting for SS implants with expanded lifetimes.

2.2.1.2 Cobalt-Chrome

Ever since the utilization of SS as the first biomaterial in Total Hip Replacement surgeries, biomedical makers have aimed research at the production of additional alloys with greater mechanical properties [91]. Currently, Co-based alloys are among the most secure implant materials for orthopedic prostheses, on account of their excellent corrosion properties and mechanical strength [22]. The main trait of Co-based alloys are its corrosion resistance in chloride environments, which is due to alloying augmentations and the development of the chromium oxide Cr_2O_3 passive layer [75]. Orthopedic implants fabricated with Co-based alloys can be cast, wrought, or forged [33]. The phenomenal mechanical properties and corrosion resistances of cobalt based alloys derive from the categorical weight proportions of base elements and alloy additions in their compositions.

As indicated by Table 2.4, casting and forging bars made with Co-based alloys with low amounts of nickel are designated as F75 and F799, and alloys with more immensely colossal nickel content are deputed as F90 and F562 [62, 74, 83, 87]. Contrasted with the wrought alloys, Co-based casting alloys are distinguished by extreme contents of high melting metals, for example, tantalum, tungsten, chromium, zirconium and titanium and by higher carbon contents [63]. In all designations, molybdenum turns out finer grains, which consequences in higher strength and silicon and manganese ameliorate oxidation resistance [26]. The CoNiCrMo alloy initially called MP35N (Standard Pressed Steel Co.) contain around 35% cobalt and nickel each. The alloy is highly corrosion resistant to seawater under stress. The abrasive wear properties of the wrought CoNiCrMo alloy are alike to the cast CoCrMo alloy, however; the prior is not advocating for the bearing surfaces of joint prosthesis in view of its low frictional properties with itself or different materials. The better fatigue and ultimate tensile strength of the wrought CoNiCrMo alloy make it congruous for the applications which require long service life with no fracture or stress fatigue. Such is the case for the stems of the hip joint prostheses. This favorable position is better esteemed when the implant must be supplanted, since it is fully arduous to remove the failed piece of implant embedded deep in the femoral medullary canal. Furthermore, the revision arthroplasty is conventionally inferior to the primary surgery in terms of its function because of the shoddier fixation of the implant.

The common microstructure of cobalt-based alloys consists of a cobalt-rich solid-solution matrix containing carbides (i.e., Cr_7C_3, and $M_{23}C_6$) within the grains and at grain boundaries, where chromium, tungsten, tantalum, silicon, zirconium, nickel, and cobalt, may be present in a

single carbide particle [62, 63]. Table 2.5 presents the mechanical properties of heat treated, surgical grade Co-based alloys [82, 83, 87, 92, 93].

Fujihara et al. [22] concentrated early forms of Co-based alloys utilized for hip implants contained comparatively high carbon contents, i.e. 0.2%, and were typically engendered via investment casting. Depending on the casting method, the manufacturing process has the capability to produce not less than three microstructural features that can vigorously influence implant properties, both positively and inimically [62]. The elements comprise: (i) if not the typical F75 microstructure, then the arrangement of interdendritic locales that emerge as solute (chromium, molybdenum, cobalt) rich and contain carbides, while dendrites become depleted in chromium and richer in cobalt, (ii) dendrite arrangement and relatively large grain sizes that decrease yield strength, and (iii) casting defects [62]. In spite of fabrication of cast materials may result in the microscopic voids within their structures, techniques for example hot isostatic pressing (HIPing) can be utilized for full densification of the material to enhance mechanical properties [47]. More recently, low-carbon wrought versions of Co-based alloys have superior mechanical properties and corrosion resistance and incline to be more vigorous than cast alloys [94]. Alike to cast alloys, hot forging or HIP of components significantly minimizes the shrinkage voids and alters the grain structures leading to better mechanical and fatigue properties [95].

Table 2.4 Chemical compositions of cobalt-based alloys for biomedical implants

Material	ASTM	Common Trade Names	Composition (wt.%)
Co-Cr-Mo Forged	F799	Forged Co-Cr-Mo Thermomechanical Co-Cr-Mo FHS	58-59 Co 26.0-30.0 Cr 5.0-7.00 Mo < 1.00 Mn < 1.00 Si < 1.00 Ni < 1.5 Fe < 0.35 C < 0.25 N
Co-Cr-Mo Cast	F75	Vitallium Haynes-Stellite 21 Protasul-2 Micrograin-Zimaloy	58.9-69.5 Co 27.0-30.0 Cr 5.0-7.0 Mo < 1.0 Mn < 1.0 Si < 2.5 Ni < 0.75 Fe

| Co-Ni-Cr-Mo-Ti Wrought | F562 | MP 35 N Biophase Protasul-1( ) | < 0.35 C 29-38.8 Co 33.0-37.0 Ni 19.0-21.0 Cr 9.0-10.5 Mo < 1.0 Ti < 0.15 Si < 0.010 S < 1.0 Fe < 0.15 Mn |
| Co-Cr-W-Ni Wrought | F90 | Haynes-Stellite 25 Wrought Co-Cr | 45.5-56.2 Co 19.0-21.0 Cr 14.0-16.0 W 9.0-11.0 Ni < 3.00 Fe 1.00-2.00 Mn 0.05-0.15 C < 0.04 P < 0.40 Si < 0.03 S |

Table 2.5 Mechanical behavior of heat treated Cobalt based alloys used in THR

Material:	Cast CoCrMo	Wrought CoCrMo		Wrought CoNiCrMo		Wrought CoNiCrMoFe		Wrought CoNiCrMoWFe	
Condition	annealed	annealed	cold worked	hot worked	annealed	cold worked aged	cold worked	cold worked aged	annealed	cold worked
Density (g/cm^3)	7.8	9.15	9.15	-	-	-	-	-	-	-
E (tensile) (GPa)	198	230	228	-	-	-	-	-	-	-
Hardness (Hv)	298	239	445	28	-	-	-	-	-	-
σ0.2% (MPa)	450	308	1000	665	242-448	1583	-	1242-1448	275	1310
σUTS (MPa)	660	858	1500	1000	794-1000	1794	1515-1794	1862-2273	600	1172
Elong.(min. %)	8	30	9	12	50	8	-	1.0-17	50	12

2.2.1.3 Titanium and its Alloys

Titanium and Ti based alloys are lighter than the distinct metals and have good mechanochemical properties. Ti has poor shear strength, making it less enviable for bone screws, plates and similar applications. Ti alloy has an excellent biocompatibility and presently the most commonly used [27]. Shenhar et al. [96], Alvarado et al. [91], Budzynski et al. [97], Geetha et al.

[49] and Navarro et al. [98], described the Titanium-based materials properties. Titanium alloys because of the blend of its excellent characteristics, for example, high strength, low density, high specific strength, good corrosion resistance, complete inertness to body environment, enhanced biocompatibility, moderate elastic modulus of around 110 GPa are a apposite option for implantation. Table 2.6 presents the four distinct categories of unalloyed commercially pure titanium for surgical implant applications [27, 82, 83, 99]. The impurity contents split them; oxygen, iron, and nitrogen should be controlled carefully. Oxygen specifically greatly affects the ductility and strength.

Titanium and its alloy additionally have this competency to become tightly integrated into bone. This high capacity to join with bone and other tissues impressively ameliorates the long-term behavior of the implanted devices, lessening the risks of loosening and failure. Normally great clinical results from rough surfaces of Titanium and its alloy is resulted when compared to smooth-surfaced implants as a result of good osseointegration between the bone and the implant [100]. The mechanical properties of material are of immense significance when designing load-bearing orthopedic and dental implants. A number of mechanical properties of metallic biomaterials are presented in Table 2.7. The mechanical properties of a particular implant depend not only on the type of metal, but additionally on the processes used to fabricate the material and device. The elastic moduli of the metals (see in Table 2.7) are no less than seven times better than natural bone [10, 27, 82, 83, 93, 99].

Imam et al. [101] described, titanium alloy for example, Ti6Al4V, is extensively utilized to manufacture implants and its chemical necessities are given in Table 2.6. The main alloying elements of the alloy are aluminum (5.5-6.5%) and vanadium (3.5-4.5%). The Ti6Al4V alloy has around the same fatigue strength i.e. 550 MPa of Cobalt Chrome alloy after rotary bending fatigue test. Titanium is an allotropic material, which subsists as an HCP structure up to 882ºC and BCC structure (bcc, β-Ti) above the temperature. Ti alloys can be invigorated and mechanical properties varied by controlled composition and thermo-mechanical processing techniques. The integration of alloying elements to titanium enables it to have a wide range of properties: (1) Aluminum has a tendency to balance out the α-phase that is increase the transformation temperature from α- to β-phase. (2) Vanadium stabilizes the β-phase by lowering the temperature of the transformation from α to β.

Table 2.6 Chemical composition of Ti and its alloy

Element	Category-1	Category-2	Category-3	Category-4	Ti6Al4V[a]
Hydrogen	0.015	0.015	0.015	0.015	0.0125
Carbon	0.10	0.10	0.10	0.10	0.08
Nitrogen	0.03	0.03	0.05	0.05	0.05
Oxygen	0.18	0.25	0.35	0.40	0.13
Iron	0.20	0.30	0.30	0.50	0.25
Titanium			Balance		

[a] Aluminum 6.00% (5.50-6.50), vanadium 4.00% (3.50-4.50), and other elements 0.1% maximum or 0.4% total.

Table 2.7 Mechanical properties of Titanium and its alloy used in THR (ASTM F136)

Properties	Category-1	Category-2	Category-3	Category-4	Ti6Al4V	Ti13Nb13Zr
Yield strength (0.2% offset) (MPa)	170	275	380	485	795	900
Tensile strength (MPa)	240	345	450	550	860	1030
Elongation (%)	24	20	18	15	10	15
Reduction of area (%)	30	30	30	25	25	45

2.3 On the basis of Tribological conditions

Tribology is defined as "the science and technology of interacting surfaces in relative motion", and embraces the study of friction, wear, and lubrication [102, 103]. Friction, wear, and lubrication are all trends familiar from day by day experience, but wear is categorically prominent because it leads to catastrophic failure and represents one of the most costly quandaries facing industry today [92]. Tribology of Total Joint Replacement is astronomically intricate. Unlike many tribological systems total joint articulation exhibits extremely low levels of wear and can function efficaciously for well over a decade. Whilst healthy natural joints show impressive tribological characteristics credited to the intrinsic properties of articular cartilage (high compliance) and synovial fluid, and ensuing optimized lubrication modes, TJRs based on current available materials experience mixed/boundary lubrication [2]. This lower lubrication performance is generally attributed to high rigidity of the artificial materials. Since some surface contact occurs during articulation, the friction between artificial materials is significantly higher than in natural joints and non-recoverable wear of the artificial joint materials takes place [2]. Among the crucial problems encountered when considering implant lubrication is the intricacy of the system. The hip joint experiences transient loading and variable sliding velocities over the

gait cycle, which results in a range of contact conditions and possible lubrication mechanisms. Typically these joints function at slow speeds, low pressures and transient loading under reciprocating sliding. For example in steady-state walking, replacement hip joints, experience two loading peaks per cycle with loads varying from 0.1 KN to 3.5 KN and linear speeds of 0-30 mm/s. The utmost contact pressures are generally low i.e. <70 MPa, when compared to engineering contacts. However, physiological kinematics and loads may vary significantly for different activities and patients reported by Bergmann et al. [104]. The other part of the problem is the lubricant, which is periprosthetic synovial fluid. Synovial fluid (SF) is an intricate combination of macromolecules (such as protein, glycoproteins, hyaluronin) and surface active species (phospholipids) discussed Kitano et al. [105] and Wang et al. [106]. The chemical composition includes hyaluronan (HA), proteins and glycoproteins, phospholipids and cholesterol [105]. A number of these species, concretely phospholipids and proteins, are thought to make contributions to the boundary lubrication of the implant. The problem is further complicated by changes to the physical and chemical properties of synovial fluid due to disease, trauma and postoperatively reported Kitano et al. [105], Wang et al. [106] and Delecrin et al. [107], so that there is no 'usual' composition. Periprosthetic SF, which refills the cavity post-implant, has different properties to healthy SF; the pH and protein concentrations increase and the effective viscosity decreases due to changes in the HA content [105,107].

2.3.1 Wear

Though advancement in biomaterial fabrication has allowed for implants to have got longer lifetimes, it is inescapable that the implants will fail because of wear. Wear is defined as the progressive removal of material with the generation of wear particles, that occur as a result of relative movement between two rival surfaces under load [7, 74, 102]. It is perhaps the most consequential yet least understood aspect of tribology and for this reason is magnetizing considerable attention at the present time. A common characteristic of the wear life of most engineering components is the relatively diminutive percentage of the weight of the device that needs to be removed afore accurate functioning is impaired. However, it is not always disadvantageous and plenty of processes such as metal cutting (e.g., polishing) rely on the phenomenon [03].

Wear determines the useful life of artificial joints, and in TJRs wear of the joint surfaces is known to be one of the most prevalent causes of failure and absence of durability of the prosthetic implants. Albeit the mechanical consequences of wear can inhibit the practical life of

the joint replacement, the clinical evils from wear more often are owing to the relinquishment of the extortionate amount of wear particles into the biological environment, and when particles within a certain size-range are phagocytosed in adequate amount, the macrophages enter into an activated state of metabolism, releasing substances that can result in periprosthetic bone resorption which leads to the eventual loosening of the implant [7].

2.3.1.1 Wear of Metals in total joint replacement (TJR)

The metal components in Total Joint Replacement are damaged by articulation (friction) even when rubbing in opposition to the soft polymeric materials. 316L stainless steel is less sensitive to wear damaging than Co-Cr-Mo (moderate), and Ti6A14V (severe) alloys [23]. Passive oxide-type films are present on implant metal surfaces that protect them from corrosion in vivo; however, small concentrations of metal ions can be detected in the body fluids and organs whenever metallic implants are placed in the body [23]. Tissue culture studies have shown that cell replication is slowed in the presence of ions found in two commonly implanted alloys Co-Cr-Mo and Ti6A14V, while other studies demonstrate that bone and fibrous tissue will grow into intimate apposition with implants fabricated from these same materials [5]. For 316L stainless steel, the passive film is provided by the chromium included in the metal. It produces a chromium oxide film (Cr_2O_3) by reacting with available oxygen in the air or with oxygen contained in the body environment. This passive film although very thin, about 2-5 nm dense, protects the underlying metal from further oxidation (corrosion). The chromium in Co-Cr-Mo provides protection in a similar fashion to that of 316L stainless steel. In Ti6A14V alloys, it is the titanium that provides the protective passive film by forming titanium oxide (TiO2) [23].

Although passive surface films form very quickly (in nanoseconds), they can be harmed or sheared off from rubbing next to another surface, exposing the metal temporarily to the environment. This exposure causes soluble metal ions to be released locally. If the rubbing occurs continuously as with hip movement; the passive film is constantly damaged and reformed, creating a constant source of metal ions. If these removed oxide films are hard, they can behave as three-body abrasives and metal wear as well as polymer wear can occur [23]. The attendance of the third material between two rubbing materials is known as three-body wear and this can expedite the wear of the two initial surfaces if the third material is harder.

Metal burnishing or micro-scratching can occur in hip replacements with body particles such as bone chips, bone cement debris, and metal particles to accelerate the passive film damage and production of metal ions. Significant levels of the major component of metal

prostheses have been quantified near the implant in synovial fluids and soft tissues, as well as throughout the body in the blood, urine and other tissues [108]. Haynes et al [109] found that, Co-Cr and 316L stainless steel particles turn out to be much less toxic but may additionally induce more bone resorbing mediators as they age in vivo. The long-term effects of ion leaching in TJR remain a concern, and await further elucidation. It has been shown by analyzing metal release rates from metal-polyethylene wear tests that Co-Cr-Mo is progressively removed at a rate of approximately 0.1 µm per year, 316L stainless steel is removed around 0.2 µm per year, and Ti6A14V around 1µm per year [110].

A novel passive film forms immediately from the reaction of the uncovered metal surface with oxygen in the environment when damaged. Implant metal surfaces gradually give up metal from this oxidative wear process and this can lead to an increased surface roughness, which in turn can increase the mating polymer wear rate [101, 111]. In TJR the wear of the polymer is greatly influenced by the roughness of the metallic counter face. Laboratory studies using screening device wear testers have shown that the wear volume of UHMWPE is approximately proportional to the mean surface roughness of the counter face raised to a power greater than 1 [110-114]. Other authors have also found different relationships between the k_o and R_a, and the conflicts in the results may be due to the different lubricants used and testing conditions [11]. The micro-topography of a surface determines its roughness and in TJR typical Ra values are initially in the range of 0.02-0.05um [110], and could increase with time due to surface abrasion especially for Ti6A14V alloy, and thus increase the mating polymer wear. This means that minimizing the surface roughness of the metal would reduce the long-term wear of the mating UHMWPE component.

- *Wear of Titanium Alloy in TJR*

Ti6A14V alloys are utilized for bone and joint replacements because of their superior biocompatibility and many auspicious attributes. Its high corrosion resistance is due to the formation of the protective oxide film TiO_2 around 1 to 4 nm thick; however, body fluids contain chloride ions that can induce the breakdown of such passive films on prostheses. Despite the various benefits of Ti6A14V alloy as an implant biomaterial, the wear resistance of an alloy is comparatively poor and has long been the concern among manufactures and surgeons who have observed a black sludge material in the vicinity of explanted artificial joints, and excessive wear of the mating UHMWPE [115-119]. Agins et al [120] have shown that Ti6A14V alloy can be concretely susceptible to wear, thus generating metallic wear debris that can lead to aseptic

loosening of the implant in joint replacements, and a sequence of other clinical retrieval and experimental wear studies [120-123] have shown that Ti6A14V alloy by itself without a surface treatment is not well suited for *in vivo* bearing applications because of the poor surface wear characteristics. Schmidt et al [124, 125] have shown utilizing a pin-on-disc tribometer that surface modification of titanium alloy implantation can improve the tribological behaviour of Ti6A14V/polymer sliding couples. They observed an increase in micro-hardness with implantation dose due to compound formation (TiN), and found wear reduction in both the implanted Ti6A14V samples and mating unmodified UHMWPE attributed to an increase in micro-hardness and a decrease in oxide film thickness on the Ti6A14V.

- *Wear of Stainless steel Alloy in TJR*

Stainless steel (316L) has been utilised for several years for joint implants because of acceptable friction and wear characteristics, and most stainless steel explanted hip prostheses do not show significant in vivo wear. They have much better friction and wear characteristics compared to Ti6A14V implants. Nevertheless, throughout long-time period contact with body fluids and tissues, they have been reported to show metallic wear and corrosion [109, 119, 126-129]. Among the most prevalent metallic biomaterials, 316L stainless steel has lowest corrosion resistance, and in vitro corrosion of the material in physiological solutions have shown that toxic ions such as Cr, Ni and Mo are present both in the solutions and in the corrosion products. Crevice corrosion, which is often associated with wear, and synergistic effects of fatigue in chlorine solutions have also been observed. Rieu [119, 127, 130] observed in a pin-on-disc test, a very low wear on untreated 316L stainless steel characterised by few scratches on the steel disc and a non-measurable weight loss of the UHMWPE wear pins. However, in a ball-on-cup tribological test where mechanical and chemical conditions are much more severe than in the human body, they observed the 316L stainless steel ball to have become dark and the UHMWPE cup showing high wear with the production of chips of polyethylene. They observed a reduction in wear of the UHMWPE cup while the 316L stainless steel ball was implanted. Besetti [131] evaluated the in vivo bone tissue response to implanted stainless steel in the tibia diaphysis (cortical bone) and proximal tibia epiphysis of New Zealand white rabbits. They demonstrated that ion implanted stainless steel had equivalent or relatively enhanced biological compatibility in contact with bone compared to untreated materials, and concluded that implanted 316L stainless steel may be a utilizable material in biomedical purposes where reduced ion release or enhanced mechanical properties are required, such as in TJR.

- *Wear of Co-Cr Alloy in TJR*

Co-Cr-Mo alloys are facile to obtain in intricate shapes making use of casting techniques. Their orthopaedic prostheses are durable and wear resistant however, the mating component of ultra high molecular weight polyethylene (UHMWPE) easily wears down over time as a result of articulation against the hard alloy. In joint simulator studies conducted to 2×10^6 cycles, ion implantation treated and untreated Co-Cr-Mo femur heads were tested against UHMWPE, and wear was calculated via weight loss measurements by Taylor et al. [118]. Results showed a 25% reduction in wear against treated components in contrasting to untreated components. The wear of the UHMWPE against the treated Co-Cr-Mo alloy used to be nearly that against zirconia. Brummitt et al. [132] studied retrieved implants consisting of both titanium and cobalt chromium alloys. The Co-Cr alloys demonstrated higher wear resistance after twelve years in vivo use contrasted with the Ti alloys that were significantly damaged over twelve years. Both metallic alloys were combined with the similar UHMWPE components. The surface finish of Co-Cr alloy used to be maintained uniformly over the articulation zones; nevertheless, the Ti implants were consistently damaged. Davidson et al. [110] determined Co-Cr-Mo was a superior alloy. The experiment dealt with lots of alloys and provided data on the material properties and how these properties influenced the amount of wear on the metal-polyethylene implants.

2.3.2 Wear Testing and Measurements

Since 1970s, the procedure for the development of orthopedic bearings initiated with screening of several candidate materials by simple and affordable testing machines. The promising candidates would then be tested in a joint simulator followed by in vivo testing of the most promising material was reported by Dumbleton et al. [133]. There are significant distinctions between pin-on-disc material testing and full artificial joint simulator testing. The latter tests the overall amalgamation of implant design as well as the bearing materials, and therefore is ineluctably more complex and costly reported by Haider and Garvin [134], Haider and Kaddick [135] and Haider et al. [136]. This makes it more indispensable to have the pin-on-disk testing done right with meaningful and conclusive results, hopefully predictive of their in vivo wear resistance. Consequently, identifying the pair of parameters that would allow screening of materials on a simplified apparatus such as a pin-on-disk tester has been the focus of various studies was reported McKellop et al. [137]. Dumbleton [138] and Dumbleton et al. [133] endeavoured to compare wear rates obtained in the laboratories with clinical wear rates of 0.13mm/year for Charnley prostheses in an endeavour to validate testing conditions. While,

Dowson and Harding [139], Dumbleton and Shen [140], McKellop et al. [137] and Tetreault and Kennedy [141] studied the effects of lubricants using dry, water and serum lubrication, there was clearly no agreement about the wear measurement technique [142, 143]. Measurements were either based on changes in polyethylene weight or height. Although the volumetric measurements camp advocated their method on the grounds that attached wear debris and fluid up take did not affect the specimen height [143-145], gravimetric measurements were not affected by creep and plastic deformation [137]. Dowson and Harding [139] and McKellop et al. [137] compared both the techniques reported that volumetric measurements yielded higher scatter. The complexity of obtaining a linear wear rate based on height changes due to creep [146] helped establish gravimetric measurements as the standard wear measurement technique in pin-on-disk testing. Caution is necessary with wear estimates which rely on thickness quantifications due to potential creep and shape recovery errors allied with viscoelastic deformation and some shape memory properties of UHMWPE reported by Lee and Pienkowski [147].

It was acknowledged at this time that obtaining a wear rate similar to clinical values did not guarantee that similar wear mechanisms were active due to the simplifications introduced by the setup reported by McKellop et al. [137] and Dumbleton [138]. Consequently, researchers began examining articulating surfaces and comparing them to those from retrieved implants in order to evaluate whether the wear mechanisms were similar [137, 142]. Dowson and Harding [139], Dumbleton and Shen [140], Tetreault and Kennedy [141] described, surface evaluations revealed that dry lubrication resulted in melting of the surface, which caused delamination and polyethylene transfer and led to the high wear rates when the product of pressure and velocity limit of the material was exceeded [140, 145, 148]. While water lubrication also displayed polyethylene transfer discussed McKellop [137], Tetreault and Kennedy [141] and Cooper [149], which was not clinically relevant, serum lubrication produced scratches on other wise burnished surfaces similar to those of retrieved implants [137, 148, 150, 151]. Thus, it was established that serum or other protein containing lubrication was required in laboratory tests to facilitate wear mechanisms similar to those in vivo [148-154].

Even after serum lubrication and gravimetric quantification of wear were established, wear factors on simplified testers such as unidirectional pin-on-disk and reciprocating pin-on-flat testers [155] were one to three orders of magnitude smaller than in vivo wear factors in total hip arthroplasty and in total knee arthroplasty due to simplified geometry and testing conditions

[156-159]. The goal of studies employing pin-on-disk testing was to obtain ranking of materials that is free from uncontrolled implant design effects based on their relative wear rates rather than absolute wear rates [137, 138, 151]. For instance, McKellop et al. [160] showed on a reciprocating pin-on-disk tester that both polytetrafluoroethylene (PTFE) and polyester displayed significantly higher wear rates than UHMWPE, which was in agreement with clinical findings. Bragdon et al. [161] compared a multidirectional motion hip simulator with a bi-directional pin-on-disk tester and produced similar wear rates (10 mg/MC compared to 35 mg/MC).These findings, which were clinically relevant, established the importance of multidirectional motion in eliciting wear behaviour similar to in vivo. The importance of multidirectional motion to in vivo wear mechanisms was also evidenced by quasi-elliptical tracks observed in implants from hip and knee joints [162].

2.3.2.1 Friction

Studies of friction in total hip replacements have been carried out utilizing both free and driven pendulum machines. The head and cup of a hip replacement act as the fulcrum of a pendulum within the free pendulum studies, with the desired load affixed to the pendulum. The pendulum swing is initiated from known amplitude, and the decay of the swing monitored. Frictional damping forces occurring between the head and cup resist the motion of the pendulum, causing the decay in swing amplitude and ultimately halting the motion. Charnley [163] determined that a linear decay indicated boundary lubrication, with increasing time to decay indicating improved lubrication. Early studies demonstrated MoP implants had better frictional properties compared with MoM [163, 164]. Friction and wear processes are known to be affected by the surface wettability of the prosthetic materials [110, 165, 166], but definite correlations between wettability and tribological behavior are still to be established. A couple of studies [105, 153, 167, 168] have been reported on the effect of the various components of synovial fluid on friction and wear but different authors attain to distinct conclusions. Nevertheless, there is general agreement that hyaluronic acid (HA) and albumin are the main components for the tribological behavior of the systems when synovial fluid is the lubricant: HA is responsible for the high viscosity and albumin enhances boundary lubrication through adsorption on the joint material surfaces. Recently, Wang et al. [169] and Dowson [170] commented that friction measurement is liable to be particularly valuable in perspective of the growing appreciation of the importance of surface tractions on sub-surface strains and wear mechanisms. The surface traction plays a vital role in the orientation of the polymeric molecules of UHMWPE and

therefore the manner of wear encountered. Current and experimental prostheses are characterized in terms of frictional performance using mainly single axis joint simulators [171-176]. Studies have generally contemplated only current prostheses with reference to relative performance between distinct designs and material combinations. However, latest studies have incorporated explanted prostheses [171, 176] and both the universities of Durham and Leeds are directing frictional studies utilizing experimental soft-layer components comprising polyurethane, as opposed to UHMWPE, as the bearing surface [174, 177-178]. Studies on the frictional behavior of orthopedic material combinations and the effect of other tribological parameters have also been done utilizing wear screening machines [145, 179-187].

2.3.2.2 Lubrication

In lots of cases both short and long term failure of artificial joints is due to wear of the articulating surfaces. Material loss and damage of the surfaces may originate in physical (abrasion or adherence) or chemical (corrosion) mechanisms. These outcome in the formation of micron (for polymer) or nanometer (for metal) sized wear debris which is biologically active and often instigates an adverse cellular response [188-189]. The development of wear-resistant materials, including cross-linked polyethylene described by Wang et al. [190], metal treatment by Varano et al. [191] and ceramics by Essner et al. [192] has been the focus of a lot research over the years reported by Katti et al. [193]. However, the variety of materials available to the implant designer is limited as these must be low wearing, biocompatible; both in bulk and particulate and easy to manufacture to a reliable standard [193].

The other way to improving wear performance is to optimize the lubrication function of the joint, to exploit this we necessitate to know the film formation mechanisms taking place during articulation. Presently there are two general theories; fluid film EHL mechanism [194] and boundary lubrication [195] mechanism. Although these theories are often treated separately it is highly likely, based on the implant operating conditions, both will contribute to lubricant film formation during articulation.

Boundary lubrication dominates under conditions where a fluid film is not formed (by hydrodynamic action); these are generally high loads, low speeds and low fluid viscosity. Gale et al. [196] identified a number of synovial fluid (SF) species as potential boundary lubricants; these include hyaluronic acid (HA), proteins, glycoproteins and phospholipids. HA is a high molecular weight (105-106 Da) linear polysaccharide and in diseased SF the concentration and molecular weight of HA are decreased [197]. HA is thought to contribute to viscoelasticity and

viscosity enhancement presented Swann et al. [198] but to have insignificant boundary lubrication function [199]. Phospholipids are a main component of biological membranes, which form structured mono and multiple layers at interfaces [195]. A major class is the zwitterionic phosphatidylcholines which have a positively charged quaternary ammonium ion (polar head) and adjacent phosphate ion. The positively-charged head group adsorbs at surfaces to form an oligolamellar layer [200] with the long hydrocarbon chains forming a hydrophobic surface.

Other synovial fluid (SF) components have been identified as having boundary lubrication capabilities. In the late 1970s attention turned to lubricin, a highly purified glycoprotein fraction of SF as the primary boundary lubricant of articular cartilage [200, 201]. Analysis of lubricin showed it contains protein and carbohydrate with a small percentage (nearly 12%) of phospholipid. The phospholipid fraction was identified as the primary boundary lubricant in lubricin [296, 201]. The water-soluble glycoprotein component is thought to act as a carrier for the insoluble phospholipid.

Surface analysis of explanted joints from hip simulator and retrieval studies has been reported by Wimmer et al. [202]. In this study surface layer formation on forty-two retrieved MoM hip joints was compared to results from in vitro test specimens. The paper reported evidence of thick carbon-rich deposited layers on over 80% of the components. These films were conventionally within or at the border of the formerly articulating surfaces". They concluded the films were formed by denatured proteins deposited from solution in the high pressure contact regions. It was suggested the proteins acted as a solid lubricant reducing adhesion and abrasion. There is supporting evidence from Wang and co-workers (1998) for this idea; they concluded that the protein layer acts as a "solid" boundary layer which prevents adhesive wear.

Organic reacted or deposited layers also appear to play a role in conditioning the alloy subsurface and thus affecting wear. Recent studies of the CrCoMo alloy published by Pourzal et al. [203, 204] have examined the micro structural changes that arise in the subsurface region of retrieved (resurfacing) and simulator-tested MoM implants. The hip-simulator test samples indicated the formation of a carbon-rich nanocrystalline layer approximately 200nm thick [204]. The formation of this layer through mechanical mixing [205] is reported to be the origin of the excellent wear resistance of the CrCoMo alloy [203].

A couple of studies have analyzed bulk fluid remaining in the simulator test chamber to obtain insights into lubrication mechanism [206]. Bovine calf serum (BCS) solution speedily forms precipitates during the test [190] and must be regularly replaced. In a recent article

Maskiewicz and co-workers [206] examined protein degradation products formed during simulator tests of serum-based lubricants. They reported the formation of "high molecular weight aggregates which precipitated out of solution". There was no proof of protein molecular fragmentation. The main conclusion out of this work was that high shear rates within the articulating interface were responsible for protein agglomeration.

The alternative theory is that MoM hip joints operate in the "fluid-film" regime where the rubbing surfaces are dissevered by Elasto Hydrodynamic lubricant (EHL) film [194, 207, 208]. In EHL the film formation mechanisms are very different to boundary lubrication. Friction is now a result of fluid forces (lubricant rheological properties) and not surface asperity interaction. EHL requires the entrainment of a viscous fluid which combined with the deformation of the surfaces contributes to the development of a separating film. Wear is, now, caused by chemical corrosion or 3rd body abrasion and not mechanical wear mechanisms between the main contacting bodies. For simple hydrocarbon oils the film thickness can be exactly predicted for different load and speed conditions and this has been verified by numerous experimental studies utilizing optical interferometry [209].

For predictive purposes, an artificial neural network (ANN) approach has, therefore, been introduced recently in the field of wear of polymers and composites by Velten et al. [210] and Zhang et al. [211]. An ANN is a computational modeling tool and found agreement in the field of bio-tribology for modeling real-world problems. It is an advanced simulation technique that comprises database training to predict response precisely from a set of inputs. This technique is an iterative process and used to solve complex, non-linear problems because it is able to emulate the learning ability of human beings. This means the ANN learns directly from the examples, it is not needed for it to know the theory (nature of the problem) behind a phenomenon. The main benefit of the ANN methodology over conventional regression analysis is that the network makes a solution without the need to designate the associations between variables. Artificial neural network is basically constructed of numerous cross-linked simple processing units called neurons. Neuron collects numerous input signals but it delivers only one output signal at a time. The basic architecture of network normally composed of three types of neurons layers connected in series: input, hidden and output layer. The input and output layer in the network are fixed and equal to that of input and output variables whereas, hidden layer can include more than one layer and in each layer the number of neurons is flexible. ANN modelling in the field of tribology has been examined by various authors [211-214]. Arun Rout and Alok Satapathy [215] reported an

ANN model for understanding to predict the influence of rice husk on wear resistance potential of epoxy resin. The ANNs are also employed in material science and tool condition monitoring for the machining of conventional engineering materials. ANN can frequently solve various problems quicker compared to other techniques with the additional ability to learn. Many researchers were used ANNs to predict the mechanical, tribological and the physical properties of metal matrix composites also [216-218]. The prediction of sliding friction and wear properties of polymer composites was investigated by means of pin-on-disc sliding wear tests of polyphenylene sulphide matrix composites using ANN was reported by Lada et al. [219]. Altinkok and Koker [220] studied the prediction of mechanical properties in composites with the help of ANN. The use of neural network to predict the tribological examination of diverse material/mechanical systems was done by Jones et al. [211]. Prediction of wear behavior of A356/SiCp MMCs using ANN was examined by Rashed and Mahmoud [221]. Velten et al. [210] examined the potential of Artificial Neural Network to predict and analyze the wear performance of short fiber reinforced polymeric materials for bearing application.

2.4 On the basis of Corrosion and biocompatibility

To work prosperously, it is vital for metallic biomaterials to have satisfactory corrosion resistance against the antagonistic environment of the human body [31, 222]. Though corrosion accounts for the destructive assault of a metal by chemical or electrochemical reaction with its surroundings, there are infrequent, but scarce component failures [47, 223]. If and when metallic implants fail because of corrosion, immense concentrations of corrosion products are liberated in the body and respond to the tissue fluids, dissolved gases, inorganic, and organic ions [31]. The corrosion assessments of implant materials might be completed both in highly corrosive media, for example, 3.5% (w/w) or 0.9% (w/w) NaCl, 0.1 M HCl or 0.1 M H_2SO_4 and in media simulating biological electrolytes such as Ringer [224, 225], Hank [226, 227] and Tyrode [228] solutions or artificial saliva [229] at the body temperature of 37^0C as specified in ASTM F 2129. Clark and Williams [224] completed corrosion tests of miscellaneous implant materials in serum albumin and fibrinogen containing electrolytes, representing biological media and found that the corrosion of aluminum and titanium were not influenced by such media, while there was a slight increment in the corrosion of chromium and nickel and a significant increment in the corrosion of copper and cobalt. They also noticed that the corrosion of molybdenum was considerably repressed. In another study, Williams et al. [225] expressed that the incorporation of protein to the test solution improved the corrosion rate of stainless steel, but caused no adjustment in the

corrosion rate of Ti6Al4V. The fretting corrosion of stainless steel was observed to diminish in the protein containing medium and there was no adjustment in the corrosion of pure Titanium and its alloys. Hsu et al. [230] examined the corrosion behaviour of Ti6Al4V using phosphate buffered salt (PBS) at different pH values and temperatures.

The main corrosion mechanism of CoCrMo alloys in the body fluids is passive dissolution. In vitro [231, 232] and in vivo [233, 234] tests affirm the metal liberate from the CoCrMo alloys through that corrosion mechanism. Hanawa [235] reported the distinctive variety of phenomena as a result of metal particles release takes place in the human body, for example, transportation, metabolism, and accumulation in organs, allergy and carcinoma. These effects can be generally most harmful for human health, chiefly in the case of the CoCrMo where the alloying elements Chromium and Cobalt produce a high risk of carcinogenicity. Although the definitive effects of these metal ions have not been determined, toxicity and metallalergy are the most noteworthy concerns. For instance, it has been demonstrated that Cr^{3+} and Co^{+2} have a toxicity effect on osteoblasy and incited cell mortality reported by Fleury et al. [236]. Consequently, there is still a need of basic comprehension of the electrochemical behavior of CoCrMo alloys so as to improve their corrosion resistance and minimize the metal ion releases in the human body.

Biocompatibility is a word extensively utilized as a part of biomaterial science, but there still exist a lot of uncertainty about what it really implies and about the mechanism that are subsumed within the phenomenon that collectively constitute biocompatibility [223]. Bumgardner et al. [237] described, the materials utilized in devices must be harmless in addition to effective. It is important to realize that (i) none material will be felicitous for all medical device applications (ii) the material, its composition and degradation product may affect host cells and tissues; and (iii) the host environment may also affect material properties and device performances. Biocompatibility is defined as the capacity of a material to perform with a suitable host response in a particular situation [1]. The way to understanding biocompatibility is in the determination of which chemical, biochemical, physiological, physical or other mechanisms becomes operative, under the highly specific conditions connected with contact between biomaterials and tissues of the body, and what are the consequences of these interactions.

The assessment of biological responses to a medical device is made to determine that the medical device executes as proposed and presents no significant harm to the patient or user. This assessment is to predict whether a biomaterial, medical device, or prosthesis presents potential

harm to the patient or user by assessing conditions that simulate clinical use [122]. The determination of biocompatibility of materials and implant devices involves detailed characterization of the material and extensive testing, first at the cell/tissue level and then in in-vivo animal models and ultimately in human clinical trials. The design and utilize of biocompatibility testing protocols is provided by a variety of professional and regulatory organizations, including ASTM, ISO, ADA, NIH and FDA. The methods and evaluation criteria for determining biocompatibility are regularly reviewed and amended as additional information is accumulated.

2.5 On implementation of DOE and optimization techniques

Wear processes in alloys are complex phenomena including a set of operating variables and it is important to comprehend how the wear attributes of the alloys are influenced by various operating conditions. Although a countless researchers have reported on properties, performance and on wear characteristics of alloys, neither the optimization of wear processes nor the influence of process parameters on wear rate has adequately been studied yet. Selecting the accurate operating conditions is always a vital concern as traditional experimental design would necessitate many experimental trials to achieve acceptable results. In any process, the desired testing parameters are either decided in view of experience or by utilization of a handbook. It, however, does not provide optimal testing parameters for a specific condition. In this manner, numerous mathematical models based on statistical regression techniques have been built to choose the best possible testing conditions. The numbers of trials required for full factorial design increase geometrically, whereas fractional factorial design is effective and importantly decreases the time. This method is well known due to its simplicity; however, this very effortlessness has prompted unreliable results and insufficient conclusions. The fractional design might not contain the finest design point. Moreover, the conventional multi-factorial experimental design is the "change-one-factor-at-a-time" technique. Under this method one and only factor is varied, while the various variables are kept fixed at a particular arrangement of conditions. To conquer these problems, Taguchi and Konishi [238] supported the utilization of orthogonal arrays and Taguchi [239] formulated another experiment design that applied signal-to-noise ratio with orthogonal arrays of the powerful plan of items and procedures. In this technique, the impact of a variable is measured by average results and accordingly, the trial results can be reproducible. Phadke [240], Wu and Moore [241] and other researchers [242–245] have subsequently applied the Taguchi method to design the products and process parameters.

This is a power full tool of Design of experiment and it works on orthogonal array. Data acquiring through Taguchi technique was in a systematic way to understand the effect of operating parameters on output response parameters, which was an unknown function of these operating variables. The vital stage in the process is selection of factors which have effects on the sliding wear process. An orthogonal array was formed by using Taguchi techniques to consider the influence of various factors on the target value and defines the plan of experiments.

Taguchi experimental design is utilized in different fields for, example, environment sciences, agriculture sciences, management and business, engineering, physics, chemistry, statistics and medicine [246]. Some researchers utilized Taguchi experimental design technique for the optimization of process parameters includes in mechanical behavior, fabrication and machining processes [247-252]. The Thong and Shahidan [253] worked on the optimization of cutting parameters such as cutting speed, feed rate, and depth of cut under flooded coolant condition in turning process using Taguchi method for Nickel-based alloy. They reported that the feed rate is most significant parameter, spindle speed is significant and depth of cut is least significant parameter in effecting surface roughness. Fei et al. [254] had done a review on the practical utilizations of Taguchi method for optimization of processing parameters for plastic injection moulding process. Basavarajappa and Chandramohan [255] utilized Taguchi method to study the effect of operating parameters on the wear rate and also found that the sliding distance was the parameter which has highest physical and statistical significance on the wear rate. Uysal et al. [252] utilized the Taguchi method and ANOVA to get the optimal cutting parameter and to study the influence of parameters on tool wear. Bagci and Aykut [256] utilized Taguchi methodology to examine the optimum surface roughness in CNC face milling of Co-based alloy.

2.6 On the basis of multi criteria decision making (MCDM) method

Basically, MCDM is a sub-branch of operations research that deals with decision problems containing a numbers of alternatives and criteria's [257]. MCDM can be defined as the compilation of procedures for the comparison, ranking and selecting numerous alternatives having diverse attributes [258]. MCDM is like a process of making decisions when there is having several conflicting criteria. An MCDM method ranks the doable alternatives and the highest ranked one is recommended as the best choice. There are numerous MCDM methods such as: AHP (Analytic Hierarchy Process), TOPSIS (Technique for Order Preference by Similarity to Ideal Solution), GRA (Grey Relation Analysis), VIKOR (Vise

Kriterijumska Optimizacija Kompromisno Resenje), PSI (Preference Selection Index), ELECTRE (Elimination and Choice Translating Reality), PROMETHEE (Preference Ranking Organization Method for Enrichment Evaluations), ROVM (Range of value method) etc. have been proposed to help in selecting the best compromise alternatives. Various MCDM methods have been applied to a number of applications by many researchers to solve the problem of suitable material selection.

Wang and Chang [259] proposed a fuzzy MCDM approach to assist selecting the best suited tool steel material for a manufacturing application, such as jig and fixture design. Tretheway et al. [260] developed a structure for materials selection based on material performance and failure analysis. Jee and Kang [261] applied the TOPSIS method to rank the alternative materials with, entropy method to evaluate the weight factor for each material property. Sapuan [262] build a knowledge-based system (KBS) in the selection of best suited polymeric-based composite materials. Bahraminasab and Jahan [263] used comprehensive VIKOR approach to rank the material for femoral component of knee joint replacement. Ermatita et al. [264] utilized ELECTRE method to identify gene mutations that can cause cancer. Rouyendegh and Erkan [265] used fuzzy ELECTRE approach for the selection of academic staff. Mazumder [266] utilized the ELECTRE method for decision making in manufacturing atmosphere. They implemented this method for material selection, robot selection, flexible manufacturing system selection, rapid prototyping process selection, material handling equipment selection and automated inspection device selection.

Smith et al. [267] implemented the AHP approach in selection of the bridge material for different states in india. Sapuan et al. [268] utilized AHP method to find out the most appropriate natural fiber composites for automotive application such as dashboard panel and found that the kenaf polypropylene composites is the best choice for this application. Shanian and Savadogo [269] evaluated some of MCDMs for solving a material selection problem of highly sensitive components involving conflicting and multiple design objectives. Athawale et al. [270] utilized the utility additive method (UAM) for solving the problems of material selection. Rathod and Kanzaria [271] implemented two MCDMs, such as TOPSIS and fuzzy TOPSIS to identify the best suited of phase change material in solar domestic hot water system. Chatterjee et al. [272] used COPRAS (complex proportional assessment) and EVAMIX (evaluation of mixed data) methods for selection of the most suitable materials for two industrial applications. Maniya and Bhatt [273] observed three different material selection problems using PSI (preference selection

index) method, and validated the ranking results with those obtained from GTMA and TOPSIS method. Jahan et al. [274] examined the quantitative procedures that had been developed to solve the material selection problems for various engineering components.

Gervasio and Silva [275] projected a probabilistic hybrid method between the AHP and PROMETHEE techniques to assess the life-cycle sustainability of three different bridge types. Jahan and Bahraminasab [276] used MCDA approach to selecting the best suited design made by functionally graded material of Co-Cr femoral component. Chen et al. [277] and Zhi-hong [278] utilized entropy method for determination of weight of evaluating factors for ground water and quality assessment of a river. The results are found more precise after implementation of entropy weight of each criterion and responses were more subjectivity of expert evaluation.

It is understood from above literature that optimization technique utilization for optimize process parameters is necessary and influence of these parameters affect the responses. In multi-criteria decision making situation, optimal solution is formulated by optimization techniques.

2.7 The Knowledge Gap in Earlier Investigations

The extensive literature survey presented above reveals the following knowledge gap in the research reported so far:

1. Though much work has been reported on various wear characteristics of polymer, composites, metals, alloys and homogeneous materials, comparatively less has been reported on the sliding wear performance of unfilled/particulate filled metal alloy and in fact no study has been found particularly on addition of filler as metal in the based metal.

2. Study on mechanical characterization of particulate filled metal based alloy is scarcely reported in literature

3. Study on surface morphology of friction-wear mechanism behavior of particulates filled metal based alloy with the combination of SEM and AFM is very rare.

4. Studies carried out worldwide on sliding behavior of alloys have largely been experimental and utilize of statistical techniques in analyzing wear characteristics is infrequent.

5. Taguchi method, in spite of being a simple, efficient and systematic approach to optimize designs for performance, quality and cost, is used only in a limited number of applications worldwide. Its implementation in parametric appraisal of wear processes has hardly been reported.

6. ENTROPY-PROMETHEE method is a proficient tool for solving many multi criteria decision making (MCDM) problems. However, it is hardly been utilized for selection of materials for femoral head of hip joint replacement.

2.8 Objectives of the Present Work

The knowledge gap in the existing literature summarized above has helped to set the objectives of this research work which are outlined as follows:

1. Developing a high strength metal alloy composite for femoral head of prosthesis replacement.

2. Determination of physic-mechanical properties such as density, compressive strength and micro-hardness test of particulate filled metal alloy composites in experimentally.

3. Characterization of surface morphology of friction-wear mechanism with SEM & AFM, and to correlate the tribo-performance of the surface layers on worn surfaces of designed alloy.

4. Parametric appraisal of sliding wear process of unfilled/particulate filled alloy composite and optimization.

5. Prediction of wear volume using artificial neural networks (ANN) and comparison with experimental results.

6. Evaluation the corrosion and biocompatibility performance of designed alloy composites in experimentally.

7. Finally, the optimal performance analysis of particulate filled metal alloy composite for analysis of physical, mechanical, wear volume and friction coefficient analysis of the said fabricated composites using ENTROPY-PROMETHEE method.

Chapter summary

This chapter was all about the different consideration that has been taken for the research purpose. The various aspects of metal and metal alloy composites reported as:

— The knowledge gap in past research.

— The objective of the present work.

The next chapter discusses the materials and methods used for the fabrication of the alloy composites, the experimental planning, the Taguchi DOE method, neural computations, and corrosion and biocompatibility analysis. Finally, it also presents the PROMETHEE multi-criteria-decision-making approach for formulation ranking.

*****

Introduction

Raw materials are the starting point for development of new materials and quality of new material itself is dependent upon the raw materials. Then the next step is the role of different processing techniques to fabricate the new materials and their physical and mechanical characterizations to ensure the quality of the materials. This chapter describes the materials and methods used for the processing of all the biomedical alloy composites under this investigation. It presents the details of the physical and mechanical characterizations, sliding wear behavior, corrosion analysis and biocompatibility test which the alloy composite samples are subjected to. It also reviews additional techniques used for the present investigation such as micro-indentation, as well as the post-test analysis methods involving various microscopic techniques such as scanning electron microscopy (SEM) attached with EDS, X-ray diffraction (XRD) and atomic force microscopy (AFM). The methodology related to the design of experiment technique based on Taguchi method and the statistical analyses inspired by artificial neural network and in order to obtain the optimal ranking of the formulations based on their physical, mechanical and sliding wear properties ENTROPY-PROMETHEE (Preference Ranking Organization Method for Enrichment Evaluations) MCDM (Multi Criteria Decision Making) technique also presented in this part of the thesis.

3.1 Matrix Material

3.1.1 The formulation design of metal alloy composites

The formulation design of the metal alloy composite materials for hip implant was carried out on the basis of three classes of ingredients viz., fillers (i.e. Molybdenum, Nickel and Tungsten) with varying percentages by weight. Three types of formulation design for the alloy composites viz. Type-1 (A-Series), Type-2 (B-Series) and Type-3 (C-Series) were carried out. Type-1 represents the A-Series metal alloy composites based on the variation of molybdenum filled particulate, Type-2 represents the B-Series metal alloy composites based on the variation of nickel filled particulate and Type-3 represents the C-Series metal alloy composites based on the variation of tungsten filled particulate in cobalt-chromium as a base metal. The chemical compositions of 'A' series, 'B' Series and 'C' Series alloy composite are shown in Tables 3.1, 3.2 and 3.3

---

respectively. Table 3.4 shows the chemical composition of final alloy composites of femoral head material for orthopedic hip implant.

Table 3.1 Formulation design of A-Series alloy composites

Elements	Designation				
	A0	A1	A2	A3	A4
Cobalt (Co)	Bal	Bal	Bal	Bal	Bal
Chromium (Cr)	30%	30%	30%	30%	30%
Molybdenum (Mo)	0%	1%	2%	3%	4%

Table 3.2 Formulation design of B-Series alloy composites

Elements	Designation				
	B0	B1	B2	B3	B4
Cobalt (Co)	Bal	Bal	Bal	Bal	Bal
Chromium (Cr)	30%	30%	30%	30%	30%
Molybdenum (Mo)	4%	4%	4%	4%	4%
Nickel (Ni)	0%	1%	2%	3%	4%

Table 3.3 Formulation design of C-Series alloy composites

Elements	Designation				
	C0	C1	C2	C3	C4
Cobalt (Co)	Bal	Bal	Bal	Bal	Bal
Chromium (Cr)	30%	30%	30%	30%	30%
Molybdenum (Mo)	4%	4%	4%	4%	4%
Nickel (Ni)	1%	1%	1%	1%	1%
Tungsten (W)	0%	1%	2%	3%	4%

Table 3.4 Final Formulation design of alloy composites

Elements	Designation				
	D0	D1	D2	D3	D4
Cobalt (Co)	Bal	Bal	Bal	Bal	Bal
Chromium (Cr)	30%	30%	30%	30%	30%
Molybdenum (Mo)	4%	4%	4%	4%	4%
Nickel (Ni)	1%	1%	1%	1%	1%
Tungsten (W)	2%	2%	2%	2%	2%

3.2 Fabrication of metal alloy composites

In the presented work, rectangular plates (100×65×10mm) with varying weight percentage of molybdenum, nickel and tungsten particulate (less than 44 microns) filled alloy composites were fabricated using the casting method and were manufactured using the facilities of our laboratory (i.e. Centre for Tribology, MNIT, Jaipur, India). For this purpose, the metals (i.e. Co, Cr, Mo, Ni and W) were melted by induction furnace shown in Figure 3.1.

(a)   (b)
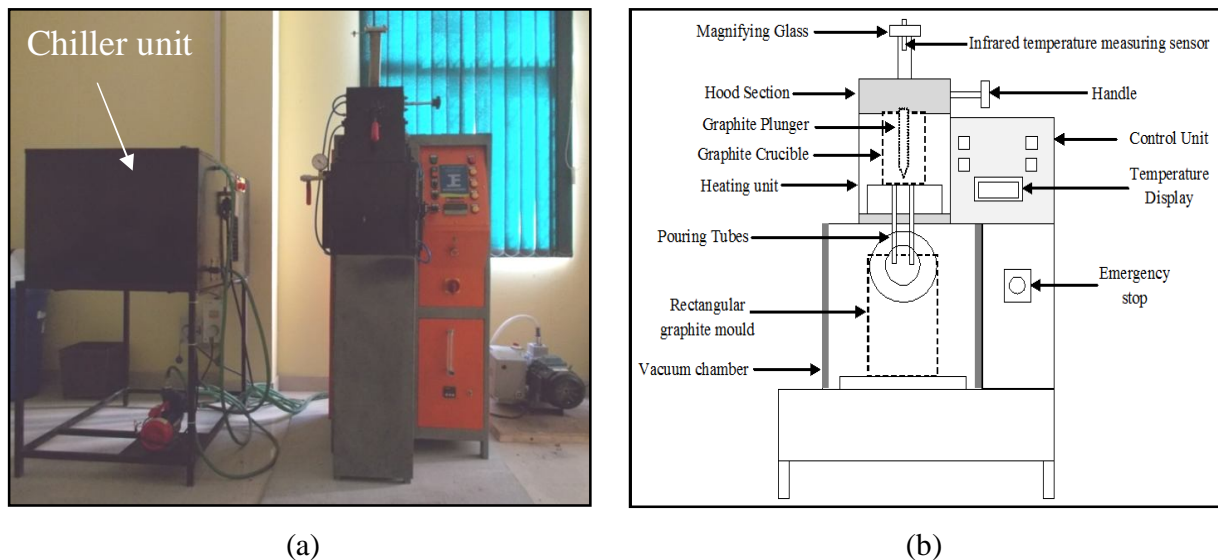
Figure 3.1: Experimental setup of casting machine, (a) Image of the casting setup (b) Schematic diagram of the casting machine

In this furnace respective weight percentages of all the proposed materials according to 'A', 'B' and 'C' series metal alloy composites formulation are melted above 1800 ºC for 15mins and then poured into the rectangular graphite mold in vacuum conditions. There are two separate chambers are available specifically in the high temperature vacuum centrifugal casting machine. One is the melting unit and just below the melting chamber one more chamber is the casting section. Here both the chambers are under vacuum environment attach with chiller unit. The lower chamber is coupled with motor for function of vertical centrifugal casting while pouring the molten alloy. In this analysis the rotational speed is maintained around 200rpm for homogeneous mixing of all the metals present in the matrix. After casting the rectangular mold is removed from the vacuum chamber and the samples were then sized as per the sample size and the surface is grounded/polished by semi automatic Buehler MetaServ 250 polisher/grinder (see Figure 3.2) and then samples were cleaned in ethanol with an ultrasonic cleaner and dried with a

commercially available blower. After that the prepared samples were electrolytically etched with 100ml ethanol and 20ml 1.0M HCl mixed with copper (II) chloride ($CuCl_2$) for 10sec for examining the various characterization like physical, mechanical, wear behavior and surface morphology.

Figure 3.2: Semi automatic Grinder/polisher

3.3 Mechanical characterization

3.3.1 *Micro-hardness*

Micro-hardness measurement is done using a USL Vickers micro-hardness tester (see Figure 3.3) equipped with a square based pyramidal (angle 136° between opposite faces) diamond indenter by applying a load of 0.5N for 15s. The micro-hardness is measured at six different locations and after measuring the micro-hardness of the entire identified region, the mean micro-hardness is taken in this study. All measurements are carried out as per ASTM E-92 [279] standard.

Figure 3.3: Micro hardness testing machine   **Figure 3.4:** Compression testing machine

3.3.2 *Compressive strength*

Compressive test is done as per ASTM E9-09 [280] standard using AIMIL compression testing machine (see Figure 3.4) on the fabricated composite specimens. The test is carried out with the specimen dimension of 25×10×10mm at a crosshead speed of 2mm/min. The sample is fixed between the discs and force is applied from the top disc of the specimen.

3.4 Scanning electron microscopy (SEM)

The worn out surfaces after wear testing are examined directly via FEI NOVA NANO 450 scanning electron microscope operating at 15 KV as shown in Figure 3.5. This machine is attached with energy dispersive X-ray (EDAX) to identified the different chemical composition of materials under FE-SEM. The samples are mounted on stubs and analyze the associated wear features such as scars, continuous and parallel groves, micro ploughing effect, micro cracks etc.

3.5 X-Ray diffraction studies

The fabricated alloy composites are examined for the identification of the (crystalline) phases with a Panalytical X Pert Pro X-ray diffractometer (XRD) with monochromatic Cu-K (alpha) radiation (see Figure 3.6) over 20º≤ 2θ ≤ 120. X'Pert High Score software and the PCPDF data bank was used to carried out the pattern analysis of the samples.
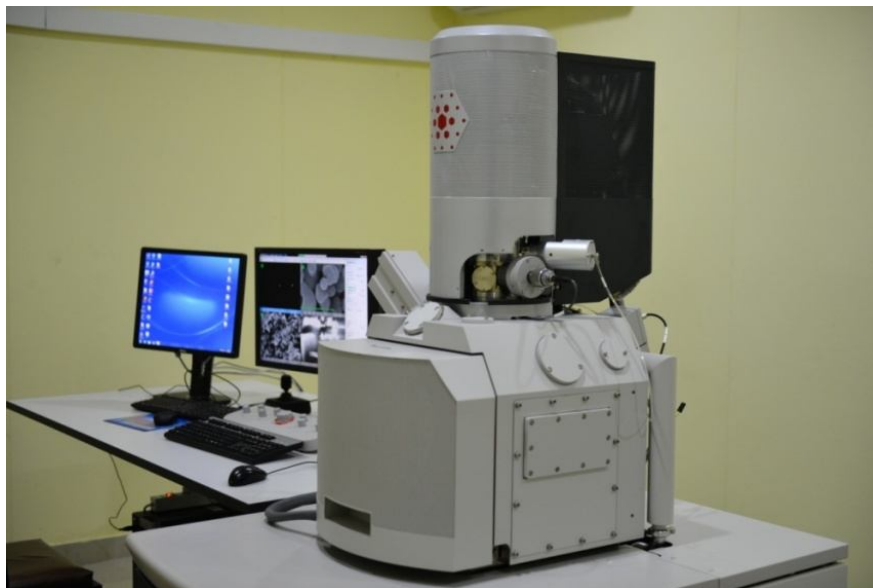
Figure 3.5: Scanning Electron Microscope along with EDAX

Figure 3.6: X-ray diffractometer

3.6 Tribometer

A pin-on-disk tribometer (CSM Instruments) confirming to ASTM G 99 as shown in Figure 3.7 was used for carried out the tribology tests. As the name 'tribometer' suggests, 'tribos' meaning rubbing and 'meter' meaning measurement, is an instrument which is used to measure the friction and sliding wear of different materials. The tribometer runs under stationary conditions with constant applied normal forces of up to 60 N and at constant rotational speeds of up to 2000 rpm. A load cell is used to measure the tangential force acting on the pin. The counter body is a disc made of hardened alloy steel (EN-31) with 60–70 rockwell hardness (HRC) and surface roughness of 1.6mm. The pin (see Figure 3.8b) is held stationary against the rotating disc and the normal force is applied through a lever mechanism as shown in Figure 3.8a. The normal contact load (F_n) on the pin was varying from 5N to 25N, corresponding to the sliding velocity of the disc varying from 0.26 to 1.3m/s. The wear track was 50mm in diameter is used for all test under dry and wet conditions respectively. After each experimental run, every sample is cleaned with cotton dipped in acetone and dried with a hot air blower for 2 min. Thereafter, a precision electronic balance with accuracy ±0.1 mg is used to find the material loss from the fabricated alloy composite surface during sliding test and the wear is then calculated as volumetric wear loss (mm^3):

$$Volumetric\ wear\ loss = \Delta m/\rho_n \tag{3.1}$$
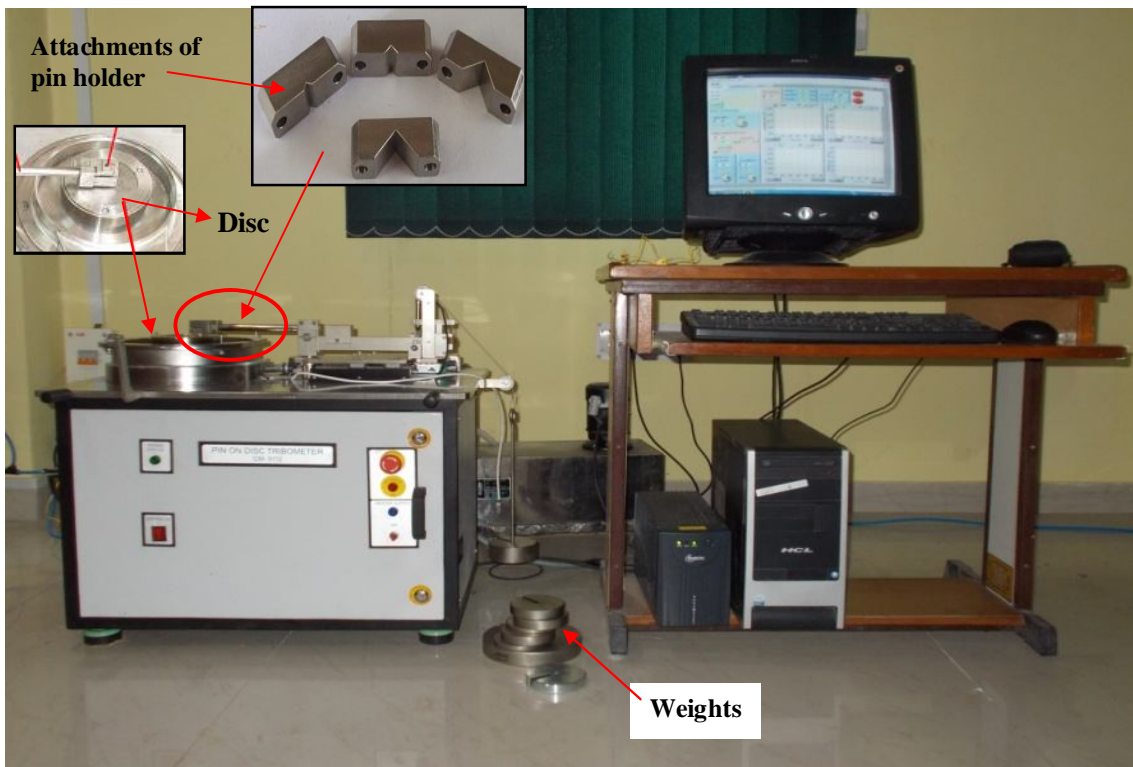
Figure 3.7: Pin on Disc Tribometer
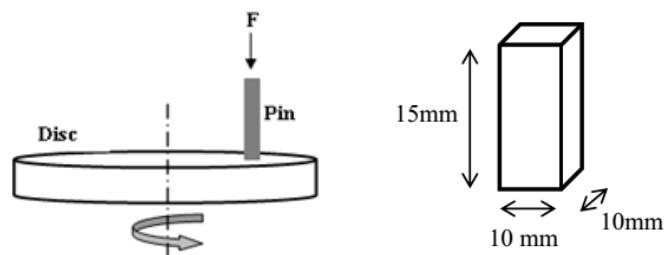
Figure 3.8: (a) Arrangement of disc and pin; (b) Pin sample

Where, Δm is the mass loss in the test duration (g), ρ is the density of the fabricated alloy composite (g/mm^3). The friction coefficient was incessantly recorded WINDCOM 2007 software during each test run.

3.7 Atomic force microscopy

Contact mode NANO SCOPE V SYSTEM (Surface Imaging Systems, Bruker, CA USA) equipped with a 125µm×125µm×5µm XYZ scanner (see Figure 3.9) and an optical microscope was used to characterize the surface topography and roughness of the sample surfaces, and to obtain initial arithmetic mean surface roughness values (Ra).
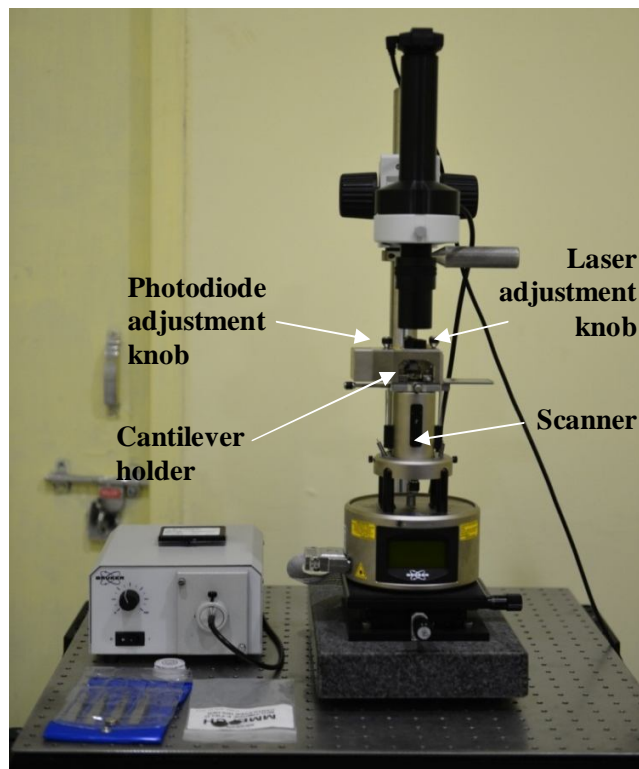
Figure 3.9: Atomic force microscopy

The initial mean Ra values for all materials were calculated from three measurements from three different areas on the surface. All 3D images are recorded at room temperature. The AFM was positioned on an active vibration isolation table (Newport, vision Isostation, USA) to eliminate external noise.

3.8 Corrosion Analysis

Traditional corrosion test methods include weight loss measurements, electrochemical test methods including potentiodynamic and impedance measurements. Electrochemical test methods are familiar as they are completed in a short period of time. GAMRY potentiostat VFP600 (see Figure 3.10) instrument was utilized for conducting electrochemical tests by accelerating corrosion with appropriate current and voltages. This instrument is allied to a PC and accessed with the assistance of Gamry Framework software as shown in Figure 3.11. A potentiostat with corrosion software (Echem Analyst) was used for electrochemical control and data analysis. The corrosion current density (i_{corr}) and corrosion parameters, such as anodic and cathodic Tafel slopes (b_a and $-b_c$), were calculated from the polarization curves by Tafel extrapolation. Saline solution was prepared using 8g/L NaCl, pH 7.4 at body temperature 37ºC.
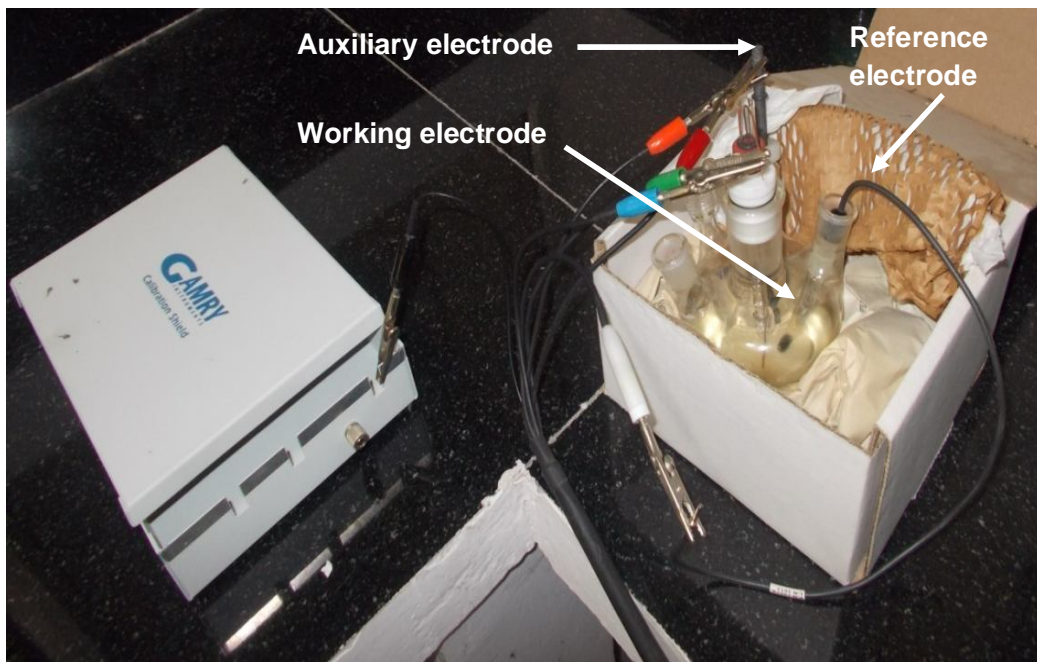
Figure 3.10: Photograph of the three-electrode system.
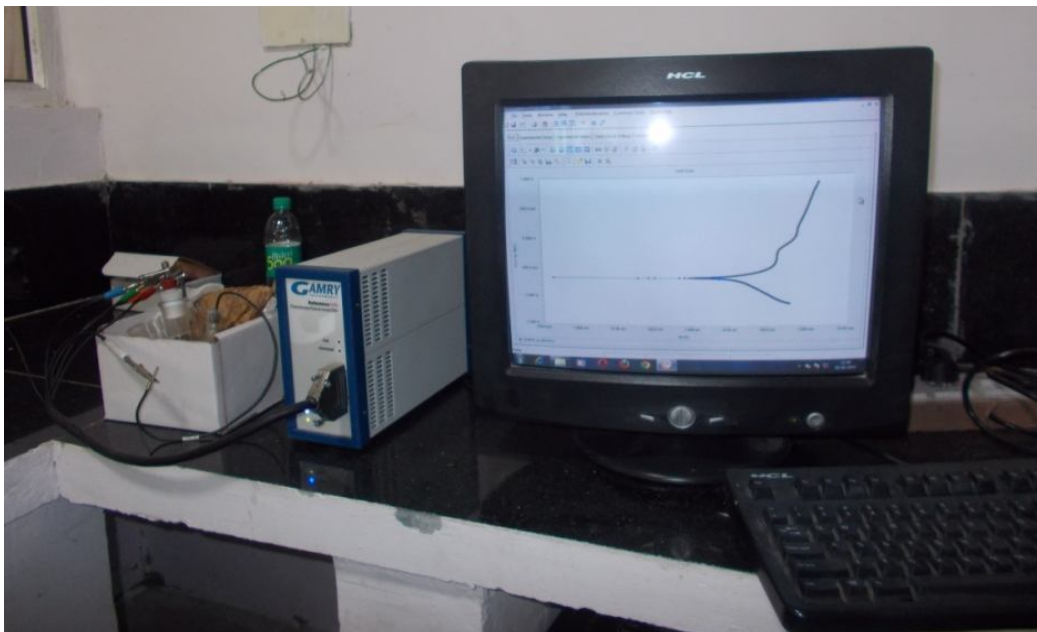
Figure 3.11: Corrosion analysis setup

The volume of the cell was 100 ml. The anodic polarization curve for the Tafel analysis was measured from −150 to +150mV versus E_{corr} with a scanning rate of 1mV/s after immersing in electrolyte about 30min. The potentiodynamic curves were obtained at a constant voltage scan rate of 10mV/s. The specimen area exposed was 8cm^2 with scan frequencies ranging from -1 to 1 V. Electrochemical tests were conducted in a corrosion cell by using three electrodes, one is

working electrode which is the coated or uncoated sample whose degradation property has to be tested, the second electrode is graphite, and the third electrode used is Saturated Calomel Electrode (SCE) which senses the reaction happening within the corrosion cell and inputs the values to the software where necessary data is shown in the form of graphs.

3.9 Biocompatibility Test

To assess, as a first approach, the biocompatibility of fabricated alloy composites with variation of fillers such as molybdenum, nickel and tungsten particulates, histological tests in subcutaneous tissue in three rats were performed according to the International Standard ISO 10993-1 [281]. The rats were implanted circular alloys (i.e. Co30Cr4Mo, Co30Cr4Mo1Ni and Co30Cr4Mo2W) plates (3mm diameter, and 1mm thickness) between the subcutaneous tissue and muscular fascia in the backs of three adult male rats. Prophylactic antibiotics were given to the rats, and the skin was sutured with resorbable material. After 6 weeks of implantation the animals sacrificed by cervical dislocation. The skin tissue samples were excised and fixed in 10% buffered formalin. After proper fixation pieces of tissues samples were processed by dehydration in graded series of alcohol and toluene in tissue processor (Leica TP 1020) as shown in Figure 3.12.

Figure 3.12: Tissue processor

The processed tissues were embedded in paraffin wax (Leica). Multiple sections of 4-5 µm thickness from each block were cut on rotatory microtome (Microm, Germany), mounted on coated slide and air dried overnight. The sections were deparaffinised and stained with

hematoxylin and eosin (McMannus and Mowry, 1965) [316] in auto-stainer (Leica, Germany) and cover slipped using auto cover slipper (Leica, Germany). After drying sections were photographed in light microscope (Leica, DMLB) using DCM 500 camera at 20X magnification (Leica, Germany).

3.10 Process optimization and Taguchi method

Statistical methods are commonly used to improve the quality of a product or process. Such methods enable the user to define and study the effect of every single condition possible in an experiment where numerous factors are involved. Wear processes such as sliding is such processes in which a number of control factors collectively determine the performance output i.e. the wear volume. Hence, in the present work a statistical technique called Taguchi method is used to optimize the process parameters leading to minimum sliding wear of the designed alloys under study. This part of the chapter presents the Taguchi experimental design methodology in detail.

Table 3.5 Parameter settings for sliding wear test.

Control Factors	Symbols	Fixed parameters	
Normal load	Factor A	Disc	EN-31 (hardened alloy steel)
Sliding velocity	Factor B	Test temperature	Room Temperature
Sliding distance	Factor C	Running Time	10 min
Filler content	Factor D	Wear track diameter	50 mm

3.10.1 Taguchi Experimental Design

Taguchi design of experiment is a powerful analysis approach for exploring the influence of control factors on output performance [282]. It is commonly adopted approach for optimizing design parameters because of its simple, efficient, and systematic. The method is originally proposed as a means of improving the quality of products through the application of statistical and engineering concepts, since experimental procedures are usually complex, costly, time consuming, and difficult to perform real experiments with entire accuracy. Therefore, the need to satisfy the design objectives with the least number of experiments is evidently a vital requirement. The most important stage in the design of experiment lies in the selection of the control factors. Therefore, a large number of factors are initially included so that non-significant variables can be identified at earliest opportunity. Exhaustive literature review on sliding wear behavior of metallic alloys reveal that parameters viz., normal load, sliding velocity, sliding

distance and filler content etc largely influence the wear rate of metallic alloys [283, 284]. In the present work, the impact of four such parameters are studied using L_{25} (5^6) orthogonal design. The operating conditions under which wear tests are carried out are given in Table 3.6. The tests are conducted at room temperature as per Taguchi experimental design by the use of MINITAB 16 software given in Table 3.6. Four parameters viz., normal load, sliding velocity, sliding distance and filler content, each at three levels, are considered in this study. In Table 3.7, each column represents a test parameter and a row gives a test condition which is nothing but combination of parameter levels. In conventional full factorial experiment design, it would require $5^4 = 625$ runs to study four parameters each at five levels, whereas Taguchi's factorial experiment approach reduces the same to 25 runs only, thereby offering a great advantage in terms of experimental time and cost.

Table 3.6 Levels of the variables used in the experiment

Control factor	Level					Units
	I	II	III	IV	V	
A: Normal Load	5	10	15	20	25	N
B: Sliding Velocity	0.26	0.52	0.78	1.04	1.30	m/s
C: Sliding distance	500	1000	1500	2000	2500	m
D: Filler Content	0	1	2	3	4	wt.%

This method achieves the integration of design of experiments (DOE) with the parametric optimization of the process yielding the desired results. The orthogonal array requires a set of well-balanced experiments. Taguchi's method uses a statistical measure of performance called signal-to-noise ratio (S/N), which is logarithmic function of desired output to serve as objective functions for optimization. The S/N ratio considers both the mean and the variability into account. It is defined as the ratio of the mean (signal) to the standard deviation (noise). The ratio depends on the quality characteristics of the product/process to be optimized. The three categories of S/N ratios are used: lower-the-better (LB), higher-the-better (HB) and nominal-the best (NB). The experimental observations are transformed into a signal-to-noise (S/N) ratio. The S/N ratio for minimum wear volume coming under smaller is better characteristic, which can be calculated as logarithmic transformation of the loss function as shown below.

$$(\eta) = -10 \, log \left[\frac{1}{n}\Sigma_{i=1}^{n} \, y_i^2\right] \qquad (3.2)$$

Where n is the number of tests and y_i is the value of experimental result (i.e. sliding wear volume) of the *i*th test. To obtain optimal performance, smaller-the-better characteristic for sliding wear must be taken [285].

The plan of the experiments is as follows: the first column is assigned to load (A), the second column to sliding velocity (B), the third column to sliding distance (C) and the forth column to filler content (D). The response to be studied is wear volume in both dry and wet conditions and the runs are repeated with three times corresponding to 150 runs and reported the mean value to allow the analysis of variance of the results.

Table 3.7 Taguchi L_{25} (5^6) orthogonal array design

Runs	Normal Load (N)	Sliding velocity (m/s)	Sliding distance (m)	Filler Content (wt.%)
1	5	50	500	0
2	5	100	1000	1
3	5	150	1500	2
4	5	200	2000	3
5	5	250	2500	4
6	10	50	1000	2
7	10	100	1500	3
8	10	150	2000	4
9	10	200	2500	0
10	10	250	500	1
11	15	50	1500	4
12	15	100	2000	0
13	15	150	2500	1
14	15	200	500	2
15	15	250	1000	3
16	20	50	2000	1
17	20	100	2500	2
18	20	150	500	3
19	20	200	1000	4
20	20	250	1500	0
21	25	50	2500	3
22	25	100	500	4
23	25	150	1000	0
24	25	200	1500	1
25	25	250	2000	2

3.11 Artificial neural network

Artificial neural network (ANN) is an advanced simulation technique that comprises database training to predict response precisely from a set of inputs. This technique is an iterative process

and used to solve complex, non-linear problems because it is able to emulate the learning ability of human beings. This means the ANN learns directly from the examples, it is not needed for it to know the theory (nature of the problem) behind a phenomenon. The main benefit of the ANN methodology over conventional regression analysis is that the network makes a solution without the need to designate the associations between variables. Artificial neural network is basically constructed of numerous cross-linked simple processing units called neurons. Neuron collects numerous input signals but it delivers only one output signal at a time. The basic architecture of network normally composed of three types of neurons layers connected in series: input, hidden and output layer. The input and output layer in the network are fixed and equal to that of input and output variables whereas, hidden layer can include more than one layer and in each layer the number of neurons is flexible [286]. The coarse information is accepted by the input layer and processed in the hidden layer and then the results are exported via the output layer as shown in Figure 3.13.
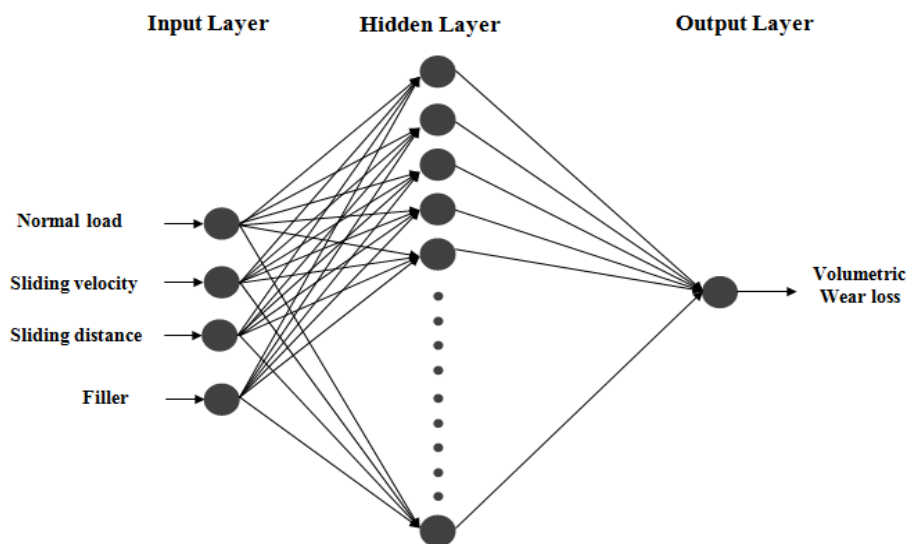
Figure 3.13: A schematic illustration of an artificial neural network.

In the present analysis, the normal load, sliding velocity, sliding distance and filler are taken as the four input parameters. Each of these parameters is characterized by one neuron and consequently the input layer in the ANN structure has four neurons. The database is built considering experiments at the limit ranges of each parameter. Experimental result sets are used to train the ANN in order to understand the input-output correlations. The database is then divided into three categories, namely: (i) a training category, which is exclusively used to adjust the network weights and (ii) a test category, which corresponds to the set that validates the

results of the training protocol. Usually seventy five percent data (patterns) is used for training and twenty five percent for testing [286]. The input variables are normalized so as to lie in the same range group of 0-1. The output layer of the network has only one neuron to represent wear volume. Different ANN structures (Input-Hidden-Output nodes) with varying number of neurons in the hidden layer are tested at constant cycles, learning rate, error goal, momentum parameter and epochs by using a user-friendly neural network toolbox in MATLAB R2008a software. The number of cycles selected during training is high enough so that the ANN models could be rigorously trained.

3.12 ENTROPY- PROMETHEE Method

In recent years, several MCDM (Multi Criteria Decision Making) methods such as: AHP (Analytic Hierarchy Process), TOPSIS (Technique for Order Preference by Similarity to Ideal Solution), GRA (Grey Relation Analysis), VIKOR (Vise Kriterijumska Optimizacija Kompromisno Resenje), PSI (Preference Selection Index), ELECTRE (Elimination and Choice Translating Reality), PROMETHEE (Preference Ranking Organization Method for Enrichment Evaluations) etc. have been proposed to help in selecting the best compromise alternatives. Among all, PROMETHEE is a quite simple ranking method in conception and application compared with the other methods. Brans proposed the PROMETHEE in 1982. The PROMETHEE methods use pair wise comparisons and outranking relationships to choose the best alternatives. Specifically, they compute positive and negative preference flows for each alternative and help the designer to make final selection. The positive preference flow indicates how an alternative is outranking all the other alternatives and the negative preference flow indicates how an alternative is outranked by all the other alternatives. The determination of weight for each criterion is important for the smooth functioning of PROMETHEE, which is determined by entropy method. The hybrid entropy-PROMETHEE approach was successfully applied to surpass the ambiguities involved in the complete ranking of alternatives. The evaluation methodology consists of the following four basic phases viz.

Phase I: Determination of alternatives and criterions

Phase II: Construction of decision matrix

Phase III: Determination of weight

Phase IV: Selection of optimal composition

Phase I: Determination of alternatives and criterions

In this phase, the number of alternatives $(A_i, i = 1, 2....m)$ and criterions $(C_j, j = 1, 2....n)$ for a given MCDM problems are identified.

Phase II: Construction of decision matrix

After the identification of alternatives and criterions, the value of experimental results for each alternative with respected criterion is expressed in the form of a decision matrix as:

$$D = \begin{array}{c} \\ A_1 \\ A_2 \\ \vdots \\ A_i \\ \vdots \\ A_m \end{array} \begin{array}{cccccc} C_1 & C_2 & \cdots & C_j & \cdots & C_n \\ \left[\begin{array}{cccccc} g_{11} & g_{12} & \cdots & g_{1j} & \cdots & g_{1n} \\ g_{21} & g_{22} & \cdots & g_{2j} & \cdots & g_{2n} \\ \vdots & \vdots & \cdots & \vdots & \cdots & \vdots \\ g_{i1} & g_{i2} & \cdots & g_{ij} & \cdots & g_{in} \\ \vdots & \vdots & \cdots & \vdots & \cdots & \vdots \\ g_{m1} & g_{m2} & \cdots & g_{mj} & \cdots & g_{mn} \end{array} \right] \end{array} \tag{3.3}$$

Where, element g_{ij} represent the value of jth criterion (C_j) for the ith alternative (A_i).

Phase III: Determination of weight: Entropy method

The entropy of the jth criterion in the decision matrix is given by:

$$H_j = -\lambda \sum_{i=1}^{m} \alpha_{ij} \ln(\alpha_{ij}) \tag{3.4}$$

Where $\alpha_{ij} = \dfrac{g_{ij}}{\sum\limits_{i=1}^{m} g_{ij}}$; $i = 1, 2, \cdots, m; j = 1, 2, \cdots, n$ and $\lambda = \dfrac{1}{\ln(m)}$

Finally the weight of each criterion is calculated as:

$$\omega_j = \dfrac{E_j}{\sum\limits_{j=1}^{n} E_j} \tag{3.5}$$

Where E_j is the degree of diversity of the information for the jth criterion output and given as

$$E_j = 1 - H_j. \tag{3.6}$$

Phase IV: Selection of optimal composition: PROMETHEE method

First of all the decision matrix is normalized by using the following equations:

Larger the better,

$$g'_{ij} = \frac{g_{ij} - \min\{g_{ij}\}}{\max\{g_{ij}\} - \min\{g_{ij}\}} \qquad (3.7)$$

Smaller the better,

$$g'_{ij} = \frac{\max\{g_{ij}\} - g_{ij}}{\max\{g_{ij}\} - \min\{g_{ij}\}} \qquad (3.8)$$

In the next step, the preference functions $(p_j(i,i'))$ are calculated for each criterion as:

$$p_j(i,i') = 0 \quad if \ g'_{ij} \le g'_{i'j}, \text{and}$$

$$p_j(i,i') = (g'_{ij} - g'_{i'j}) \quad if \ g'_{ij} > g'_{i'j} \qquad (3.9)$$

Thereafter, the weighted preference function is determined by using following equation:

$$\varpi(i,i') = \sum_{j=1}^{n} \omega_j \times p_j(i,i') \qquad (3.10)$$

In the next step, the positive and negative outranking flows are determined by using following equations:

$$\theta_i^+ = \frac{1}{m-1} \sum_{i'=1}^{m} \varpi(i,i'), \text{ and} \qquad (3.11)$$

$$\theta_i^- = \frac{1}{m-1} \sum_{i'=1}^{m} \varpi(i',i) \qquad (3.12)$$

Finally the net outranking flow for each alternative is calculated as:

$$\theta_i = \theta_i^+ - \theta_i^- \qquad (3.13)$$

Thus, the best alternative is the one having the highest θ_i value.

Chapter summary

This chapter has provided:

— The descriptions of materials used in the experiments.

— The details of fabrication and characterization of the alloy composites.

— The description of sliding wear test.

— The description of corrosion resistance analysis and biocompatibility test.

— An explanation of the Taguchi experimental design and neural network model.

— The details of ENTROPY-PROMETHEE MCDM technique to obtain the optimal ranking of formulations based on their physical, mechanical, sliding wear and friction coefficient.

The next chapter presents the effect of particulates (i.e. molybdenum, nickel and tungsten) on physical, mechanical and wears characterization of the alloy composite under study.

*****

PHYSICAL, MECHANICAL AND WEAR CHARACTERIZATION ON METAL ALLOY COMPOSITES

Introduction

This chapter discusses the result based on the physical, mechanical and wears characterization of the fabricated alloy composites according to the formulations discussed in previous chapter. The effect of particulates (i.e. molybdenum, nickel and tungsten) on various properties of fabricated Co-30Cr base metal alloy composite is discussed. The effects of sliding velocity and normal load on the sliding wear response of the fabricated alloy composites are also presented. The interpretation of the results and the comparison among various alloy composite samples are also presented. The results of this chapter are divided into three parts. Part I represents the physical, mechanical and wear behavior of A-Series alloy composites based on the variation of molybdenum filled particulate, Part II represents the physical, mechanical and wear behavior of B-Series alloy composites based on the variation of nickel filled particulate and Part III represents the physical, mechanical and wear behavior of C-Series alloy composites based on the variation of tungsten filled particulate in cobalt-chromium as a base metal matrix.

4.1. Part I: A-Series alloy composite (Co30Cr) based on the variation of molybdenum filled particulate

The characterization of the fabricated alloy composites revealed that inclusion of weight fraction of molybdenum (Mo) has strong influence not only on the mechanical properties of the alloy composites but also on their wear behavior under with and without water. The XRD diffractograms with a comparison for each sample are presented in Figure 4.1. These five different alloy composites are fabricated by the casting method [287]. It can be seen that the microstructure of 0wt.% Mo consists of a Co matrix with Cr regions. It is clear that the Co, in alliance with O forms Co_xO_y in the microstructure. The necessary oxides could have arrived from two sources: from Co or from the atmosphere for the period of mixing. Also, the hexagonal close-packed (HCP) Co structure has been formed for the reason that of the martensitic transformation [288]. No carbides are present in the microstructure, which corresponds well with the XRD peaks identified in 0-4wt. % Mo content. On the other hand, in all the samples, the fcc (111) cobalt base α matrix (d=2.04°A, a=b=c= 3.545°A), bcc (110) Cr (d=2.039°A, a=b=c=2.884°A), bcc (110) Mo (d=2.225°A, a=b=c= 3.147°A), and hcp (201) Co_3Mo (d=1.953°A, a=b=5.125°A, c=4.113°A) were

identified. An additional rhombohedral Co_7Mo_6 (116) phase (d=2.08°A), Co_7Mo_6 (027) phase (d=1.796°A, a=b=4.762°A, and c= 25.61 7°A) and a tetragonal Co_2Mo_3 (411) phase (d=2.031°A, a=b=9.229 and c=4.827°A) were identified.
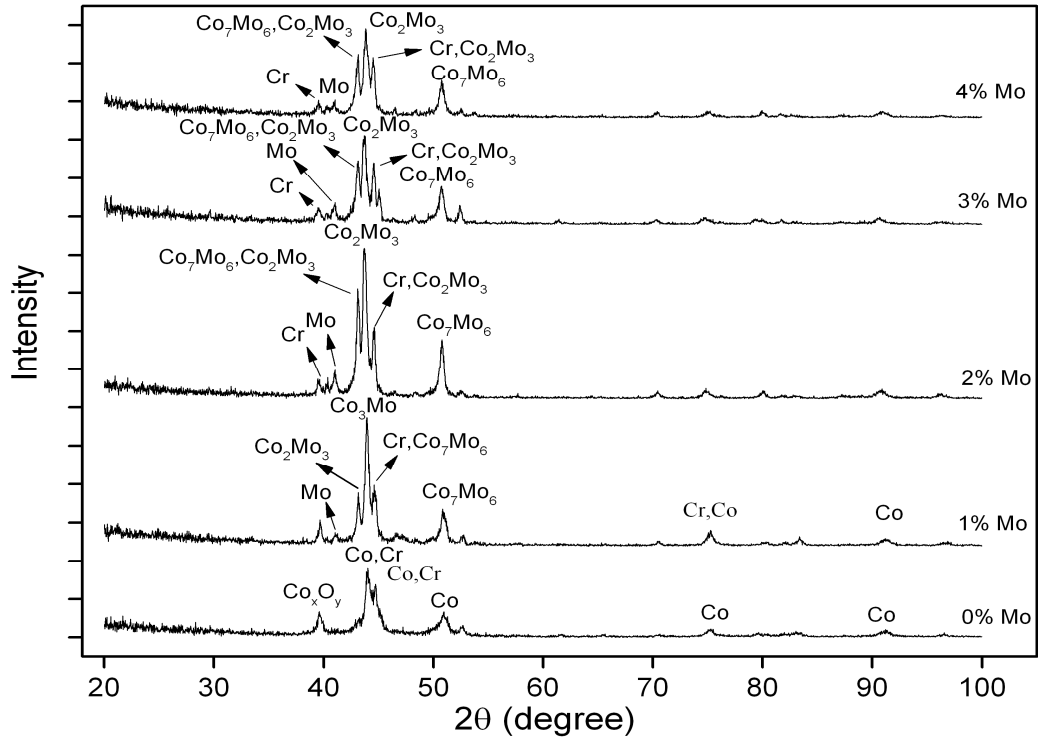
Figure 4.1: XRD patterns of fabricated molybdenum filled Co-30Cr alloy composite
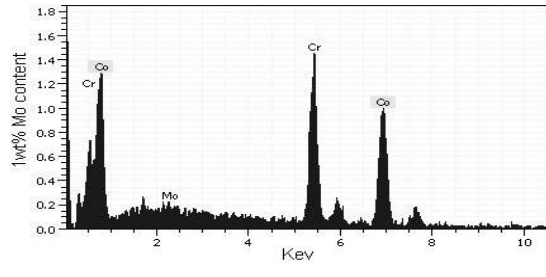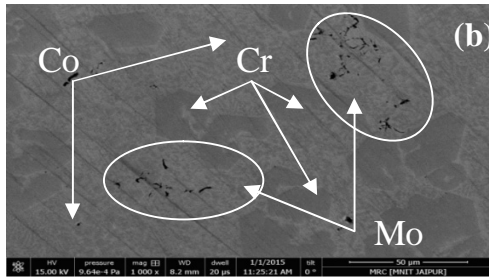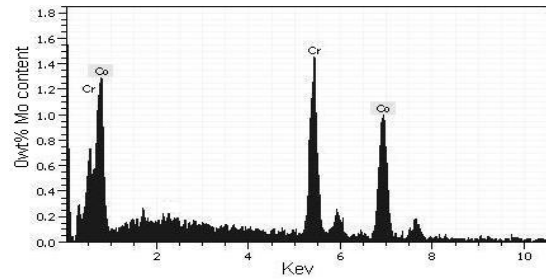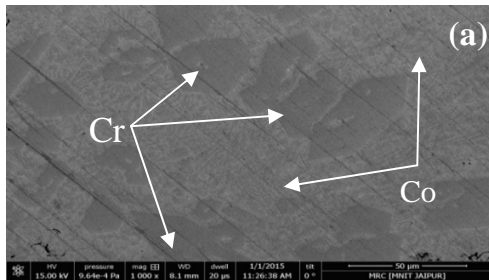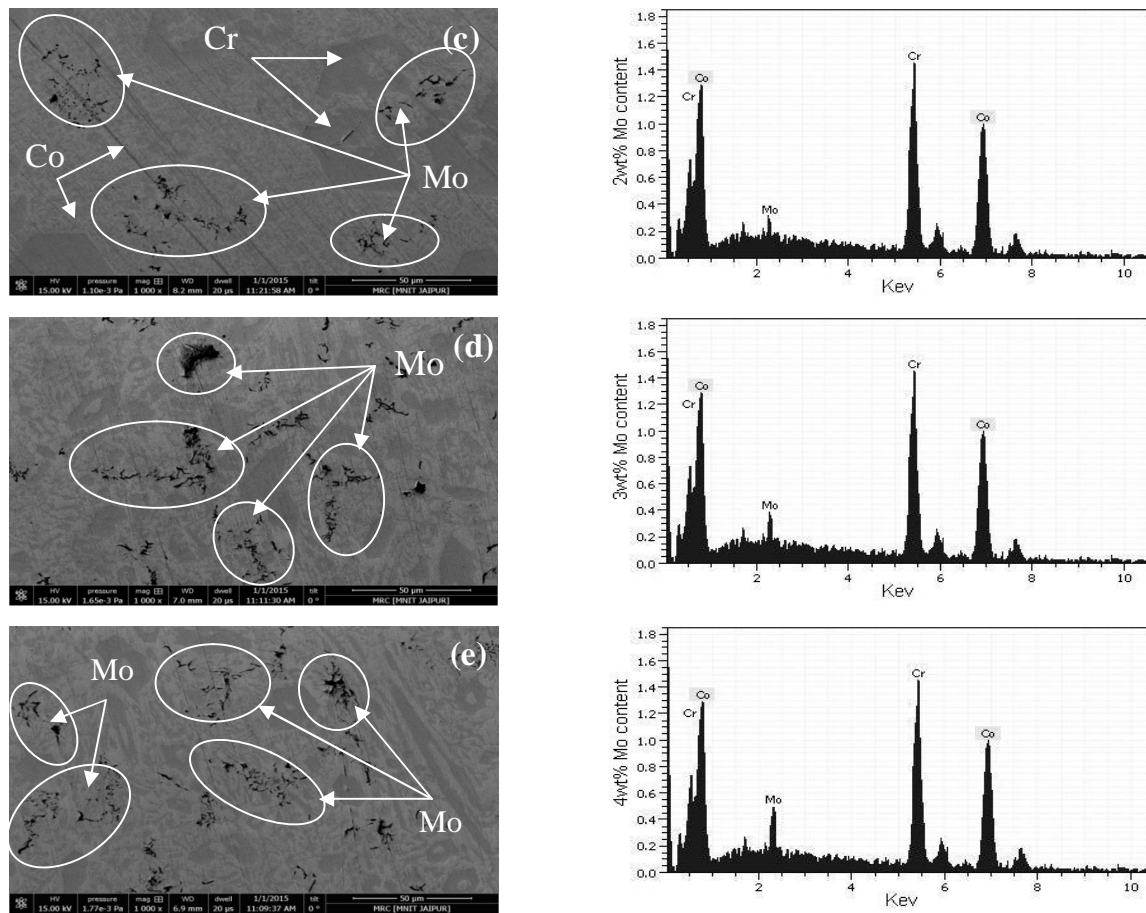
Figure 4.2: SEM micrographs and corresponding EDAX results of molybdenum filled Co-30Cr alloy composite: (a) 0wt.% Mo, (b) 1wt.% Mo, (c) 2wt.% Mo,(d) 3wt.% Mo and (e) 4wt.% Mo

The XRD patterns obtained have a number of similarities with other Co-Cr-Mo alloys viz ASTM F75, ASTM F1537 or studied in the literature [289-293]. Scanning electron microscopy images of the microstructure of samples M0, M1, M2, M3 and M4, with addition of molybdenum content are shown in Figure 4.2. It can be seen that the cobalt based solid solution is in light grey, chromium is in dark grey and, in different shades of black, the molybdenum contents.

4.1.1 Physical and Mechanical Properties of alloy composites

4.1.1.1 Density

The density of the fabricated molybdenum (0-4wt.%) filled Co-30Cr alloy composites are shown in Figure 4.3a. As shown in the figure, the density has significantly increased with the addition of molybdenum content. This increased in density may be attributed to the addition of particulate reinforcement with their increased bonding and better intermixing in the matrix causing an

increase in the bulk entanglement density. The densities obtained with the addition of molybdenum content (0-4wt. %) have near about as per ASTM F75 [56, 291].
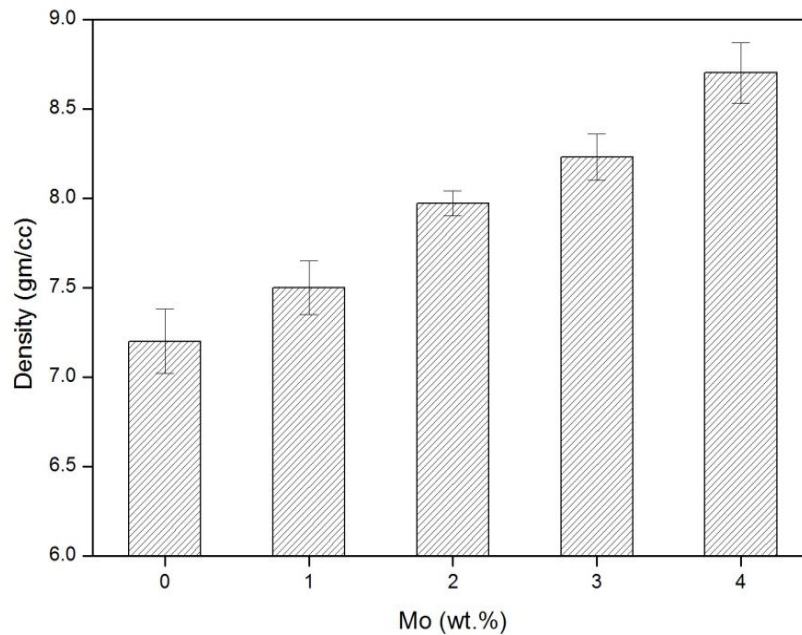
Figure 4.3: (a) Variation of density with Mo filled alloy composites

4.1.1.2 Micro-hardness

Micro-hardness of the fabricated alloy composite at different weight fractions of molybdenum is shown in Figure 4.3b. The micro-hardness is measured at six different locations and after measuring the micro-hardness of the entire identified region, the mean micro-hardness is taken in this study. It is observed that in all the samples, the hardness of the fabricated alloy composites increases with increase in weight percentage of molybdenum (see Table 4.1) due to vertical centrifugal casting. As the wt.% of Mo increases, the hardness of the alloy composites also increases i.e. at 4wt.% of Mo particulate filler added in metal matrix Co-30Cr alloy composite has exhibited the maximum hardness. Similar trend also reported by Ahmed and Lovelock [294] and Balagna et al. [295].

4.1.1.3 Compression strength

Figure 4.3c shows the variation of compression strength of the fabricated alloy composites with the Mo contents. A gradual increase in compressive strength with increased in wt.% of Mo is observed. It evidently indicates that the addition of Mo improves the load bearing capacity of the alloys.
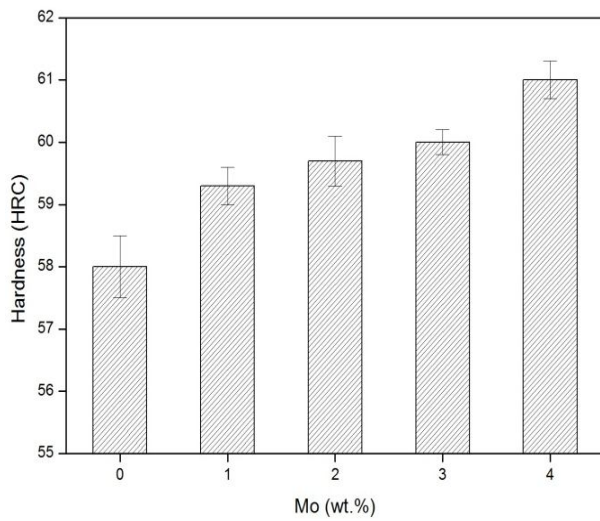
Figure 4.3: (b) Variation of micro-hardness with Mo filled alloy composites
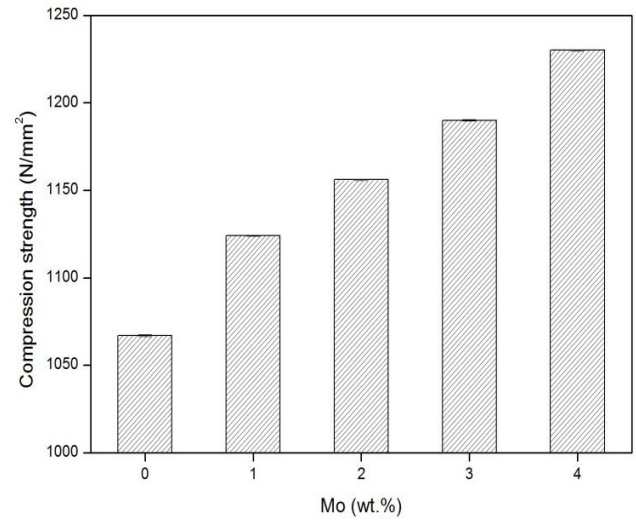
Figure 4.3: (c) Variation of compression strength with Mo filled alloy composites

Table 4.1 Physical and mechanical properties of molybdenum filled alloy composite

Alloys	Density (gm/cc)	Hardness (HRC)	Compression strength (N/mm^2)
A0	7.2	58	1067
A1	7.5	59.3	1124
A2	7.97	59.7	1156
A3	8.23	60	1190
A4	8.70	61	1230

4.1.2 Sliding wear behavior of alloy composites

4.1.2.1 Effect of sliding velocity on volumetric wear of Molybdenum filled alloy composites

Each test is conducted for 1500 m of sliding distance. In this way easily measurable wear loss is obtained and a comparatively long steady-state wear period is ensured. Figure 4.4a represents the volumetric wear loss (mm^3) of fabricated unfilled and Mo filled (1, 2, 3 and 4 wt.%) particulates alloy composites as a function of sliding velocity at constant load 15N under dry and wet conditions. The volumetric wear loss (mm^3) of unfilled and Mo particulate filled alloy composites (i.e. 0-3wt.% Mo) are gradually increases with further increased in sliding velocity up to 1.3m/s.

This is because at higher sliding velocity, surface contact between the disc and the pin is more and consequently the wear loss is more. It is interesting to note that the volumetric wear loss of fabricated alloy composites obtained in this study is very close to the previous researchers [288, 290]. Whereas, in 4wt.% Mo particulate filled alloy composites show less volumetric wear loss as compared with other wt. % of Mo particulate filled alloy composites in both dry and wet medium.

Figure 4.4b shows the variation in the friction coefficient with sliding velocity for the effect of molybdenum particulate filled alloy composites under dry and wet condition. At the primary epoch of rubbing, friction is low and the factors accountable for this low friction are due to the attendance of a layer of foreign material on the disc surface. This layer generally constitutes; moisture; oxide of metals; deposited lubricating material, etc. After initial rubbing, the upper layer separates and fresh surfaces directly come in contact which increases the bonding force between the contacting surfaces. A similar finding is observed by Savarimuthu et al. [296] for sliding wear behavior of tungsten carbide thermal spray coatings for replacement of chromium electroplate in aircraft applications. The 4wt.% Mo particulates display least effect in the variation of friction coefficient with sliding velocity. The mean steady state values of the friction coefficient with respect to sliding velocity tested in both the conditions at 15N load is illustrated in Figure 4.4b for the addition of Mo particulate filled Co30Cr alloy composites. It is seen from Figure 4.4b that, at the lowest sliding velocity (0.26 m/s) friction coefficient of almost all the combination of alloys are low after which it increases and then decreases parallel to increase in the sliding velocity up to 0.785 m/s.

4.1.2.2 Effect of normal load on volumetric wear of Molybdenum filled alloy composites

The volumetric wear loss with normal load (5–25N) at constant sliding velocity (0.785 m/s) for unfilled and Mo particulate filled fabricated alloy composites are presented in Figure 4.5a. As shown in Figure 4.5a, the volumetric wear loss increases as the normal load increases up to 25N. Out of all the samples, 4wt.% Mo exhibits a lesser wear loss than the others in both dry and wet conditions. As the load on the pin is increased the actual area of contact would enhance towards the nominal contact area, consequently that increase the frictional force between two sliding surfaces. The enhanced frictional force and real surface area in contact cause higher wear. This implies that the shear force and frictional thrust force are increased with increase of normal load and this accelerates the volumetric wear loss. In this study, the material used for pin and counter disc are both different and the value obtained of volumetric wear (mm^3) is in the range of cobalt

based alloy [29-31]. Some authors used the same material of both pin and disc instead of EN31 steel. Firkins et al. [297] used CoCr alloy for both the pin and disc material and found the wear behavior is likely similar to our study. Doni et al. [298] compared the dry sliding wear behavior under 1N normal load of hot pressed CoCrMo implant material with commercially cast CoCrMo and Ti6Al4V implant materials and found the wear loss of Ti6Al4V alloy is 14 and 47 times higher than the cast and hot pressed CoCrMo samples respectively.
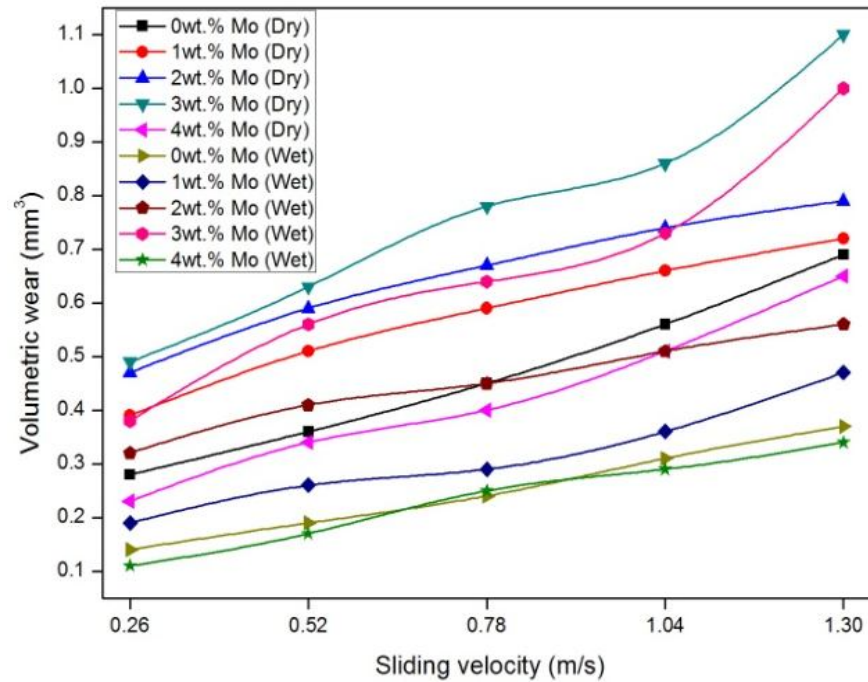
Figure 4.4a: Variation of volumetric wear with sliding velocity for molybdenum filled alloy composite under dry and wet condition (load: 15 N and sliding distance 1500m)

Figure 4.5b shows the friction coefficient versus normal load for unfilled and Mo particulate filled Co30Cr alloy composites under steady state condition. As shown in Figure 4.5b, the friction coefficient of the fabricated alloy (i.e. Co30Cr) composites both dry and wet conditions with various Mo filler contents exhibited considerably low coefficient of friction up to 15N normal load. The current experimental results are explicable: during starting stages, the surfaces of both the alloy specimens and the disc are smooth due to the presence of reinforcing particulate materials including moisture, oxide of metals, deposited lubricating materials, etc. and thus resulting in a low friction coefficient. As the wear continued, the layer break up and the clean surface come in directly contact with the specimen and gradually increases the friction coefficients are accomplished when a steady wear stage is attained up to 25N load[32].
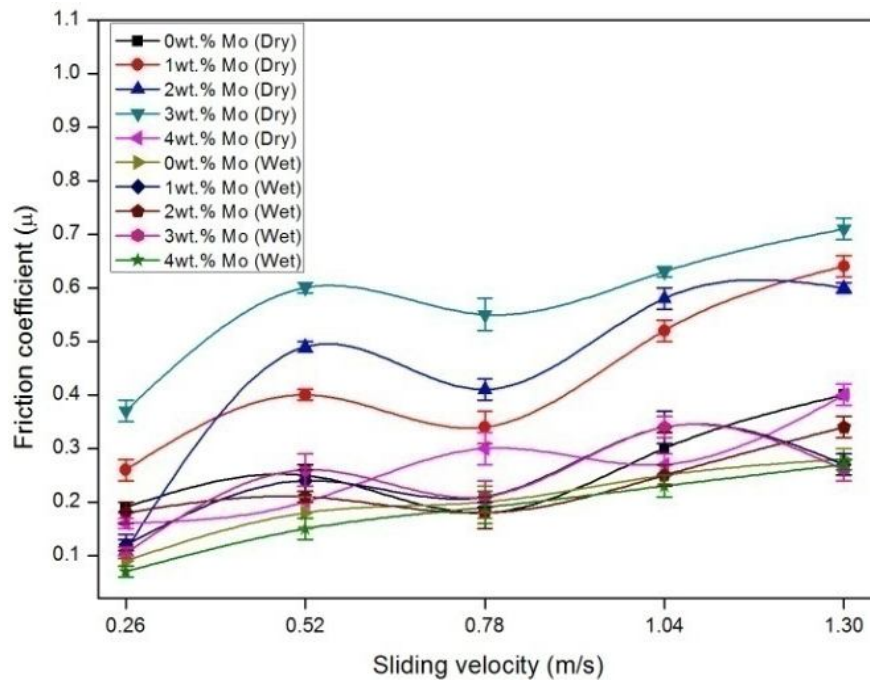
Figure 4.4b: Variation of friction coefficient with sliding velocity for molybdenum filled alloy composite under dry and wet condition (load: 15 N and sliding distance 1500m)
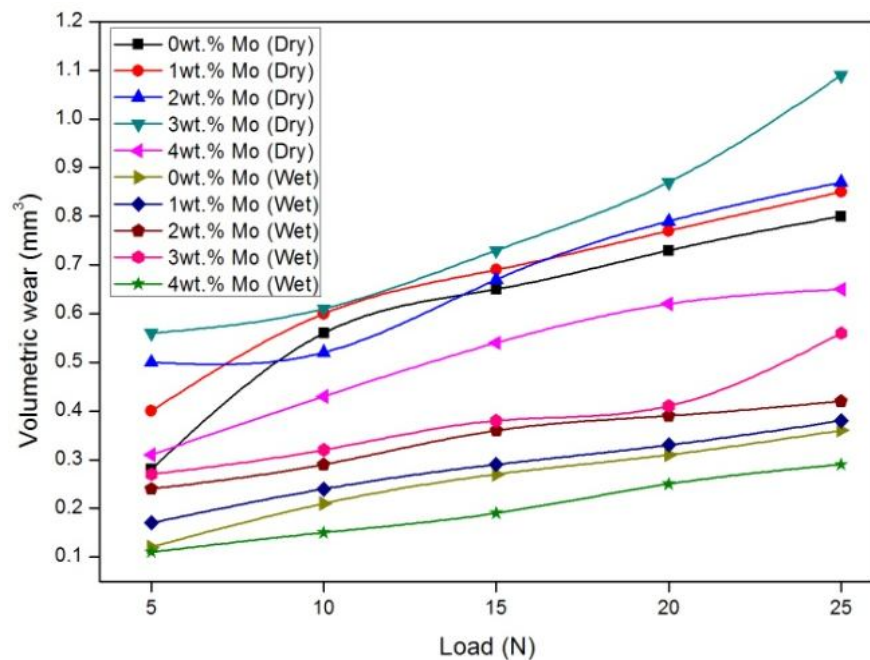
Figure 4.5a: Variation of volumetric wear with normal load for molybdenum filled alloy composite under dry and wet condition (Sliding velocity: 0.785 m/s and sliding distance 1500m)
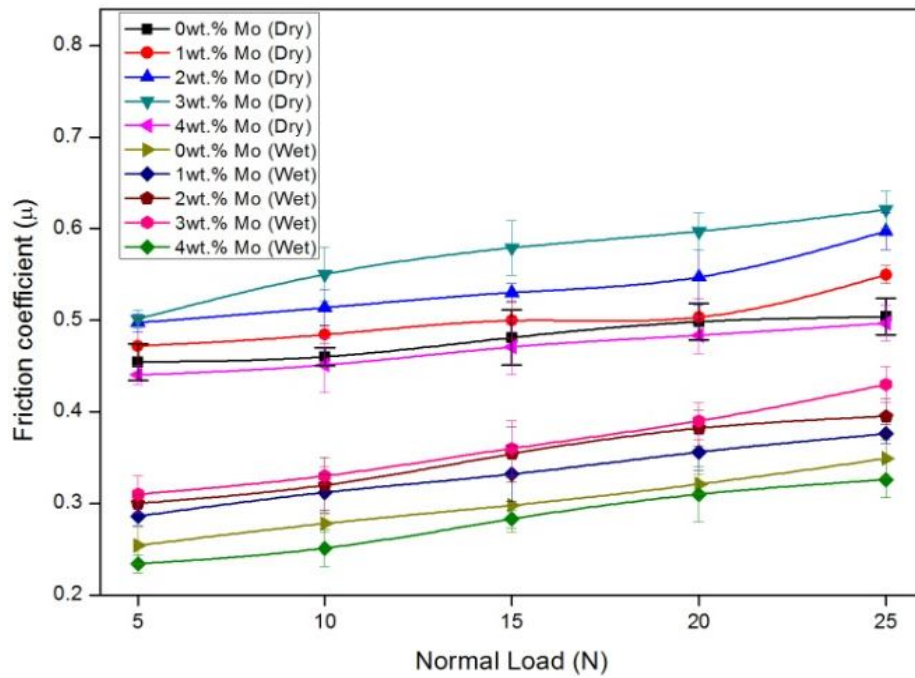
Figure 4.5b: Variation of friction coefficient with normal load for molybdenum filled alloy composite under dry and wet condition (Sliding velocity: 0.785m/s and sliding distance 1500m)

4.1.3 Taguchi Experimental Analysis

Table 4.2 shows the volumetric wear loss of unfilled and particulate filled metal alloy composites and their respective S/N ratio values. The sixth and tenth columns represent the volumetric wear loss (mm^3) whereas; eighth and twelfth column represents the friction coefficient of the dry and wet condition of the fabricated alloy composites. The overall mean for the S/N ratio of the wear loss under dry and wet sliding condition are found to be -9.777 dB and 35.218 dB respectively. Similarly, the overall mean for the S/N ratio of the friction coefficient for both sliding conditions are found to be 6.670 dB and 20.924 dB respectively. Figures 4.6a-4.6d show graphically the effect of the four control factors on wear volume and friction coefficient in dry and wet sliding conditions. Analysis of the result leads to the conclusion that factor combination of A_4, B_1, C_5 and D_5 gives minimum sliding wear loss in dry condition and A_5, B_1, C_4 and D_5 in wet conditions for the fabricated alloy composites respectively (Figure 4.6a and Figure 4.6b). Similarly, the factor combination of A_1, B_2, C_4 and D_5 gives minimum friction coefficient in dry condition and A_2, B_2, C_4 and D_5 in wet conditions for the fabricated alloy composites respectively (Figure 4.6c and Figure 4.6d).

Table 4.2 Experimental design using L_{25} orthogonal array

Runs	A	B	C	D	Dry Condition					Wet Condition				
					wear loss (mm^3)	Standard deviation	S/N Ratio (db)	Friction Coeff.	S/N Ratio (db)	wear loss (mm^3)	Standard deviation	S/N Ratio (db)	Friction Coeff.	S/N Ratio (db)
1	5	0.26	500	0	7.2222	0.0004	-17.17	0.297	10.532	0.087322	0.0005	21.1775	0.030	30.5317
2	5	0.523	1000	1	9.5524	0.0005	-19.60	0.176	15.072	0.069553	0.0002	23.1536	0.018	35.0724
3	5	0.785	1500	2	7.3059	0.0002	-17.27	0.455	6.839	0.079725	0.0002	21.9680	0.155	16.1905
4	5	1.04	2000	3	6.0753	0.0002	-15.67	0.458	6.791	0.011275	0.0003	38.9574	0.096	20.3766
5	5	1.3	2500	4	2.2069	0.0003	-6.876	0.170	15.370	0.021269	0.0002	33.4450	0.017	35.3696
6	10	0.26	1000	2	9.0376	0.0002	-19.12	0.471	6.545	0.100376	0.0004	19.9673	0.047	26.5453
7	10	0.523	1500	3	3.2402	0.0002	-10.21	0.238	12.481	0.032402	0.0002	29.7886	0.024	32.4812
8	10	0.785	2000	4	2.1494	0.0002	-6.646	0.203	13.852	0.011544	0.0002	38.7526	0.020	33.8520
9	10	1.04	2500	0	3.1111	0.0002	-9.858	0.431	7.304	0.016711	0.0005	35.5398	0.043	27.3044
10	10	1.3	500	1	8.3333	0.0004	-18.41	0.350	9.108	0.133333	0.0005	17.5012	0.035	29.1080
11	15	0.26	1500	4	1.4541	0.0004	-3.252	0.463	6.679	0.004985	0.0004	46.0460	0.046	26.6790
12	15	0.523	2000	0	4.4753	0.0003	-13.01	0.466	6.634	0.014198	0.0004	36.9557	0.047	26.6344
13	15	0.785	2500	1	1.7067	0.0003	-4.643	0.731	2.722	0.017173	0.0003	35.3029	0.331	9.60373
14	15	1.04	500	2	6.6918	0.0004	-16.51	0.730	2.734	0.068384	0.0003	23.3008	0.298	10.5227
15	15	1.3	1000	3	1.6201	0.0004	-4.191	0.855	1.362	0.016401	0.0003	35.7026	0.255	11.8733
16	20	0.26	2000	1	0.3333	0.0003	9.542	0.347	9.185	0.003408	0.0002	49.3491	0.147	16.6341
17	20	0.523	2500	2	1.6524	0.0003	-4.363	0.702	3.070	0.006584	0.0004	43.6295	0.202	13.883
18	20	0.785	500	3	4.8603	0.0002	-13.73	0.888	1.032	0.048603	0.0002	26.2668	0.351	9.09385
19	20	1.04	1000	4	1.5747	0.0004	-3.944	0.753	2.469	0.005747	0.0002	44.8109	0.153	16.3299
20	20	1.3	1500	0	1.4630	0.0002	-3.305	0.696	3.151	0.00463	0.0004	46.6890	0.086	21.3376
21	25	0.26	2500	3	1.4977	0.0002	-3.508	0.787	2.086	0.002041	0.0002	53.8035	0.287	10.8572
22	25	0.523	500	4	7.8276	0.0004	-17.87	0.403	7.894	0.078276	0.0002	22.1274	0.103	19.7442
23	25	0.785	1000	0	2.8889	0.0002	-9.215	0.771	2.259	0.008889	0.0004	41.0230	0.271	11.3409
24	25	1.04	1500	1	2.6637	0.0002	-8.510	0.505	5.940	0.00677	0.0002	43.3877	0.205	13.7792
25	25	1.3	2000	2	2.2509	0.0002	-7.047	0.523	5.636	0.002569	0.0002	51.8033	0.123	18.2257
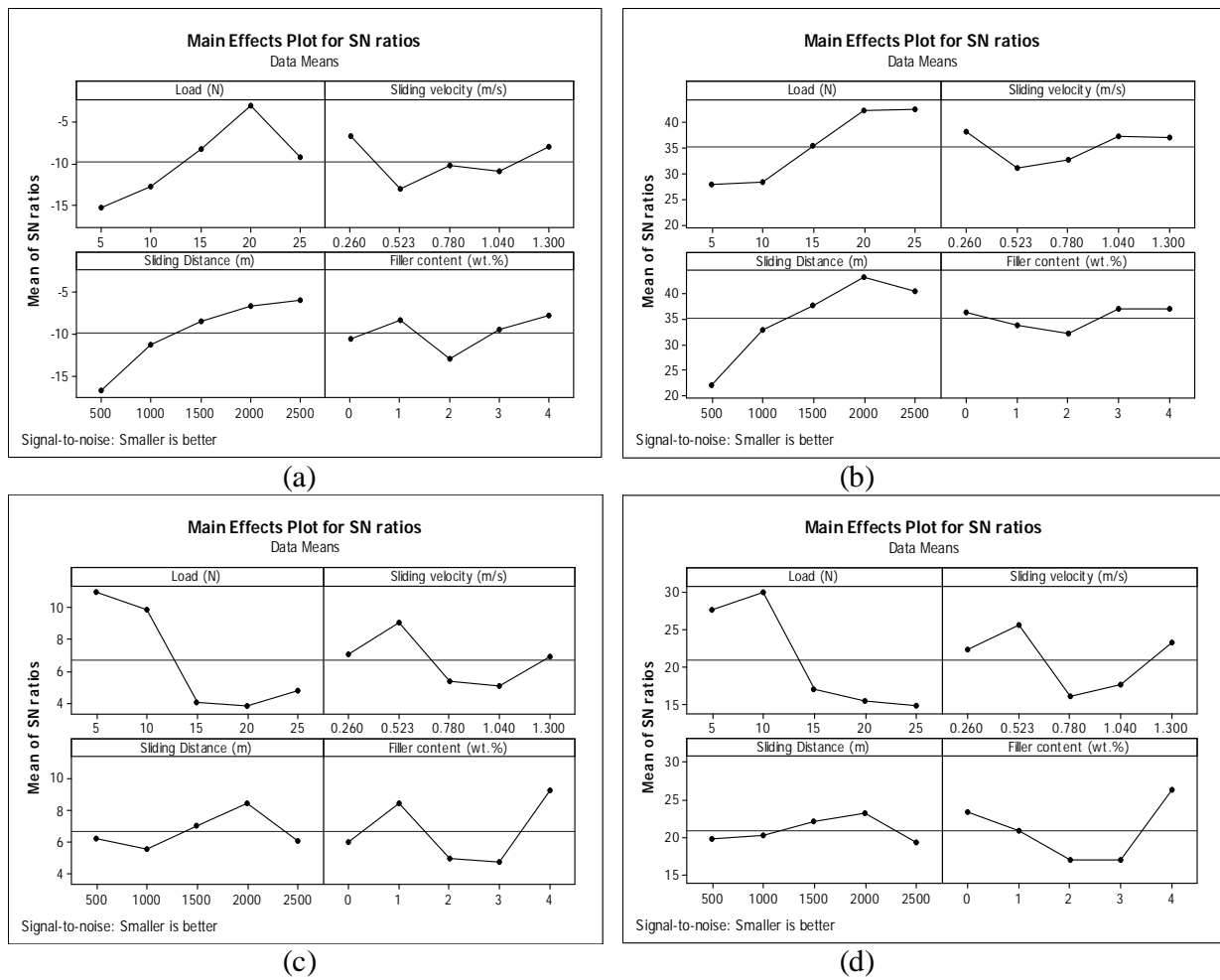
Figure 4.6: (a) Effect of control factors on volumetric wear loss for Mo filled Co30Cr alloy composites under dry condition; (b) Effect of control factors on volumetric wear loss for Mo filled Co30Cr alloy composites under wet condition; (c) Effect of control factors on friction coefficient for Mo filled Co30Cr alloy composites under dry condition; (d) Effect of control factors on friction coefficient for Mo filled Co30Cr alloy composites under wet condition

4.1.4 Confirmation Experiment

The last step in any design of experiment approach is to conduct the confirmation experiment. The purpose of the confirmation experiment is to validate the conclusions drawn during the analysis phase. The confirmation experiment is performed by conducting a new set of factor settings $A_3B_4C_1D_2$ and $A_4B_2C_3D_1$ to predict the wear volume for dry and wet sliding condition respectively. Similarly, a new set of factor settings $A_2B_4C_3D_1$ and $A_3B_5C_2D_1$ to predict the friction coefficient for both the conditions. The estimated S/N ratio for wear volumes can be calculated by predictive equation:

$$\hat{\eta}_{dry_w} = \bar{\eta} + (\overline{A_3} - \bar{\eta}) + (\overline{B_4} - \bar{\eta}) + (\overline{C_1} - \bar{\eta}) + (\overline{D_2} - \bar{\eta}) \tag{4.1}$$

$$\hat{\eta}_{dry_\mu} = \bar{\eta} + (\overline{A_2} - \bar{\eta}) + (\overline{B_4} - \bar{\eta}) + (\overline{C_3} - \bar{\eta}) + (\overline{D_1} - \bar{\eta}) \tag{4.2}$$

$$\hat{\eta}_{wet_w} = \bar{\eta} + (\overline{A_4} - \bar{\eta}) + (\overline{B_2} - \bar{\eta}) + (\overline{C_3} - \bar{\eta}) + (\overline{D_1} - \bar{\eta}) \tag{4.3}$$

$$\hat{\eta}_{wet_\mu} = \bar{\eta} + (\overline{A_3} - \bar{\eta}) + (\overline{B_5} - \bar{\eta}) + (\overline{C_2} - \bar{\eta}) + (\overline{D_1} - \bar{\eta}) \tag{4.4}$$

Where, $\hat{\eta}_w$: predicted average of wear volume, $\hat{\eta}_\mu$: predicted average of friction coefficient, $\bar{\eta}$: overall experimental average, $\overline{A_3}, \overline{B_4}, \overline{C_1}, \overline{D_2}$ for wear volume and $\overline{A_2}, \overline{B_4}, \overline{C_3}, \overline{D_1}$ for friction coefficient under dry condition and $\overline{A_4}, \overline{B_2}, \overline{C_3}, \overline{D_1}$ for wear volume and $\overline{A_3}, \overline{B_5}, \overline{C_2}, \overline{D_1}$ for friction coefficients under wet condition are the mean response for factors at designated level. By combining like terms, the equation reduces to:

$$\hat{\eta}_{dry_w} = \overline{A_3} + \overline{B_4} + \overline{C_1} + \overline{D_2} - 3\bar{\eta} \tag{4.5}$$

$$\hat{\eta}_{dry_\mu} = \overline{A_2} + \overline{B_4} + \overline{C_3} + \overline{D_1} - 3\bar{\eta} \tag{4.6}$$

$$\hat{\eta}_{wet_w} = \overline{A_4} + \overline{B_2} + \overline{C_3} + \overline{D_1} - 3\bar{\eta} \tag{4.7}$$

$$\hat{\eta}_{wet_\mu} = \overline{A_3} + \overline{B_5} + \overline{C_2} + \overline{D_1} - 3\bar{\eta} \tag{4.8}$$

A new combination of factor levels $\overline{A_3}, \overline{B_4}, \overline{C_1}, \overline{D_2}$ and $\overline{A_4}, \overline{B_2}, \overline{C_3}, \overline{D_1}$ are used to predict the wear volume by using prediction equations (Eq. 4.5 and Eq. 4.7) and the S/N ratio is found to be -14.9564 dB and 41.4790dB for dry and wet sliding condition respectively. Similarly, factor levels $\overline{A_2}, \overline{B_4}, \overline{C_3}, \overline{D_1}$ and $\overline{A_3}, \overline{B_5}, \overline{C_2}, \overline{D_1}$ are used to predict the friction coefficient by using prediction equations (Eq. 4.6 and Eq. 4.8) and the S/N ratio is found to be 7.89037 dB and 21.1033 dB for dry and wet sliding condition respectively. The resulting model seems to be capable of predicting wear volume to a reasonable accuracy. An error under dry and wet sliding condition for S/N ratio of wear volume and friction coefficient is observed as shown in Table 4.3. However, the error can be further reduced if the number of measurement will be increased. This validates the development of the mathematical model for predicting the measures of performance based on knowledge of the input parameters.

Table 4.3 Results of the confirmation experiments for wear volume and friction coefficient

	Dry condition		Wet condition	
	S/N ratio for wear volume	S/N ratio for friction coefficient	S/N ratio for wear volume	S/N ratio for friction coefficient
Levels	$A_3B_4C_1D_2$	$A_2B_4C_3D_1$	$A_4B_2C_3D_1$	$A_3B_5C_2D_1$
Prediction	-14.9564	7.89037	41.4790	21.1033
Experimental	-15.1408	8.03455	42.2989	21.6954
Error (%)	1.2	1.79	1.9	2.72

4.1.5 ANOVA and the Effect of Factors

In order to understand a concrete visualization of impact of various factors like normal load (A), sliding velocity (B), sliding distance (C) and filler content (D) on volumetric wear loss, it is enviable to develop analysis of variance (ANOVA) table to find out the order of significant factors. Tables 4.4 and 4.5 demonstrates the results of the ANOVA with the wear loss and friction coefficient assuming a level of significance of 5% under dry and wet sliding condition respectively.

Table 4.4 ANOVA table for volumetric wear

Source	Degree of freedom (DF)	Seq SS	Adj SS	Adj MS	F	P
Dry condition						
A	4	62.806	62.806	15.702	5.21	0.023
B	4	12.736	12.736	3.184	1.06	0.437
C	4	75.678	75.678	18.920	6.28	0.014
D	4	17.102	17.102	4.276	1.42	0.312
Error	8	24.113	24.113	3.014		
Total	24	192.436				
Wet condition						
A	4	0.0085991	0.0085991	0.0021498	7.42	0.008
B	4	0.0011142	0.0011142	0.0002785	0.96	0.478
C	4	0.0181137	0.0181137	0.0045284	15.62	0.001
D	4	0.0037213	0.0037213	0.0009303	3.21	0.075
Error	8	0.0023191	0.0023191	0.0002899		
Total	24	0.0338674				

The last column of the table designates the probability of significance of major control factors. It has been noticed that sliding distance (p = 0.014), load (p = 0.023), filler content (p = 0.312) and sliding velocity (p = 0.437) for dry sliding condition and sliding distance (p = 0.001), load (p = 0.008), filler content (p = 0.075) and sliding velocity (p = 0.478) for wet sliding condition are significant in the declining order of importance on wear loss whereas, load (p = 0.000), filler content (p = 0.005), sliding velocity (p = 0.017) and sliding distance (p = 0.021) for dry sliding condition and filler content (p = 0.000), load (p = 0.000), and sliding velocity (p = 0.000) and sliding distance (p = 0.001) for wet sliding condition are significant in the declining

order of importance on friction coefficient respectively. From this analysis it is observed that filler content has the most significant contribution compared to other factor.

Table 4.5 ANOVA table for friction coefficient

Source	Degree of freedom (DF)	Seq SS	Adj SS	Adj MS	F	P
Dry condition						
A	4	0.618329	0.618329	0.154582	25.54	0.000
B	4	0.141318	0.141318	0.035330	5.84	0.017
C	4	0.130989	0.130989	0.032747	5.41	0.021
D	4	0.215729	0.215729	0.053932	8.91	0.005
Error	8	0.048427	0.048427	0.006053		
Total	24	1.154792				
Wet condition						
A	4	0.128710	0.128710	0.032178	64.90	0.000
B	4	0.067684	0.067684	0.016921	34.13	0.000
C	4	0.030158	0.030158	0.007540	15.21	0.001
D	4	0.058367	0.058367	0.014592	29.43	0.000
Error	8	0.003966	0.003966	0.000496		
Total	24	0.288886				

4.1.6 Surface Morphology

The worn surface morphology of molybdenum particulate filled Co30Cr alloy composites under dry and wet mediums is examined by scanning electron microscopy (SEM). The SEM characterization is carried out by using FEI NOVA NANOSEM 450 with an energy dispersive spectroscopy (EDS) attached to analyze the chemical composition of different phases and wear mechanisms induced by the pin-on-disc test. These micrographs have taken after 30 min of the test duration with a sliding velocity of 0.785 m/s and a normal load of 15N. Figures 4.7-4.10 show the microstructure of worn surfaces of fabricated Mo particulate filled Co30Cr alloy composites by varying sliding velocity under dry condition (Taken from Figure 4.4a) at constant normal load: 15N and sliding distance: 1500m. The wear sample surfaces with high resolution AFM are plotted in Figures 4.11 and 4.12 for dry and wet condition respectively. The corresponding surface roughness (R_a) is reported in Table 4.5 after the Taguchi design of experiment test run for dry and wet condition respectively.

Figure 4.7a shows the worn surface morphology of fabricated unfilled particulate alloy composites where the attendance of reinforced particles becomes negligible. In Figure 4.7b, parallel and continuous grooves are found due to the attendance of Mo (1wt.%) particulate filled alloy composite and due to which the interfacial bonding in between the particles is not so strong and the material is removed from surfaces during the sliding wear process and formed a continuous grooves on the fabricated alloy composite surface. As far as 2wt.% and 3wt.% Mo particulate filled Co30Cr alloy composites the volumetric wear loss starts increasing under similar operating conditions as shown in Figures 4.7c and 4.7d respectively. The increased in volumetric wear loss is due to poor bonding between the hard particulates and matrix material (See steady state Figure 4.5a) and there may be chances of formation of delamination wear in the subsurface of the worn area which leads to removal of material (see Figure 4.7c) during the sliding wear process. However, under similar operating condition the worn surface morphology of 4wt. % Mo particulate filled Co30Cr alloy composite the formation of wear track is minimum as compared with 0-3wt.% Mo particulate fillers (see Figure 4.7a-4.7d). The reduction of volumetric wear loss is minimum due reinforcement of hard molybdenum particulates in the alloy matrix composite.

Similar trend is also observed under the wet condition (i.e. Introduction of smooth layer of distilled water between the pin and the disc) as shown in Figure 4.8. This layer is almost fully covers the wear track in place of dry condition (See Figures 4.8a-4.8e) along the sliding direction for 0-4wt.% particulate filled Co30Cr alloy composite at constant sliding velocity 0.785m/sec, normal load 15N and sliding distance 1500m respectively (See Figure 4.4a). However, under steady state condition the worn surface morphology of fabricated unfilled particulate alloy composites are shown in Figure 4.8a, where the attendance of reinforced particles becomes negligible. Again, with further increased particulate fillers in the fabricated alloy composite i.e. 1wt.% Mo the volumetric wear loss is slightly more in the form of parallel and continuous cracks instead of unfilled particulate as shown in Figure 4.8b. This shows less abrasion grooves as compared to dry condition under similar test condition due to the presence of a layer of distilled water between the pin and the counter disc and no directly contact between the pin and the disc and hence a reduced amount of wear loss attained (see Figure 4.8b). Figure 4.8c shows the surface morphology of 2wt.% Mo particulate filled alloy composites. This shows the volumetric wear loss starts increasing due to improper bonding between the hard particulates and matrix material causes continuous wear scars are occurred. Due to the presence of a layer of distilled water between the

pin and the disc the volumetric wear loss is considerable less as compared to dry condition shown in Figure 4.7c. As the filler content further increases to 3wt.% (Figure 4.8d) the wear loss also increased and the formation of micro cracks are more in place of 2wt.% Mo particulate filled alloy composites but less as compared to dry condition under similar operating condition (see Figure 4.7d) along the sliding wear direction. The surface morphology of 4wt.% Mo particulate filled alloy composite, shown in Figure 4.8e, appears to be smooth with no shallow grooves and continuous ploughing effect as compared to other filler content of alloy composites. The fine surface occurs may be due to reinforcement of hard tungsten particulates in the alloy matrix composite. The obtained worn surfaces are similar to many other researchers by their research study [32-34].

Figure 4.9 shows the worn surface morphology of molybdenum particulate filled Co30Cr alloy composites under different normal loads without water (Taken from Figure 4.4a) at constant sliding velocity: 0.785 m/s and sliding distance: 1500 m. Figure 4.9a shows the worn surface of the alloy composites containing 0wt.% of Mo particulate filler exhibited wear scars and micro cracks along the sliding direction at constant sliding velocity 0.785m/sec, normal load 15N and sliding distance 1500m respectively(See Figure 4.4a). However, under similar operating condition the worn surface morphology of 1wt.% Mo particulate filled alloy composite the formation of crack is more due to the oversize carbides and their less uniform distribution in the matrix as compared with 0wt. % Mo particulate filled alloy composites (Figure 4.9b). Again, with further increased in filler content in the alloy composite i.e. 2 and 3wt.% Mo the volumetric wear loss starts increasing and wear track becomes larger under similar operating conditions as shown in Figs. 4.9c and 4.9d respectively. The increased in wear volume is due to poor bonding between the hard particulates and matrix material. The obtained worn surfaces are alike to previous studies in our research group [33]. However, under similar steady state condition the worn surface morphology of 4wt.% Mo particulate filled alloy composite the formation of parallel and continuous groves and ploughing strip is reduced on the damaged surface due to reinforcement of hard molybdenum particulates in the alloy matrix composite as compared with other two compositions (See steady state Figure 4.4a and morphology Figure 4.9e).
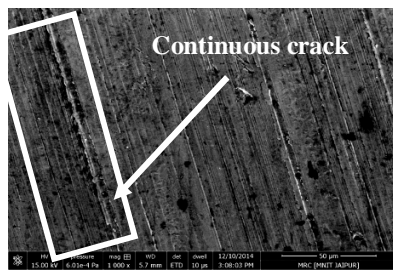
(a): 0wt.% Mo
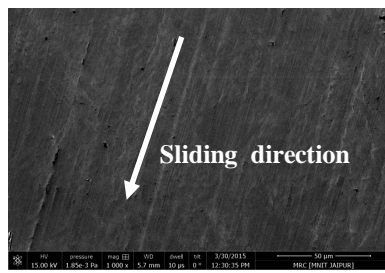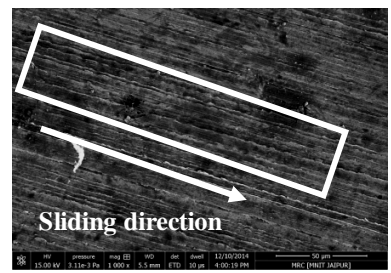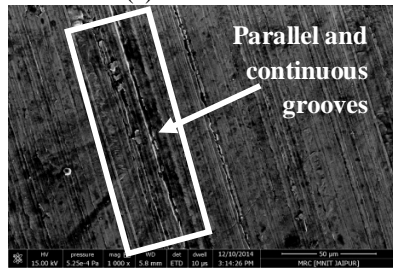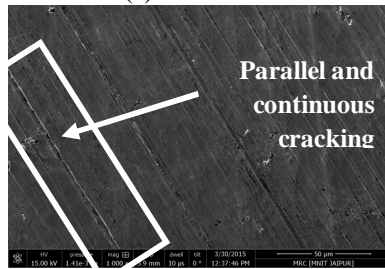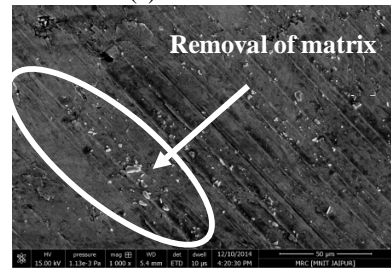
(b): 1wt.% Mo
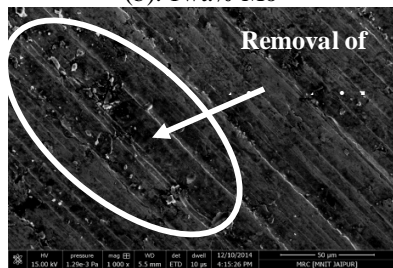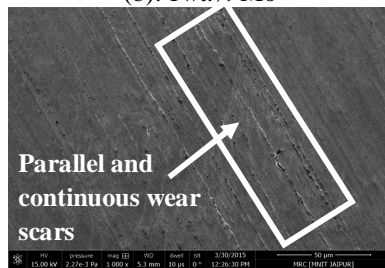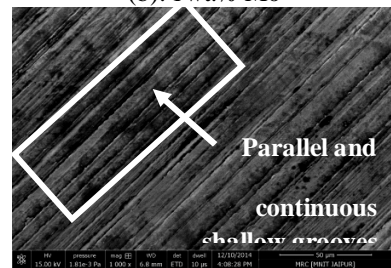
(c): 2wt.% Mo
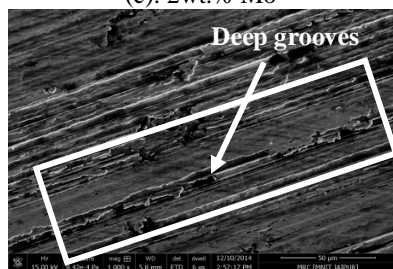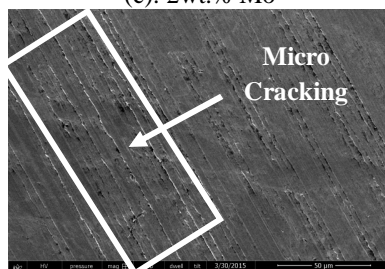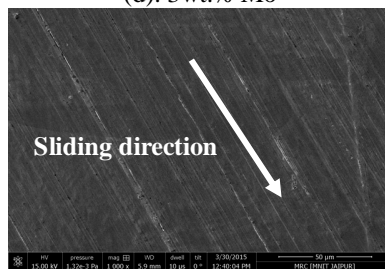
(d): 3wt.% Mo
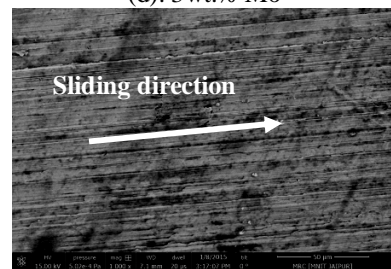
(e): 4wt.% Mo

Figure 4.7: SEM micrograph of different Mo content under dry conditions (load: 15 N and sliding distance: 1500 m)

(a): 0wt.% Mo

(b): 1wt.% Mo

(c): 2wt.% Mo

(d): 3wt.% Mo

(e): 4wt.% Mo

Figure 4.8: SEM micrograph of different Mo content under wet conditions (load: 15 N and sliding distance: 1500 m)

(a): 0wt.% Mo

(b): 1wt.% Mo

(c): 2wt.% Mo

(d): 3wt.% Mo

(e): 4wt.% Mo

Figure 4.9: SEM micrograph of different Mo content under dry condition (sliding velocity: 0.785 m/s and sliding distance: 1500 m)

(a): 0wt.% Mo   (b): 1wt.% Mo   (c): 2wt.% Mo

(d): 3wt.% Mo   (e): 4wt.% Mo
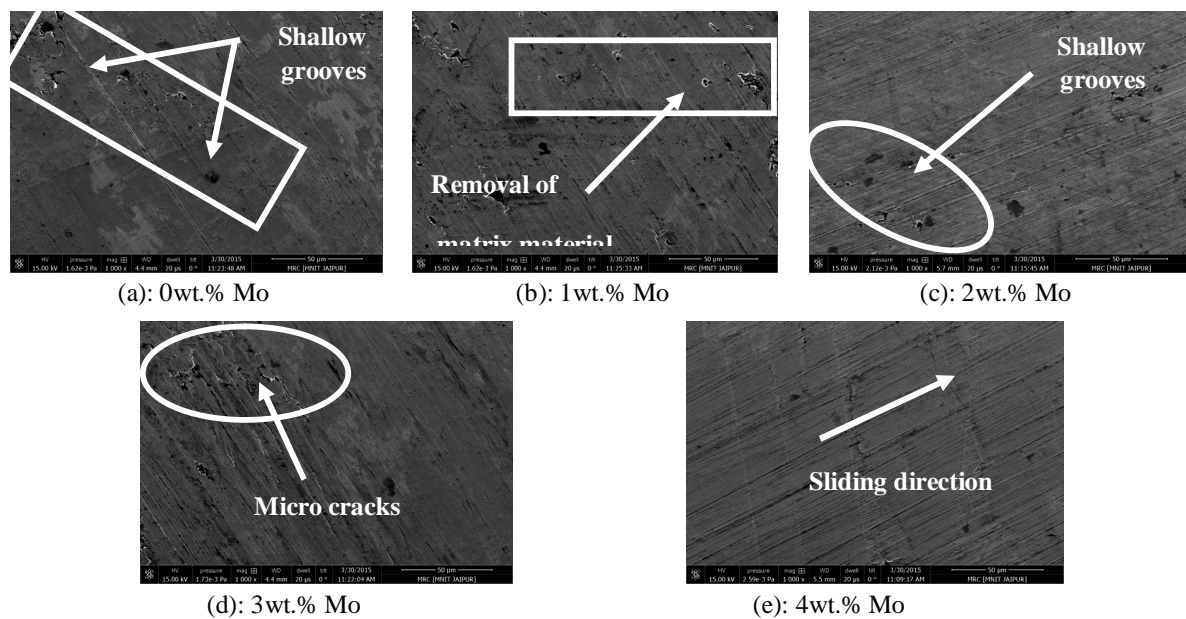
Figure 4.10: SEM micrograph of different Mo content under wet condition (sliding velocity: 0.785 m/s and sliding distance: 1500 m)

Similar, trend is observed under the wet condition as shown in Figure 4.10, the fabricated alloy composites i.e. pin is not directly contact with the counter disc because it fully covers with a layer of distilled water. Figure 4.10a shows the worn surface morphology of 0wt.% Mo particulate filled Co30Cr alloy composite at similar steady state condition as discussed earlier. This shows the formation of parallel and continuous abrasion grooves are less in place of dry condition shown in Figure 4.9a. This may be due to the presence of layer of distilled water between the pin and the counter disc along the sliding direction. As the filler content increases to 1wt.% (Figure 4.10b) the volumetric wear loss increases compared to 1wt.% of reinforcing particulates due to improper bonding in the matrix material. As far as 2wt.% and 3wt.% Mo particulate filled alloy composites the volumetric wear loss starts increasing under similar operating conditions as shown in Figures 4.10c and 4.10d respectively. The increased in wear loss is due to less uniform distribution in the matrix. Figure 4.10e shows the surface morphology of 4wt.% Mo particulate filled alloy composites. This shows the reduction of abrasion grooves and ploughing effect along the sliding wear direction due to reinforcement of hard molybdenum particulates in the alloy matrix composite as compared with other filler contents.
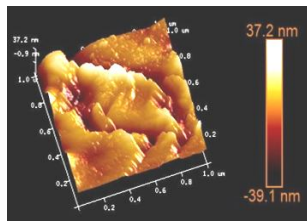
(a) 0 wt% Mo
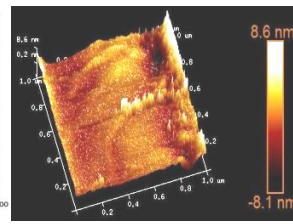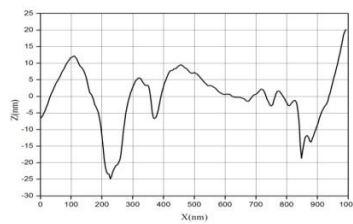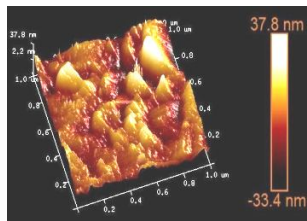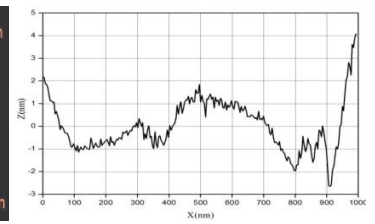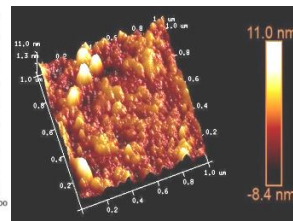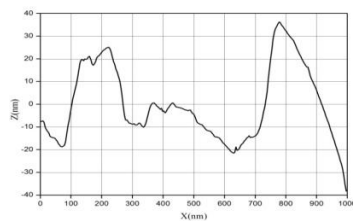
(b) 1 wt% Mo
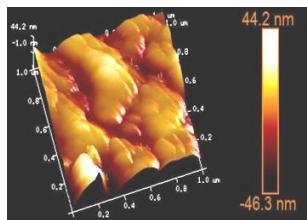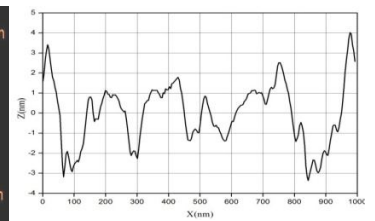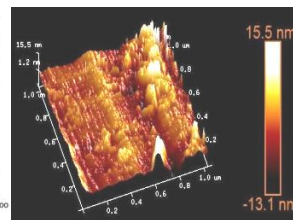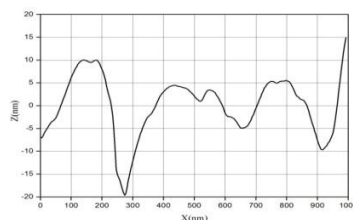
(c) 2 wt% Mo
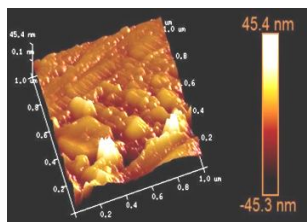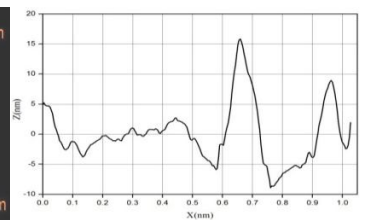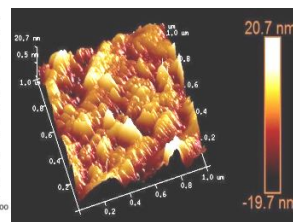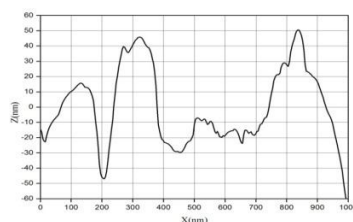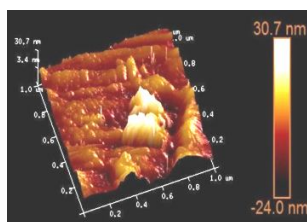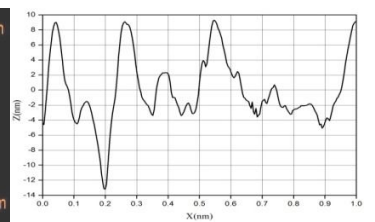
(d) 3 wt% Mo
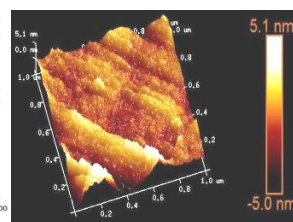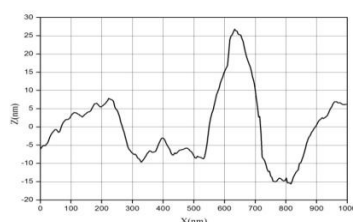
(e) 4 wt% Mo
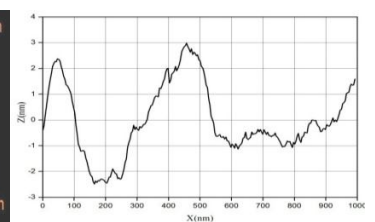
Figure 4.11: The 3D AFM micrographs and the line profiles of the molybdenum filled Co30Cr alloy composite under dry condition.

(a) 0 wt% Mo

(b) 1 wt% Mo

(c) 2 wt% Mo

(d) 3 wt% Mo

(e) 4 wt% Mo

Figure 4.12: The 3D AFM micrographs and the line profiles of the molybdenum filled Co30Cr alloy composite under wet condition.

Table 4.6 Surface Roughness of the fabricated molybdenum filled alloy composites

Designed alloys	Average surface roughness (R_a)	
	Dry Condition (nm)	Wet Condition (nm)
Co30Cr + 0 wt.% Mo	7.19	1.28 nm
Co30Cr + 1 wt.% Mo	6.61	1.78 nm
Co30Cr + 2 wt.% Mo	8.77	2.41 nm
Co30Cr + 3 wt.% Mo	5.89	4.11 nm
Co30Cr + 4 wt.% Mo	4.52	0.862 nm

4.2 Part II: B-Series alloy composite (Co30Cr4Mo) based on the variation of nickel filled particulate

The characterization of the fabricated alloy composites reveals that inclusion of weight fraction of Ni has strong influence not only on the mechanical properties of the alloys but also on their wear behavior under with and without water. The XRD diffractograms with a comparison for each sample are presented in Figure 4.13. These five different alloys are fabricated by the casting method [287]. It can be seen that the microstructure of 0wt.% Ni consists of a Co matrix with Cr and Mo regions. It is evident that Co, Cr, Ni, in alliance with oxides forms Co_xO_y, Cr_xO_y, Ni_xO_y in the microstructure respectively. The necessary oxides (O) could have arrived from two sources: from Co or from the atmosphere during mixing. Also, the hexagonal close-packed (HCP) Co structure has been formed for the reason that of the martensitic transformation [288]. No carbides are present in the microstructure, which corresponds well with the XRD peaks identified in 0-4 wt.% Ni content. In addition the compounds Co, Cr, Mo and Ni can be seen clearly confirming its presence (Figure 4.14).On the other hand, in all the samples, the fcc (111, 200, 220) cobalt base α matrix, bcc (110) Cr, bcc (110) Mo, and fcc (111) CrNi were identified. An additional rhombohedral Co7Mo6 (116) phase, a tetragonal Co_2Mo_3 (411), $NiCr_2O_4$ (220), MoNi4 (002) phase, were identified.
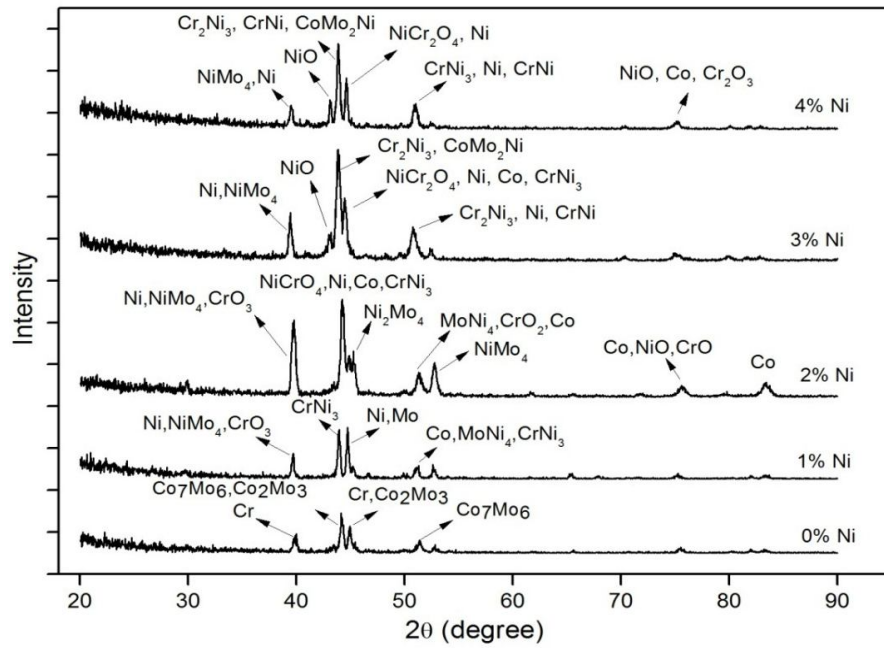
Figure 4.13: XRD patterns of fabricated nickel filled Co-30Cr-4Mo alloy composite.
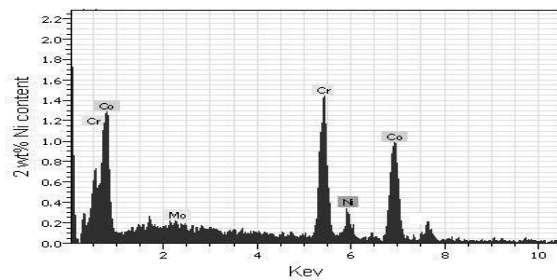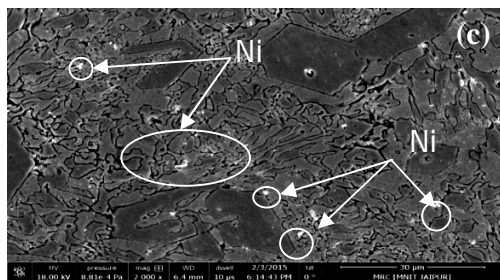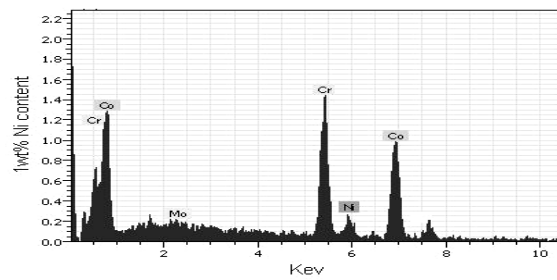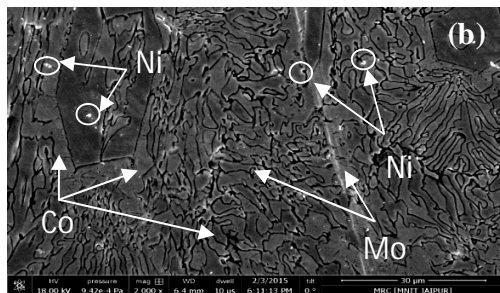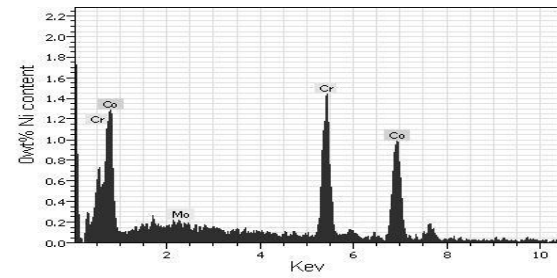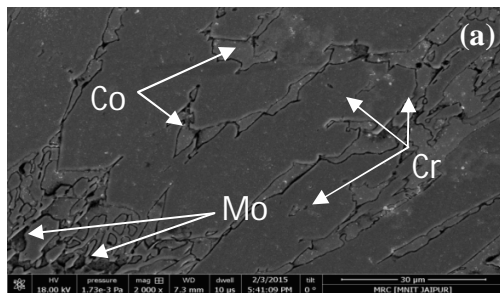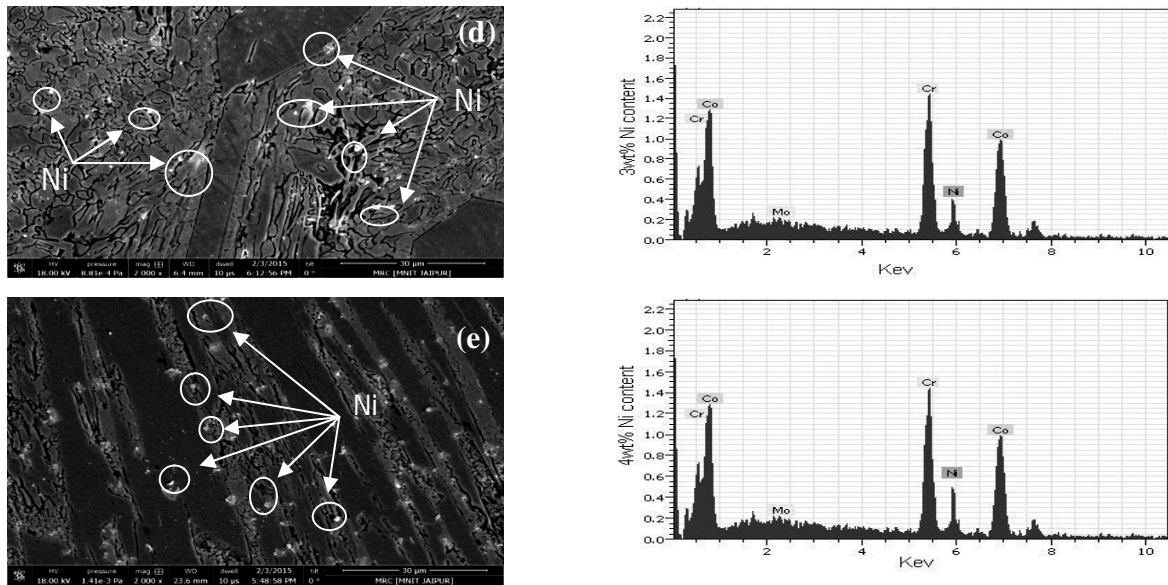
Figure 4.14: SEM micrographs and corresponding EDS results of nickel filled Co-30Cr-4Mo alloy composite:(a) 0wt.% Ni, (b) 1wt.% Ni, (c) 2wt.% Ni,(d) 3wt.% Ni and (e) 4wt.% Ni

The XRD patterns obtained have a number of similarities with other Co-Cr-Mo alloys viz ASTM F75, ASTM F1537 or studied in the literature [291-293]. Scanning electron microscopy (SEM) images and their corresponding energy dispersive spectrometer (EDS) of the microstructure of samples N0, N1, N2, N3 and N4, with inclusion of nickel content are shown in Figure 4.14. It can be seen that the cobalt based solid solution is in dark grey, chromium is in light grey and, in different shades of black, the molybdenum contents. In addition, the small white spots demonstrate the weight fraction of nickel content.

4.2.1 Physical and Mechanical Properties of alloy Composites

4.2.1.1 Density

The density of the fabricated nickel (0-4wt.%) filled Co-30Cr-4Mo alloy composites are shown in Figure 4.15a. It is clearly seen that the unfilled alloy composite (i.e. 0wt.% Ni) attained 8.7gm/cc. Afterwards, the density is decreased then significantly increased with the addition of nickel content up to 4wt.% (Table 4.7). The increase in density specifies that particle breakage may not have any significant influence on the alloy. It is believed to attain an enrichment of the bonding between the particle and metal matrix (Co-Cr-Mo). The densities obtained with the addition of nickel content (0-4wt.% Ni) are closed to the values as per ASTM F75 [56, 291].
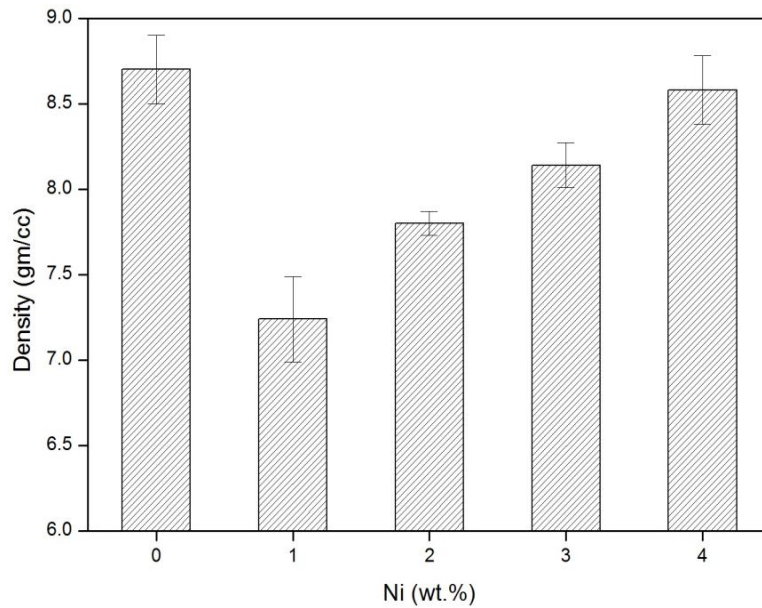
Figure 4.15a: Variation of density with Ni content

4.2.1.2 Micro-hardness

Figure 4.15b illustrates the simplified representation the variation of micro-hardness of nickel filled Co-30Cr-4Mo alloy composite. The micro-hardness is measured at six distinct locations and after measuring the micro-hardness of the entire identified region, the mean micro-hardness is taken in this study. It is noticed that the hardness attained 61 HRC at 0wt.% Ni filled alloy composite (Table 4.7). Afterwards, as the weight percentage of nickel enhances the hardness of the alloy composites also enhances. The addition of nickel particles increases the dislocation density of the matrix alloy. So the interaction bonding between the filler (Ni) and matrix increases the micro-hardness of alloy composites. Similar, trends also reported by Savas and Alemdag [79] and Choudhury et al. [299].

4.2.1.3 Compression strength

Figure 4.15c illustrates the variation of compression strength of the fabricated alloy composites (Co-30Cr-4Mo) with the Ni contents. A gradual increase in compressive strength with the weight percentage of Ni (1wt.%, 2wt.%, 3wt.% and 4wt.%) is noticed. It evidently indicates that the inclusion of Ni improves the load bearing capacity of the alloys (Table 4.7).
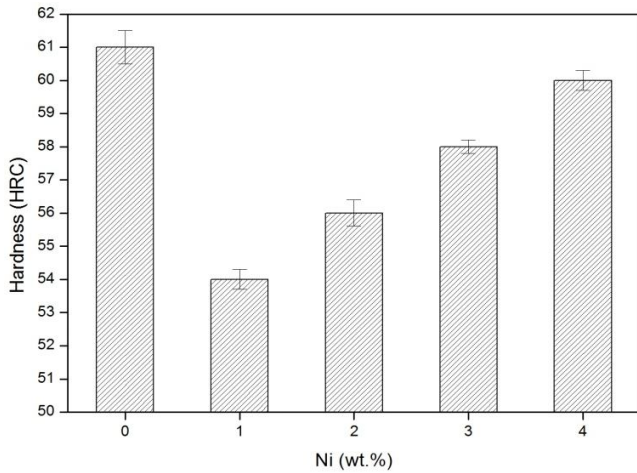
Figure 4.15b: Variation of micro-hardness with Ni content
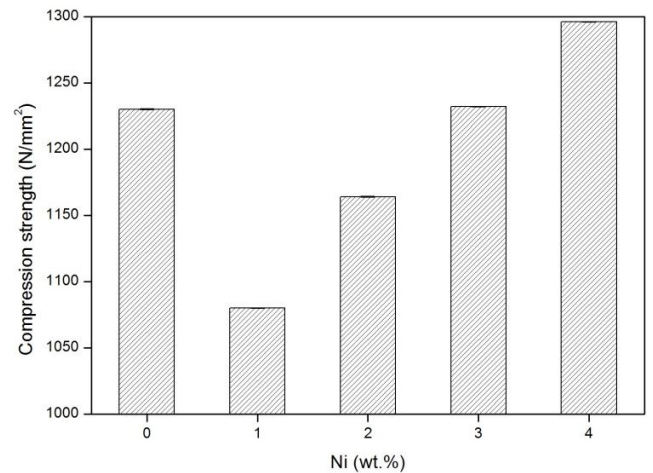
Figure 4.15c: Variation of compression strength with Ni content

Table 4.7 Physical and mechanical properties of nickel filled alloy composite

Alloys	Density (gm/cc)	Hardness (HRC)	Compression strength (N/mm2)
B0	8.70	61	1230
B1	7.24	54	1080
B2	7.80	56	1164
B3	8.14	58	1232
B4	8.58	60	1296

4.2.2 Sliding Wear Behavior of Composites

4.2.2.1 Influence of Sliding Velocity on volumetric wear loss of Particulate filled alloy composites

The steady state sliding wear analysis is carried out by varying one factor at-a-time i.e. sliding velocity and rest all other factors remaining constant (i.e. normal load: 15N and sliding distance: 1500m) respectively to obtain the volumetric wear loss of the particulate filled alloy composites. Figure 4.16a shows the volumetric wear loss gradually increased with the increased in sliding velocity irrespective of filler content in both dry and wet medium. The volumetric wear loss is maximum in 2wt.% Ni particulate filled alloy composites and minimum in 1wt.% Ni particulate filled alloy composites in both dry and wet medium (Figure 4.16a). It is interesting to note that the volumetric wear loss of fabricated alloy composite obtained in this study is very close to the previous researchers [300, 301]. Whereas, in 3wt.% and 4wt.% Ni particulate filled alloy

composites show slightly more volumetric wear loss as compared with 1wt.% Ni particulate filled alloy composites in both dry and wet medium. This may be the cause of incompatible in addition of higher percentages of nickel particulates in fabricated Co-30Cr-4Mo alloy composites. However, Figure 4.16a shows the maximum wear resistant for unfilled alloy composite as compared to nickel filled Co-30Cr-4Mo metal matrix materials.
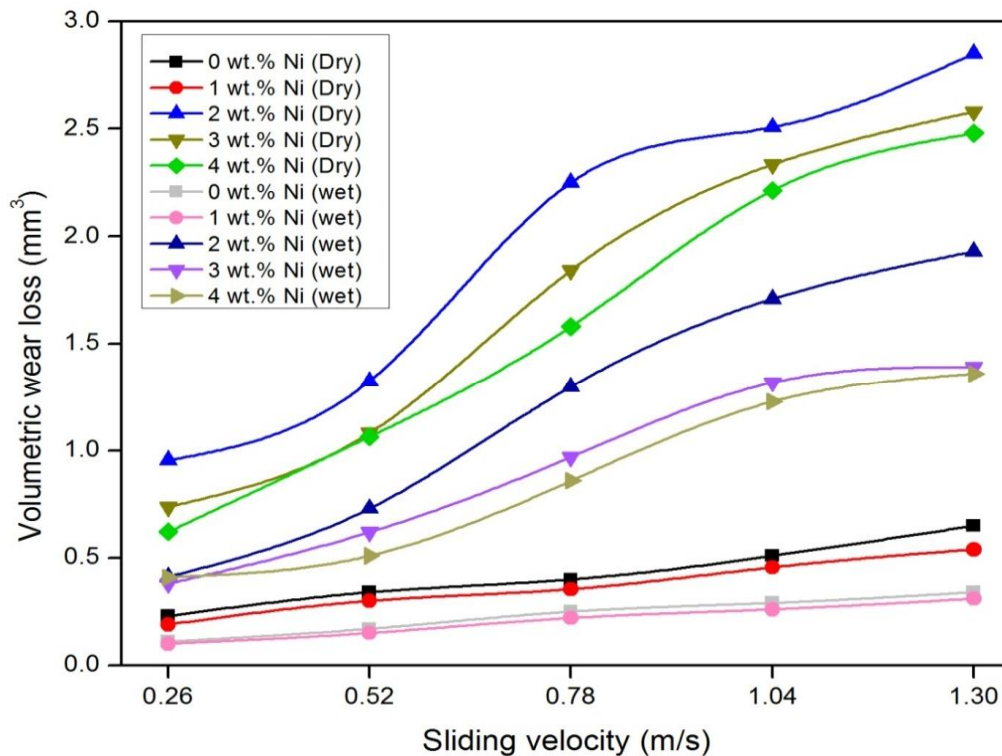
Figure 4.16a: Variation of volumetric wear with sliding velocity for Co30Cr4Mo alloy under dry and wet condition (load: 15 N and sliding distance 1500m)

Figure 4.16(b) shows the effect of sliding velocity on friction coefficient of different Ni particulates filled alloy composites (at load: 15 N and sliding distance 1500m) in both dry and wet medium. At the primary stage of rubbing, friction is low and the factors accountable for this low friction are due to the presence of a layer of foreign material on the disc surface. This layer on the disc surface in general constitutes; moisture; oxide of metals; deposited lubricating material, etc. After starting rubbing, the saved layer separates and clean surfaces come in contact which increases the bonding force between the contacting surfaces. A similar finding is reported by Savas et al. [79]. It is clear from the Figure 4.16b that the mean steady state value of friction coefficients is initially low among all the Ni filled particulates. Thereafter, it gradually increases up to

0.523m/s and then decreases further increase in the sliding velocity (i.e. 0.78m/s). The similar manner of friction coefficient is obtained further increase the sliding velocity up to 1.3m/s. It is also observed that the 1wt.% Ni displays least effect in the variation of friction coefficient with sliding velocity.
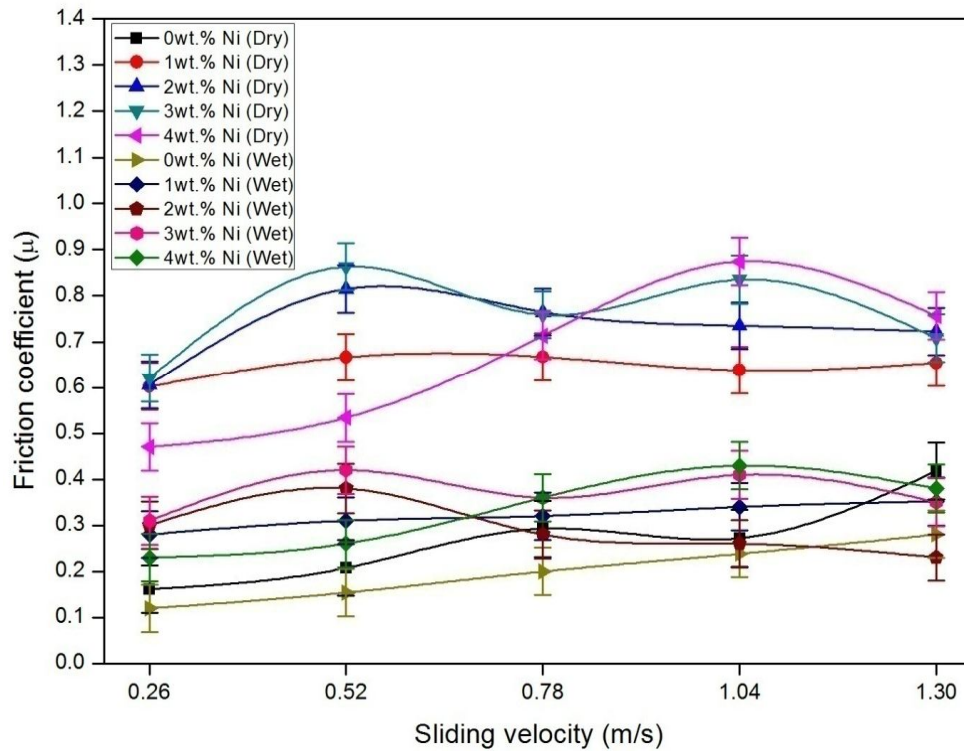
Figure 4.16b: Variation of coefficient of friction with sliding velocity for Co30Cr4Mo alloy under dry and wet condition (load: 15 N and sliding distance 1500m)

4.2.2.2 Influence of normal load on volumetric wear loss of particulate filled alloy composites

In the present study, the steady state volumetric wear loss is evaluated as a function of normal load under constant sliding velocity and sliding distance i.e. 0.785m/s and 1500m respectively for Ni filled Co30Cr4Mo alloy in dry and wet both conditions is shown in Figure 4.17(a). It is clearly seen that the volumetric wear loss steadily increases if the normal load increased from 5N to 25N. As the load on the pin is enhanced the actual area of contact would enhance towards the nominal contact area, consequently that increase the frictional force between two sliding surfaces. The enhanced frictional force and real surface area in contact cause higher wear. This implies that the shear force and frictional thrust are increased with increase of applied load and this accelerates the volumetric wear. Out of all the samples, 1wt.% Ni exhibits a lesser wear loss than the others nickel

filled (2wt.%, 3wt.% and 4wt.%) alloy composites. In this study the material used for pin and counter disc are both different and the value obtained of volumetric wear is in the range of cobalt based alloy [66, 302]. Some authors used the same material of both pin and disc instead of dissimilar materials. Firkins et al. [297] used CoCr alloy for both the pin and disc material and found the wear behavior is likely similar to the present study. Doni et al. [298] compared the dry sliding wear behavior under 1N normal load of hot pressed CoCrMo implant material with commercially cast CoCrMo and Ti6Al4V implant materials and found the wear loss of Ti6Al4V alloy is 14 and 47 times higher than the cast and hot pressed CoCrMo samples respectively. Similar trends of variation were also observed for mild steel–mild steel couples, i.e. wear loss increases with the increase in normal load [303, 304].
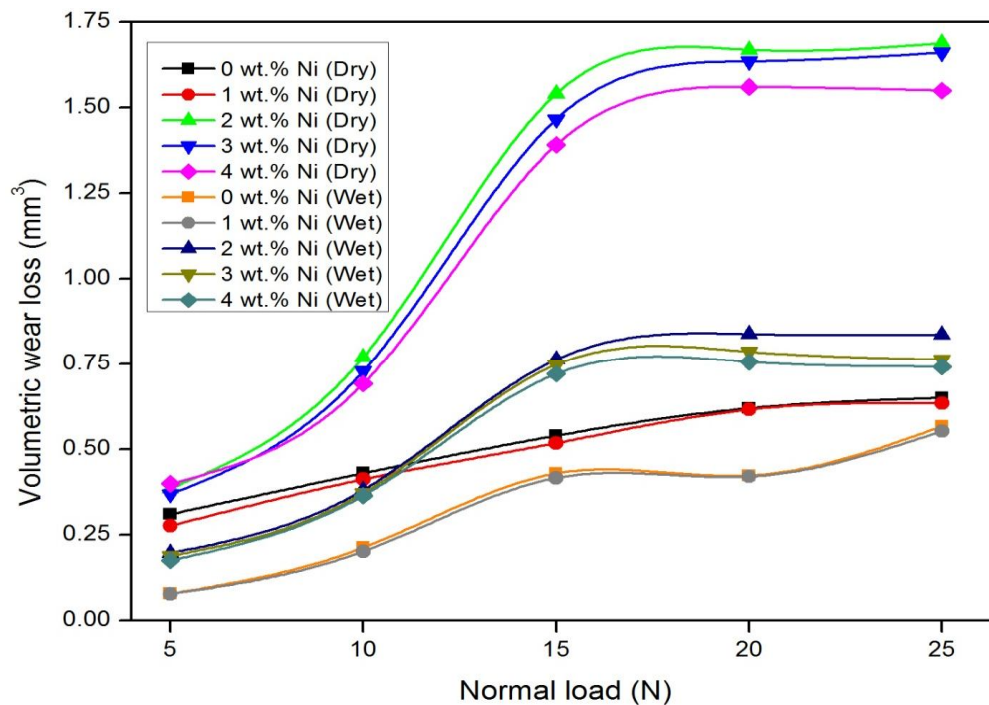
Figure 4.17a: Variation of volumetric wear with normal load for Co30Cr4Mo alloy under dry and wet condition (Sliding velocity: 0.785 m/s and sliding distance 1500m)

The coefficient of friction versus normal load, i.e. operating duration at sliding conditions of 0.785 m/s and 1500 m, are presented in Figure 4.17(b). As shown in Figure 4.17b, the coefficient of friction of the fabricated alloy composites (i.e. Co30Cr4Mo) for both dry and wet conditions with various nickel filler contents exhibited considerably low at the initial stage. The current experimental results are explicable: during initial stages, the surfaces of both the alloy

specimens and the steel counterpart were smooth due to the presence of a layer of foreign materials including moisture, oxide of metals, deposited lubricating materials, etc. and thus strong saved layer between the specimen and the counterpart, resulting in a low friction coefficient. As the wear continued, the layer break up and the clean surface come in directly contact with the specimen and gradually increases the coefficients of friction are achieved when a steady wear stage is reached up to 10N load when inclusion of 1-3wt.% of Ni in the fabricated alloy composite whereas, in 4wt.% of Ni friction coefficient is gradually decrease up to same loading condition (i.e. 10N) under dry condition. Thereafter, it rapidly increases up to 20N load and it again steadily decreased up to 25N load for similar operating conditions (see Figure 4.17b). At 15N load, the friction coefficient of 1wt.% and 2wt. % of Ni particulate filled alloy composites rapidly decreases while 3wt.% of Ni filled alloy composites gradually increases the friction coefficient up to 25N load. Similar behavior is attained, for 1wt.% of Ni particulate filled alloy composites under similar loading condition (i.e. 25N load). For similar operating conditions 2wt.% and 4wt.% of Ni particulate filled alloy composites the friction coefficient is first increased and it again gradually decrease for the rest of the experiment load (i.e. 25N) for dry conditions. However, the friction coefficient of unfilled alloy composite is gradually increased from 5N to 25N under dry condition.
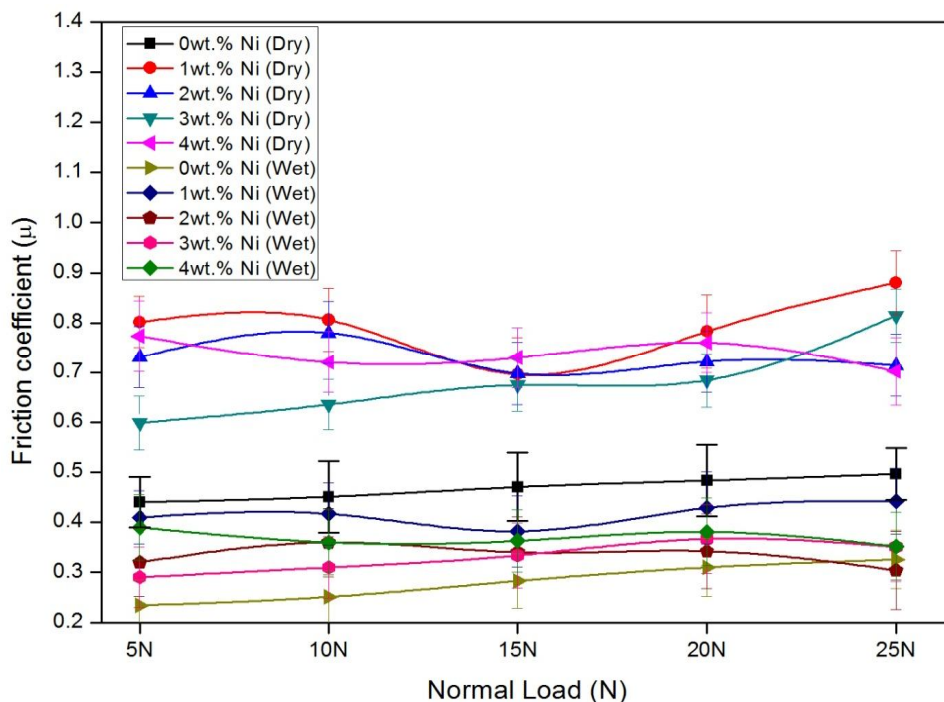
Figure 4.17b: Variation of coefficient of friction with normal load for Co30Cr4Mo alloy under dry and wet condition (Sliding velocity: 0.785m/s and sliding distance 1500m)

For wet condition (i.e. pin slides on the disc which covers the layer of distilled water) 1wt.%, 2wt.% and 3wt.% of Ni particulate filled alloy composites the friction coefficient first increases up to 10N load then it decreases at 15N load under similar operating condition as considered for dry medium. Whereas, 4wt.% of Ni particulate filled alloy composites works as opposite in nature i.e. the friction coefficient gradually decreases up to 15N load (see Figure 4.17b). Thereafter, it slightly increases at 20N load and again it decrease for the rest of the experiment load i.e. 25N. Similar manner observed for 1, 2 and 3wt. % Ni particulate filled alloy composites on same loading condition i.e. 25N. A similar finding is reported by Yamanoglu et al. [300].

4.2.3 Taguchi Experimental Analysis

Table 4.8 shows the wear loss of particulate filled alloy composites and their respective S/N ratio values. The sixth and eleventh column represents the volumetric wear loss of the dry and wet medium of the proposed alloy composites and each experiment is repeated three times and the mean value of wear loss and their corresponding standard deviation is reported in Table 4.8. The overall mean for the S/N ratio of the wear loss under dry and wet sliding condition are found to be 43.30232 dB and 62.70246 dB respectively. Similarly, the overall mean for the S/N ratio of the friction coefficient for both sliding conditions are found to be 7.9878 dB and 15.311 dB respectively. Figures 4.16a-4.16d show graphically the effect of the four control factors on volumetric wear loss in dry and wet sliding conditions. Analysis of the result leads to the conclusion that factor combination of $A_5B_1C_5D_2$ and $A_5B_1C_5D_2$ gives minimum wear volume in dry and wet conditions respectively for the fabricated alloy composite (Figure 4.16a and Figure 4.16b). Similarly, the factor combination of $A_2B_2C_3D_2$ gives minimum friction coefficient in dry condition and $A_1B_2C_3D2$ in wet condition for the fabricated alloy composites respectively (Figure 4.16c and Figure 4.16d).

Table 4.8 Experimental design using L_{25} orthogonal array

Runs	A	B	C	D	Dry Condition					Wet Condition				
					wear loss (mm^3)	Standard deviation	S/N Ratio (db)	Friction Coeff.	S/N Ratio (db)	wear loss (mm^3)	Standard deviation	S/N Ratio (db)	Friction Coeff.	S/N Ratio (db)
1	5	0.26	500	0	0.0858	0.000306	21.3320	0.26	15.947	0.0092000	0.00002	40.7242	0.03	31.375
2	5	0.523	1000	1	0.0276	0.000200	31.1818	0.18	15.072	0.0026400	0.00001	51.5679	0.03	31.903
3	5	0.785	1500	2	0.0343	0.000200	29.3026	0.06	11.867	0.0042800	0.00003	47.3711	0.04	28.707
4	5	1.04	2000	3	0.0123	0.000200	38.2019	0.26	11.640	0.0010800	0.00002	59.3315	0.11	19.514
5	5	1.3	2500	4	0.0119	0.000361	38.4745	0.37	8.626	0.0011520	0.00002	58.7710	0.13	17.804
6	10	0.26	1000	2	0.0231	0.000100	32.7278	0.17	15.356	0.0028000	0.00003	51.0568	0.10	20.291
7	10	0.523	1500	3	0.0115	0.000230	38.8113	0.04	19.679	0.0011267	0.00003	58.9641	0.02	34.563
8	10	0.785	2000	4	0.0073	0.000310	42.7335	0.20	13.852	0.0006900	0.00001	63.2230	0.10	19.933
9	10	1.04	2500	0	0.0027	0.000152	51.3727	0.43	7.304	0.0002200	0.00001	73.1515	0.21	13.654
10	10	1.3	500	1	0.0662	0.000143	23.5828	0.05	10.161	0.0068000	0.00001	43.3498	0.13	18.020
11	15	0.26	1500	4	0.0044	0.000306	47.2191	0.46	6.679	0.0003956	0.00002	68.0559	0.22	13.288
12	15	0.523	2000	0	0.0033	0.000200	49.7179	0.47	6.634	0.0002500	0.00003	72.0412	0.22	13.193
13	15	0.785	2500	1	0.0018	0.000102	55.0897	0.73	2.722	0.0001413	0.00003	76.9951	0.47	6.6430
14	15	1.04	500	2	0.0548	0.000107	25.2244	0.53	5.515	0.0060000	0.00002	44.4370	0.26	11.556
15	15	1.3	1000	3	0.0142	0.000198	36.9542	0.85	1.362	0.0014400	0.00001	56.8328	0.49	6.2380
16	20	0.26	2000	1	0.0015	0.000176	56.1934	0.33	9.596	0.0001550	0.00001	76.1934	0.25	12.200
17	20	0.523	2500	2	0.0010	0.000173	60.1755	0.83	1.598	0.0009600	0.00003	60.3546	0.35	9.0380
18	20	0.785	500	3	0.0209	0.000157	33.5971	0.75	2.469	0.0019800	0.00003	54.0667	0.38	8.4830
19	20	1.04	1000	4	0.0046	0.000200	46.6509	0.84	1.495	0.0003750	0.00002	68.5194	0.43	7.2740
20	20	1.3	1500	0	0.0017	0.000306	55.2224	0.75	2.524	0.0001800	0.00002	74.8945	0.36	8.8490
21	25	0.26	2500	3	0.0004	0.000361	67.6181	0.69	3.267	0.0000448	0.00002	86.9744	0.29	10.759
22	25	0.523	500	4	0.0105	0.000100	39.5928	0.14	12.494	0.0010240	0.00001	59.7940	0.31	10.286
23	25	0.785	1000	0	0.0048	0.000157	46.3752	0.77	2.259	0.0004840	0.00001	66.3031	0.41	7.7260
24	25	1.04	1500	1	0.0012	0.000200	58.6116	0.50	5.940	0.0001013	0.00002	79.8850	0.24	12.357
25	25	1.3	2000	2	0.0015	0.000200	56.5948	0.52	5.636	0.0001840	0.00001	74.7036	0.35	9.1270

(a)

(b)

(c)

(b)
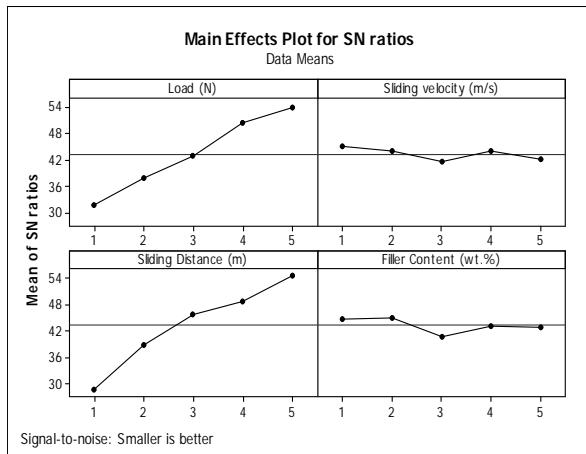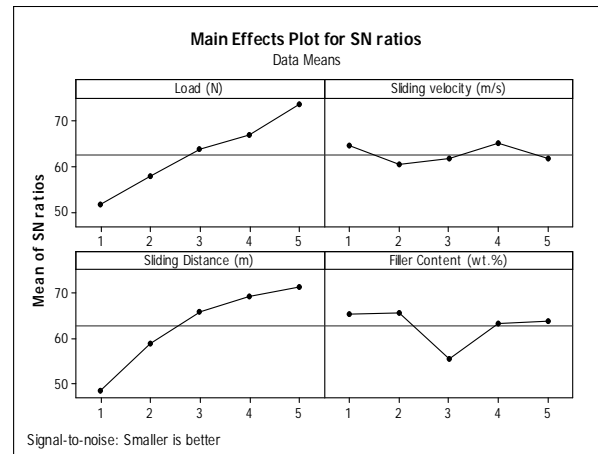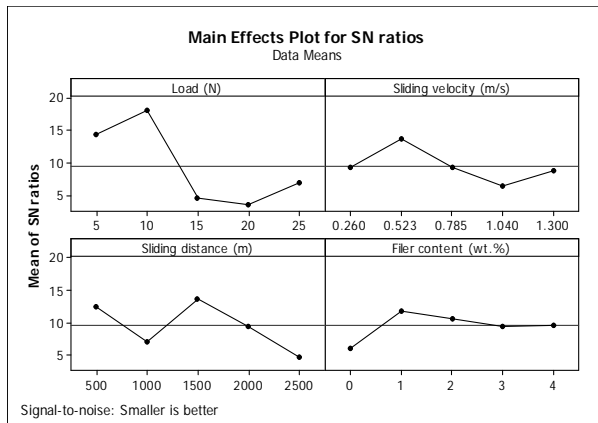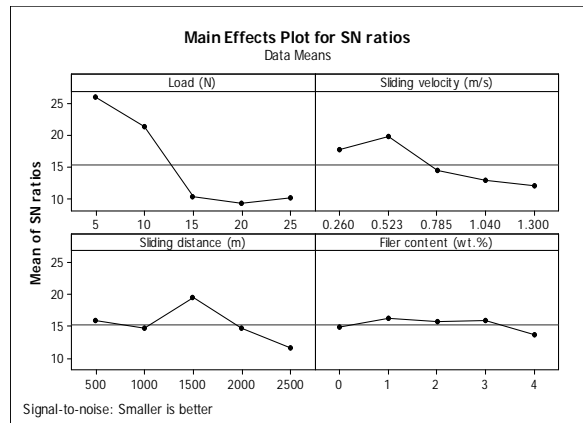
Figure 4.18: (a) Effect of control factors on volumetric wear loss for Ni filled Co-30Cr-4Mo alloy composites under dry condition; (b) Effect of control factors on volumetric wear loss for Ni filled Co-30Cr-4Mo alloy composites under wet condition; (c) Effect of control factors on friction coefficient for Ni filled Co-30Cr-4Mo alloy composites under dry condition; (d) Effect of control factors on friction coefficient for Ni filled Co-30Cr-4Mo alloy composites under wet condition

4.2.4 Confirmation Experiment

The confirmation experiment is the final step in the design of experiment process. The purpose of the confirmation experiment is to validate the conclusions drawn during the analysis phase. The confirmation experiment is performed by conducting a new set of factor settings $A_4B_2C_5D_3$ for dry condition and $A_5B_2C_4D_1$ for wet condition to predict the volumetric wear loss. Similarly, a new set of factor settings $A_3B_1C_2D_3$ and $A_3B_1C_2D_2$ to predict the friction coefficient for both the conditions. The estimated S/N ratio for wear loss can be calculated by the predictive equation:

$$\hat{\eta}_{dry_w} = \bar{\eta} + (\overline{A_4} - \bar{\eta}) + (\overline{B_2} - \bar{\eta}) + (\overline{C_5} - \bar{\eta}) + (\overline{D_3} - \bar{\eta}) \tag{4.9}$$

$$\hat{\eta}_{dry_\mu} = \bar{\eta} + (\overline{A_3} - \bar{\eta}) + (\overline{B_1} - \bar{\eta}) + (\overline{C_2} - \bar{\eta}) + (\overline{D_3} - \bar{\eta}) \tag{4.10}$$

$$\hat{\eta}_{wet_w} = \bar{\eta} + (\overline{A_5} - \bar{\eta}) + (\overline{B_2} - \bar{\eta}) + (\overline{C_4} - \bar{\eta}) + (\overline{D_1} - \bar{\eta}) \tag{4.11}$$

$$\hat{\eta}_{wet_\mu} = \bar{\eta} + (\overline{A_3} - \bar{\eta}) + (\overline{B_1} - \bar{\eta}) + (\overline{C_2} - \bar{\eta}) + (\overline{D_2} - \bar{\eta}) \tag{4.12}$$

Where $\hat{\eta}_w$: predicted average of wear volume, $\hat{\eta}_\mu$: predicted average of friction coefficient, $\bar{\eta}$: overall experimental average, $\overline{A_4}, \overline{B_2}, \overline{C_5}, \overline{D_3}$ for wear volume and $\overline{A_3}, \overline{B_1}, \overline{C_2}, \overline{D_3}$ for friction coefficient under dry condition and $\overline{A_5}, \overline{B_2}, \overline{C_4}, \overline{D_1}$ for wear volume and $\overline{A_3}, \overline{B_1}, \overline{C_2}, \overline{D_2}$ for friction coefficient under wet condition are the mean response for factors at designated levels. By combining like terms, the equation reduces to:

$$\hat{\eta}_{dry_w} = \overline{A_4} + \overline{B_2} + \overline{C_5} + \overline{D_3} - 3\bar{\eta} \tag{4.13}$$

$$\hat{\eta}_{dry_\mu} = \overline{A_3} + \overline{B_1} + \overline{C_2} + \overline{D_3} - 3\bar{\eta} \tag{4.14}$$

$$\hat{\eta}_{wet_w} = \overline{A_5} + \overline{B_2} + \overline{C_4} + \overline{D_1} - 3\bar{\eta} \tag{4.15}$$

$$\hat{\eta}_{wet_\mu} = \overline{A_3} + \overline{B_1} + \overline{C_2} + \overline{D_2} - 3\bar{\eta} \tag{4.16}$$

A new combination of factor levels $\overline{A_4}, \overline{B_2}, \overline{C_5}, \overline{D_3}$ and $\overline{A_5}, \overline{B_2}, \overline{C_4}, \overline{D_1}$ are used to predict volumetric wear loss by using prediction equation (Eqs. 4.13 and 4.15) and the S/N ratio is found to be 59.6589 dB and 80.4095 dB for dry and wet sliding condition respectively. Similarly, factor levels $\overline{A_3}, \overline{B_1}, \overline{C_2}, \overline{D_3}$ and $\overline{A_3}, \overline{B_1}, \overline{C_2}, \overline{D_2}$ are used to predict the friction coefficient by using prediction equations (Eq. 4.14 and 4.16) and the S/N ratio is found to be 3.09734 dB and 12.7442 dB for dry and wet sliding condition respectively. The resulting model seems to be capable of predicting wear to a reasonable accuracy. An error of under dry and wet sliding condition for S/N ratio of wear volume and friction coefficient is observed as shown in Table 4.9. However, the error can be further reduced if the number of measurement will be expanded. This validates the development of the mathematical model for predicting the measures of performance based on knowledge of the input parameters.

Table 4.9 Results of the confirmation experiments for wear volume and friction coefficient

	Dry condition		Wet condition	
	S/N ratio for wear volume (db)	S/N ratio for friction coefficient (db)	S/N ratio for wear volume (db)	S/N ratio for friction coefficient (db)
Levels	$A_4B_2C_5D_3$	$A_3B_1C_2D_3$	$A_5B_2C_4D_1$	$A_3B_1C_2D_2$
Prediction	59.6589	3.09734	80.4905	12.7442
Experimental	60.198	3.4521	81.015	13.6154
Error (%)	0.89	0.10	0.64	0.063

4.2.5 ANOVA and the Effect of Factors

In order to understand a concrete visualization of impact of various factors like normal load (A), sliding velocity (B), sliding distance (C) and filler content (D) on wear loss, it is enviable to develop analysis of variance (ANOVA) table to find out the order of significant factors. Table 4.10 demonstrates the results of the ANOVA with the volumetric wear loss assuming a level of significance of 5% under dry and wet sliding condition respectively.

Table 4.10 ANOVA table for volumetric wear loss

Source	Degree of freedom (DF)	Seq SS	Adj SS	Adj MS	F	P
Dry condition						
A	4	0.0031384	0.0031384	0.0007846	6.73	0.011
B	4	0.0004580	0.0004580	0.0001145	0.98	0.469
C	4	0.0065117	0.0065117	0.0016279	13.96	0.001
D	4	0.0007970	0.0007970	0.0001993	1.71	0.240
Error	8	0.0009326	0.0009326	0.0001166		
Total	24	0.0118378				
Wet condition						
A	4	0.0000349	0.0000349	0.0000087	5.69	0.018
B	4	0.0000051	0.0000051	0.0000013	0.84	0.538
C	4	0.0000704	0.0000704	0.0000176	11.48	0.002
D	4	0.0000139	0.0000139	0.0000035	2.26	0.152
Error	8	0.0000123	0.0000123	0.0000015		
Total	24	0.0001366				

The last column of the table designates the probability of significance of major control factors. It has been noticed that sliding distance (p = 0.001), load (p = 0.011), filler content (p = 0.240), and sliding velocity (p = 0.469) for dry sliding condition and sliding distance (p = 0.002), load (p = 0.018), filler content (p = 0.152) and sliding velocity (p = 0.538) for wet sliding condition are significant in the declining order of importance on wear loss. Likewise it has been noticed that (Table 4.11) normal load (p = 0.000), sliding distance (p = 0.009), sliding velocity (p = 0.017), and filler content (p = 0.233) for dry sliding condition and normal load (p = 0.000), sliding velocity (p = 0.019), sliding distance (p = 0.021) and filler content (p = 0.754) for wet sliding condition are significant in the declining order of importance on friction coefficient.

Table 4.11 ANOVA table for friction coefficient

Source	Degree of freedom (DF)	Seq SS	Adj SS	Adj MS	F	P
Dry condition						
A	4	0.901091	0.901091	0.225273	27.02	0.000
B	4	0.192714	0.192714	0.048179	5.78	0.017
C	4	0.246511	0.246511	0.061628	7.39	0.009
D	4	0.058103	0.058103	0.014526	1.74	0.233
Error	8	0.066692	0.066692	0.008336		
Total	24	1.465112				
Wet condition						
A	4	0.375198	0.375198	0.093800	37.16	0.000
B	4	0.056570	0.056570	0.014142	5.60	0.019
C	4	0.054068	0.054068	0.013517	5.36	0.021
D	4	0.004799	0.004799	0.001200	0.48	0.754
Error	8	0.020192	0.020192	0.002524		
Total	24	0.510827				

4.2.6 Surface Morphology

Figures 4.19-4.22 show the morphology of worn surfaces of nickel particulate filled Co30Cr4Mo alloy composites under dry and wet (a layer of distilled water used between the pin and the counter disc) condition. The SEM characterization is carried out by using a FEI NOVA NANOSEM 450 with an energy dispersive spectroscopy (EDS) attached to analyze the chemical composition of different phases and wear mechanisms induced by the pin-on-disc test. Figure 4.19 shows the worn

surface morphology of nickel particulate filled Co30Cr4Mo alloy composites by varying sliding velocity under dry condition (Taken from Figure 4.16a) at constant normal load: 15N and sliding distance: 1500m. Figure 4.19a shows the worn surface morphology of the unfilled alloy composite where the presence of reinforced particles becomes negligible at constant sliding velocity 1.3m/sec, normal load 15N and sliding distance 1500m respectively (See Figure 4.16a). However, under similar operating condition the worn surface morphology of 1wt.% Ni particulate filled alloy composite the formation of micro ploughing and parallel and continuous grooves are reduced on the surface shown in Figure 4.19b. The reduction of volumetric wear loss is due to good bonding of reinforcement in the alloy matrix composite. Again, with further increased in filler content in the alloy composite (2wt.% Ni) the volumetric wear loss is more and formation of cracks and shallow grooves are more as compared with other two compositions (See steady state Figure 4.16a and morphology Figure 4.19c) due to which the interfacial bonding in between the particles is not so strong and the material is removed from surface during the sliding wear process. As far as 3wt.% and 4wt.% Ni particulate filled alloy composites the volumetric wear starts increasing and parallel and continuous shallow and deep abrasion grooves are formed along the sliding direction under similar operating conditions as shown in Figures 4.19d and 4.19e respectively. The increased in wear loss is due to poor bonding between the hard particulates and matrix material (See steady state Figure 4.16a) and there may be chances of formation of delamination wear in the subsurface of the worn area. As the subsurface cracks are clearly visible in the micrographs (Figures 4.19d and 4.19e) and delamination wear may also occurred in some worn region which covered by the adhered hard particulate filled materials under high load operating condition.

Figure 4.20 shows the worn surface morphology of nickel particulate filled Co30Cr4Mo alloy composites by varying sliding velocity under a smooth layer of distilled water i.e. wet condition (Taken from Figure 4.16a) at constant normal load: 15 N and sliding distance: 1500 m. This layer is almost fully covers the wear track as compare with dry condition (See Figure 4.20a) along the sliding direction for 0wt.% Ni particulate filled Co30Cr4Mo alloy composite at constant sliding velocity 1.3m/sec, normal load 15N and sliding distance 1500m respectively(See Figure 4.16a). However, under similar conditions the worn surface morphology of 1wt.% Ni particulate filled alloy composite, shown in Figure 4.20b, appears to be smooth with no shallow grooves and continuous ploughing effect as compared to other filler content of alloy composites under dry condition. The fine surface occurs may be due to the presence of layer of distilled water during

sliding lessens the wear of both disc and the counter pin. As the filler content further increased in the alloy composite i.e. 2wt.% Ni the volumetric wear is still further diminished from the surface and formation of crack also diminished as compared with other two compositions (See steady state Figure 4.19a and morphology Figure 4.20c). As far as 3wt.% and 4wt.% Ni particulate filled alloy composites the volumetric wear starts increasing and relatively more parallel and continuous wear scars are occurs under similar operating conditions as shown in Figures 4.20d and 4.20e respectively. The obtained worn surfaces are similar to previous studies in our research group [297]. From this analysis, it is observed that, the 1wt. % Ni particulate filled alloy composite attained minimum volumetric wear loss as compared with other composition under similar operating condition (at load: 15 N and sliding distance: 1500 m) in both dry and wet condition.
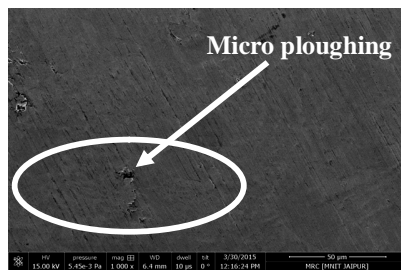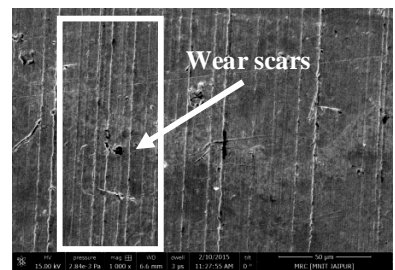
(a): 0wt.% Ni

(a): 0wt.% Ni

(a): 0wt.% Ni
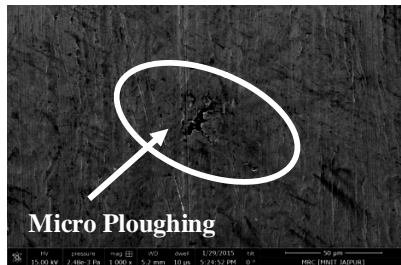
(b): 1wt.% Ni
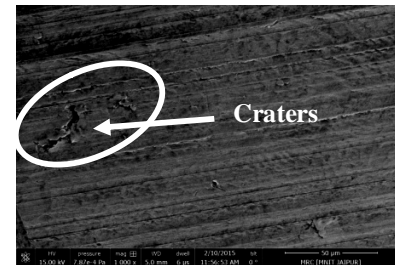
(b): 1wt.% Ni

(b): 1wt.% Ni
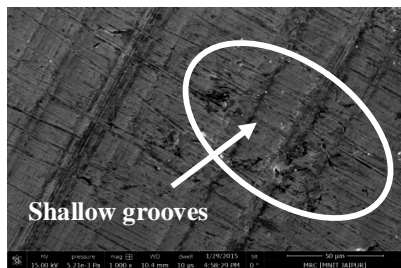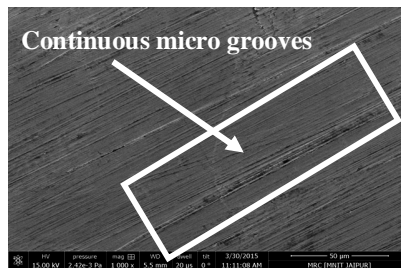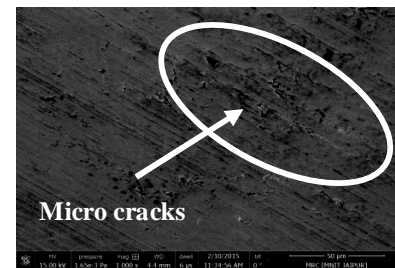
(c): 2wt.% Ni

(c): 2wt.% Ni

(c): 2wt.% Ni
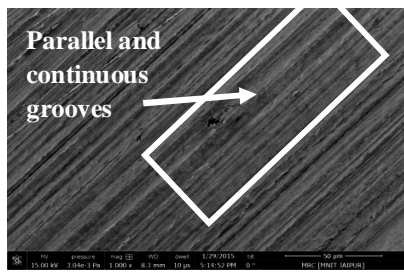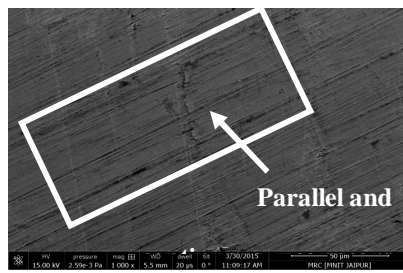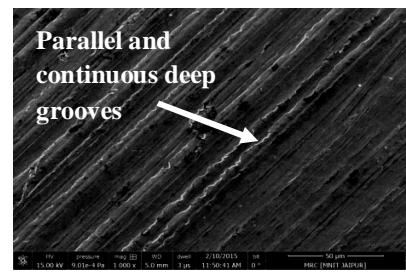
(d): 3wt.% Ni

(d): 3wt.% Ni

(d): 3wt.% Ni
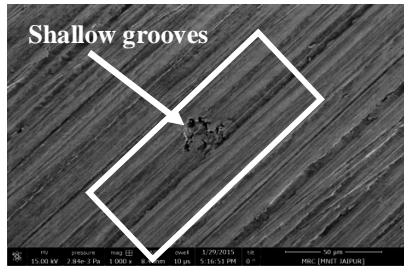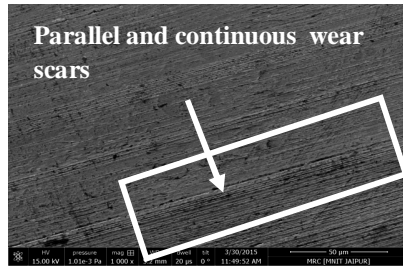
(e): 4wt.% Ni

(e): 4wt.% Ni

(e): 4wt.% Ni

Figure 4.19: SEM micrograph of different Ni content under dry condition (load: 15 N and sliding distance: 1500 m)

Figure 4.20: SEM micrograph of different Ni content under wet condition (load: 15 N and sliding distance: 1500 m)

Figure 4.21: SEM micrograph of different Ni content under dry condition (sliding velocity: 0.785 m/s and sliding distance: 1500 m)
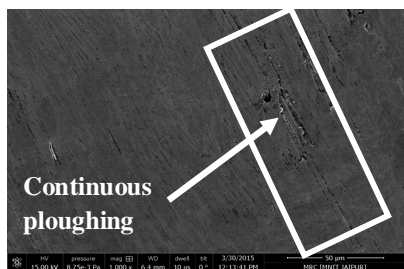
(a): 0wt.% Ni
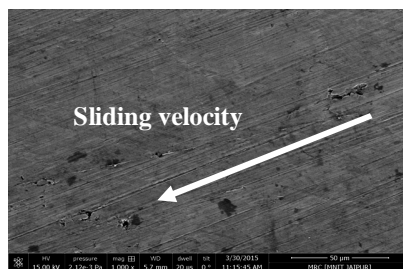
(b): 1wt.% Ni
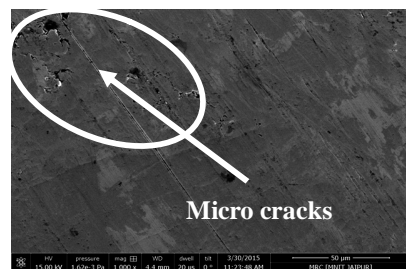
(c): 2wt.% Ni
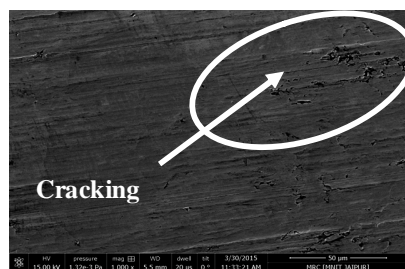
(d): 4wt.% Ni
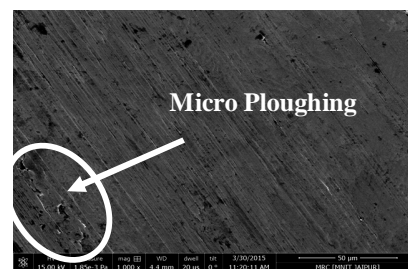
(e): 5wt.% Ni

Figure 4.22: SEM micrograph of different Ni content under wet condition (sliding velocity: 0.785 m/s and sliding distance: 1500 m)

Similar trend is observed the worn surface morphology of nickel particulate filled Co30Cr4Mo alloy composites under different loads at constant sliding velocity: 0.785m/s and sliding distance: 1500m under dry condition as shown in Figure 4.21. Figure 4.21a shows the worn surface morphology of the unfilled alloy composite where the presence of reinforced particles becomes negligible along the sliding direction at an applied load of 15N. However, the worn surface (Figure 4.21b) of the 1wt.% Ni particulate alloy alloy composite the volumetric wear loss is slight reduction and the formation of the craters were thin in nature and contained fewer cracks due to reinforcement of nickel particulates in the alloy matrix composite as compared with other compositions (See steady state Figure 4.17a and morphology Figure 4.21b). Again, with further increased in filler content in the alloy composite (2wt.% Ni) the volumetric wear starts increasing under similar operating conditions as shown in Figure 4.21c. The increased in wear is due to poor bonding between the hard particulates and matrix material (See steady state Figure 4.17a) and there may be chances of formation of delamination wear in the subsurface of the worn area. As far as further increased in filler content i.e. 3wt. % and 4wt. % Ni particulate filled alloy composites the volumetric wear loss further increased under similar operating conditions (See steady state Figure 4.17a) due to less uniform distribution in the matrix as shown in Figures 4.21d and 4.21e respectively.The obtained worn surfaces are similar to previous studies in our research group [42].

Figure 4.22 shows the worn surface morphology of nickel particulate filled Co30Cr4Mo alloy composites under different normal loads with a layer of distilled water i.e. wet condition (Taken from Figure 4.17a) at constant sliding velocity: 0.785m/s and sliding distance: 1500m. This layer is almost fully covers the wear track in contrast to without water i.e. dry condition (See Figure 4.22a) for 0wt.% particulate filled Co30Cr4Mo alloy composite at constant sliding velocity 0.785m/sec, normal load 15N and sliding distance 1500m respectively (See Figure 4.22a). Nevertheless, under alike conditions the worn surface morphology of 1wt.% Ni particulate filled alloy composite the formation of micro cracks is minimal in contrast with 1wt.% Ni particulate filled alloy composites (Figure 4.22b) under dry condition. The reduction volumetric wear loss is minimal due to the existence of the layer of distilled water during sliding diminishes the wear of both the surfaces i.e. disc and the counter pin. A further increased in filler content in the alloy composite (i.e. 2wt.% Ni) the volumetric wear starts increasing and relatively more crack are occurs under similar operating conditions as shown in Figures 4.22c. The increased in wear is due to poor bonding between the hard particulates and matrix material (See steady state Figure 4.17a).

Again further increased in filler content i.e. 3wt.% and 4wt.% Ni particulate filled alloy composites the volumetric wear loss further increased and the formation of cracking and ploughing effect is more as compared to other compositions under alike operating conditions (See steady state Figure 4.17a). The increased in wear is due to due to less uniform distribution in the matrix (See Figures 4.22d and 4.22e).

The corresponding AFM micrographs are shown in Figures 4.23 and 4.24. The average roughness of the surfaces of the wear samples is also conducted (See Table 4.10) using computerized image analysis techniques and confocal laser scanning microscopy. The obtained worn surfaces are similar to previous studies in our research group [32]. From this analysis, it can be say that the 1wt.% Ni particulate filled alloy composite attained minimum material loss as compared with other composition under similar operating condition (at sliding velocity: 0.785m/s and sliding distance: 1500 m) in both dry and wet condition.

(a) 0 wt% Ni

(a) 0 wt% Ni

(b) 1 wt% Ni

(b) 1 wt% Ni

(c) 2 wt% Ni

(c) 2 wt% Ni

(d) 3 wt% Ni

(d) 3 wt% Ni
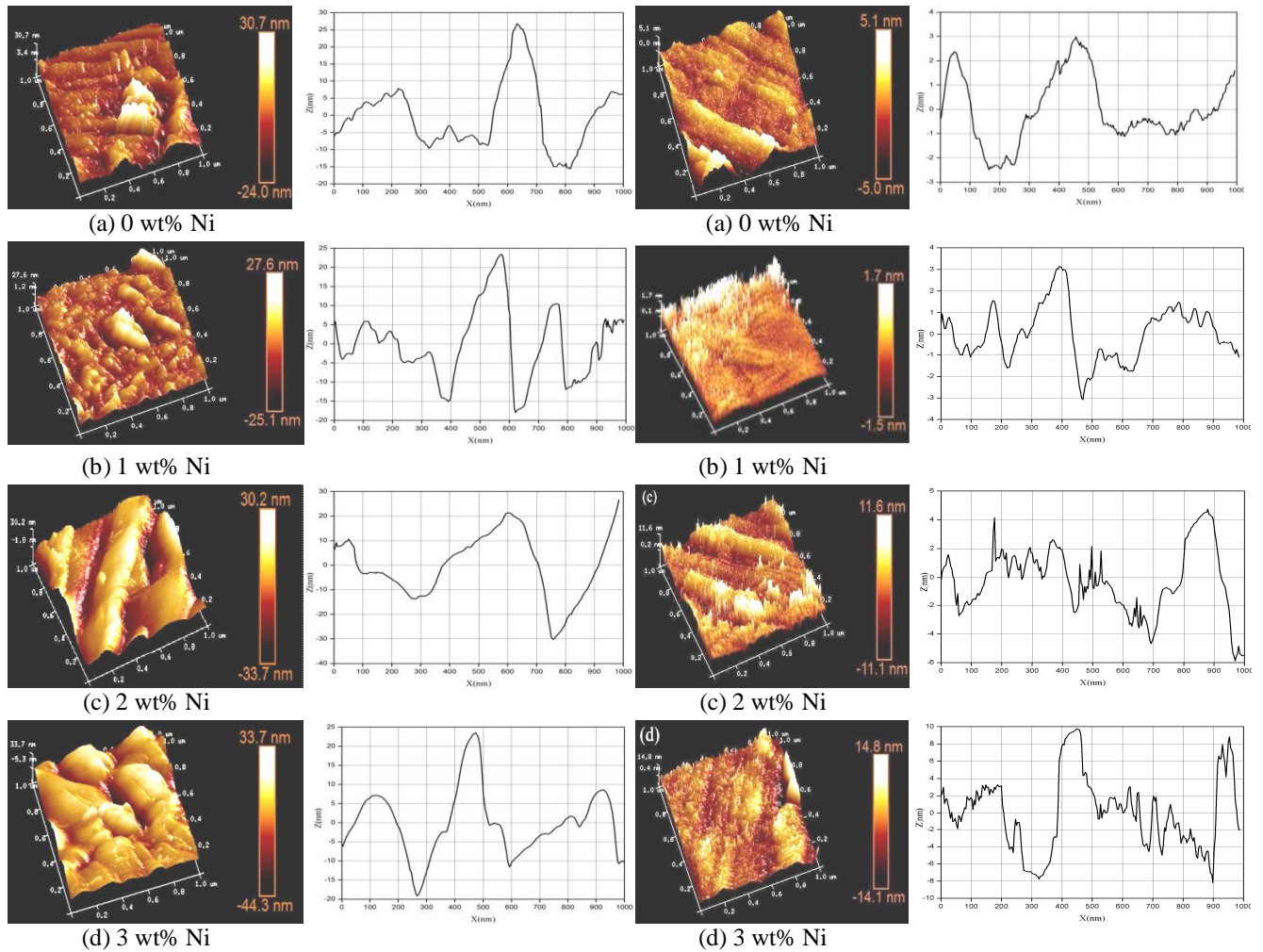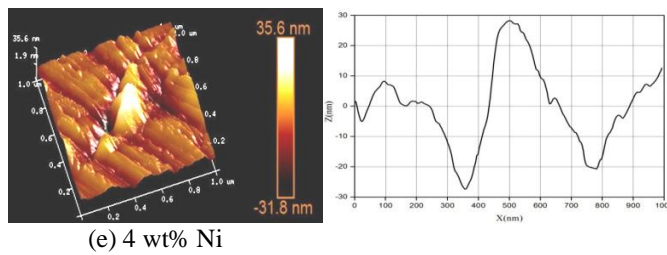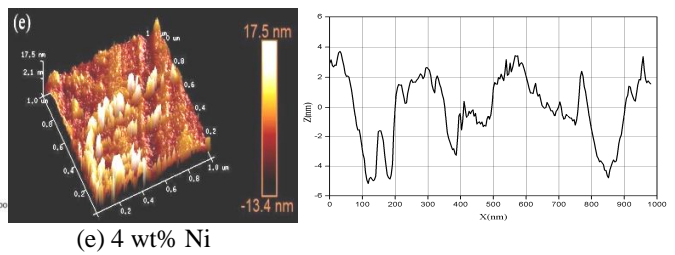
(e) 4 wt% Ni

(e) 4 wt% Ni

Figure 4.23: The 3D AFM micrographs and the line profiles of the worn surface of nickel filled Co-30Cr-4Mo alloy composite under dry condition

Figure 4.24: The 3D AFM micrographs and the line profiles of the worn surface of nickel filled Co-30Cr-4Mo alloy composite under wet condition.

Table 4.12 Surface Roughness of the fabricated alloy composites

Formulated composites	Average surface roughness (R_a)	
	Dry Condition (nm)	Wet Condition (nm)
Co30Cr4Mo + 0 wt.% Ni	4.52	0.862 nm
Co30Cr4Mo + 1 wt.% Ni	4.29	1.11 nm
Co30Cr4Mo + 2 wt.% Ni	7.61	2.29 nm
Co30Cr4Mo + 3 wt.% Ni	7.62	2.60 nm
Co30Cr4Mo + 4 wt.% Ni	5.07	2.66 nm

4.3 Part III: C-Series alloy composite (Co30Cr4Mo1Ni) based on the variation of tungsten filled particulate

The characterization of the fabricated alloy composites reveals that incorporation of tungsten (W) particulate has strong influence on the mechanical also as wear performance. The XRD diffractograms with a comparison for each sample is presented in Figure 4.25. These five different alloys are fabricated by the casting method [287]. It can be seen that the microstructure of unfilled alloy composite consists of a Co matrix with Cr, Mo and Ni regions. It is clear that the Co, Cr and W, alliance with oxide and forms Co_xO_y, Cr_xO_y, Ni_xO_y and W_xO_y in the microstructure. The oxides (O) could have arrived from two sources either from Co or from the atmosphere for the period of mixing. For this, the hexagonal close-packed (HCP) Co structure has been formed for the reason that of the martensitic transformation [288]. It is also observed that no carbides are present in the microstructure in all the fabricated alloy composites (0-4wt.% W). In addition the compounds Co, Cr, Mo, Ni and W can be seen clearly confirming its presence (Figure 4.25). On the other hand, in all the samples, the fcc (111) cobalt base α matrix (d=2.04°A), bcc (110) Cr (d=2.039°A), bcc

(110) Mo (d=2.225°A), bcc (210) W (d=2.258°A) and fcc (111) CrNi (d=2.073°A) are identified. An additional rhombohedral Co_7Mo_6 (116) phase (d=2.08°A), a tetragonal Cr_2W_6 (110), Ni_4W (121) (d=2.078°A), a hexagonal Co_3W (201) (d=1.952°A) and a cubic $Cr_4Ni_{15}W$ (200) (d=1.786°A), $Ni_{17}W_3$ (220) (d=1.269°A) major phases are also identified. The XRD patterns obtained have a number of similarities with other Co-Cr-Mo alloys viz ASTM F75, ASTM F1537 or studied in the literature [289-293]. Scanning electron microscopy and corresponding EDAX images of the microstructure of samples W0, W1, W2, W3 and W4, with inclusion of tungsten content are shown in Figure 4.26. It can be seen that the cobalt based solid solution is in dark grey, chromium is in light grey and, in different shades of light black, the molybdenum contents. In addition, the uniform distribution of small white spots demonstrate the weight fraction of nickel content and the dark black curl spots show the tungsten weight fraction content.
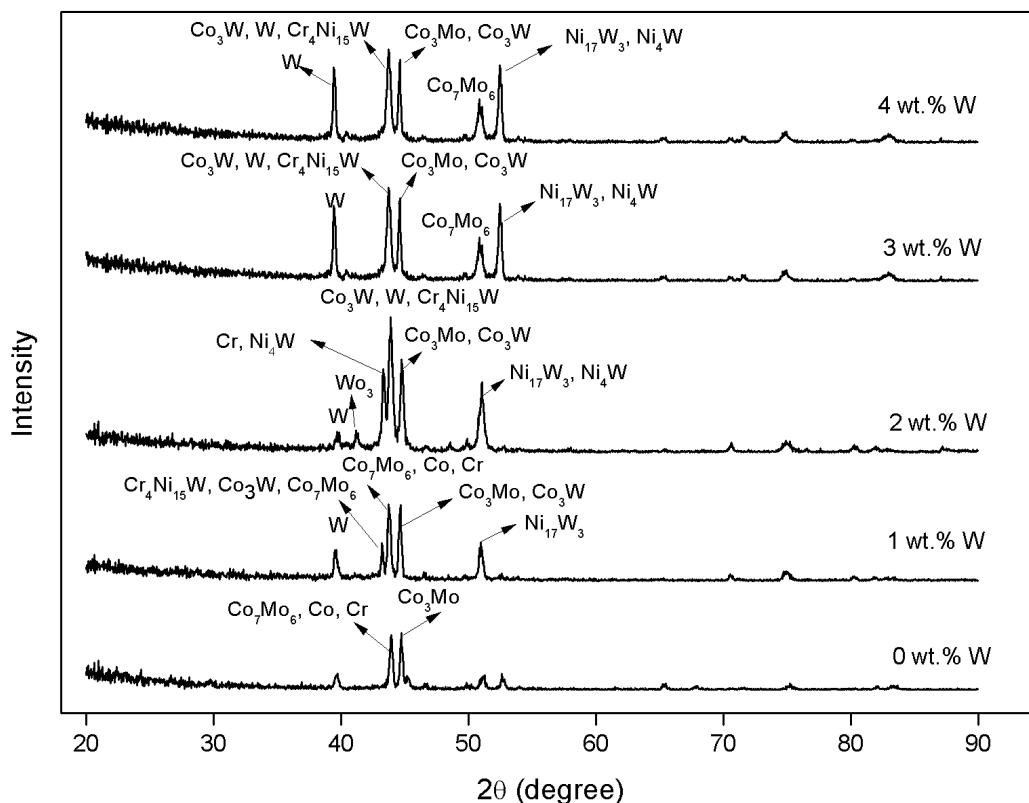
Figure 4.25: XRD patterns of fabricated tungsten filled Co-30Cr-4Mo-1Ni alloy composite.
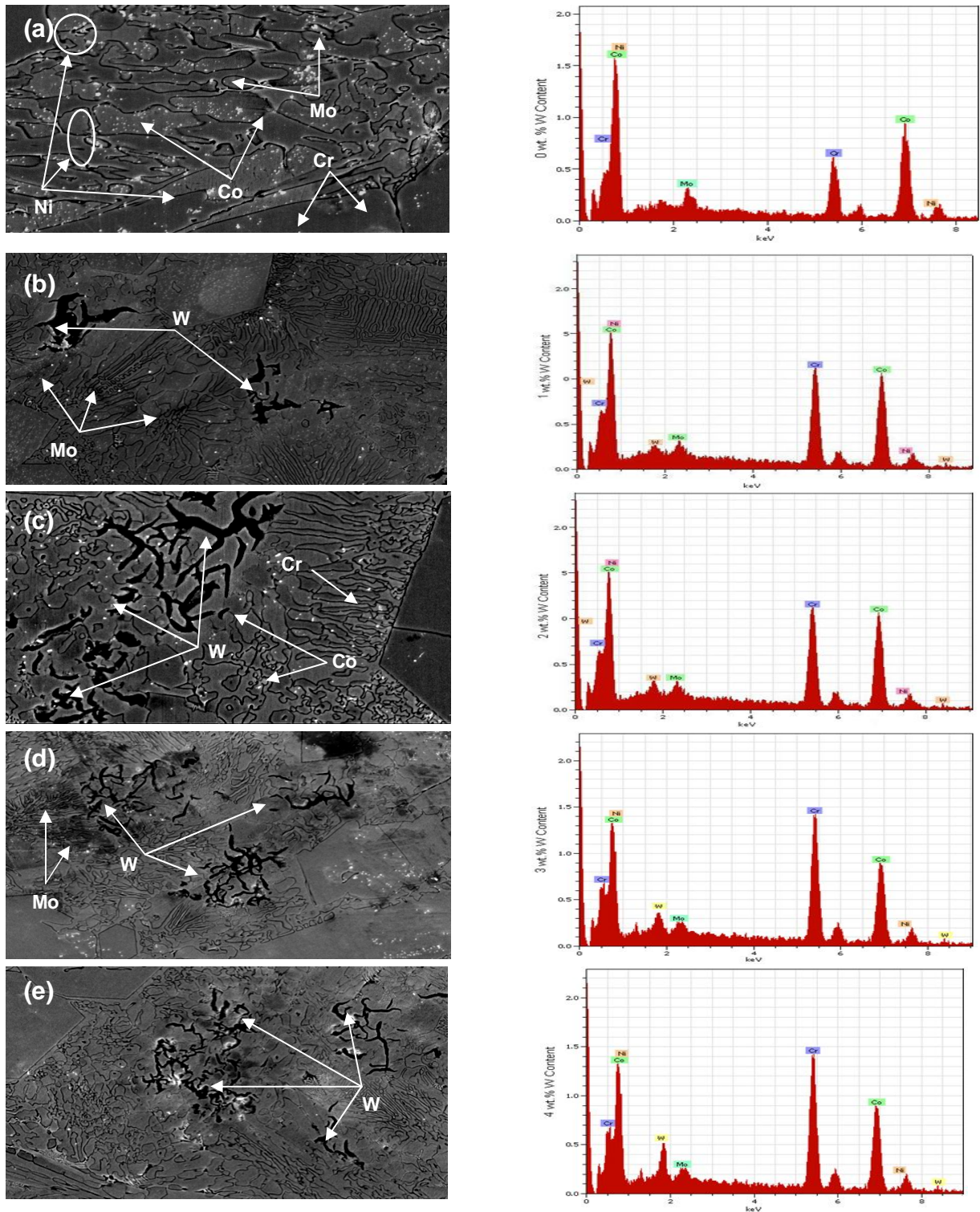
Figure 4.26: SEM micrographs and corresponding EDS results of tungsten filled Co-30Cr-4Mo-1Ni alloy composite:(a) 0 wt.% W, (b) 1wt.% W, (c) 2 wt.% W, (d) 3 wt.% W and (e) 4 wt.% W.

4.3.1 Physical and Mechanical Properties of alloy Composites

4.3.1.1 Density

The density of the fabricated tungsten (0-4wt.%) filled Co-30Cr-4Mo-1Ni alloy composites are shown in Figure 4.27a. It is clearly seen that, the density is 8.58gm/cc at 0wt.% W. Beyond 0wt.% to 4wt.% W filled alloy composite the density is increased slowly up to 8.64gm/cc. The increment of density occurred due to ample bonding between the particle and metal matrix (Co-Cr-Mo-Ni). The densities obtained with the addition of tungsten content (0-4wt% W) have near about as per ASTM F75 [26].

4.3.1.2 Micro hardness

Figure 4.27b illustrates the simplified representation the variation of micro-hardness of tungsten filled alloy composites. The micro-hardness is measured at five different locations and after measuring the micro-hardness of the entire identified region, the mean micro-hardness is taken in this study. It is observed that the tungsten filled samples (i.e. 1wt.% to 4wt.%), the hardness of the fabricated alloy composite increases (linearly) with increased in weight percentage of tungsten particulate fillers in the alloy matrix material. The increased in hardness is quite evident and expected since hard tungsten particle is combination of Co-30Cr-4Mo-1Ni metal matrix and contributes effectively to increase the hardness of the alloy composites. Therefore, from Table 4.11 it is clearly seen that for unfilled alloy composite the hardness is 60 HRC. Afterwards, as the content of W wt% increases, the hardness of the alloy composites also increases i.e. at 4wt.% of W particulate filled alloy composite has exhibited the maximum hardness (Table 4.11). This dispersion effect is likely to maintain a higher environment temperature instead of elevated temperature because the particles may not react with the matrix phase. Similar results were found earlier by previous studies on hardness of Co-Cr alloys with different content of W [27, 28].

4.3.1.3 Compression strength

Figure 4.27c shows the variation of compression strength of the fabricated alloy composites (Co-30Cr-4Mo-1Ni) with the tungsten contents. As shown in fig the compressive strength of 0wt.% W filled alloy composite is 1296 MPa. However, addition the weight percentage of tungsten particulate filler into the base matrix (i.e. Co-30Cr-4Mo-1Ni) the compressive strength also gradually increases up to 4wt.% W. It clearly indicates that the inclusion of tungsten particulate filler improves the load bearing capacity of the alloy composites.
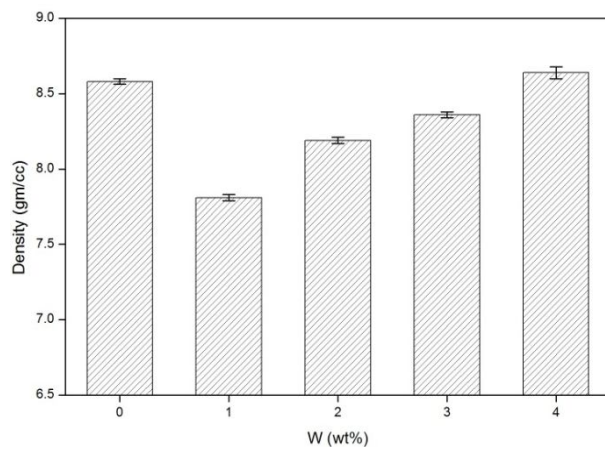
Figure 4.27a: Variation of density with W content
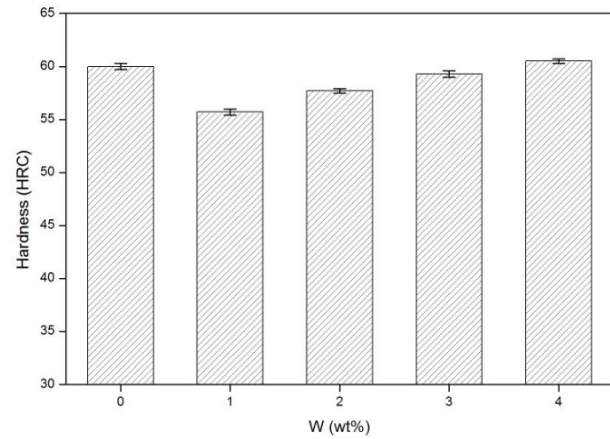
Figure 4.27b: Variation of micro-hardness with W content
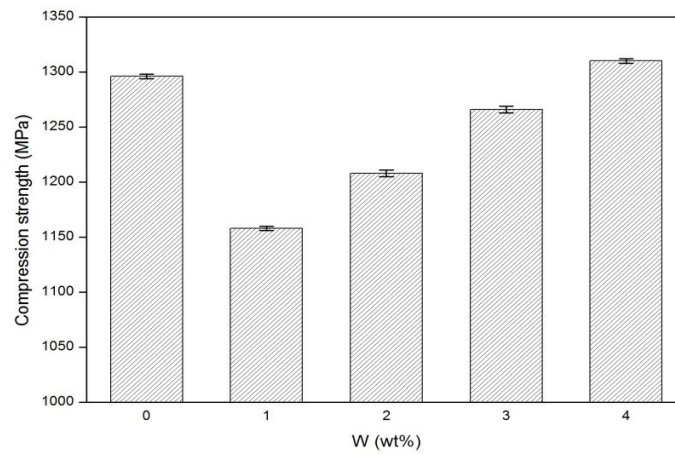
Figure 4.27c: Variation of compression strength with W content

Table 4.13 Physical and mechanical properties of tungsten filled alloy composite

Alloys	Density (gm/cc)	Hardness (HRC)	Compression strength (N/mm2)
C0	8.58	60	1296
C1	7.81	55.7	1158
C2	8.19	57.7	1208
C3	8.36	59.3	1266
C4	8.64	60.5	1310

4.3.2 Sliding Wear Behavior of alloy Composites

4.3.2.1 Effect of sliding velocity on volumetric wear loss of particulate filled alloy composites

The steady state sliding wear analysis is conducted by varying one factor at-a-time i.e. sliding velocity and all other factors remaining constant (normal load: 15 N and sliding distance 1500m) respectively to get the volumetric wear loss of the particulate filled alloy composites (Figure 4.28a). Figure 4.28a shows the volumetric wear loss gradually increased with the increased in sliding velocity irrespective of filler content in both dry and wet medium. The volumetric wear loss is maximum in 0wt.% W particulate filled alloy composites and minimum in 2wt.% W particulate filled alloy composites in both dry and wet medium (see Figure 4.28a). It is interesting to note that the volumetric wear of fabricated alloy composites obtained in this study is very close to the previous researchers [305, 306]. Whereas, in 3wt.% and 4wt.% W particulate filled alloy composites show more volumetric wear loss as compared with 2wt.% W particulate filled alloy composites in both dry and wet medium. This may be the cause of incompatible in addition of higher percentages of tungsten particulates in Co-30Cr-4Mo-1Ni alloy composites.

Figure 4.28b shows the effect of sliding velocity on friction coefficient of different tungsten particulates filled alloy composites (at load: 15N and sliding distance 1500m) in both dry and wet medium. At the primary stage of rubbing, friction is low and the factors accountable for this low friction are due to the attendance of a layer of foreign material on the disc surface. This layer generally constitutes; moisture; oxide of metals; deposited lubricating material, etc. After initial rubbing, the upper layer separates and fresh surfaces directly comes in contact which increases the bonding force between the contacting surfaces. A similar finding is reported by Savarimuthu et al. [296] for sliding wear behavior of tungsten carbide thermal spray coatings for replacement of chromium electroplate in aircraft applications. It is clear from the Figure 4.28b that the mean steady state value of friction coefficients is initially low among all the tungsten filled particulates. Thereafter, it gradually increases up to 0.523m/s and then decreases further increase in the sliding velocity (i.e. 0.78m/s). The similar manner of friction coefficient is obtained further increase the sliding velocity up to 1.3m/s. It is also observed that the 2wt. % W displays least effect in the variation of friction coefficient with sliding velocity.
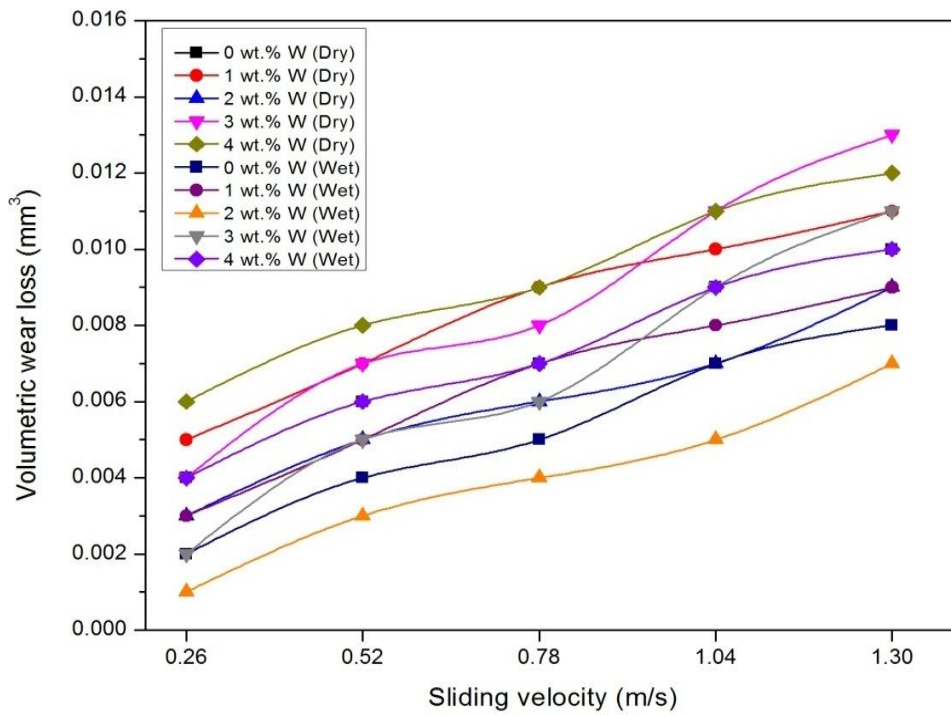
Figure 4.28a: Variation of volumetric wear with sliding velocity for Co30Cr4Mo1Ni alloy under dry and wet condition (load: 15 N and sliding distance 1500m)
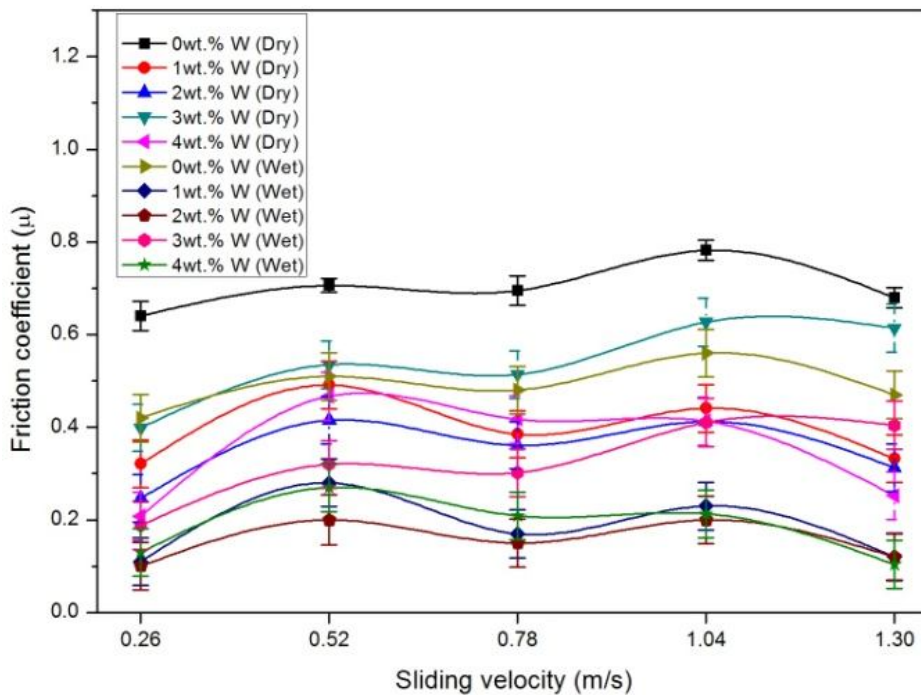
Figure 4.28b: Variation of coefficient of friction with sliding velocity for Co30Cr4Mo1Ni alloy under dry and wet condition (load: 15 N and sliding distance 1500m)

4.3.2.2 Effect of normal load on volumetric wear loss of particulate filled alloy composites

Figure 4.29a shows the mean steady state wear analysis of tungsten particulate filled Co30Cr4Mo1Ni alloy composites by varying normal load (5–25N) under constant operation conditions (Sliding velocity: 0.785 m/s and sliding distance 1500m) respectively. As shown in Figure 4.29a clearly seen that the volumetric wear loss steadily increases if the normal load increased from 5N to 25N. As the load on the pin is enhanced the actual area of contact would enhance towards the nominal contact area, consequently that increase the frictional force between two sliding surfaces. The enhanced frictional force and real surface area in contact cause higher wear. This implies that the shear force and frictional thrust force are increased with increase of normal load and this accelerates the volumetric wear loss. Out of all the samples, 2wt% W exhibits a lesser wear loss than the others. In this study the material used for pin and counter disc are both different and the value obtained of volumetric wear is in the range of Cobalt based alloy [307-309]. Few authors used the same material of both pin and disc instead of dissimilar materials. Firkins et al. [297] used CoCr alloy for both the pin and disc material and found the wear behavior is likely similar to the present study. Doni et al. [298] compared the dry sliding wear behavior under 1N normal load of hot pressed CoCrMo implant material with commercially cast CoCrMo and Ti6Al4V implant materials and found the wear loss of Ti6Al4V alloy is 14 and 47 times higher than the cast and hot pressed CoCrMo samples respectively.

Figure 4.29b shows the friction coefficient versus normal load for tungsten filled Co30Cr4Mo1Ni alloy composites under steady state condition. As shown in Figure 4.29b, the friction coefficient of the fabricated alloy composites (i.e. Co30Cr4Mo1Ni) both dry and wet conditions with varying tungsten filler contents exhibited considerably low coefficient of friction up to 15N normal load. The current experimental results are explicable: during starting stages, the surfaces of both the alloy specimens and the disc are smooth due to the presence of reinforcing particulate materials including moisture, oxide of metals, deposited lubricating materials, etc. and thus resulting in a low friction coefficient. As the wear continued, the layer break up and the clean surface come in directly contact with the specimen and gradually increases the friction coefficients are accomplished when a steady wear stage is attained up to 10N loads. Thereafter, it rapidly decreases at 15N loads and it again increases for the rest of the experiment loads (i.e. 25N) [310].
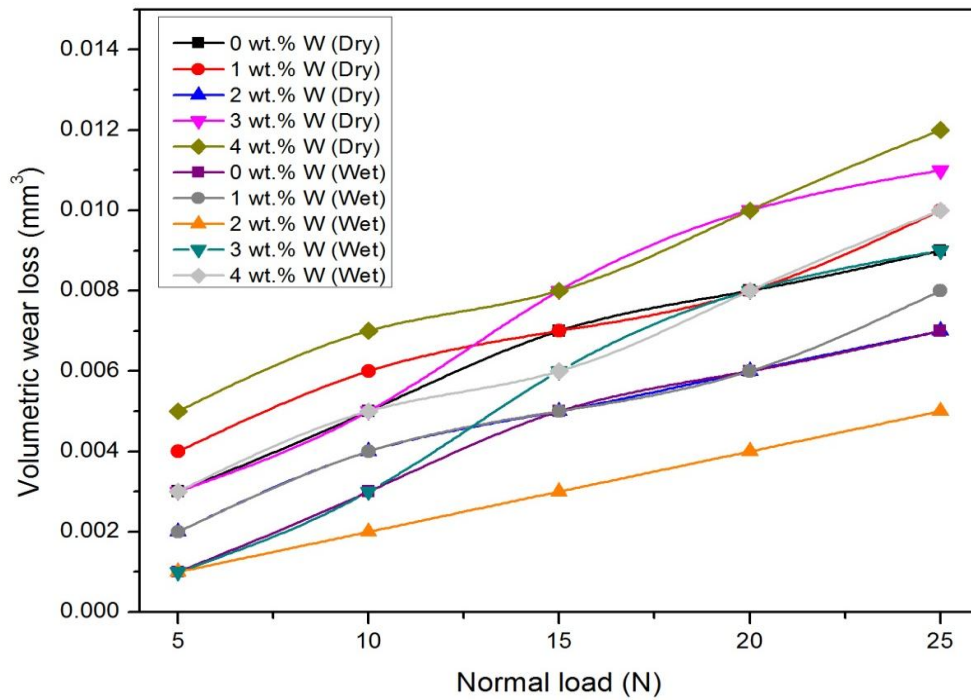
Figure 4.29a: Variation of volumetric wear with normal load for Co30Cr4Mo1Ni alloy under dry and wet condition (Sliding velocity: 0.785 m/s and sliding distance 1500m)
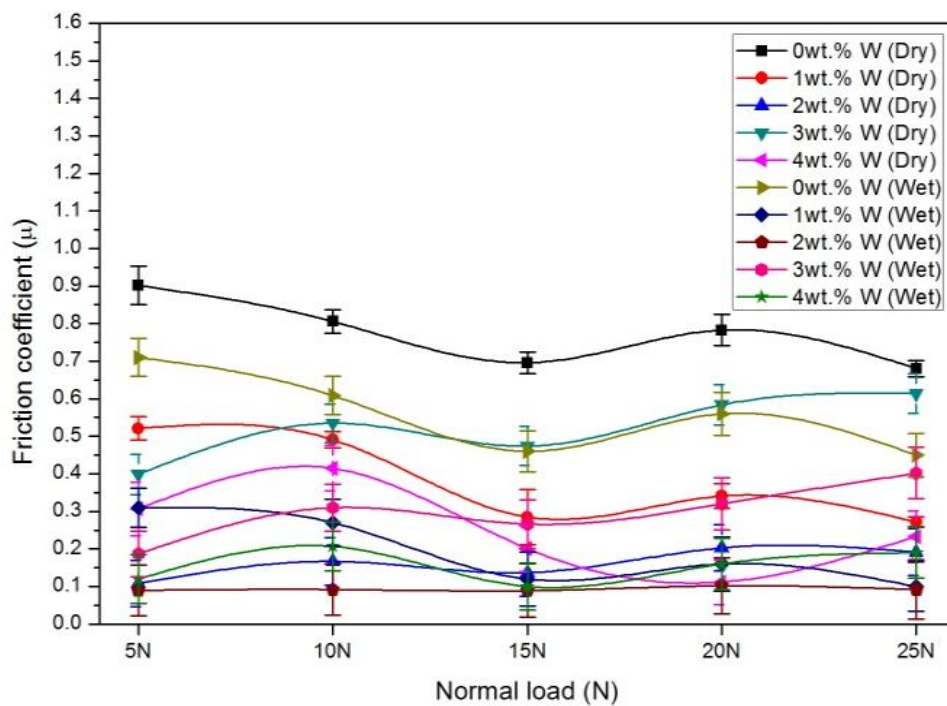
Figure 4.29b: Variation of coefficient of friction with normal load for Co30Cr4Mo1Ni alloy under dry and wet condition (Sliding velocity: 0.785m/s and sliding distance 1500m)

4.3.3 Taguchi experimental analysis

Table 4.12 shows the volumetric wear loss of particulate filled alloy composites and their respective S/N ration values. The sixth and ninth column represents the volumetric wear loss of the dry and wet medium of the proposed alloy composites and each experiment is repeated three times and the mean wear loss and their corresponding standard deviation is reported in Table 4.12.

Table 4.14 Experimental design using L_{25} orthogonal array

Runs	A	B	C	D	Dry Condition					Wet Condition				
					wear loss (mm^3)	Standard deviation	S/N Ratio (db)	Friction Coeff.	S/N Ratio (db)	wear loss (mm^3)	Standard deviation	S/N Ratio (db)	Friction Coeff.	S/N Ratio (db)
1	5	0.26	500	0	0.045819	0.000203	26.7792	0.463	6.6790	0.004592	0.00001	46.759	0.036	28.849
2	5	0.523	1000	1	0.033800	0.000300	29.4217	0.555	5.1141	0.004000	0.00001	47.958	0.047	26.650
3	5	0.785	1500	2	0.015733	0.000200	36.0636	0.095	20.4455	0.000136	0.00003	77.329	0.037	28.706
4	5	1.04	2000	3	0.013500	0.000100	37.3933	0.262	11.6396	0.001260	0.00003	57.992	0.104	19.679
5	5	1.3	2500	4	0.011120	0.000251	39.0779	0.377	8.48450	0.000928	0.00002	60.649	0.303	10.363
6	10	0.26	1000	2	0.011000	0.000200	39.1721	0.195	14.1993	0.000105	0.00001	79.576	0.197	14.123
7	10	0.523	1500	3	0.009800	0.000230	40.1755	0.253	11.9391	0.000880	0.00001	61.110	0.335	9.490
8	10	0.785	2000	4	0.006250	0.000315	44.0824	0.231	12.7294	0.000063	0.00001	84.082	0.310	10.179
9	10	1.04	2500	0	0.002880	0.000122	50.8122	0.431	7.31067	0.000444	0.00002	67.052	0.360	8.882
10	10	1.3	500	1	0.034200	0.000134	29.3195	0.370	8.63596	0.002140	0.00002	53.391	0.245	12.202
11	15	0.26	1500	4	0.004356	0.000316	47.2191	0.463	6.67904	0.000560	0.00003	65.036	0.137	17.284
12	15	0.523	2000	0	0.002767	0.000100	51.1609	0.431	7.30447	0.000049	0.00002	86.137	0.290	10.759
13	15	0.785	2500	1	0.002933	0.000122	50.6528	0.655	3.67517	0.000248	0.00001	72.110	0.311	10.144
14	15	1.04	500	2	0.013067	0.000127	37.6767	0.433	7.27024	0.000135	0.00003	77.414	0.218	13.230
15	15	1.3	1000	3	0.007467	0.000128	42.5375	0.203	13.8520	0.000793	0.00002	62.010	0.101	19.932
16	20	0.26	2000	1	0.001150	0.000136	58.7860	0.587	4.62723	0.000140	0.00002	77.077	0.101	19.939
17	20	0.523	2500	2	0.000760	0.000153	62.3837	0.138	17.2024	0.000860	0.00002	61.310	0.265	11.535
18	20	0.785	500	3	0.012100	0.000167	38.3443	0.262	11.6396	0.001360	0.00002	57.329	0.129	17.804
19	20	1.04	1000	4	0.004650	0.000220	46.6509	0.463	6.67904	0.000615	0.00001	64.222	0.241	12.367
20	20	1.3	1500	0	0.002600	0.000336	51.7005	0.431	7.30447	0.000530	0.00003	65.514	0.391	8.1597
21	25	0.26	2500	3	0.000400	0.000321	67.9588	0.787	2.08594	0.000058	0.00001	84.791	0.290	10.759
22	25	0.523	500	4	0.008640	0.000120	41.2697	0.800	1.94135	0.000936	0.00002	60.574	0.353	9.0378
23	25	0.785	1000	0	0.004080	0.000167	47.7868	0.842	1.49527	0.000500	0.00002	66.020	0.260	11.705
24	25	1.04	1500	1	0.001893	0.000230	54.4555	0.837	1.54549	0.000173	0.00001	75.222	0.289	10.782
25	25	1.3	2000	2	0.000620	0.000210	64.1522	0.682	3.32316	0.000048	0.00001	86.375	0.184	14.698
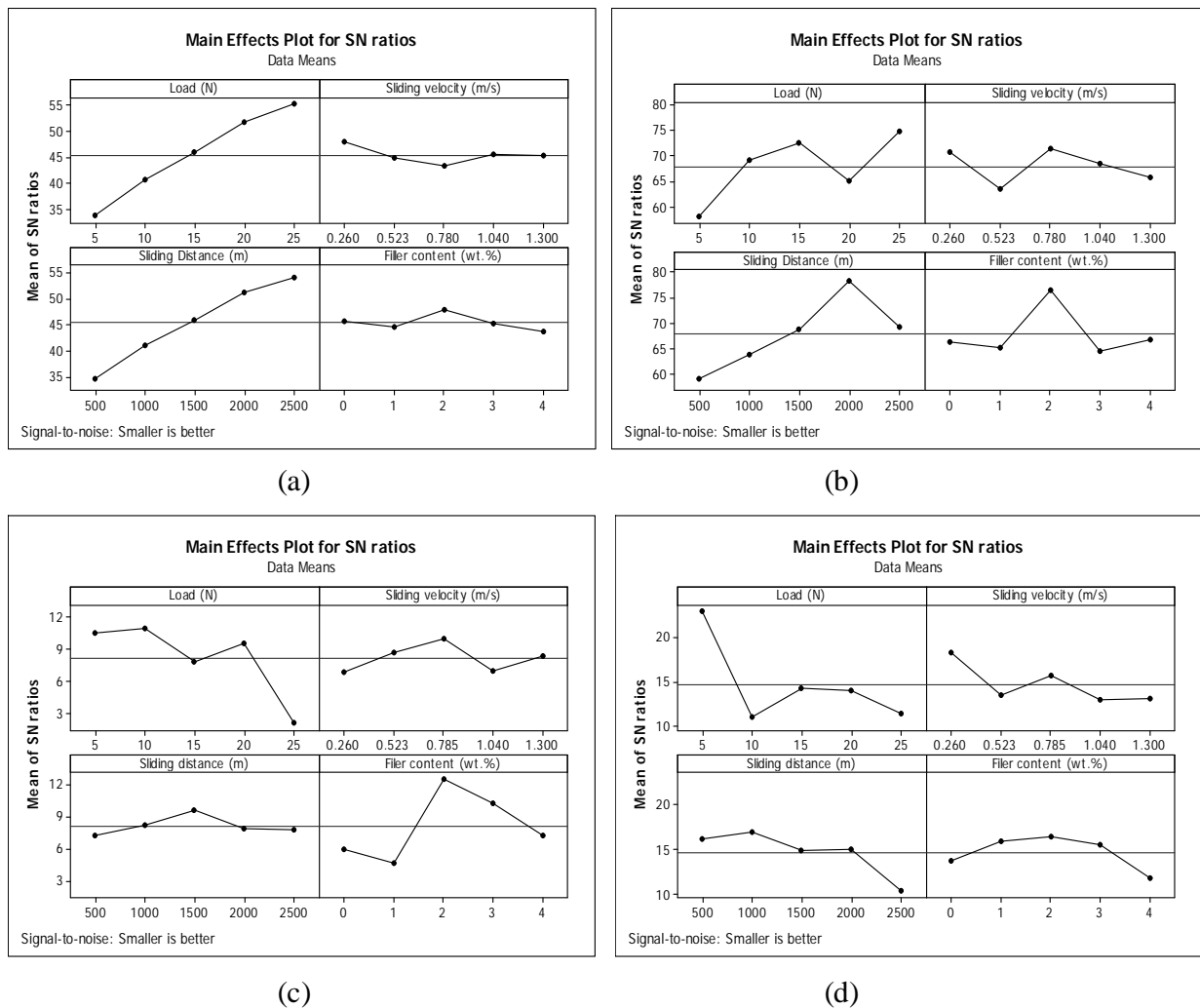
Figure 4.30: (a) Effect of control factors on volumetric wear loss for W filled Co-30Cr-4Mo-1Ni alloy composites under dry condition; (b) Effect of control factors on volumetric wear loss for W filled Co-30Cr-4Mo-1Ni alloy composites under wet condition; (c) Effect of control factors on friction coefficient for W filled Co-30Cr-4Mo-1Ni alloy composites under dry condition; (d) Effect of control factors on friction coefficient for W filled Co-30Cr-4Mo-1Ni alloy composites under wet condition

The overall mean for the S/N ratio of the wear loss under dry and wet sliding condition are found to be 45.4013 dB and 67.8820 dB respectively. Similarly, the overall mean for the S/N ratio of the friction coefficient for both sliding conditions are found to be 8.152 dB and 14.69 dB respectively. Figures 4.30a and 4.30b show graphically the effect of the four control factors on volumetric wear loss in dry and wet sliding conditions. Analysis of the result leads to the conclusion that factor combination of $A_5B_1C_5D_3$ and $A_5B_3C_4D_3$ gives minimum wear loss in dry

and wet conditions respectively for the fabricated alloy composites (Figure 4.30a and Figure 4.30b). Similarly, the factor combination of A_2, B_3, C_3, D_3 gives minimum friction coefficient in dry condition and A_1, B_1, C_2 and D_3 in wet conditions for the fabricated alloy composites respectively (Figure 4.30c and Figure 4.30d).

4.3.4 Confirmation Experiment

Confirmation experiment is the last step of design of experiment process. The purpose is to validate the conclusions drawn during the analysis phase. The confirmation experiment is executed by conducting a novel set of factor settings $A_4B_2C_3D_1$ and $A_4B_5C_3D_2$ to predict the wear loss for dry and wet sliding condition respectively. Similarly, a new set of factor settings $A_3B_2C_1D_2$ and $A_2B_3C_1D_2$ to predict the friction coefficient for both the conditions. The estimated S/N ratio for wear loss can be calculated by predictive equation:

$$\hat{\eta}_{dry_w} = \bar{\eta} + (\overline{A_4} - \bar{\eta}) + (\overline{B_2} - \bar{\eta}) + (\overline{C_3} - \bar{\eta}) + (\overline{D_1} - \bar{\eta}) \qquad (4.17)$$

$$\hat{\eta}_{dry_\mu} = \bar{\eta} + (\overline{A_3} - \bar{\eta}) + (\overline{B_2} - \bar{\eta}) + (\overline{C_1} - \bar{\eta}) + (\overline{D_2} - \bar{\eta}) \qquad (4.18)$$

$$\hat{\eta}_{wet_w} = \bar{\eta} + (\overline{A_4} - \bar{\eta}) + (\overline{B_5} - \bar{\eta}) + (\overline{C_3} - \bar{\eta}) + (\overline{D_2} - \bar{\eta}) \qquad (4.19)$$

$$\hat{\eta}_{wet_\mu} = \bar{\eta} + (\overline{A_2} - \bar{\eta}) + (\overline{B_3} - \bar{\eta}) + (\overline{C_1} - \bar{\eta}) + (\overline{D_2} - \bar{\eta}) \qquad (4.20)$$

Where, $\widehat{\eta_w}$: predicted average of wear volume, $\widehat{\eta_\mu}$: predicted average of friction coefficient $\bar{\eta}$: overall experimental average, $\overline{A_4}, \overline{B_2}, \overline{C_3}, \overline{D_1}$ for wear volume and $\overline{A_3}, \overline{B_2}, \overline{C_1}, \overline{D_2}$ for friction coefficient under dry condition and $\overline{A_4}, \overline{B_5}, \overline{C_3}, \overline{D_2}$ for wear volume and $\overline{A_2}, \overline{B_3}, \overline{C_1}, \overline{D_2}$ for friction coefficient under wet condition are the mean response for factors at designated levels. By combining like terms, the equation reduces to:

$$\hat{\eta}_{dry_w} = \overline{A_4} + \overline{B_2} + \overline{C_3} + \overline{D_1} - 3\bar{\eta} \qquad (4.21)$$

$$\hat{\eta}_{dry_\mu} = \overline{A_3} + \overline{B_2} + \overline{C_1} + \overline{D_2} - 3\bar{\eta} \qquad (4.22)$$

$$\hat{\eta}_{wet_w} = \overline{A_4} + \overline{B_5} + \overline{C_3} + \overline{D_2} - 3\bar{\eta} \qquad (4.23)$$

$$\hat{\eta}_{wet_\mu} = \overline{A_2} + \overline{B_3} + \overline{C_1} + \overline{D_2} - 3\bar{\eta} \qquad (4.24)$$

A new combination of factor levels $\overline{A_4}, \overline{B_2}, \overline{C_3}, \overline{D_1}$ and $\overline{A_4}, \overline{B_5}, \overline{C_3}, \overline{D_2}$ are used to predict wear volume by using prediction equation (Eq. 4.21 and Eq. 4.23) and the S/N ratio is found to be 51.8222 dB and 61.0277 dB for dry and wet sliding condition respectively. Similarly, factor levels $\overline{A_3}, \overline{B_2}, \overline{C_1}, \overline{D_2}$ and $\overline{A_2}, \overline{B_3}, \overline{C_1}, \overline{D_2}$ are used to predict the friction coefficient by using prediction equations (Eq. 4.22 and Eq. 4.24) and the S/N ratio is found to be 3.953 dB and 14.780 dB for dry

and wet sliding condition respectively. The resulting model seems to be capable of predicting wear volume to a reasonable accuracy. An error under dry and wet sliding condition for S/N ratio of wear volume and friction coefficient is observed as shown in Table 4.15. However, the error can be diminished if the number of measurement will be increased.

Table 4.15 Results of the confirmation experiments for wear loss

| | Optimal control parameters | | Error (%) |
	Prediction	Experimental	
Dry condition			
Level	$A_4B_2C_3D_1$	$A_4B_2C_3D_1$	
S/N ratio for volumetric wear loss (db)	51.8222	52.928	2.08
	$A_3B_2C_1D_2$	$A_3B_2C_1D_2$	
S/N ratio for friction coefficient (db)	3.953	4.325	0.08
Wet condition			
Level	$A_4B_5C_3D_2$	$A_4B_5C_3D_2$	
S/N ratio for volumetric wear loss (db)	61.0277	61.987	1.54
	$A_2B_3C_1D_2$	$A_2B_3C_1D_2$	
S/N ratio for friction coefficient (db)	14.780	15.329	0.03

4.2.5 ANOVA and the Effect of Factors

In order to comprehend an actual visualization of impact of various factors like normal load (A), sliding velocity (B), sliding distance (C) and filler content (D) on wear loss, it is desirable to build up analysis of variance (ANOVA) table to determine the order of significant factors. Table 4.16 and 4.17 demonstrates the results of the ANOVA with the volumetric wear loss and friction coefficient assuming a level of significance of 5% under dry and wet sliding condition respectively. The last column of the table designates the probability of significance of major control factors. It has been noticed that normal load (p = 0.001), sliding distance (p = 0.002), filler content (p = 0.212), and sliding velocity (p = 0.483) for dry sliding condition and normal load (p = 0.039), sliding distance (p = 0.085), filler content (p = 0.306) and sliding velocity (p = 0.448) for wet sliding condition are significant in the declining order of importance on wear volume whereas, normal load (p = 0.000), filler content (p = 0.011), sliding velocity (p = 0.578) and sliding distance (p = 0.887) for dry sliding condition and normal load (p = 0.027), sliding distance (p= 0.112), filler content (p = 0.233) and sliding velocity (p = 0.242) for wet sliding condition are significant in the

declining order of importance on friction coefficient respectively. From this analysis it is observed that normal load has the most significant contribution compared to other factor.

Table 4.16 ANOVA table for volumetric wear loss

Source	Degree of freedom (DF)	Seq SS	Adj SS	Adj MS	F	P
Dry condition						
A	4	0.0014958	0.0014958	0.0003740	14.04	0.001
B	4	0.0001013	0.0001013	0.0000253	0.95	0.483
C	4	0.0012234	0.0012234	0.0003059	11.48	0.002
D	4	0.0001977	0.0001977	0.0000494	1.86	0.212
Error	8	0.0002131	0.0002131	0.0000266		
Total	24	0.0032313				
Wet condition						
A	4	0.0000116	0.0000116	0.0000029	4.25	0.039
B	4	0.0000028	0.0000028	0.0000007	1.03	0.448
C	4	0.0000083	0.0000083	0.0000021	3.03	0.085
D	4	0.0000039	0.0000039	0.0000010	1.44	0.306
Error	8	0.0000054	0.0000054	0.0000007		
Total	24	0.0000320				

Table 4.17 ANOVA table for friction coefficient

Source	Degree of freedom (DF)	Seq SS	Adj SS	Adj MS	F	P
Dry condition						
A	4	0.77228	0.77228	0.19307	18.50	0.000
B	4	0.03181	0.03181	0.00795	0.76	0.578
C	4	0.01143	0.01143	0.00286	0.27	0.887
D	4	0.28625	0.28625	0.07156	6.86	0.011
Error	8	0.08351	0.08351	0.01044		
Wet condition						
A	4	0.105591	0.105591	0.026398	4.94	0.027
B	4	0.036445	0.036445	0.009111	1.70	0.242
C	4	0.056641	0.056641	0.014160	2.65	0.112
D	4	0.037285	0.037285	0.009321	1.74	0.233
Error	8	0.042788	0.042788	0.005348		
Total	24	0.278751				

4.3.6 Surfaces Morphology

Figures 4.31-4.34 show the morphology of worn surfaces of tungsten particulate filled Co30Cr4Mo1Ni alloy composites under dry and wet (a layer of distilled water used between the pin and the counter disc) condition. The SEM characterization is carried out by using FEI NOVA NANOSEM 450 with an energy dispersive X-ray analysis (EDAX) attached to analyze the chemical composition of diverse phases and wear mechanisms induced by the pin-on-disc test.

Figure 4.31 shows the worn surface morphology of tungsten particulate filled Co30Cr4Mo1Ni alloy composites by varying sliding velocity under dry condition (Taken from Figure 4.28a) at constant normal load: 15N and sliding distance: 1500 m. Fig 4.31a shows the worn surface morphology of the unfilled alloy composite where the attendance of reinforced particles becomes negligible at constant sliding velocity 1.3m/sec, normal load 15N and sliding distance 1500m respectively (See Figure 4.28a). However, under similar operating condition the worn surface morphology of 1wt% W particulate filled alloy composite the formation of micro ploughing and parallel and continuous wear scars on the surface shown in Figure 4.31b. It is clearly seen that the volumetric wear loss is more and formation of cracks are more as compared with unfilled alloy composite due to which the interfacial bonding in between the particles is not so sturdy and the material is removed from surface during the sliding wear process. Again, with further increased in filler content in the alloy composite i.e. 2wt.% W the wear loss is reduced and formation of scars also reduced as compared with other two compositions (See steady state Figure 4.28a and morphology Figure 4.31c). As far as 3wt.% and 4wt.% W particulate filled alloy composites the volumetric wear loss starts increasing under similar operating conditions as shown in Figs. 4.31d and 4.31e respectively. The increased in wear loss is due to poor bonding between the hard particulates and matrix material (See steady state Figure 4.28a) and there may be chances of formation of delamination wear in the subsurface of the worn area. As the subsurface cracks are clearly visible in the micrographs (Figures 4.31d and 4.31e) and delamination wear may also occurred in some worn region which covered by the adhered hard particulate filled materials under high load operating condition.

Figure 4.32 shows the worn surface morphology of tungsten particulate filled Co30Cr4Mo1Ni alloy composites by varying sliding velocity under a smooth layer of distilled water (Taken from Figure 4.28a) at constant normal load: 15 N and sliding distance: 1500 m. This layer is almost fully covers the wear track as compare to dry condition (See Figure 4.32a) along

the sliding direction for 0wt.% W particulate filled Co30Cr4Mo1Ni alloy composite at constant sliding velocity 1.3m/sec, normal load 15N and sliding distance 1500m respectively (See Figure 4.28a). However, under similar conditions the worn surface morphology of 1wt.% W particulate filled alloy composite appears to be smooth with no micro ploughing effect but formation of parallel and multiple wear scars is more as compared with 0wt.% W particulate filled alloy composites (Figure 4.32b). Again, with further increased in filler content in the alloy composite i.e. 2wt.% W the volumetric wear is still further diminished from the surface and formation of crack also diminished and the surface appears to be smooth as compared with other two compositions (See steady state Figure 4.28a and morphology Figure 4.32c). The fine surface occurs may be due to the presence of layer of distilled water during sliding lessens the wear of both disc and the counter pin. As far as 3wt.% and 4wt.% W particulate filled alloy composites the volumetric wear loss starts increasing and relatively more scars and micro ploughing are occurs under similar operating conditions as shown in Figures 4.32d and 4.32e respectively. The obtained worn surfaces are similar to previous studies in our research group [310]. From this analysis, it is observed that, the 2wt. % W particulate filled alloy composite attained minimum volumetric wear loss as compared with other composition under similar operating condition (at load: 15 N and sliding distance: 1500 m) in both dry and wet condition.

Similar trend is observed the worn surface morphology of tungsten particulate filled Co30Cr4Mo1Ni alloy composites under different loads at constant sliding velocity: 0.785m/s and sliding distance: 1500m under dry condition as shown in Figure 4.33. Figure4.33a shows the worn surface morphology of the unfilled alloy composite in which the attendance of reinforced particles becomes negligible along the sliding direction at an applied load of 15N. However, under similar operating condition the worn surface morphology of 1wt.% W particulate filled alloy composite the formation of continuous deep grooves is more due to the oversize carbides and their less uniform distribution in the matrix as compared with unfilled particulate filled alloy composites (Figure 4.33b). Again, with further increased in filler content in the alloy composite i.e. 2wt.% W the wear loss is reduced and formation of grooves also reduced due to reinforcement of hard tungsten particulates in the alloy matrix composite as compared with other two compositions (See steady state Figure 4.29a and morphology Figure 4.33c). As far as further increased in filler content i.e. 3wt.% and 4wt.% W particulate filled alloy composites the volumetric wear loss starts increasing and wear track becomes larger under similar operating conditions (See steady state

Figure 4.29a) are shown in Figs. 4.33d and 4.33e respectively. The increased in wear loss is due to poor bonding between the hard particulates and matrix material. The obtained worn surfaces are alike to previous studies in our research group [311].

(a): 0wt.% W

(a): 0wt.% W

(a): 0wt.% W

(b): 1wt.% W

(b): 1wt.% W

(b): 1wt.% W

(c): 2wt.% W

(c): 2wt.% W

(c): 2wt.% W

(d): 3wt.% W

(d): 3wt.% W

(d): 3wt.% W
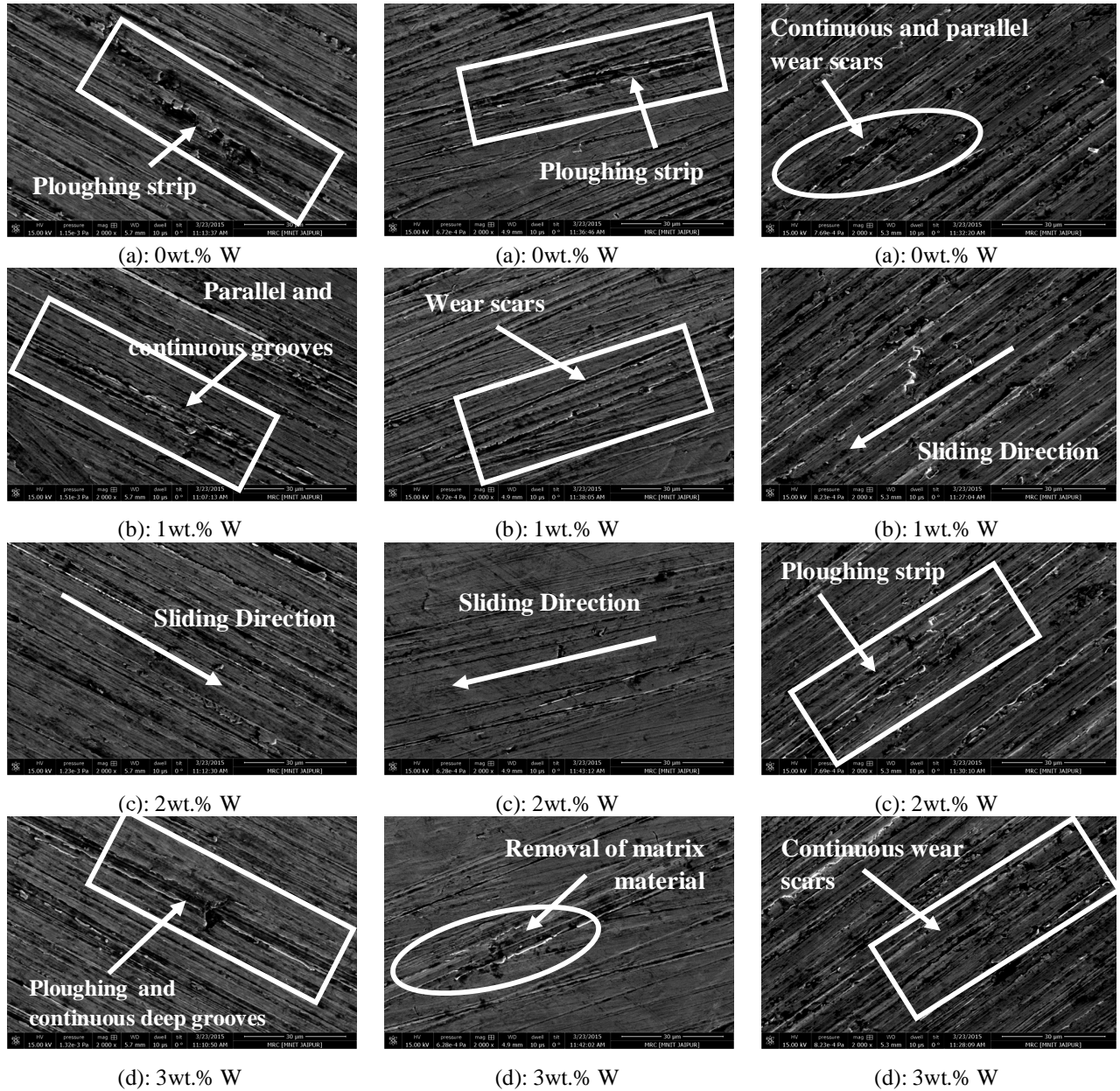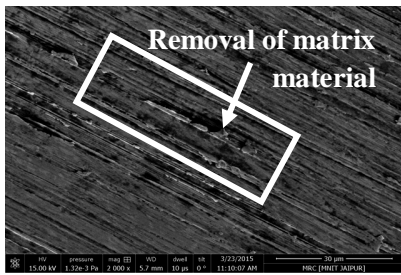
(e): 4wt.% W

Figure 4.31: SEM micrograph of different W content under dry condition (load: 15 N and sliding distance: 1500 m)
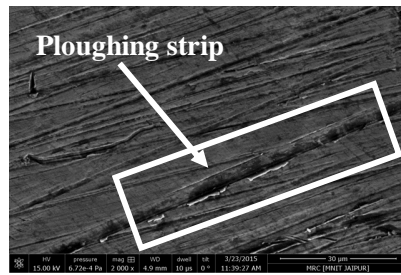
(e): 4wt.% W

Figure 4.32: SEM micrograph of different W content under wet condition (load: 15 N and sliding distance: 1500 m)
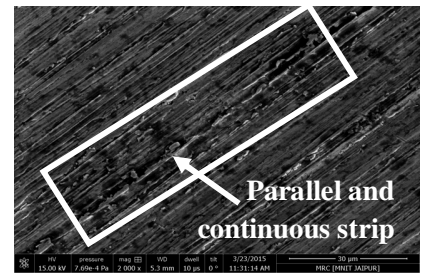
(e): 4wt.% W

Figure4.33: SEM micrograph of different W content under dry condition (sliding velocity: 0.785 m/s and sliding distance: 1500 m)
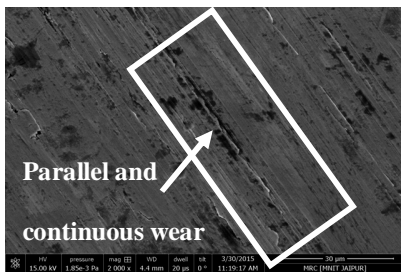
(a): 0wt.% W
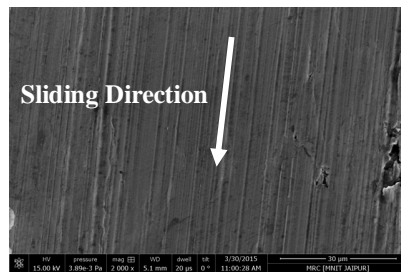
(b): 1wt.% W
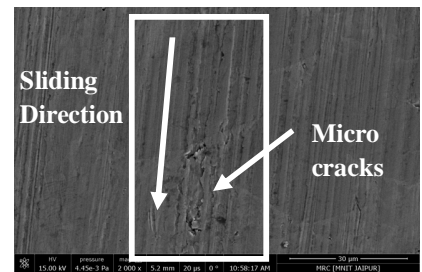
(c): 2wt.% W
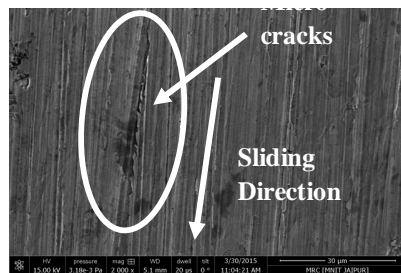
(d): 3wt.% W
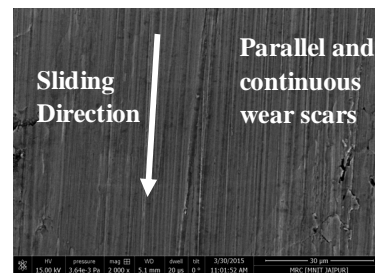
(e): 4wt.% W

Figure 4.34: SEM micrograph of different W content under wet condition (sliding velocity: 0.785 m/s and sliding distance: 1500 m)

Figure 4.34 shows the worn surface morphology of tungsten particulate filled Co30Cr4Mo1Ni alloy composites under different normal loads with a layer of distilled water (Taken from Figure 4.35a) at constant sliding velocity: 0.785 m/s and sliding distance: 1500 m. This layer is almost fully covers the wear track in contrast to without water i.e. dry condition (See Figure 4.34a) for 0wt.% particulate filled Co30Cr4Mo1Ni alloy composite at constant sliding velocity 1.3m/sec, normal load 15N and sliding distance 1500m respectively (See Figure 4.29a).

Nevertheless, under alike conditions the worn surface morphology of 1wt.% W particulate filled alloy composite the formation of micro ploughing is large as shown in Figure 4.34b. The increased in wear is due to poor bonding between the hard particulates and matrix material. A further increased in filler content in the alloy composite (i.e. 2wt.% W) the volumetric wear is reduced and formation of micro ploughing also reduced in contrast with other two compositions (See steady state Figure 4.29a and morphology Figure 4.34c). The reduction volumetric wear loss is minimal due to the existence of the layer of distilled water during sliding diminishes the wear of both the surfaces (disc and the counter pin). As far as 3wt.% and 4wt.% W particulate filled alloy composites the volumetric wear loss starts increasing and relatively more micro crack and parallel and continuous wear scars are occurs under similar operating conditions as shown in Figs. 4.34d and Figure4.34e respectively due to less uniform distribution in the matrix as compared with dry condition. From this analysis, it can be say that the 2wt% W particulate filled alloy composite attained minimum material loss as compared with other composition under similar operating condition (at sliding velocity: 0.785m/s and sliding distance: 1500 m) in both dry and wet condition

The high resolution 3D AFM topographies and their corresponding wear profiles of the worn out surfaces of different tungsten particulates alloy composites were obtained, and the representative images were presented in Figure 4.35 and 4.36 respectively. The cross sectional view not only used to quantify the wear surface mechanism but also helps to illustrates the profile of wear track with the formation of grooves and other defects on the upper surfaces. The wear profile obtained during sliding demonstrates simply the quantity of material loss and also shows the depth of the formation of grooves on the worn out surface. From this analysis, the wear profiles attained for various tungsten particulates were close to as per ASTM standards (F75 and F1537) [42]. It is clear from the Figure 4.35 and Figure 4.36 that the wear profile of 2wt.% of tungsten particulate filled alloy composites obtained reduced ploughing action and shallow depth i.e. 14.8nm for dry sliding condition and 3.5nm for wet sliding condition (See Figure 4.35c and Figure 4.36c) in contrast with 16.7, 19.7, 19.8 and 21.1nm for dry (see Figure 4.35a-4.35e) and 16.3, 7.6, 15.0 and 13.5nm for wet (Figure 4.36a-4.36e) sliding condition relative to the 0, 1, 3 and 4 wt.% of tungsten filled Co-30Cr-4Mo-1Ni alloy composites, respectively, due to minimum wear loss of fabricated alloy composites. From this analysis it can be said that the 2wt.% W particulate filled alloy composite attained minimum material loss from

the surface as compared with other weight percentage of W content (i.e. 1, 3 and 4wt.%) for both dry and wet conditions respectively.

(a) 0 wt% W

(b) 1 wt% W

(c) 2 wt% W

(d) 3 wt% W

(e) 4 wt% W
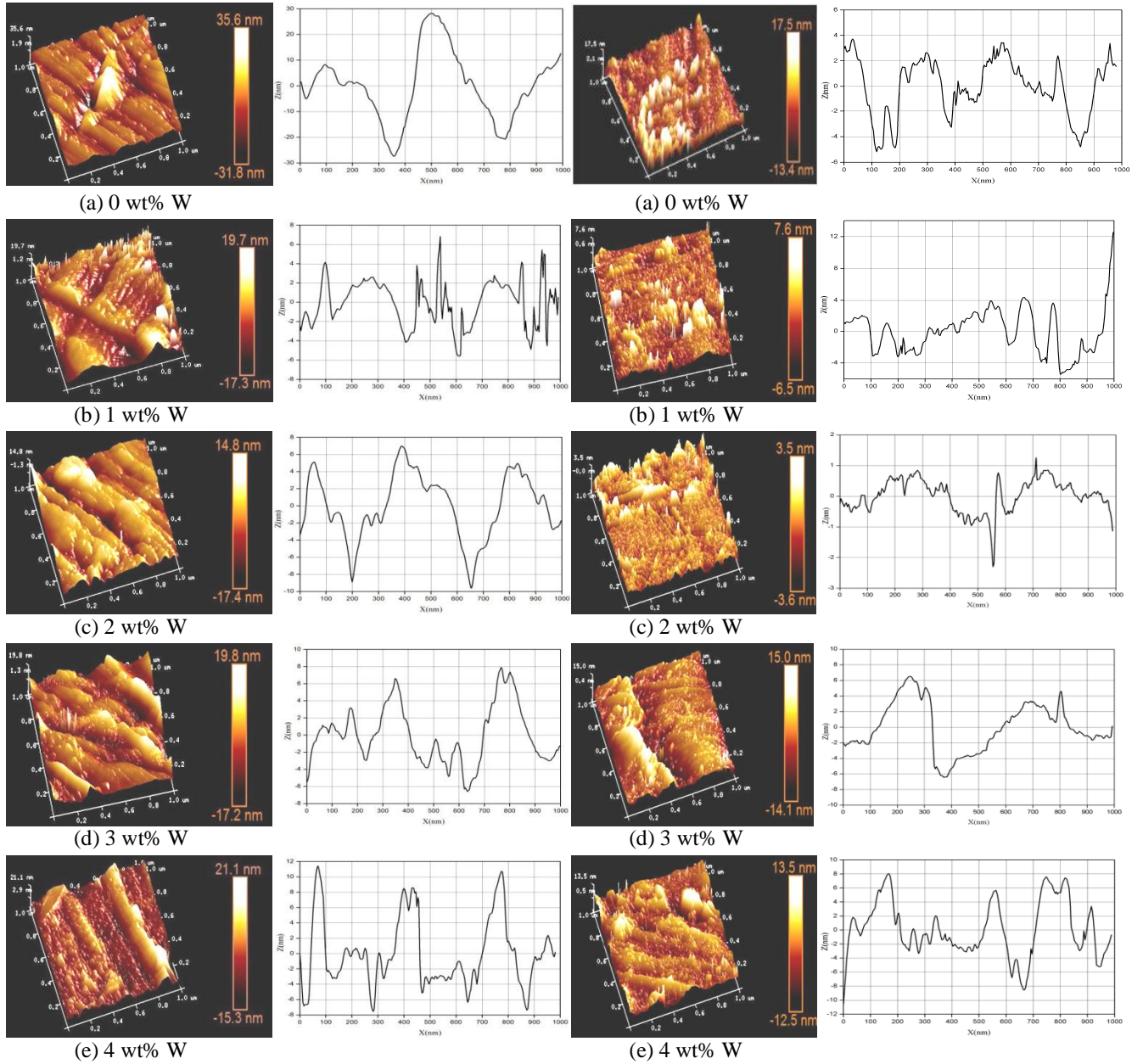
Figure 4.35: The 3D AFM micrographs and the line profiles of the worn surface of tungsten filled Co-30Cr-4Mo-1Ni alloy composite under dry condition.

Figure 4.36: The 3D AFM micrographs and the line profiles of the worn surface of tungsten filled Co-30Cr-4Mo-1Ni alloy composite under wet condition.

Table 4.18 Surface Roughness of the fabricated alloy composites

Designed alloys	Average surface roughness (R_a)	
	Dry sliding condition (nm)	Wet sliding condition (nm)
Co-30Cr-4Mo-1Ni + 0 wt.% W	16.7 nm	16.3 nm
Co-30Cr-4Mo-1Ni + 1 wt.% W	19.7 nm	7.6 nm
Co-30Cr-4Mo-1Ni + 2 wt.% W	14.8 nm	3.5 nm
Co-30Cr-4Mo-1Ni + 3 wt.% W	19.8 nm	15.0 nm
Co-30Cr-4Mo-1Ni + 4 wt.% W	21.1 nm	13.5 nm

Chapter summary

This chapter has provided:

— The effect of three different particulates (molybdenum, nickel and tungsten) on the physical and mechanical behaviour of the fabricated alloy composites.

— The effects of sliding velocity and normal load on the sliding wear response of the fabricated alloy composites.

— The results of experimental analysis using Taguchi method.

— The morphology and 3D profiles of the worn surfaces of alloy composites using SEM and AFM.

The next chapter presents to predict the wear volume of the above fabricated metal alloy composites under different operating conditions using Artificial Neural Network tool and compared with experimental results.

*****

CHAPTER 5

NEURAL NETWORK ANALYSIS ON METAL ALLOY COMPOSITES

Introduction

This chapter discusses to predict the wear volume of the fabricated alloy composites under different operating conditions and compared with experimental results by using neural network. The wear performance is considered as a non-linear problem with respect to its variables: either materials or operating conditions. To attain minimum wear volume, appropriate combinations of operating parameters has to be designed. Therefore a powerful methodology like neural network analysis is preferred to learn these interrelated effects. It is a structure comprised of numerous cross-linked simple processing units (neurons). A neural network generally consists of three parts connected in series: input layer, hidden layer and output layer respectively. In the present analysis, the normal load, sliding velocity, sliding distance and filler content are taken as the four input parameters for both the conditions (dry and wet condition).

Each of these parameters is characterized by one neuron and consequently the input layer in the ANN structure has four neurons. Experimental results sets are used to train the ANN in order to understand the input–output correlations. The input variables are normalized so as to lie in the same range group of 0–1. The outer layer of the network has only one neuron to represent volumetric wear loss. To train the neural network used for this work, about 75% of data sets obtained during sliding wear trials on different alloys samples are taken. Different ANN structures with varying number of neurons in the hidden layer are tested at constant cycles, learning rate, transfer function, transfer algorithm, error goal, momentum rate and epochs. The number of cycles selected during training is high enough so that the ANN models could be rigorously trained. A user-friendly neural network toolbox in MATLAB R2008a environment is used to perform network training using feed-forward back propagation algorithm and prediction with the ANN [41]. The results of this chapter are also divided into three parts. Part I represent the wear analysis and prediction of A-Series alloy composites based on the variation of Molybdenum filled particulates, Part II represents the wear analysis and prediction of B-Series alloy composites based on the variation of nickel filled particulates and Part III represents the wear analysis and prediction of C-Series alloy composites based on the variation of tungsten filled particulates in the Co-30Cr metal matrix as a base metal.

5.1 Part I: A-Series alloy composite (Co30Cr) based on the variation of molybdenum filled particulate

Based on the least error criterion, one structure, shown in Table 5.1, is selected for training by the input-output data of A-series alloy composites. The three-layer neural network used in this work is shown in Figure 5.1. The learning rate is varied in the range of 0.001-0.100 during the training of the input–output data. Neuron number in the hidden layer is varied and in the optimized structure of the network, this number is 15 and 13 (dry and wet conditions) for this case.
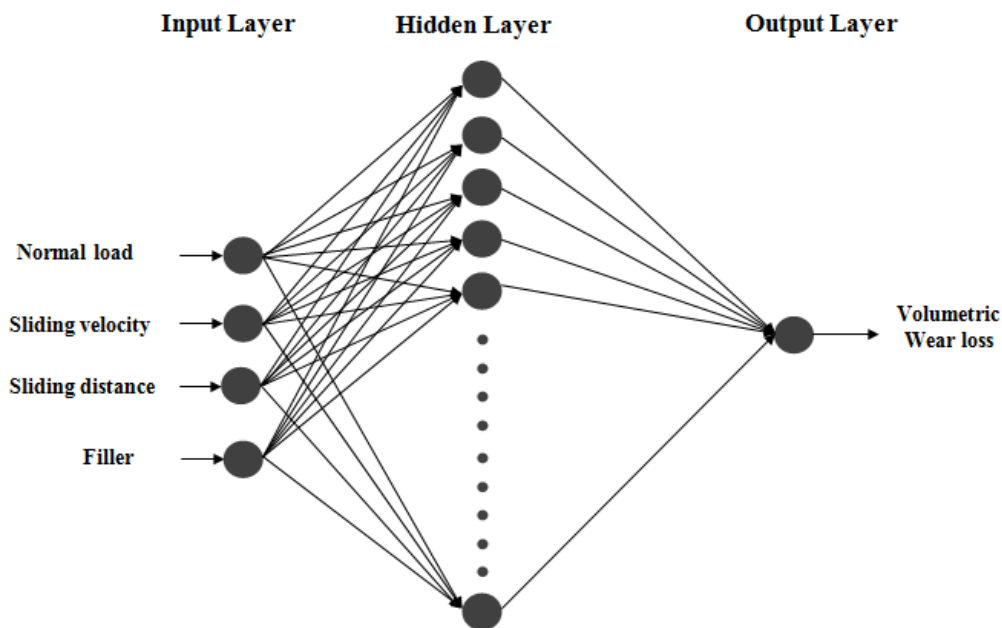
Figure 5.1: ANN structure for 'A' series alloy composite

Table 5.2 presents a comparison between the experimental values and the ANN predicted results for all 25 runs of fabricated alloy composite under both dry and wet sliding conditions. The corresponding graphs are shown in Figures 5.2 and 5.3 for dry and wet conditions. The percentage errors allied in each test run with respect to the experimental results are also shown in the Table 5.2. It is found that the error under both the conditions (i.e. dry and wet) in ANN prediction lies in the range of 0–7% which establishes the validity of the neural computation.

Table 5.1 Network architecture parameters for sliding wear behaviour.

Type	Values (Dry condition)	Values (Wet condition)
Architecture	Feed-forward back propagation	Feed-forward back propagation
Number of hidden layer (H)	15	13
Number of input layer (I)	4	4
Number of output layer (O)	1	1
Transfer function	Tan sigmoid	Tan sigmoid
Training algorithm	Gradient descent learning	Gradient descent learning
Learning rate	0.001	0.001
Error goal	1×10^{-4}	1×10^{-4}
Epochs	10,00,000	10,00,000
Momentum rate	0.001	0.001

Table 5.2 Comparison of experimental and ANN results

Test Run	Volumetric wear loss (mm^3)				Error (%)	
	Dry condition		Wet condition		Dry condition	Wet condition
	Experimental wear loss	ANN Predicted wear loss	Experimental wear loss	ANN Predicted wear loss		
1	7.2222	6.94	0.087322	0.0836	3.91	4.24
2	9.5524	8.923	0.069553	0.0683	6.59	1.87
3	7.3059	6.7345	0.079725	0.0778	7.82	2.39
4	6.0753	5.9156	0.011275	0.0107	2.63	4.83
5	2.2069	2.1983	0.021269	0.0204	0.39	4.26
6	9.0376	8.8876	0.100376	0.1012	1.66	0.85
7	3.2402	3.1776	0.032402	0.0318	1.93	1.71
8	2.1494	2.087	0.011544	0.0113	2.90	1.88
9	3.1111	2.8976	0.016711	0.0152	6.86	8.86
10	8.3333	7.8475	0.133333	0.1242	5.83	6.83
11	1.4541	1.354	0.004985	0.0047	6.88	4.91
12	4.4753	4.253	0.014198	0.0140	4.97	1.39
13	1.7067	1.6475	0.017173	0.0167	3.47	2.75
14	6.6918	6.543	0.068384	0.0670	2.22	2.02
15	1.6201	1.5342	0.016401	0.0156	5.30	4.88
16	0.3333	0.311	0.003408	0.0034	6.69	1.12
17	1.6524	1.5738	0.006584	0.0062	4.76	5.26
18	4.8603	4.7635	0.048603	0.0477	1.99	1.96
19	1.5747	1.5634	0.005747	0.0056	0.72	3.20
20	1.463	1.411	0.00463	0.0046	3.55	0.43
21	1.4977	1.3987	0.002041	0.0020	6.61	2.99
22	7.8276	7.5363	0.078276	0.0753	3.72	3.74
23	2.8889	2.7645	0.008889	0.0085	4.31	3.93
24	2.6637	2.5343	0.00677	0.0065	4.86	3.55
25	2.2509	2.154	0.002569	0.0024	4.30	5.41
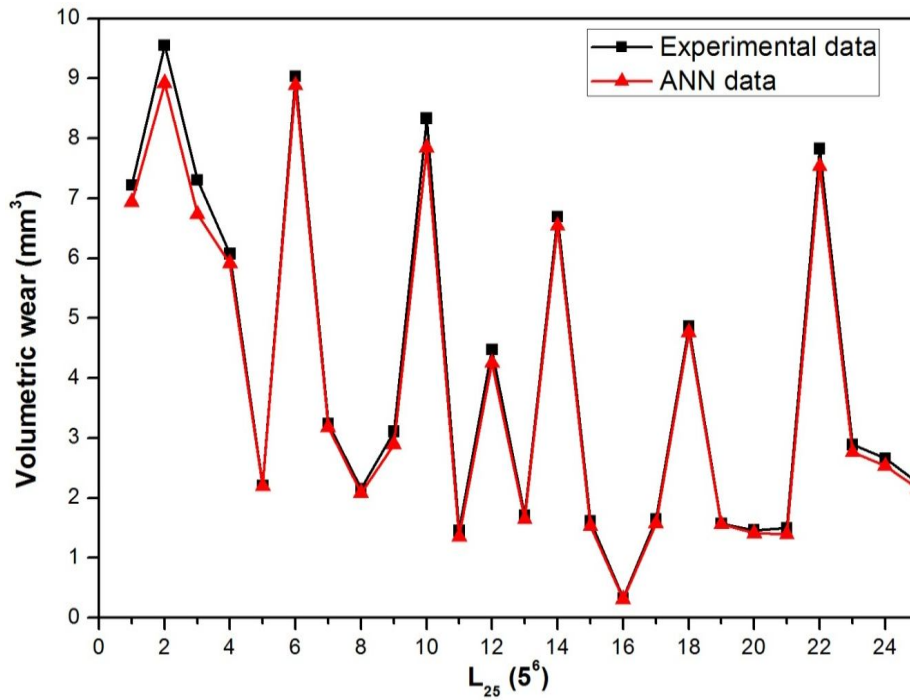
Figure 5.2: Experimental versus predicted ANN data of wear volume under dry condition as a function of L_{25} orthogonal array
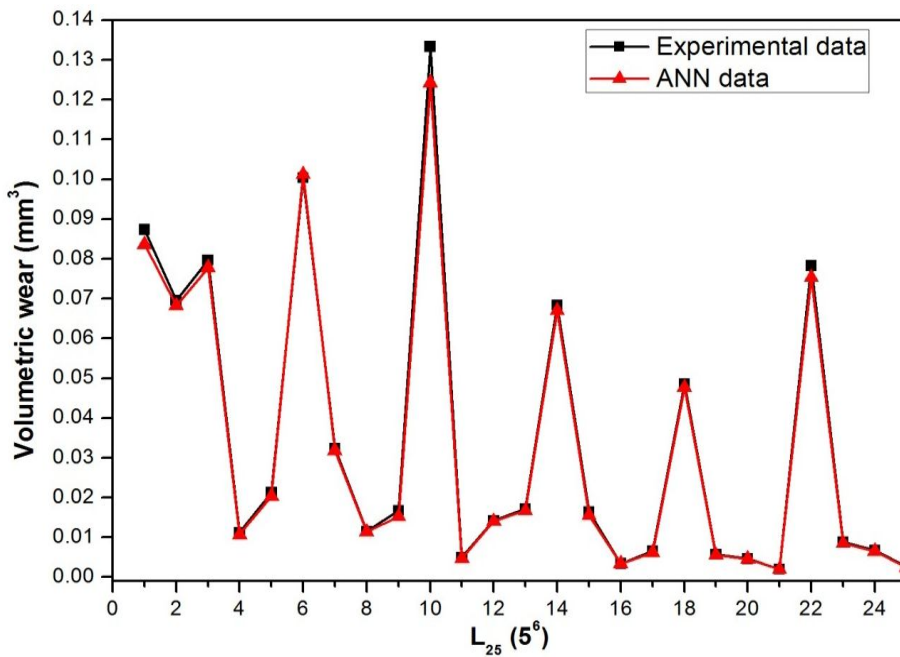
Figure 5.3: Experimental versus predicted ANN data of wear volume under wet condition as a function of L_{25} orthogonal array

5.2 Part II: B-Series alloy composite (Co30Cr4Mo) based on the variation of nickel filled particulate

Depending on the least error criterion, one structure (Table 5.3) is selected for training by the input-output data. The three-layer neural network used in this work is shown in Figure 5.4. The learning rate is varied in the range of 0.001-0.100 during the training of the input–output data. Neuron number in the hidden layer is varied and in the optimized structure of the network, this number is 11 for dry and 10 for wet conditions in this case. Table 5.4 presents a comparison between the experimental values and the ANN predicted results for all 25 runs of fabricated alloy composite. The corresponding graphs are shown in Figures 5.5 and 5.6 for dry and wet conditions. The percentage errors allied in each test run with respect to the experimental results are also shown in the table. It is found that the error in ANN prediction lies in the range of 0–10%, which establishes the validity of the neural computation.
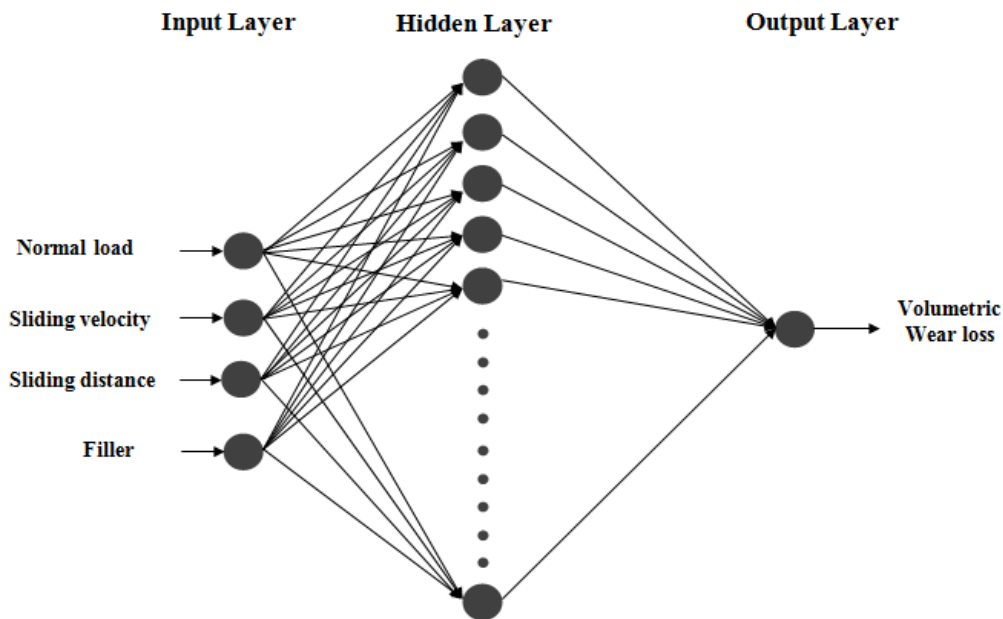
Figure 5.4: ANN structure for 'B' series alloy composite

Table 5.3 Network architecture parameters for sliding wear behaviour.

Type	Values (Dry condition)	Values (Wet condition)
Architecture	Feed-forward back propagation	Feed-forward back propagation
Number of hidden layer (H)	11	10
Number of input layer (I)	4	4
Number of output layer (O)	1	1
Transfer function	Tan sigmoid	Tan sigmoid
Training algorithm	Gradient descent learning	Gradient descent learning
Learning rate	0.001	0.001
Error goal	1×10^{-4}	1×10^{-4}
Epochs	10,00,000	10,00,000
Momentum rate	0.001	0.001

Table 5.4 Comparison of experimental and ANN results

Test Run	Volumetric wear loss (mm^3)				Error (%)	
	Dry condition		Wet condition		Dry condition	Wet condition
	Experimental wear loss	ANN Predicted wear loss	Experimental wear loss	ANN Predicted wear loss		
1	0.0858	0.0822	0.0092	0.0091	4.196	1.087
2	0.0276	0.0256	0.00264	0.00261	7.246	1.136
3	0.0343	0.0332	0.00428	0.00421	3.207	1.636
4	0.0123	0.0121	0.00108	0.00101	1.626	6.481
5	0.0119	0.0113	0.00115	0.00112	5.042	2.431
6	0.0231	0.0229	0.0028	0.0027	0.866	3.571
7	0.0115	0.0112	0.001126	0.00109	2.609	2.902
8	0.0073	0.0069	0.00069	0.00065	5.479	5.797
9	0.0027	0.0026	0.0002	0.00021	3.704	4.545
10	0.0662	0.066	0.0068	0.0067	0.302	1.471
11	0.0044	0.0042	0.00039	0.00038	4.545	3.943
12	0.0033	0.0031	0.00025	0.00024	6.061	4.000
13	0.0018	0.00175	0.00014	0.00014	2.778	0.920
14	0.0548	0.0547	0.006	0.0056	0.182	6.667
15	0.0142	0.0139	0.00144	0.00142	2.113	1.389
16	0.0015	0.00145	0.00015	0.00015	3.333	1.935
17	0.001	0.00097	0.00096	0.00094	2.500	2.083
18	0.0209	0.0201	0.00198	0.0019	3.828	4.040
19	0.0046	0.0043	0.00037	0.00036	6.522	2.667
20	0.0017	0.00164	0.00018	0.00016	3.529	6.111
21	0.0004	0.00038	0.000044	0.00004	5.000	6.250
22	0.0105	0.0101	0.001024	0.001	3.810	2.344
23	0.0048	0.0045	0.000484	0.00045	6.250	7.025
24	0.0012	0.0011	0.000101	0.0001	8.333	1.283
25	0.0015	0.00139	0.000184	0.00017	7.333	4.348
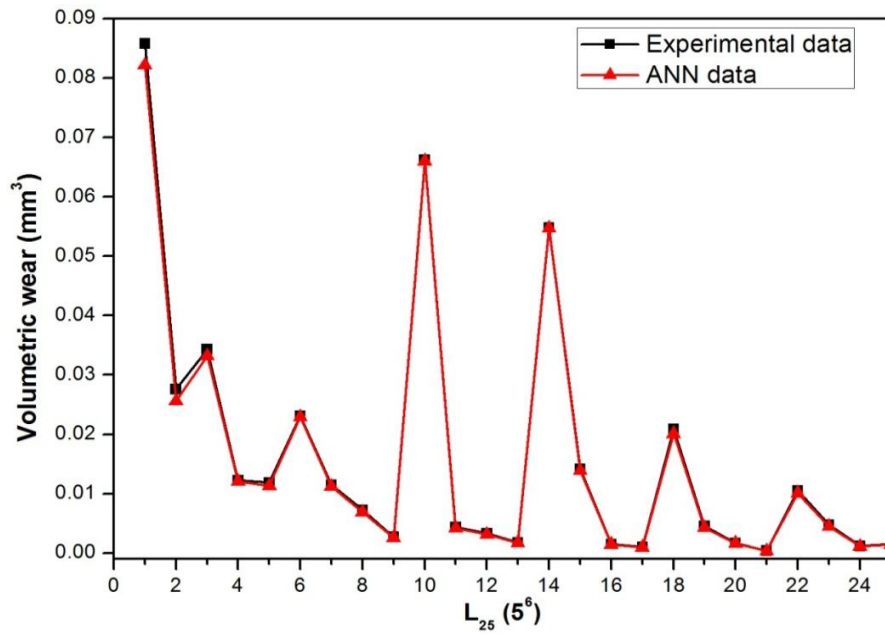
Figure 5.5: Experimental versus predicted ANN data of wear volume under dry condition as a function of L_{25} orthogonal array
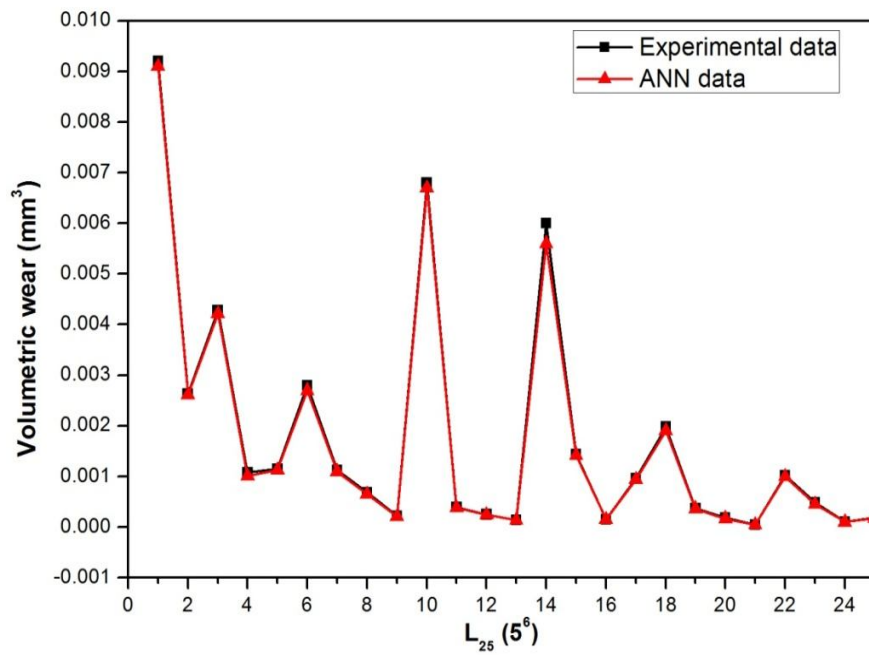
Figure 5.6: Experimental versus predicted ANN data of wear volume under wet condition as a function of L_{25} orthogonal array

5.3 Part III: C-Series alloy composite (Co30Cr4Mo1Ni) based on the variation of tungsten filled particulate

Depending on the least error criterion, one structure, shown in Table 5.5, is selected for training by the input-output data. The three-layer neural network used in this work is shown in Figure 5.7. The learning rate is varied in the range of 0.001– 0.100 during the training of the input–output data. Neuron number in the hidden layer is varied and in the optimized structure of the network, this number is 14 and 15 (i.e. dry and wet condition) for this case. Table 5.6 presents a comparison between the experimental values and the ANN predicted results for all 25 runs of fabricated alloy composites under both dry and wet sliding conditions. The corresponding plots are shown in Figures 5.8 and 5.9 for dry and wet conditions .The percentage errors allied in each test run with respect to the experimental results are also shown in the table. It is found that the error under both the conditions (dry and wet) in ANN prediction lies in the range of 0–10%, which establishes the validity of the neural computation.
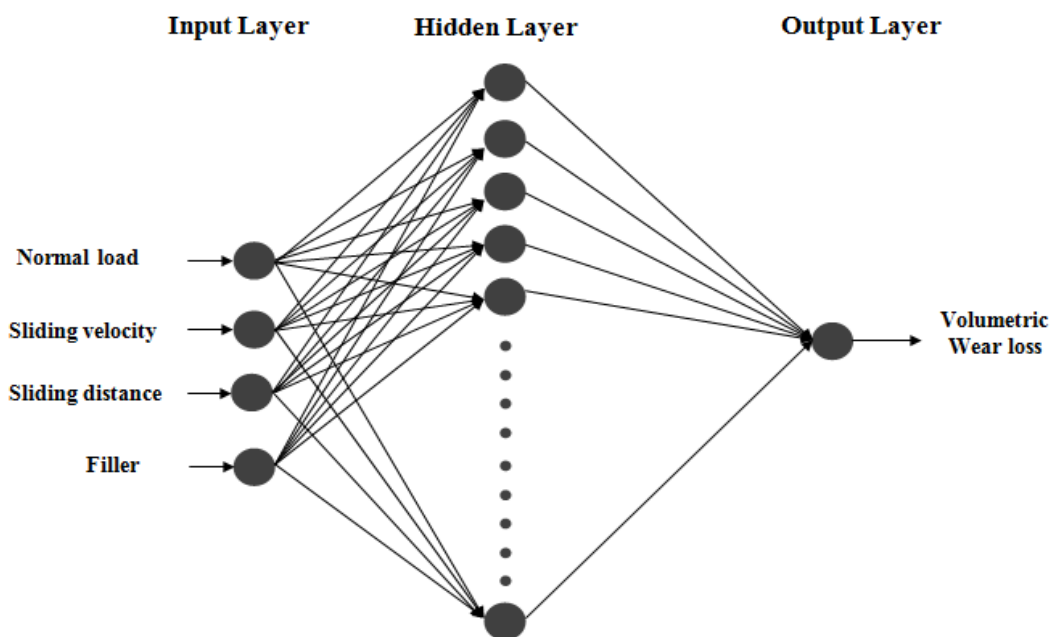
Figure 5.7: ANN structure for 'C' series alloy composite

Table 5.5 Network architecture parameters for sliding wear behaviour.

Type	Values (Dry condition)	Values (Wet condition)
Architecture	Feed-forward back propagation	Feed-forward back propagation
Number of hidden layer (H)	14	15
Number of input layer (I)	4	4
Number of output layer (O)	1	1
Transfer function	Tan sigmoid	Tan sigmoid
Training algorithm	Gradient descent learning	Gradient descent learning
Learning rate	0.001	0.001
Error goal	1×10^{-4}	1×10^{-4}
Epochs	10,00,000	10,00,000
Momentum rate	0.001	0.001

Table 5.6 Comparison of experimental and ANN results

Test Run	Volumetric wear loss (mm^3)				Error (%)	
	Dry condition		Wet condition		Dry condition	Wet condition
	Experimental wear loss	ANN Predicted wear loss	Experimental wear loss	ANN Predicted wear loss		
1	0.045819	0.04376	0.004592	0.00447	4.493	2.657
2	0.033800	0.03198	0.004000	0.003764	5.385	5.900
3	0.015733	0.01465	0.000136	0.000127	6.886	6.324
4	0.013500	0.01276	0.001260	0.001157	5.481	8.151
5	0.011120	0.01063	0.000928	0.000864	4.406	6.897
6	0.011000	0.01054	0.000105	9.94E-05	4.182	5.333
7	0.009800	0.00886	0.000880	0.00083	9.592	5.739
8	0.006250	0.005897	0.000063	0.000058	5.648	7.200
9	0.002880	0.002647	0.000444	0.000423	8.090	4.730
10	0.034200	0.03176	0.002140	0.002035	7.135	4.907
11	0.004356	0.004174	0.000560	0.000518	4.168	7.500
12	0.002767	0.002654	0.000049	0.000046	4.072	6.757
13	0.002933	0.002874	0.000248	0.000227	2.023	8.306
14	0.013067	0.012334	0.000135	0.000123	5.607	8.663
15	0.007467	0.00694	0.000793	0.000728	7.054	8.298
16	0.001150	0.001076	0.000140	0.000129	6.435	7.857
17	0.000760	0.000695	0.000860	0.000844	8.526	1.860
18	0.012100	0.011835	0.001360	0.001295	2.190	4.779
19	0.004650	0.00428	0.000615	0.000604	7.957	1.854
20	0.002600	0.002534	0.000530	0.000504	2.538	4.906
21	0.000400	0.00039	0.000058	0.000057	2.500	1.042
22	0.008640	0.00849	0.000936	0.000902	1.736	3.632
23	0.004080	0.0038	0.000500	0.000476	6.863	4.800
24	0.001893	0.001734	0.000173	0.000165	8.415	5.038
25	0.000620	0.000562	0.000048	0.000045	9.306	6.250
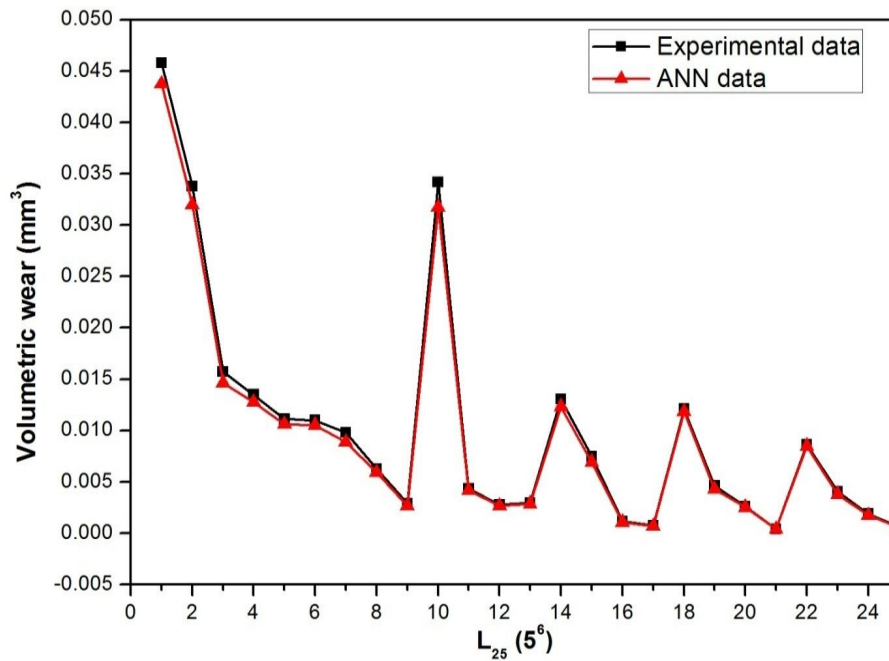
Figure 5.8: Experimental versus predicted ANN data of wear volume under dry condition as a function of L_{25} orthogonal array
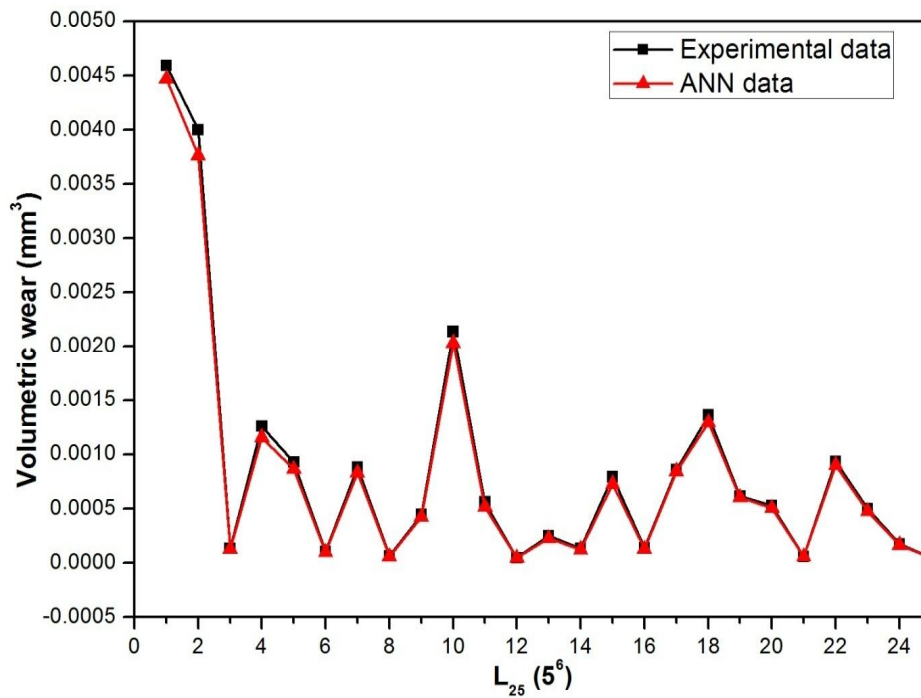
Figure 5.9: Experimental versus predicted ANN data of wear volume under wet condition as a function of L_{25} orthogonal array

Chapter summary

The research presented in this chapter illustrates that the use of a neural network tool to simulate experiments with parametric design strategy is effective, efficient and helps to predict the wear response of fabricated alloy composites under different test conditions within and beyond the experimental domain. The predicted and the experimental values of wear volume exhibit good agreement and validate the remarkable prediction capability of a well-trained neural network for this kind of processes.

The next chapter presents the corrosive nature and biocompatibility behaviour of the fabricated metal alloy composites according to the formulation.

*****

CHAPTER 6
CORROSION AND BIOCOMPATIBILITY ANALYSIS ON METAL ALLOY COMPOSITES

Introduction

This chapter discusses the results of corrosion behaviour and to analyze the biocompatibility of the fabricated metal alloy composites according to the formulations discussed in the previous chapter. The effect of particulates such as molybdenum, nickel and tungsten with different weight percentage of corrosion resistance property of the fabricated alloy composites is discussed. The interpretation of the results and the comparison among various samples are also presented. The results of this chapter are divided into two parts. First part represents the corrosion resistance behaviour of 'A', 'B' and 'C' series alloy composite based on the variation of molybdenum, nickel and tungsten filled particulates. Second part represents the biocompatibility analysis of the optimum weight percentage of particulates (i.e. molybdenum, nickel and tungsten) in 'A', 'B' and 'C' series alloy composite under wear characterization. Corrosion resistance measurement is analyzed by the electrochemical test method and by using histological test to analyze the biological response (i.e. inflammatory or macrophage cells) of the fabricated alloy composites.

6.1 Part I: A-Series alloy composite (Co30Cr) based on the variation of molybdenum filled particulate

6.1.1 Electrochemical test

Figure 6.1a shows the open circuit potential (OCP) for 'A' series (i.e. Co30Cr) fabricated alloy composite, addition with different wt.% of molybdenum works as stationary electrodes submerged in a NaCl solution at 37ºC and pH 7.4.The open circuit potential (E_{OC}), of a metal varies as a function of time but stabilizes at a fixed value after a long period of immersion. If open circuit potential is higher than material characterized better corrosion resistance. Based on that, Figure 6.1a clearly shows that after 1 hr exposure, an approximately constant value of -0.12 V is attained when addition of 4wt.% of molybdenum content in the matrix material which shows higher (see Figure 6.1a) as compared to the other weight fraction of molybdenum.

Figure 6.1b and Table 2 show the anodic polarization curves and data respectively. Table 2 shows the corrosion potential of fabricated 'A' series alloy composites with different weight percentage of molybdenum filled particulate. It is clearly seen that the 1wt. % of particulate

filled molybdenum alloy under NaCl solution is much more negative than those of the rest of the particulate filled alloys in a metal matrix. Furthermore, the corrosion current of 1wt. % of particulate filled molybdenum is much larger as compared to 0wt.%, 2wt.%, 3wt.% and 4wt.% of molybdenum filled particulate alloy composites respectively. This is an expected outcome, since the corrosion current is directly proportional to the corrosion rate, the lower the corrosion current the better its resistance against corrosion. Similarly, the more positive or anodic the corrosion current, the higher the resistance against corrosion. By definition, the corrosion of implants implies that a certain amount of ions is released from the implanted metal into the body [312]. The released ions may be deposited in certain parts of the body, causing systematic reactions [313, 314]. The obtained results are alike to previous studies in our research group [315]. When the corrosion potentials and currents of fabricated alloy composites with different wt.% of molybdenum filled particulates are compared, it can be seen that Co-30Cr with addition of 4wt.% Mo has a more positive corrosion potential and lower corrosion current as compared to the other weight percentage of molybdenum content. Thus, it can be concluded that Co-30Cr with addition of 4wt.% Mo is more stable against corrosion in 'A' series alloy composites.
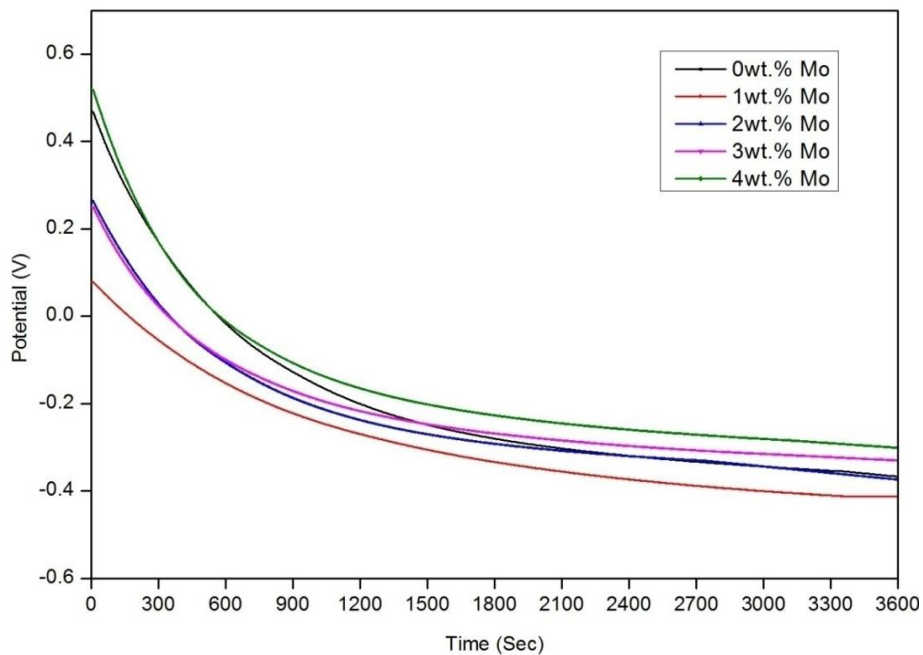
Figure 6.1a: Open Circuit Potential (OCP) curves for different wt.% of Mo
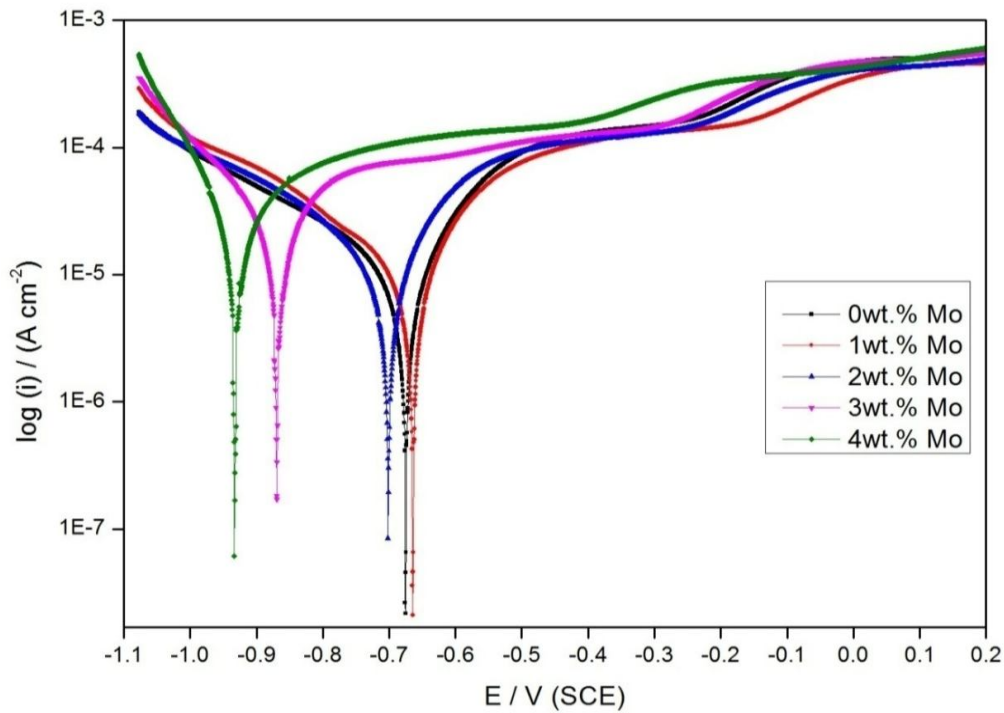
Figure 6.1b: Tafel polarization curves for different wt.% of Mo

Table 6.1 Corrosion parameters obtained with Tafel polarization method for 'A' series alloy composites at 37ºC

Sample	I_{corr} ($\mu A/cm^2$)	E_{corr} (mV)	Corrosion rate (mm/yr)
Co30Cr + 0 wt.% Mo	221	-751	0.411
Co30Cr + 1 wt.% Mo	256	-773	0.315
Co30Cr + 2 wt.% Mo	172	-722	0.251
Co30Cr + 3 wt.% Mo	74	-702	0.105
Co30Cr + 4 wt.% Mo	65	-675	0.104

6.2 Part II: B-Series alloy composite (Co30Cr4Mo) based on the variation of nickel filled particulate

6.2.1 Electrochemical test

Figure 6.2a shows the open circuit potential (OCP) for 'B' series (i.e. Co30Cr4Mo) alloy composites, addition with different wt.% of nickel works as stationary electrodes submerged in a NaCl solution at 37ºC and pH 7.4.The open circuit potential (E_{OC}), of a metal varies as a function of time but stabilizes at a fixed value after a long period of immersion. If open circuit potential is higher than material characterized better corrosion resistance. Based on that, Figure 6.2a clearly

shows that after one hour exposure, an approximately constant value of -0.25V is attained when addition of 4 wt.% of nickel content in the matrix material which shows higher (see Figure 6.2a) as compared to other wt.% Ni.

Figure 6.2b and Table 6.2 show the anodic polarization curves and data respectively. Table 6.2 shows the corrosion potential of fabricated 'B' series alloy composites with different weight percentage of nickel particulates. It is clearly seen that the unfilled alloy composite under NaCl solution is much more negative than those of particulate (i.e. 1wt.%, 2wt.%, 3wt.% and 4wt.%) filled nickel alloys. Furthermore, the corrosion current of 0wt.%Ni is much larger as compared to nickel filled particulate alloys. This is an expected outcome, since the corrosion current is directly proportional to the corrosion rate, the lower the corrosion current the better its resistance against corrosion. Similarly, the more positive or anodic the corrosion current, the higher the resistance against corrosion. By definition, the corrosion of implants implies that a certain amount of ions is released from the implanted metal into the body [312]. The released ions may be deposited in certain parts of the body, causing systematic reactions [313, 314]. The obtained results are alike to previous studies in our research group [315]. When the corrosion potentials and currents of fabricated alloys with different wt. % of particulate filled nickel are compared, it can be seen that Co30Cr4Mo with addition of 4wt.% of particulate filled nickel in the metal matrix has a more positive corrosion potential and lower corrosion current as compared to the other weight percentage of nickel content. Thus, it can be concluded that Co30Cr4Mo with addition of 4wt.% Ni particulate filled alloy composite is more stable against corrosion in 'B' series metal matrix.
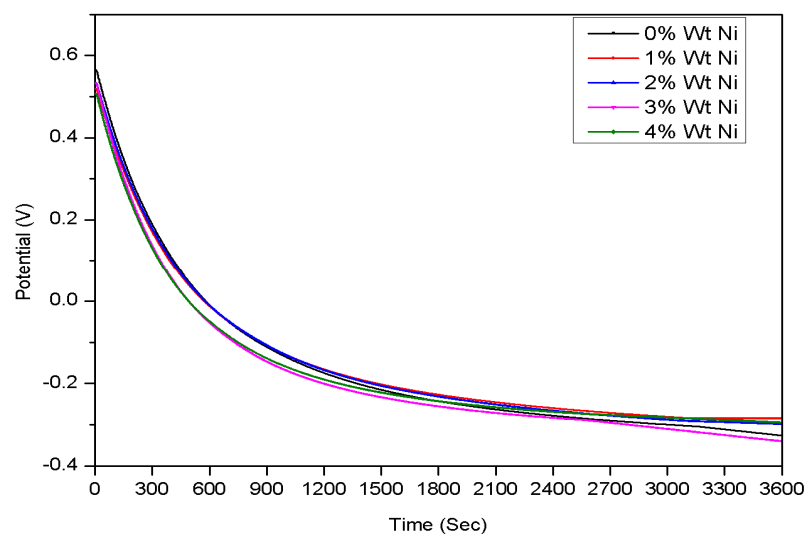
Figure 6.2a: Open Circuit Potential (OCP) curves for different wt. % of Ni
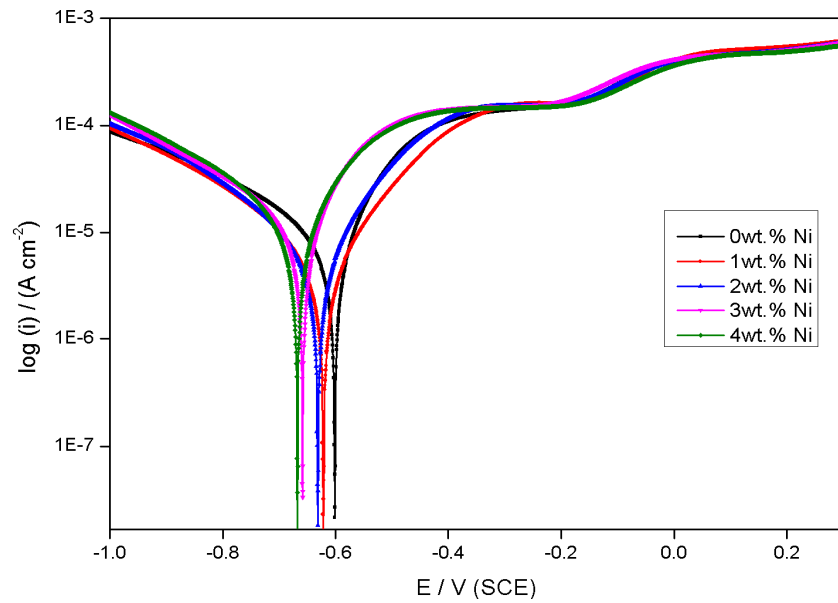
Figure 6.2b: Tafel polarization curves for different wt. % of Ni

Table 6.2 Corrosion parameters obtained with Tafel polarization method for 'B' series alloy composites at 37ºC

Sample	I_{corr} ($\mu A/cm^2$)	E_{corr} (mV)	Corrosion rate (mm/yr)
Co30Cr4Mo + 0 wt.% Ni	300	-689	0.499
Co30Cr4Mo + 1 wt.% Ni	184	-677	0.458
Co30Cr4Mo + 2 wt.% Ni	170	-658	0.432
Co30Cr4Mo + 3 wt.% Ni	164	-641	0.239
Co30Cr4Mo + 4 wt.% Ni	124	-626	0.221

6.3 Part III: C-Series alloy composite (Co30Cr4Mo1Ni) based on the variation of tungsten filled particulate

6.3.1 Electrochemical test

Figure 6.3a shows the open circuit potential (OCP) for 'C' series alloy composites (i.e. Co30Cr4Mo1Ni) addition with different wt.% of tungsten works as stationary electrodes submerged in a NaCl solution at 37ºC and pH 7.4.The open circuit potential (E_{OC}), of a metal varies as a function of time but stabilizes at a fixed value after a long period of immersion. In open circuit potential is higher than material characterized better corrosion resistance. Based on that, Figure 6.3a clearly shows that after 1 hr exposure, an approximately constant value of -0.30 V is attained when addition of 2wt.% of tungsten content in the matrix material which shows higher as compared to other weight percentage of tungsten. Figure 6.3b and Table 6.3 show the

anodic polarization curves and data respectively. Table 6.3 shows the corrosion potential of fabricated 'C' series alloy composite with different weight percentage of tungsten filled particulate. It is clearly seen that the 4wt.% of particulate filled tungsten alloy under NaCl solution is much more negative than 0-3wt.% particulate filled tungsten alloys. Furthermore, the corrosion current of 4wt.% W is much larger as compared to the rest of all the particulate filled tungsten alloys. This is an expected outcome, since the corrosion current is directly proportional to the corrosion rate, the lower the corrosion current the better its resistance against corrosion. Similarly, the more positive or anodic the corrosion current, the higher the resistance against corrosion. By definition, the corrosion of implant implies that a certain amount of ions is released from the implanted metal into the body [312]. The released ions may be deposited in certain parts of the body, causing systematic reactions [313, 314]. The obtained results are similar to previous studies in our research group [315]. When the corrosion potentials and currents of fabricated alloy composites with different wt.% W are compared, it can be seen that Co30Cr4Mo1Ni with addition of 2wt.% W in the matrix has a more positive corrosion potential and lower corrosion current as compared to the other weight percentage of tungsten content. Thus, it can be concluded that Co30Cr4Mo1Ni with addition of 2wt.% of particulate filled tungsten alloy is more stable against corrosion in 'C' series metal matrix.
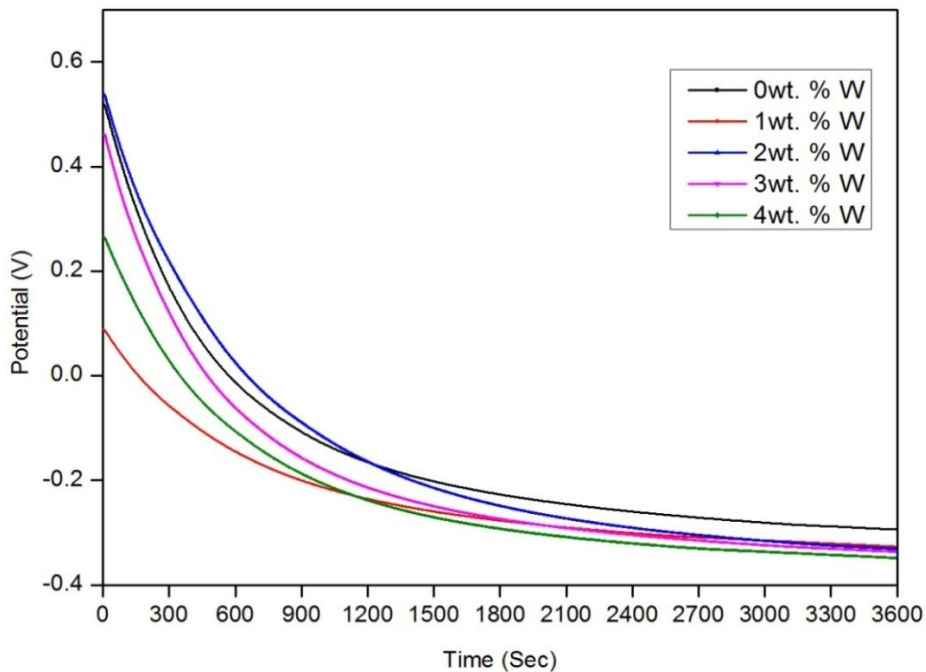
Figure 6.3a: Open Circuit Potential (OCP) curves for different wt. % of W
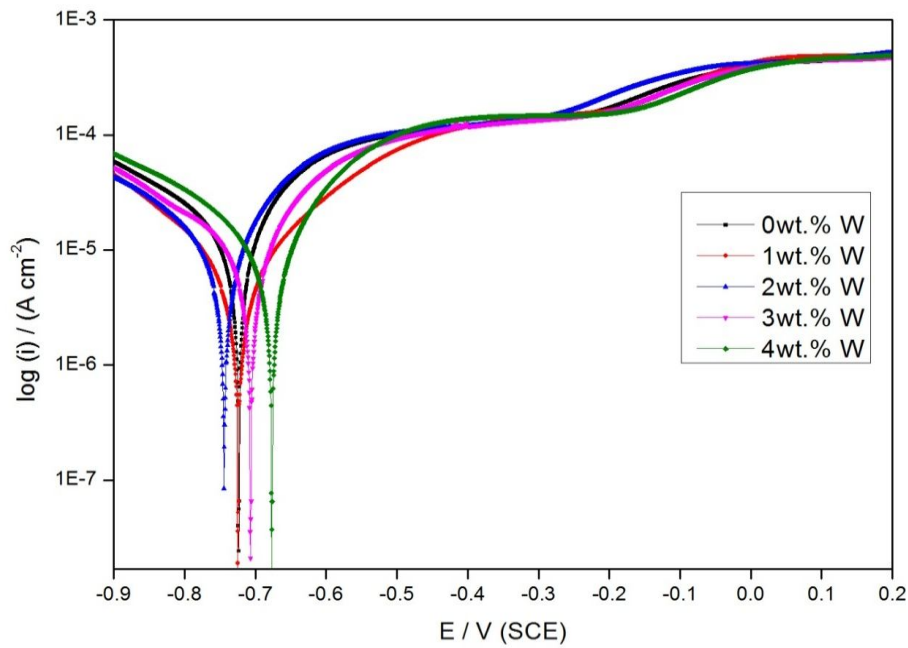
Figure 6.3b: Tafel polarization curves for different wt. % of W

Table 6.3 Corrosion parameters obtained with Tafel polarization method for 'C' series alloy composites at 37ºC

Sample	I_{corr} ($\mu A/cm^2$)	E_{corr} (mV)	Corrosion rate (mm/yr)
Co30Cr4Mo1Ni + 0 wt.% W	142	-691	0.239
Co30Cr4Mo1Ni + 1 wt.% W	134	-671	0.218
Co30Cr4Mo1Ni + 2 wt.% W	102	-653	0.152
Co30Cr4Mo1Ni + 3 wt.% W	175	-710	0.266
Co30Cr4Mo1Ni + 4 wt.% W	193	-733	0.276

6.4 Biocompatibility test

After examine the optimum wear loss and corrosion resistance analysis of fabricated alloy composites for femoral head material, there is also need to observe the biological response before implanted in the human body. For this, a histological test is conducted on 3 male adult rats to check the biocompatibility of the fabricated alloy composites (i.e. Co30Cr4Mo, Co30Cr4Mo2Ni and Co30Cr4Mo2Ni1W). Figure 6.4a shows the microscopic observation of control rat skin showed stratified epithelium which is united to the dermis by thin basal lamina without showing any degenerative changes.

Figures 6.4b-6.4d shows the biopsy micrograph of rat skin implanted with fabricated alloy composites i.e. Co30Cr4Mo, Co30Cr4Mo1Ni and Co30Cr4Mo2Ni1W. Microscopic observation of these figures shows that same structure as that of control rats. There is no inflammatory cell immigration, no epidermal necrosis, no vacuolar degeneration of basal cell, no edema, no adenexal atrophy and vesicle formation. These changes are usually observed in the skin of rat implanted with metal plates. Thus implantation of metal plates (i.e. fabricated alloy composites) has not caused any histopathological lesions in the skin of rats. Thus the novel fabricated alloy composite is safe in animal (rat) model.
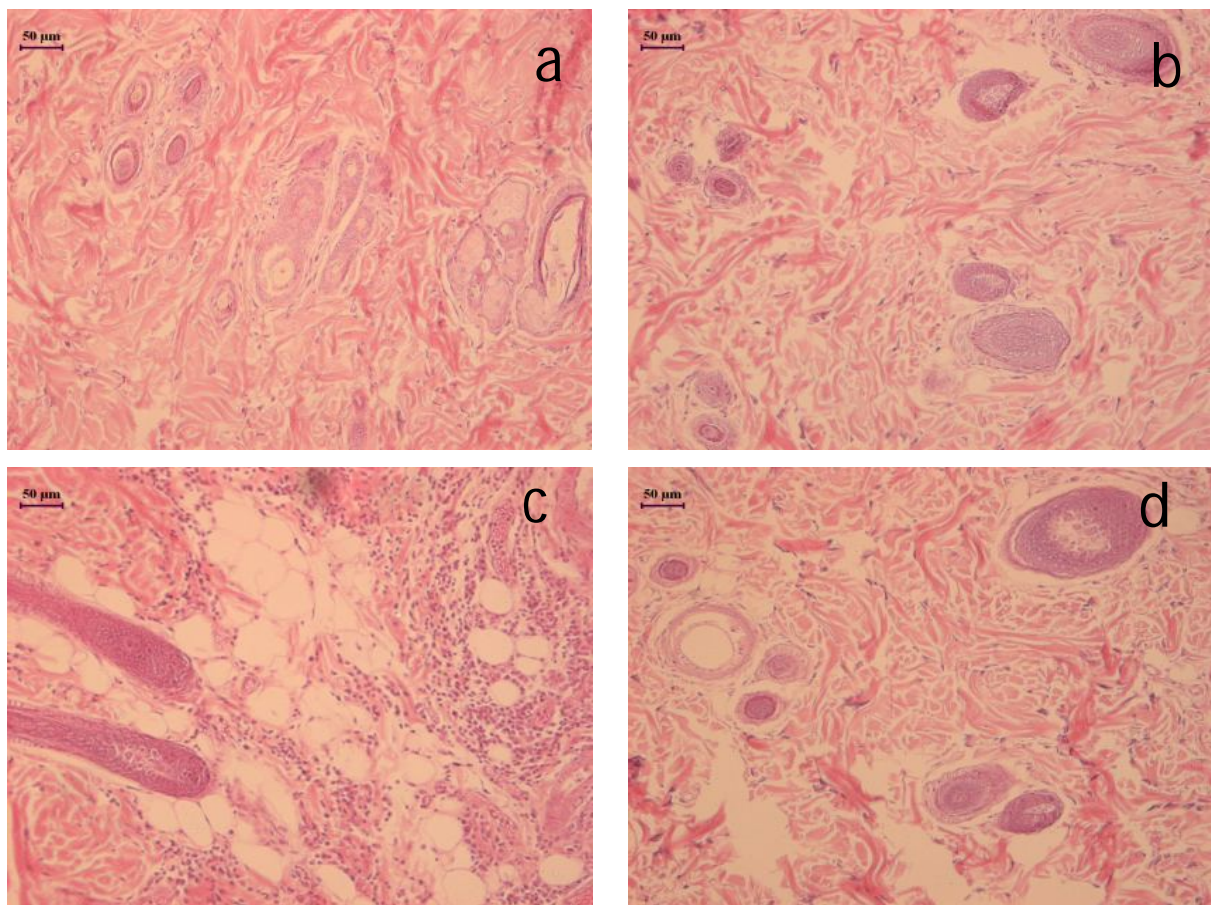
Figure 6.4: Histopathological micrographs of (a) Control rat skin, (b) Co30Cr4Mo rat skin, (c) Co30Cr4Mo1Ni rat skin and (d) Co30Cr4Mo1Ni2W rat skin

Chapter summary

This chapter summarises that:

- The corrosion resistance behaviour and biological response of the fabricated metal alloy composites.

- The inclusion of particulates i.e. 4wt. % Mo, 4wt.% Ni and 2wt.%W with Co-30Cr metal matrix exhibited superior resistance against corrosion for A, B and C series metal alloy composites respectively.

- The histology test of the samples (i.e. fabricated alloy composites) showed that there is no inflammatory cell immigration, no epidermal necrosis, no vacuolar degeneration of basal cell, no edema, no adenexal atrophy and vesicle formation.

The next chapter briefly discusses the ranking of the fabricated metal alloy composites by using ENTROPY-PROMETHEE approach under a set of conflicting performance defining criteria.

*****

CHAPTER 7

RANKING OF THE PHYSICAL, MECHANICAL AND SLIDING WEAR PROPERTIES METAL ALLOY COMPOSITES

Introduction

In the present study, a multi criteria decision making (MCDM) technique called ENTROPY-PROMETHEE (Preference Ranking Organization Method for Enrichment Evaluations) is applied to select the best alternatives from the fabricated alloy composite materials based on the physical, mechanical and sliding wear properties. MCDM has been one of the very fast growing areas of operational research during the two last decades. The MCDM often deals with ranking of many concrete alternatives from the best of the worst ones based on multiple conflicting criteria. The MCDM is also concerned with theory and methodology that can treat complex problems encountered in engineering, management, science, etc. There are numerous MCDM methods such as: AHP (Analytic Hierarchy Process), TOPSIS (Technique for Order Preference by Similarity to Ideal Solution), GRA (Grey Relation Analysis), VIKOR (Vise Kriterijumska Optimizacija Kompromisno Resenje), PSI (Preference Selection Index), ELECTRE (Elimination and Choice Translating Reality), PROMETHEE (Preference Ranking Organization Method for Enrichment Evaluations), ROVM (Range of value method) etc. have been proposed to help in selecting the best compromise alternatives. Among all, PROMETHEE is a quite simple ranking method of conception and application compared with the other methods. Brans [316] proposed the PROMETHEE in 1982. The PROMETHEE methods use pairwise comparisons and outranking relationships to choose the best alternatives. Specifically, they compute positive and negative preference flows for each alternative and help the designer to make the final selection. The positive preference flow indicates how an alternative is outranking all the other alternatives and the negative preference flow indicates how an alternative is outranked by all the other alternatives. The determination of weight for each criterion is important for the smooth functioning of PROMETHEE, which is determined by entropy method. The hybrid entropy-PROMETHEE approach was successfully applied to surpass the ambiguities involved in the complete ranking of alternatives.

7.1 Evaluation methodology

Multi-criteria decision making (MCDM) has been one of the very fast growing areas of operational research during the two last decades. The MCDM methods are commonly used to

---

solve this type of problems, where number of defining performance criteria or alternatives is more. For this, Entropy method is employed to determine the weight of different criteria, and the best suited alternative is selected by PROMETHEE method. The schematic of the proposed MCDM model is given in Figure 7.1. The evaluation methodology consists of the following four main phases namely:

Phase I: Determination of alternatives and criterions

Phase II: Construction of decision matrix

Phase III: Determination of weight

Phase IV: Selection of optimal composition
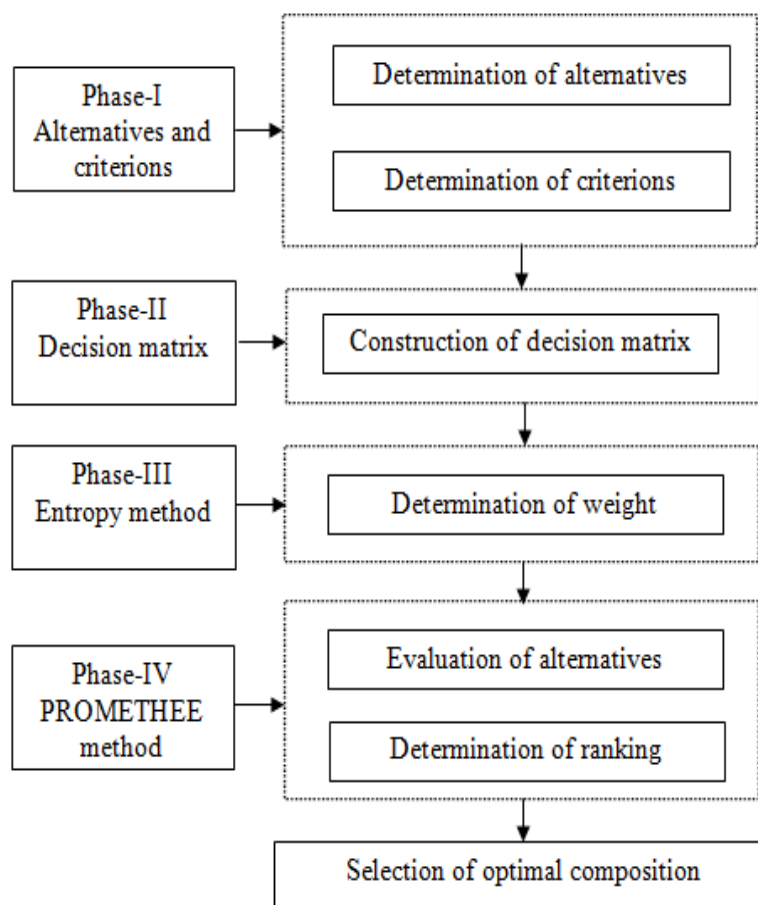
Figure 7.1: Schematic of the proposed methodology.

7.1.1 Phase I: Determination of alternatives and criterions

In this phase, the number of alternatives and criterions used in the performance evaluation of wear composite materials is identified. The various alternatives and identified criterions based on

physical performance, mechanical performance; volumetric wear performance and coefficient of friction performance are briefly described in Table 7.1 and Table 7.2 respectively.

Table 7.1 Description of the different alternatives

Composites	Sample designation	Composition
1	M-0	Base material + Filler (Co-30Cr + 0 wt.% Mo)
2	M-1	Base material + Filler (Co-30Cr + 1 wt.% Mo)
3	M-2	Base material + Filler (Co-30Cr + 2 wt.% Mo)
4	M-3	Base material + Filler (Co-30Cr + 3 wt.% Mo)
5	M-4	Base material + Filler (Co-30Cr + 4 wt.% Mo)
6	N-1	Base material + Filler (Co-30Cr-4Mo + 1 wt.% Ni)
7	N-2	Base material + Filler (Co-30Cr-4Mo + 2 wt.% Ni)
8	N-3	Base material + Filler (Co-30Cr-4Mo + 3 wt.% Ni)
9	N-4	Base material + Filler (Co-30Cr-4Mo + 4 wt.% Ni)
10	W-1	Base material + Filler (Co-30Cr-4Mo-1Ni + 1 wt.% W)
11	W-2	Base material + Filler (Co-30Cr-4Mo-1Ni + 2 wt.% W)
12	W-3	Base material + Filler (Co-30Cr-4Mo-1Ni + 3 wt.% W)
13	W-4	Base material + Filler (Co-30Cr-4Mo-1Ni + 4 wt.% W)

Table 7.2 Description of the different criterions

Criterions	Feature	Unit	Test conditions	Performance implications
C-1	Density	gm/cc		Lower-the-better
C-2	Hardness	HRC	ASTM E-92	Higher-the-better
C-3	Compressive strength	MPa	ASTM E 209-00	Higher-the-better
C-4	Volumetric wear (5N, 0.78m/s, 1500m)	mm^3	ASTM G 99	Lower-the-better
C-5	Volumetric wear (15N, 0.78m/s, 1500m)	mm^3	ASTM G 99	Lower-the-better
C-6	Volumetric wear (25N, 0.78m/s, 1500m)	mm^3	ASTM G 99	Lower-the-better
C-7	Volumetric wear (0.26m/s, 15N, 1500m)	mm^3	ASTM G 99	Lower-the-better
C-8	Volumetric wear (0.52m/s, 15N, 1500m)	mm^3	ASTM G 99	Lower-the-better
C-9	Volumetric wear (1.04m/s, 15N, 1500m)	mm^3	ASTM G 99	Lower-the-better
C-10	Coefficient of friction (5N, 0.78m/s, 1500m)	mm^3	ASTM G 99	Lower-the-better
C-11	Coefficient of friction (15N, 0.78m/s, 1500m)	mm^3	ASTM G 99	Lower-the-better
C-12	Coefficient of friction (25N, 0.78m/s, 1500m)	mm^3	ASTM G 99	Lower-the-better
C-13	Coefficient of friction (0.26m/s, 15N, 1500m)	mm^3	ASTM G 99	Lower-the-better
C-14	Coefficient of friction (0.52m/s, 15N, 1500m)	mm^3	ASTM G 99	Lower-the-better
C-15	Coefficient of friction (1.04m/s, 15N, 1500m)	mm^3	ASTM G 99	Lower-the-better

7.1.2 Phase II: Construction of decision matrix

After identifying the alternatives and criterions, the value of experimental results for each alternative with respected criterion is expressed in the form of a decision matrix.

7.1.3 Phase III: Determination of criteria weights

Due to the distinct significance of the criterions in the performance evaluation of wear materials, one cannot presume that each criterion is of equivalent importance. There are numerous methods that can be used to determine weights [319] such as the simple additive weighting method, weighted least square method, Analytic hierarchy process method, Eigen-vector method, entropy method, and Linear Programming Techniques for Multi-dimensional of Analysis Preference (LINMAP). The selection of method depends on the nature of problems.

Shannon et al. [320] introduced a theory on information basis which known as entropy method. The quantity of information obtained by people is one of the factors for evaluation accuracy and reliability of information. In the information theory, the entropy is measured with the discrete index of system. If the index is lesser, the information provided through the index is more, thus the index should has more effect during evaluation, the weights should be larger [321]. Therefore the entropy can determine weights for factors. The entropy weight is determined by the matrix constructed based on the monitoring indicators of the factors. The evaluation result can be more objective because the weights of factors can avoid the subjective factor. Chen et al. [277] and Zhi-hong [278] utilized entropy method for determination of weight of evaluating factors for ground water and quality assessment of a river. They found more accurate results after utilization of entropy weight of each criterion and outcomes are more subjectivity of expert evaluation. In their study, the weights of the criterions are determined based on the entropy method determining the objective weight of the criterions.

7.1.4 Phase IV: Selection of optimal composition

After determination the criteria weights by using ENTROPY method finally evaluate the ranking of all alternative with PROMETHEE optimization technique. The PROMETHEE method was developed by Brans [316] in 1982. The methods of PROMETHEE have been effectively implemented in numerous fields and a number of researchers have used them in decision-making problems [275]. The PROMETHEE methods have some requisites of an appropriate MCDM method and their success is basically due to their mathematical properties and to their particular friendliness of use. Maity and Chakraborty [318] used PROMETHEE II method for the selection of tool material. The result found that the Molybdenum-type high-speed steel and tungsten base high-speed tool steel are the two best choices. Alloy steel is the least preferred tool steel material.

The steps followed in the PROMETHEE optimization technique are as follows:

Step-I: After identifying the relevant goal, criterions and alternatives of the problem, a decision matrix of criterions and alternatives is formulated based on the information available regarding the problem. The details of the different alternatives and criteria's are given in Table 7.1 and Table 7.2 respectively. If the number of alternative is M and the number of criterions are N then the decision matrix having an order of M × N is represented as:

$$D_{M \times N} = \begin{bmatrix} d_{11} & d_{12} & \ldots & d_{1N} \\ d_{21} & d_{22} & \ldots & d_{2N} \\ \vdots & \vdots & \ldots & \vdots \\ d_{M1} & d_{M2} & \ldots & d_{MN} \end{bmatrix} \qquad (7.1)$$

Where, an element d_{ij} of the performance matrix $D_{M \times N}$ represents the actual value of the ith alternative in term of jth criterion. The decision matrix is presented in Table 7.7.

Step-II: The decision matrix is normalized to making all the values of the decision matrix comparable. The normalization of the decision matrix is calculated as:

$$D'_{ij} = \frac{d_{ij}}{\left[\sum_{i=1}^{M} \left(d_{ij}^2 \right) \right]^{1/2}} \qquad (7.2)$$

Step-III: In order to convert the normalized matrix to weighted normalized matrix, the weights of various criterions are determined by the entropy method. First of all the projection value (ρ_{ij}) for each alternative is calculated as:

$$\rho_{ij} = \frac{d_{ij}}{\sum_{i=1}^{M} d_{ij}} \qquad (7.3)$$

Step-IV: After the calculation of projection value, entropy of each criterion is calculated as:

$$E_j = -\varsigma \sum_{j=1}^{N} \rho_{ij} \ln(\rho_{ij}) \qquad (7.4)$$

where k is a constant and calculated as, $\varsigma = \dfrac{1}{\ln(M)}$

Step-V: Next the dispersion value (ψ_j) of each criterion is calculated as:

$$\psi_j = 1 - E_j \tag{7.5}$$

Step-VI: Finally the weight of each criterion is calculated as:

$$\omega_j = \dfrac{\psi_j}{\sum\limits_{j=1}^{N} \psi_j} \tag{7.6}$$

PROMETHEE II Method:

Step-1: Normalization

Larger the better,

$$X'_{ij} = \dfrac{X_{ij} - \min\{X_{ij}\}}{\max\{X_{ij}\} - \min\{X_{ij}\}} \tag{7.7}$$

Smaller the better,

$$X'_{ij} = \dfrac{\max\{X_{ij}\} - X_{ij}}{\max\{X_{ij}\} - \min\{X_{ij}\}}$$

(7.8)

Step-2: calculate the preference function $P_j(i, i')$ as:

$$p_j(i,i') = 0 \quad if \ X'_{ij} \le X'_{i'j}, \ and \tag{7.9}$$

$$p_j(i,i') = (X'_{ij} - X'_{i'j}) \quad if \ X'_{ij} > X'_{i'j}$$

(7.10)

Step-3: calculate the aggregated preference function taking into account the criteria weights. Aggregated preference function:

$$\varpi(i,i') = \sum\limits_{I=1}^{N} \omega \times p_j(i,i') \tag{7.11}$$

Step-4: determine the positive and negative outranking flows as:

$$\theta_i^+ = \frac{1}{M-1}\sum_{i=1}^{M}\varpi(i,i'), \text{ and} \tag{7.12}$$

$$\theta_i^- = \frac{1}{M-1}\sum_{i=1}^{M}\varpi(i',i) \tag{7.13}$$

Step-5: calculate the net outranking flow for each alternative:

$$\theta_i = \theta_i^+ - \theta_i^- \tag{7.14}$$

Thus, the best alternative is the one having the highest θ_i value.

Table 7.3 Experimental results of the criterions

Com-posite	C-1	C-2	C-3	C-4	C-5	C-6	C-7	C-8	C-9	C-10	C-11	C-12	C-13	C-14	C-15
M-0	7.20	58.0	1067	0.120	0.270	0.360	0.140	0.190	0.310	0.25	0.30	0.35	0.09	0.18	0.25
M-1	7.50	59.3	1124	0.170	0.290	0.388	0.190	0.260	0.360	0.29	0.33	0.38	0.12	0.24	0.34
M-2	7.97	59.7	1156	0.240	0.360	0.420	0.320	0.410	0.510	0.30	0.35	0.40	0.18	0.21	0.25
M-3	8.23	60.0	1190	0.270	0.380	0.560	0.380	0.560	0.730	0.31	0.36	0.43	0.11	0.26	0.34
M-4	8.70	61.0	1230	0.110	0.190	0.290	0.110	0.170	0.290	0.23	0.28	0.33	0.07	0.15	0.23
N-1	7.24	54.0	1080	0.103	0.460	0.626	0.300	0.620	1.050	0.41	0.38	0.44	0.28	0.31	0.34
N-2	7.80	56.0	1164	0.197	0.763	0.836	0.612	1.130	2.010	0.32	0.34	0.30	0.30	0.38	0.26
N-3	8.14	58.0	1232	0.188	0.983	1.310	0.380	0.570	1.320	0.29	0.33	0.35	0.31	0.42	0.41
N-4	8.58	60.0	1296	0.353	1.165	1.390	0.430	0.710	1.310	0.39	0.36	0.35	0.23	0.26	0.43
W-1	7.81	55.7	1158	0.002	0.005	0.008	0.003	0.005	0.008	0.31	0.12	0.10	0.11	0.28	0.23
W-2	8.19	57.7	1208	0.001	0.003	0.005	0.001	0.003	0.005	0.09	0.09	0.09	0.10	0.20	0.20
W-3	8.36	59.3	1266	0.001	0.006	0.009	0.002	0.005	0.009	0.19	0.27	0.40	0.19	0.32	0.41
W-4	8.64	60.5	1310	0.003	0.006	0.010	0.004	0.006	0.009	0.12	0.10	0.19	0.13	0.27	0.21

Table 7.4 Criteria weights evaluated by entropy method

Criterion	H_j	E_j	ω_j
C-1	0.9994	0.0006	0.0005
C-2	0.9998	0.0002	0.0002
C-3	0.9993	0.0007	0.0005
C-4	0.8348	0.1652	0.1277
C-5	0.7995	0.2005	0.1549
C-6	0.8107	0.1893	0.1463
C-7	0.8213	0.1787	0.1381
C-8	0.8068	0.1932	0.1493
C-9	0.7891	0.2109	0.1630
C-10	0.9758	0.0242	0.0187
C-11	0.9694	0.0306	0.0236
C-12	0.9702	0.0298	0.0230
C-13	0.9576	0.0424	0.0328
C-14	0.9855	0.0145	0.0112
C-15	0.9868	0.0132	0.0102

Table 7.5 Normalized decision matrix

Alternative	C-1	C-2	C-3	C-4	C-5	C-6	C-7	C-8	C-9	C-10	C-11	C-12	C-13	C-14	C-15
M-0	1.000	0.571	0.000	0.662	0.770	0.744	0.773	0.834	0.848	0.500	0.276	0.257	0.917	0.889	0.783
M-1	0.800	0.757	0.235	0.520	0.753	0.723	0.691	0.772	0.823	0.375	0.172	0.171	0.792	0.667	0.391
M-2	0.487	0.814	0.366	0.321	0.693	0.700	0.478	0.639	0.748	0.344	0.103	0.114	0.542	0.778	0.783
M-3	0.313	0.857	0.506	0.236	0.676	0.599	0.380	0.506	0.638	0.313	0.069	0.029	0.833	0.593	0.391
M-4	0.000	1.000	0.671	0.690	0.839	0.794	0.822	0.852	0.858	0.563	0.345	0.314	1.000	1.000	0.870
N-1	0.973	0.000	0.053	0.710	0.607	0.552	0.511	0.453	0.479	0.000	0.000	0.000	0.125	0.407	0.391
N-2	0.600	0.286	0.399	0.443	0.346	0.400	0.000	0.000	0.000	0.281	0.138	0.400	0.042	0.148	0.739
N-3	0.373	0.571	0.679	0.469	0.157	0.058	0.380	0.497	0.344	0.375	0.172	0.257	0.000	0.000	0.087
N-4	0.080	0.857	0.942	0.000	0.000	0.000	0.298	0.373	0.349	0.062	0.069	0.257	0.333	0.593	0.000
W-1	0.593	0.243	0.374	0.997	0.998	0.998	0.997	0.998	0.999	0.313	0.897	0.971	0.833	0.519	0.870
W-2	0.340	0.529	0.580	1.000	1.000	1.000	1.000	1.000	1.000	1.000	1.000	1.000	0.875	0.815	1.000
W-3	0.227	0.757	0.819	1.000	0.997	0.997	0.998	0.998	0.998	0.688	0.379	0.114	0.500	0.370	0.087
W-4	0.040	0.929	1.000	0.994	0.997	0.996	0.995	0.997	0.998	0.906	0.966	0.714	0.750	0.556	0.957

Table 7.6 Weighted preference functions for all the pairs of alternatives

	M-0	M-1	M-2	M-3	M-4	N-1	N-2	N-3	N-4	W-1	W-2	W-3	W-4
M-0		0.0618	0.1708	0.2477	0.0005	0.2640	0.5579	0.4590	0.5723	0.0065	0.0017	0.0302	0.0097
M-1	0.0002		0.0007	0.0011	0.0004	0.0019	0.0026	0.0024	0.0027	0.0005	0.0003	0.0006	0.0005
M-2	0.0003	0.0003		0.0007	0.0002	0.0018	0.0021	0.0021	0.0022	0.0004	0.0002	0.0007	0.0003
M-3	0.0003	0.0015	0.0096		0.0002	0.0854	0.3439	0.2460	0.3260	0.0010	0.0001	0.0166	0.0033
M-4	0.0421	0.1077	0.2137	0.2931		0.3024	0.5988	0.5005	0.6136	0.0158	0.0063	0.0361	0.0132
N-1	0.0062	0.0244	0.0545	0.0790	0.0030		0.3186	0.2249	0.3322	0.0002	0.0003	0.0039	0.0005
N-2	0.0035	0.0089	0.0231	0.0403	0.0023	0.0215		0.0925	0.1855	0.0000	0.0001	0.0134	0.0003
N-3	0.0003	0.0022	0.0245	0.0387	0.0002	0.0174	0.1887		0.1317	0.0014	0.0001	0.0034	0.0002
N-4	0.0005	0.0023	0.0036	0.0055	0.0002	0.0162	0.1636	0.0178		0.0004	0.0002	0.0034	0.0000
W-1	0.2275	0.2855	0.3922	0.4692	0.1910	0.4748	0.7718	0.6769	0.7899		0.0001	0.0530	0.0101
W-2	0.2433	0.3067	0.4127	0.4921	0.2054	0.4988	0.7958	0.6995	0.8128	0.0240		0.0691	0.0193
W-3	0.2020	0.2550	0.3567	0.4397	0.1662	0.4334	0.7376	0.6338	0.7485	0.0079	0.0002		0.0015
W-4	0.2309	0.2899	0.3958	0.4759	0.1928	0.4795	0.7764	0.6800	0.7935	0.0141	0.0003	0.0510	

Table 7.7 Positive, negative and net outranking flows with ranking of the alternatives

Alternatives	θ_i^+	θ_i^-	θ_i	Ranking
M-0	0.1985	0.0798	0.1187	6
M-1	0.0011	0.1122	-0.1111	7
M-2	0.0010	0.1715	-0.1705	10
M-3	0.0862	0.2153	-0.1291	9
M-4	0.2286	0.0635	0.1651	5
N-1	0.0873	0.2163	-0.1290	8
N-2	0.0326	0.4382	-0.4056	12
N-3	0.0341	0.3529	-0.3188	11
N-4	0.0178	0.4426	-0.4248	13
W-1	0.3618	0.0060	0.3558	3
W-2	0.3816	0.0008	0.3808	**1**
W-3	0.3319	0.0235	0.3084	4
W-4	0.3650	0.0049	0.3601	2
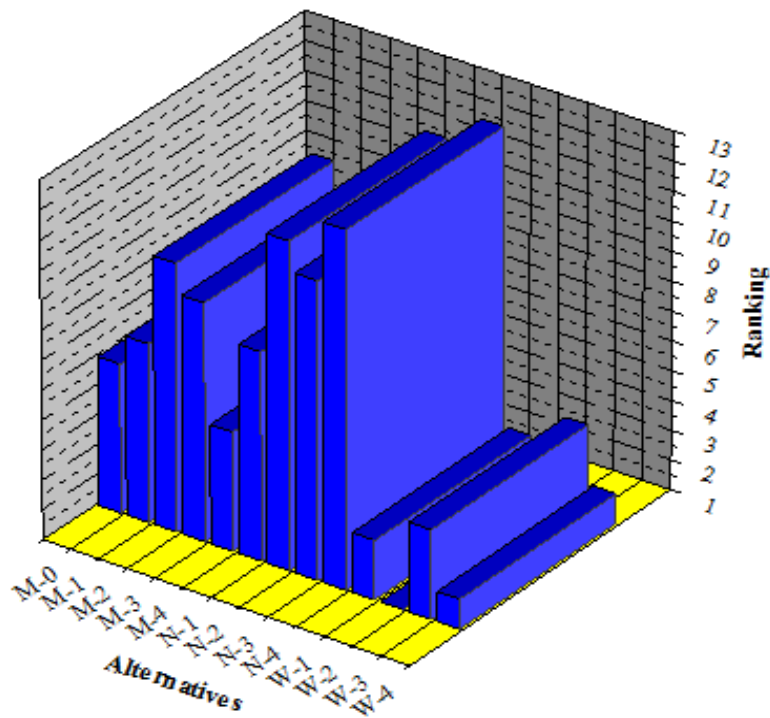
Figure 7.2: Ranking of the alternatives

Chapter Summery

This chapter has provided:

— PROMETHEE method is applied for the selection of optimal composition by using ENTROPY method.

— The weights of the criteria used for ranking of the materials.

— Based on final optimization by ENTROPY/ PROMETHEE approach, overall ranking order is: W-2>W-4>W-1>W-3>M-4>M-0>M-1>M-2>M-3>N-1>N-3>N-2>N-4 and the formulation W-2 exhibits the optimal performance among all considered set of composition in this study.

The next chapter refers to the conclusions of the present study, recommendations for the potential applications and scope for future research.

*****

CHAPTER 8

SUMMARY AND FUTURE SCOPE

Introduction

This chapter contains the summary of the work done along with objectives, conclusions based on the research work presented in this thesis followed by scope for future work in this field.

8.1 Background to the research work

The research reported in this thesis consists of three parts: the first part has provided the description of the experimental program and has presented the physical-mechanical characteristics of the alloy composites under this study; the second part has reported the effect of different particulate fillers (i.e. molybdenum, nickel and tungsten) on the sliding wear characteristics of these cobalt chromium base matrix and the third part has described the nature of corrosion resistance and its biocompatibility behaviour of fabricated alloy composites. Following three different types of metal alloy composites were developed:

Type-1: A-Series alloy composite (Co30Cr) based on the variation of molybdenum filled particulate

Type-2: B-Series alloy composite (Co30Cr4Mo) based on the variation of nickel filled particulate

Type-3: C-Series alloy composite (Co30Cr4Mo1Ni) based on the variation of tungsten filled particulate

The selected three different types of alloy composites were developed under identical processing conditions and were studied for following performance properties:

— Physical, mechanical properties and characterization of surface morphology of sliding wear mechanism and performance optimization using Taguchi method (Chapter-4)

— Prediction the wear volume using ANN technique and compared with experimental results (Chapter-5)

— Evaluation the nature of corrosion and biocompatibility behavior of fabricated alloy composite in experimentally (Chapter-6)

— Multi criteria decision making (MCDM) technique called ENTROPY- PROMETHEE is applied to select the best alternatives from the fabricated composite materials based on the physical, mechanical and sliding wear properties (Chapter-7)

8.2 Summary of the research findings

The summary based on the studies conducted in this research work are presented chapter wise.

8.2.1 Summary of research finding of physical and mechanical characteristics of metal alloy composites

The studied on the evaluation of physical and mechanical properties on the developed 'A', 'B' and 'C' series of alloy composites based on the variation of molybdenum, nickel and tungsten particulate filled cobalt-chromium (Co-30Cr) metal matrix have summarized as:

— Successful fabrication of particulates filled alloy composites at different wt.-% (0, 1, 2, 3 and 4) of molybdenum (Mo), nickel (Ni) and tungsten (W) have been done by using high temperature vacuum casting machine.

— It has been observed that physical property like density for the series 'A' alloy composite is increased with the increase in filler (Mo) content in the matrix material. For series 'B' alloy composites, the density of the unfilled alloy composite is more. Afterwards it decreases at 1wt.% Ni then it gradually increases with the increase in filler (Ni) content (2wt.%, 3wt.% and 4wt.%) into the matrix material. Similar manner found in series 'C' alloy composites.

— The incorporation of particulates i.e. molybdenum, nickel and tungsten into base matrix (i.e. Co30Cr) have lead to an enhancement in hardness. It remains in the range of 58-61 HRC for 'A' series alloy composites based on the variation of molybdenum particulate whereas it is in the range of 61-60 HRC for 'B' series alloy composites based on the variation of nickel filled particulate and 60-60.5 HRC for 'C' series alloy composites based on the variation of tungsten filled particulate. This has led to the conclusion that the hardness values have been found to have marginally improved for most of the particulates filled alloy composites.

— The compressive strength for the series 'A' alloy composites is enhanced with the increase in weight percentage of Mo into the matrix material. For series 'B' alloy

composites, the compressive strength of 0wt.% Ni filled alloy composite is 1230 MPa. Afterwards, it decreases at 1wt.% Ni filled matrix material then it gradually increases up to 1296 MPa with the increase in weight percentage of nickel into the matrix material. Similar manner reported for series 'C' alloy composites and the maximum compressive strength i.e. 1310 MPa is computed at 4wt.% tungsten filled metal matrix.

8.2.2 Summary of research findings of wear characteristics of the alloy composites

The assessment of possible wear behaviour during sliding on the developed alloy composites led to the following conclusions:

— Sliding wear volume of the alloy composites is decreased with the inclusion of filler, i.e. molybdenum in the metal matrix and the maximum wear resistance is found to be for 4wt.% of Mo filled composite as compared to other composition for 'A' series metal matrix. For series 'B', 1wt.% Ni filled alloy composite shows better wear resistance than other alloy compositions. Similarly, for 'C' series alloy composites, 2wt.% W filled particulate shows less wear volume for both dry and wet sliding conditions than other alloy compositions.

— The surface morphology of the worn out samples is performed by using a Scanning Electron Microscope (SEM) to understand the wear mechanism/behaviour at rubbing surfaces and then Atomic Force Microscopy (AFM) analysis is studied to evaluate the 3D surface profile of the worn sample. At the end, Energy dispersive X-ray analysis (EDAX) has also been performed to find out the elemental compositions of the worn alloy composites. Micro-cracks, micro-ploughing, wear scar, parallel and continuous grooves and wear debris were observed on the rubbing surfaces of the composites.

— Sliding wear characteristics of the alloy composites using Taguchi methodology have been analyzed. The optimal parameter settings are obtained from Series 'A', 'B' and 'C' alloy composite. The experimental results are also validated using confirmation test and it is found that the predicted and experimental values of the S/N ratio of wear volume and friction coefficient are in close agreement under dry and wet sliding condition.

— Significant control factors affecting the wear volume have been identified through successful implementation of analysis of variance (ANOVA). For series 'A' alloy composites, based on the variation of molybdenum filled particulate normal load emerged

as the most significant control factor, followed by sliding distance, filler content and sliding velocity for both dry and wet sliding conditions. Similarly, for series 'B' alloy composites, based on the variation of nickel filled particulate sliding distance emerged as the most significant control factor, followed by normal load, filler content and sliding velocity for dry and wet both sliding conditions. Whereas, normal load emerged as the most significant control factor, followed by sliding distance, filler content and sliding velocity for dry and wet sliding condition for series 'C' alloy composites, based on the variation of tungsten filled particulate.

— Significant control factors affecting the friction coefficient have been identified through successful implementation of analysis of variance (ANOVA). For series 'A' alloy composites normal load emerged as the most significant control factor followed by filler content, sliding velocity and sliding distance for dry sliding conditions. Whereas, normal load, sliding velocity and filler content the most significant factor and sliding distance is the least significant factor under wet sliding condition. Similarly, for 'B' series alloy composites normal load emerged as the most significant control factor followed by sliding distance, sliding velocity and filler content for dry sliding conditions. For wet sliding condition, normal load emerged as the most significant factor followed by sliding velocity, sliding distance and filler content. For 'C' series alloy composites normal load emerged as the most significant control factor followed by filler content, sliding velocity and sliding distance for dry condition. Similarly, normal load is the most significant factor and the sliding distance, filler content and sliding velocity is the least significant factor under wet sliding condition.

— The wear property of the alloy composite depends on many factors, such as normal load, sliding velocity, sliding distance and filler (wt.%). Computation through neural networks is one of the recently growing areas of artificial intelligence. Neural networks are promising due to their ability to learn highly non-liner relationship. It can also be gainfully employed to simulate property-parameters co-relationship in a space larger than the experimental domain. It is evident from the present study that the artificial neural technique has the potential to predict and analyze the wear behavior of composites if it is properly trained.

8.2.3 Summary of research findings of corrosion resistance analysis and biocompatibility response of the alloy composites

The assessment of possible corrosion resistance analysis and biocompatibility response on the developed alloy composites led to the following conclusions:

— It has been observed that with addition of 4wt.% of molybdenum filled particulate exhibited superior resistance against corrosion for the series 'A' alloy composite. Similar operating conditions with addition of 4wt.% of nickel particulate filled alloy composite and 2wt % of tungsten particulate filled alloy composites exhibited better corrosion resistant for series 'B' and series 'C' alloy composites respectively.

— The histology test of the fabricated alloy composites, i.e. Co-30Cr-4Mo, Co-30Cr-4Mo-1Ni and Co-30Cr-4Mo-1Ni-2W showed no inflammatory cell immigration, no epidermal necrosis, no vacuolar degeneration of basal cell, no edema, no adenexal atrophy and vesicle formation. From this analysis concluded that Co-30Cr-4Mo-1Ni-2W alloy composites may also be a good choice as an implant material for femoral head of joint replacement.

Finally, the calculation of ranking order for different physical, mechanical and sliding wear behavior of particulate filled alloy composites is found by using the PROMETHEE method. The sequence of ranking is W-2>W-4>W-1>W-3>M-4>M-0>M-1>M-2>M-3>N-1>N-3>N-2>N-4 and the formulation W-2 exhibits the optimal performance among all considered set of composition in this study.

8.3 Scope for future work

The following aspects could also be incorporated in this research work that should be taken up in future:

1. The present study may be extended further to implant in 'Horse' or 'Rabbit' to better understand the biocompatibility of fabricated alloy composite.

2. The present study has been carried out using simple stir casting technique. However, the research work can be extended further by considering other methods of composite fabrication and the effect of manufacturing techniques on the performance of alloy composites can similarly be analyzed

---

3. The present study can be extended further by the development of hybrid composites using further fillers and the study can similarly be analyzed.

4. The present study may be extended further by the development of composites with vacuum coating and analyzed the behaviour of the composite.

<center>*****</center>

References

1.   Williams D.F. Definitions in Biomaterials: Proceedings of a Consensus Conference of the European Society for Biomaterials, Elsevier, Amsterdam, 1987.

2.   Boretos JW, Eden M. Contemporary Biomaterials. Material and Host Response, Clinical Applications New Technology and Legal Aspects Noyes Publications, Park Ridge, NJ. 1984:232–233.

3.   Recum V. (Ed.), Handbook of Biomaterials Evaluation, Scientific, Technical and Clinical Testing of Implant Materials, Second edition, Taylor and Francis, *PA*, 1999: 915.

4.   Van Blitterswijk C.A, Grote J.J, Kuijpers W, Daems W.Th, Groot De K. Macropore tissue in growth: a quantitative and qualitative study on hydroxyapatite ceramic. Biomaterials, 1986; 7: 137-143.

5.   Currey J.D. The Mechanical Adaptations of Bones, Princeton University Press. 1984.

6.   Schmitt F.O. Adventures In Molecular Biology. Ann. Rev. Biophys. Biophys. Chem., 1985; 14:1-22.

7.   Stenzel K.H, Miyata T, Rubin A.L, in: L.J. Mullins (Ed.), Collagen as a Biomaterial in Annual Review of Biophysics and Bioengineering, Annual Reviews Inc., Palo Alto, CA, 1974; 3:231.

8.   Fratzl P, Misof K, Zizak I, Rapp G, Amenitsch H, Bernstorff S. Structure and mechanical properties of collagen. J. Struct. Biology, 1998; 122 (1-2):119-22.

9.   Wiles P. The surgery of the osteoarthritic hip. British Journal of Surgery, 1958; 45 (193):488-497.

10.   McKee GK. Developments in total hip joint replacement. Symposium on lubrication and wear in living and artificial human joints. London: Inst Mech Eng; 1967:85.

11.   Haboush EJ. A new operation for arthroplasty of the hip based on biomechanics, photoelasticity, fast-setting dental acrylic, and other considerations. Bull Hosp Joint Disease, 1953; 14: 242-277.

12.   Urist MR. The principles of hip-socket arthroplasty. J Bone Joint Surg Am. 1957; 39(4):786-810.

13.   McBride ED. A metallic femoral head prosthesis for the hip joint. J Int Coll Surg. 1951; 15(4):498-503

14.   Walker P S., Gold B L. The tribology (friction, lubrication and wear) of all-metal artificial hip joints. Wear, 1971; 17: 285-299.

15. Charnley J. Arthroplasty of the hip. A new operation. Lancet, 1961; 1(7187): 1129-32.

16. Charnley J. Long-term results of low-friction arthroplasty. Hip, 1982: 42- 9.

17. Rushton N, Rae T. The intra-articular response to particulate carbon fibre reinforced high density polyethylene and its constituents: an experimental study in mice. Biomaterials, 1984; 5(6): 352-356.

18. Gillett A, Brown S A, Dumbleton J H, Pool R P. The use of short carbon fibre reinforced thermoplastic plates for fracture fixation. Biomaterials, 1985; 6(2): 113-121.

19. Jockisch K A, Brown S A, Bauer T W, Merritt K. Biological response to chopped-carbon-fiber-reinforced peek. J. Biomed. Res., 1992; 26(2): 133-146.

20. Corvelli A A, Roberts J C, Biermann P J, Cranmer J H. Characterization of a peek composite segmental bone replacement implant. Journal Material Science, 1999; 34(10): 2421-2431.

21. Lopes M A, Monteiro F J, Santos J D. Glass-reinforced hydroxyapatite composites: fracture toughness and hardness dependence on microstructural characteristics. Biomaterials, 1999; 20(21): 2085-2090.

22. Fujihara K, Huang Z M, Ramakrishna S, Satknanantham K, Hamada H. Performance study of braided carbon/PEEK composite compression bone plates. Biomaterials, 2003; 24(15): 2661-2667.

23. Lewandowska-Szumiel M, Komender J, Chlopek J. Interaction between carbon composites and bone after intrabone implantation. J. Biomedical Materials. Res. Part A, 1999; 48(3): 289-296.

24. Boutin P, Christel P, Dorlot J M, Meunier A, Deroquancourt A, Blanquaert D, Herman S, Sedel L, Witvoet J. The Use of Dense Alumina Ceramic Combination in Total Hip-Replacement. Journal of Biomedical Materials Research, 1988; 22: 1203-1232.

25. Bizot P, Nizard R, Lerouge S, Prudhommeaux F, Sedel L. Ceramic/ceramic total hip arthroplasty. Journal of Orthopaedic Science: Official Journal of the Japanese Orthopaedic Association. 2000; 5(6): 622-627.

26. Cales B. Zirconia as a sliding material-Histologic, laboratory, and clinical data. Clinical Orthopaedics and Related Research, 2000; 379:94-112.

---

27. Park J, Lakes R S, Biomaterials: An introduction, 2nd ed., Plenum Press, New York, 1992.

28. Baker D A. Macro-and Microscopic Evaluation of Fatigue in Medical Grade Ultrahigh Molecular Weight Polyethylene. PhD Theses. May 2001, University of California: Berkeley: 1-223.

29. Sargeant A, Goswami T. Hip implants: Paper V. Physiological effects. Material and Design, 2006; 27(4): 287–307.

30. Nasab M B, Hassan M R. Metallic Biomaterials of Knee and Hip - A Review. Trends Biomaterial Artificial Organs, 2010; 24(1): 69-82.

31. Bhat V S. Biomaterials (2nd ed.). Harrow, UK: Alpha Science International Ltd. 2005.

32. Wintermantel E, Ha S. Biocompatible materials and methods of construction: Implants for Medicine and Envinroment. Springer, 1998.

33. Pilliar R M. Metallic Biomaterials, in Biomedical Materials (R. Narayan, ed.), Springer US. 2009: 41–81.

34. Abusafieh A, Siegler S, Kalidindi S R, Development of self-anchoring bone implants. I. Processing and material characterization. J. Biomed. Mater. Res. (Appl. Biomater.), 1997; 38(4): 314-327.

35. Chang F K, Perez J L, Davidson J A. Stiffness and strength tailoring of a hip prosthesis made of advanced composite materials. Journal Biomedical Material Research, 1990; 24: 873.

36. Simoes J A, Marques A T, Jeronimidis G. Design of a controlled-stiffness composite proximal femoral prosthesis. Composite Science and Technology, 1999; 60: 559.

37. Yoshimura M, Suda H, Okamoto K, Ioku K. Hydrothermal synthesis of biocompatible whiskers. Journal of Material Science, 1994; 29: 3399.

38. Suchanek W, Yoshimura M. Processing and Properties of Hydroxyapatite-Based Biomaterials for Use as Hard Tissue Replacement Implants. Journal of Material Research, 1998; 13: 94-98.

39. Mortier A, Lemaitre J, Rodvique L, Rouxhet. Synthesis and thermal behavior of well-crystallized calcium-deficient phosphate apatite. Journal of Solid State Chemistry, 1989; 78: 215.

40. Yoshimura M, Suda H, Okamoto K, Ioku K, Hydrothermal synthesis of biocompatible whiskers. Journal of Material Science,1994; 29: 3399.

41. Ota Y, Iwashita T, Kasuga T, Abe Y. Preparation of CaF$_2$ Fibers. Journal of the American Ceramic Society, 1996; 79(11): 2986-2988.

42. Toshihiro K, Hirotaka M, Katsuhito K, Masayuki N, Ken-ichiro H, Minoru U. Preparation of poly(lactic acid) composites containing calcium carbonate (vaterite) Biomaterials, 2001; 22: 19, 3247.

43. Williams D F, Review: Tissue-biomaterial interactions. Journal of Material Science, 1987; 22 (10): 3421- 3445.

44. Long M, Rack H J. Titanium alloys in total joint replacement--a materials science perspective. Biomaterials, 1998; 19(18):1621–39.

45. Wang K. The use of titanium for medical applications in the USA. Material Science and Engineering, 1996; 213:134-7.

46. Bakos D, Soldan M, Hernandez-Fuentes I. Hydroxyapatite-collagen-hyaluronic acid composite. Biomaterials, 1999; 20(2): 191-5.

47. Katz J L. Anisotropy of Young's modulus of bone. Nature, 1980; 283(5742):106-107.

48. Luke G, Gutwein, Webster Thomas. Increased viable osteoblast density in the presence of nanophase compared to conventional alumina and titania particles. Biomaterials, 2004; 25: 4175–83.

49. Geetha M, Singh A K, Asokamani R, Gogia A K. Ti based biomaterials, the ultimate choice for orthopaedic implants–A review. Progress in Materials Science, 2009; 54: 397-425.

50. Hallab N J, Anderson S, Stafford T, Glant T, Jacobs J J. Lymphocyte responses in patients with total hip arthroplasty. Journal of Orthopedic Research, 2005; 23(2):384-91.

51. Viceconti M, Muccini R, Bernakiewicz M, Baleani M, Cristofolini L. Large-sliding contact elements accurately predict levels of bone-implant micromotion relevant to osseointegration. Journal of Biomechanics, 2000; 33(12): 1611-1618.

52. Goodman S B, mez Barrena E O, Takagi M, Konttinen Y T. Biocompatibility of total joint replacements: A review. Journal of Biomedical Materials Research, 2009: 90A (2):603–618.

53. Langton D J, Jameson S S, Joyce T J, Hallab N J, Natu S, Nargol A V. Early failure of metal-on-metal bearings in hip resurfacing and large-diameter total hip replacement: A consequence of excess wear. J. Bone Joint Surg. Br., 2010; 92(1): 38–46.

54. Merritt K, Brown A S. Distribution of cobalt chromium wear and corrosion products and biologic reactions. Clin. Orthop. Relat. R., 1996; 329: S233–S243.

55. Marti A. Cobalt-base alloys used in bone surgery. Injury 2000; 31: D18–D21.

56. ASTM F75, Standard Specification for Cast Cobalt–Chromium–Molybdenum Alloy for Surgical Implant Applications, ASTM International, West Conshohocken, PA, 1998.

57. ASTM F1537, Standard Specification for Wrought Cobalt–28Chromium–6Molybdenum Alloys for Surgical Implants, ASTM International, West Conshohocken, PA, 2000.

58. ASTM F799, Standard Specification for Cobalt–28Chromium–6Molybdenum Alloy Forgings for Surgical Implants, ASTM International, West Conshohocken, PA, 1999.

59. Huang P, Salinas-Rodriguez A, Lopez H F. Tribological behavior of cast and wrought Co–Cr–Mo implant alloys. Material Science and Technology, 1999; 15: 1324–1330.

60. Unsworth A, Dowson D, Wright V. Introduction to the Biomechanics of Joints and Joint Replacement. Mechanical Engineering Publications Limited, London. 1981: 134–139.

61. Sieber H P, Rieker C B, Kottig P. Analysis of 118 second-generation metal-on-metal retrieved hip implants. Joint of Bone Joint Surgery, 1999:81: 46–50.

62. Yildiz H, Chang FK, Goodman S. Composite hip prosthesis design II. Simulation. J Biomedical Material Research, 1998; 39(1):102-19.

63. Ramsden J J, Allen David M, Stephenson David J. The Design and Manufacture of Biomedical Surfaces. CIRP Annals-Manufacturing Technology, 2007; 56(2):687-711.

64. Brooks C R. Heat treatment, structure, and properties of nonferrous alloys. Ohio American Society for Metals. 1982: 229.

65. Crook P, Metals handbook. Nonferrous alloys and special-purpose materials. Ohio American Society for Metals: ASM International: Materials Park. 1990: 447.

66. Rabinowicz E. Friction and Wear of Materials. 2nd edition John Wiley and Sons 1995.

67. Williams J A. The influence of repeated loading, residual stresses and shakedown on the behaviour of tribological contacts. Tribology International, 2005; 38: 863.

68. Devaraju A, Elayaperumal A. Tribological behaviour of Plasma nitrided AISI 316 LN type stainless steel in air and high vacuum atmosphere at room temperature. International Journal of Engineering Science and Technology, 2010; 2: 4137.

69. Kumar N. Das C R, Dash S, Tyagi A K, Bhaduri A K, Baldev R. Evaluation of tribological properties of nuclear-grade steel. Tribology Transactions, 2011; 54: 62.

70. Dumbleton J H. Tribology of natural and artificial joints. Amsterdam: Elsevier 1981.

71. Dowson D. New joint for the millennium: wear control in total replacement hip joint. In proceedings of Institution of Mechanical Engineers (H), 2001; 215 (4): 335-358.

72. [72] Tipper J L, Ingham E, Jin Z M, Fisher J. The science of metal-on-metal articulation. Current Orthopadedics, 2005; 19: 280-287.

73. Breme J, Kirkpatrick C J, Thull R. Metallic Biomaterial Interfaces. Wiley-VCH Verlag GmbH & Co. KGaA. 2008.

74. Niinomi M. Recent Metallic Materials for Biomedical Applications. Metallurgical and Material Transaction, 2002; 33 A: 477-486.

75. Yildiz H, Ha SK, Chang FK. Composite hip prosthesis design I Analysis. Journal of Biomedical and Material Research, 1998; 39(1):92-101.

76. Kutz M. Materials and Engineering Mechanics, Mechanical Engineer's Handbook fourth edition, John Wiley & Sons, 2014.

77. Hill D. Design engineering of biomaterials for medical devices. John Wiley & Sons, Chchester, 1998.

78. Beatty M W, Swartz M L, Moore B K. Effect of microfiller fraction and silane treatment on resin composite properties. Journal of Biomedical Materials Research, 1998; 40:12-23.

79. Savas T, kan Alemdag Y. Effect of nickel additions on the mechanical and sliding wear properties of Al–40Zn–3Cu alloy. Wear, 2010; 268: 565-570.

80. Parker D R, Bajpai P K. Effect of locally delivered testosterone on bone healing. Transaction Soco. Biomaterial, 1993; 26: 293.

81. Lewis G. Selection of Engineering Materials, Adapted by permission of Prentice Hall 1990: 189.

82. Ratner B D, Hoffman A S, Shoen F J, Lemons F J. Biomaterials Science: An Introduction to Materials in Medicine, Academic Press, San Diego. 1996: 37–50.

83. American society for testing and materials. Annual Book of ASTM standards, vol. 13, Medical Devices and Services, American Society for testing and materials, Philadelphia, PA, 1992.

84. Au AG. Contribution of loading conditions and material properties to stress shielding near the tibial component of total knee replacements. Journal of Biomechanics, 2007. 40(6): 1410-1416.

85. Dearnley P A. A review of metallic, ceramic and surface-treated metals used for bearing surfaces in human joint replacements. Proc. I Mech. Part H; J. Eng. in Med, 1999. 213: 107-135.

86.   Mirhosseini N,   Crouse P L, Schmidth M J J, Li L, Garrod D. Laser surface micro-texturing of Ti–6Al–4V substrates for improved cell integration. Applied Surface Science, 2007; 253(19): 7738-7743.

87.   Davis JR. ed. Metallic Materials, Chapter 3, in Handbook of Materials for Medical Devices, ASM International, Materials park, Ohio, USA, 2003.

88.   Englewood Cliffs N J, Gibbons D F, Materials for Orthopedic Joint Prostheses, Biocompatibility of Orthopedic Implants, Vol. I, D. F.Williams, CRC Press, Boca Raton, FL. 1982; 4: 116.

89.   Fini M, Giavaresi G, Torricelli P, Borsari V, Giardino R, Nicolini A, Carpi A. Osteoporosis and biomaterial osteointegration. Biomedicine & Pharmacotherapy, 2004. 58(9): 487-493.

90.   Xulin S, Ito A, Tateishi T, Hoshino A. Fretting corrosion resistance and fretting corrosion product cytocompatibility of ferritic stainless steel. Journal of Biomedical Material Research Part A, 1996; 34.1: 9-14.

91.   Alvarado J, Maldonado R, Marxuach J, Otero R. Biomechanics of Hip and Knee Prostheses. Applications of Engineering Mechanics in Medicine, GED – University of Puerto Rico Mayaguez, 2003.

92.   Yamada K, Nakamura S, Tsuchiya T, Yamashita K. Electrical Properties of Polarized Partially Stabilized Zirconia for Biomaterials. Key Engineering Materials, 2002; 216: 149-152.

93.   LeGeros RZ, Craig RG, Strategies to affect bone remodeling: osteointegration. J Bone Miner Res., 1993; 8(2): 583-596.

94.   Yan Y. Biotribocorrosion in biomaterials and medical implants. Woodhead Publishing series in biomaterials, 2013.

95.   Hench L.L. Bioceramics. J. American Ceramic Society. 1998; 81: 1705-1728.

96.   Shenhar A, Gotman I, Gutmanas E.Y, Ducheyne P. Surface modification of titanium alloy orthopaedic implants via novel powder immersion reaction assisted coating nitriding method. Materials science & engineering A, 1999; 268(1-2): 40-46.

97.   Budzynski P, Youssef A A, Sielanko J. Surface modification of Ti–6Al–4V alloy by nitrogen ion implantation. Wear, 2006; 261(11-12): 1271-1276.

98.   Navarro M, Michiardi A, Castano O, Planell J A. Biomaterials in orthopaedics. Journal of the Royal Society Interface, 2008; 5(27): 1137-1158.

99.   Long M, Rack H J. Titanium Alloys in Total Joint Replacement-A Materials Science Perspective. Biomaterials, 1998; 19: 1621–1639.

100. Lee B H, Lee C, Kim D G, Choi K, Lee K H, Kim Y D. Effect of surface structure on biomechanical properties and osseointegration. Materials Science & Engineering C, 2008; 28(8): 1448-1461.

101. Imam M A, Fraker A C, Harris J S, Gilmore C M. Influence of heat treatment on the fatigue lives of Ti-6Al-4V and Ti-4.5Al-5Mo-1.5CR. In Titanium Alloys is surgical implants, luckey, H.A. and Kubli, F.E. Eds Philadelphia, PA: ASTM special technical publication. 1983; 796: 105-119.

102. Oonishi H, Bioceramic in orthopaedic surgery–our clinical experiences. In: Bioceramic, J.E. Hulbert and S.F. Hulbert (Eds.). 1992; 3: 31-42.

103. Hench L L. Bioceramics: From concept to clinic. J. Am. Ceram. Soc., 1991; 74: 1487-1510.

104. Bergmann G. Realistic loads for testing hip implants. Bio-medical materials and engineering, 2010; 20: 65-75.

105. Kitano T. Constituents and pH changes in protein rich hyaluronan solution affect the biotribological properties of artificial articular joints. Journal of Biomechanics, 2001; 31:1031-7.

106. Wang A. The effects of lubricant composition on in vitro wear testing of polymericacetabular components. Journal of Biomedical Material Research, 2004; 68B: 45–52.

107. Delecrin J. Changes in joint fluid after total arthoplasty. Clin. Orthop. Rel. Res., 1994; 307: 240-249.

108. Hoeland W, Vogel W, Waumann K, Gummel J. Journal of Biomedical Materials Research, 1985; 19(3): 303-312.

109. Haynes D R, Crotti T N, Haywood M R. Corrosion of and changes in biological effects of cobalt chrome alloy and 316L stainless steel prosthetic particles with age. J. Biomed. Mater. Res., 2000; 49:167-175.

110. Davidson J A. Characteristics of Metal and Ceramic Total Hip Bearing Surfaces and Their Effect on Long-Term UHMWPE Wear. Clin. Orth. Rel. Res., 1993; 294: 360-376.

111. Davidson J A, Mishra A K. Surface modification issues for orthopaedic implant bearing surfaces, in Proc. Fifth International Conf. on Surface Modification Technology. Birmingham, UK: The Institute of Materials 1991.

112. Dowson D. A comparative study of the performance of metallic and ceramic femoral head components in total replacement hip joints. Wear, 1995; 190: 171-183.

113. Wang A. Effect of Femoral Head Surface Roughness on the Wear of Ultra high Molecular Weight Polyethylene Acetabular Cups. The Journal of Arthroplasty, 1998; 13(6): 615-620.

114. Dowson D. Proc. International Symposium on Polymer Wear and Its Control. St. Louis, MO: American Chemical Society, New York 1984.

115. Rostlund T. Wear of ion-implanted pure titanium against UHMWPE. Biomaterials, 1989; 10: 176-181.

116. Mcgovern T E. In vivo wear of Ti6A14V femoral heads: A retrieval study. J. Biomed. Mater. Res., 1996; 32: 447-457.

117. Schmidt H, Exner H E. Wear, Corrosion and Fatigue Properties of Ion Implanted Titanium Alloy Ti6AL4V. J. Physical Metallurgy, 1999; 90: 594-601.

118. Taylor S K, Serekian P, Manley M. UHMWPE debris generation from acetabular cup inserts articulating against untreated CoCr, ion implanted CoCr, and Zro2 bearings under hip joint simulation, in 39th Annual Meeting, Orthopaedic Research Society. San Francisco, California 1993.

119. Rieu J. Ion implantation effects on friction and wear of joint prosthesis materials. Biomaterials, 1991; 12: 139-143.

120. Agins H J. Metallic Wear in Failed Titanium-Alloy Total Hip Replacements. J. Bone Joint Surg., 1988; 70(3): 347-356.

121. Lombardi AV. Aseptic Loosening in Total Hip Arthroplasty Secondary to Osteolysis Induced by Wear Debris from Titanium-Alloy Modular Femoral Heads. Journal of Bone Joint Surgery, 1989; 71(9): 1337-1342.

122. Anderson J M. Biological Responses to Materials. Annu Rev Mater Res., 2001; 31:81-110.

123. Black J. Metallosis Associated with a Stable Titanium-Alloy Femoral Component in Total Hip Replacement. J. Bone Joint Surg., 1990; 72-A(l): 126-130.

124. Schmidt H, Achminke A, Ruck D M. Tribological behaviour of ion implanted Ti6AL4V sliding against polymers. Wear, 1997; 209: 49-56.

125. Schmidt H. Compound formation and abrasion resistance of ionimplanted Ti6A14V. Act Mater., 2001; 49: 487-495.

126. Leitao E, Silva R A, Barbosa M A. Electrochemical and surface modifications on N+-ion-implanted 316L stainless steel. J. Mater. Sci. Mater. Med., 1997; 8:365-368.

127. Rieu J. Structural modifications induced by ion implantation in metals and polymers used for orthopaedic prostheses. Mater. Sci. Technol., 1992; 8: 589-592.

128. Bordji K. Evaluation of the effect of three surface treatments on the biocompatibility of 316 stainless steel using human differentiated cells. Biomaterials, 1996; 17:491-500.

129. Cordier R C. Optimisation of nitrogen implantation of austenitic 316L steel by microstructural analysis. Materials Letters, 1994; 20:113-118.

130. Rieu J. Deterioration mechanisms of joint prosthesis materials. Several solutions by ion implantion surface treatments. Biomaterials, 1990; 11: 51-54.

131. Bosetti M. In vivo evaluation of bone tissue behaviour on ion implanted surfaces. J. Mater. Sci-Mater. Med., 2001; 12(5): 431-435.

132. Brummitt K, Hardaker C S, McCullagh P J, Drabu K J, Smith R A. Effect of counter face material on the characteristics of retrieved titanium alloy total hip replacements. J Eng Med., 1996; 210(3): 191–5.

133. Dumbleton J, Shen C, Miller E. A study of the wear of some materials in connection with total hip replacement. Wear, 1974; 29:163–171.

134. Haider H, Garvin K, Rotating platform versus fixed-bearing total knees: an in vitro study of wear. Clinical Orthopaedics and Related Research, 2008; 466: 2677–2685.

135. Haider H, Kaddick C. Wear of mobile bearing knees: is it necessarily less? Journal of ASTM International, 2012: 9.

136. Haider H, Weisenburger J, Kurtz S, Rimnac C, Freedman J, Schroeder D, Garvin K, Does vitamine-stabilized ultra high-molecular-weight polyethylene address concerns of cross-linked polyethylene in total knee arthroplasty? The Journal of Arthroplasty, 2012; 27:461–469.

137. McKellop H, Clarke I, Markolf K, Amstutz H. Wear characteristics of UHMW polyethylene: a method for accurately measuring extremely low wear rates. Journal of biomedical materials research, 1978; 12: 895–927.

138. Dumbleton J H. Wear and its measurement for joint prosthesis materials. Wear, 1978; 49: 297–326.

139. Dowson D, Harding R. The wear characteristics of ultra high molecular weight polyethylene against a high density alumina ceramic under wet (distilled water) and dry conditions. Wear, 1982; 75: 313–331.

140. Dumbleton J, Shen C. The wear behaviour of ultra high molecular weight polyethylene. Wear, 1976; 37: 279–289.

141. Tetreault D M, Kennedy F E. Friction and wear behaviour of ultra high molecular weight polyethylene on Co–Cr and titanium alloys in dry and lubricated environments. Wear, 1989; 133: 295–307.

142. Brown K, Atkinson J, Dowson D, Wright V. The wear of ultra high molecular weight polyethylene and a preliminary study of its relation to the in vivo behaviour of replacement hip joints. Wear, 1976; 40: 255–264.

143. Seedhom B, Dowson D, Wright V. Wear of solid phase formed high density polyethylene in relation to the life of artificial hips and knees. Wear, 1973; 24: 35–51.

144. Charnley J. The wear of plastics materials in the hip joint. Plastics and Rubber, 1976; 1: 59–63.

145. Shen C, Dumbleton J. The friction and wear behaviour of irradiated very high molecular weight polyethylene. Wear, 1974; 30: 349–364.

146. Rostoker W, Galante J. Contact pressure dependence of wear rates of ultra high molecular weight polyethylene. Journal of Biomedical Materials Research, 1979; 13: 957–964.

147. Lee K Y, Pienkowski D. Viscoelastic Recovery of Creep-Deformed Ultra-High Molecular Weight Polyethylene (UHMWPE). ASTM Special Technical Publication 1998; 1307: 30–36.

148. Rose R, Cimino W, Ellis E, Crugnola A. Exploratory investigations on the structure dependence of the wear resistance of polyethylene. Wear, 1982; 77: 89-104.

149. Cooper J, Dowson D, Fisher J. The effect of transfer film and surface roughness on the wear of lubricated ultra- high molecular weight polyethylene. Clinical Materials, 1993 14, 295–302.

150. Walker P S, Blunn G W, Lilley P A. Wear testing of materials and surfaces for total knee replacement. Journal of Biomedical Materials Research, 1996; 33: 159–175.

151. Wright K, Dobbs H, Scales J. Wear studies on prosthetic materials using the pin-on-disc machine. Biomaterials, 1982; 3: 41–48.

152. Ahlroos T. Effect of lubricant on the wear of prosthetic joint materials. Acta Polytechnica Scandinavica, Mechanical engineering series, 2001:153.

153. Saikko V. Effect of lubricant protein concentration on the wear of ultra-high molecular weight polyethylene sliding against a CoCr counter face. Journal of Tribology, 2003; 125: 638–642.

154. Yao J Q, Blanchet T A, Murphy D J, Laurent M P. Effect of fluid absorption on the wear resistance of UHMWPE orthopaedic bearing surfaces. Wear, 2003; 255: 1113–1120.

155. Saikko V. A multi directional motion pin-on-disk wear test method for prosthetic joint materials. Journal of Biomedical Materials Research, 1998; 41: 58–64.

156. Bragdon C R, O'Connor D O, Lowenstein J D, Jasty M, Biggs S A, Harris W H. A new pin-on-disk wear testing method for simulating wear of polyethylene on cobalt-chrome alloy in total hip arthroplasty. The Journal of Arthroplasty, 2001; 16: 658–665.

157. Saikko V, Ahlroos T. Type of motion and lubricant in wear simulation of polyethylene acetabular cup. Proceedings of the Institution of Mechanical Engineers, Part H: Journal of Engineering in Medicine, 1999; 213: 301–310.

158. Turell M, Friedlaender G, Wang A, Thornhill T, Bellare A. The effect of counter face roughness on the wear of UHMWPE for rectangular wear paths. Wear, 2005; 259: 984–991.

159. Wang A, Polineni V, Essner A, Sokol M, Sun D, Stark C, Dumbleton J H. The significance of non linear motion in the wear screening of orthopaedic implant materials. Journal of Testing and Evaluation, 1997; 25: 239–245.

160. McKellop H, Clarke I, Markolf K, Amstutz H. Friction and wear properties of polymer, metal, and ceramic prosthetic joint materials evaluated on a multichannel screening device. Journal of Biomedical Materials Research, 1981; 15: 619.

161. Bragdon C, O'Connor D, Lowenstein J, Jasty M, Syniuta W. The importance of multi directional motion on the wear of polyethylene. Proceedings of the Institution of Mechanical Engineers, Part H: Journal of Engineering in Medicine, 1996; 210: 157–165.

162. Korduba L, Wang A. The effect of cross-shear on the wear of virgin and highly-cross linked polyethylene. Wear, 2011; 271: 1220–1223.

163. Charnley J. An artificial bearing in the hip joint: Implications in biological lubrication. Fed Proc., 1966; 25(3):1079–1081.

164. Unsworth A. The effects of lubrication in hip joint prostheses. Phys Med Biol., 1978; 23(2): 253–268.

165. Widmer M R, Heuberger M, Voros J, Spencer N D. Influence of polymer surface chemistry on frictional properties under protein lubrication conditions: implications for hip-implant design, Tribology Letter, 2001;10: 111–116.

---

166. Borruto A, Crivellone G, Marani F. Influence of surface wettability on friction and wear tests, Wear, 1998; 222: 57–65.

167. Sawae Y, Murakami T, Chen J. Effect of synovial constituents on friction and wear of ultra-high molecular weight polyethylene sliding against prosthetic joint materials, Wear, 1998; 216: 213–219.

168. Saikko V, Calonius O, Keranen J. Effect of counter face roughness on the wear of conventional and cross linked ultrahigh molecular weight polyethylene studied with a multi-directional motion pin-on-disk device, J. Biomed. Mater. Res., 2001; 57: 506–512.

169. Wang A, Stark C, Dumbleton J H. Mechanistic and morphological origins of ultra-high molecular weight polyethylene wear debris in total joint replacement prosthesis. Proc. Inst. Mech. Engrs., 1996; 2: 141-156.

170. Dowson D, Caravia L, Fisher J, Jobbins B. The influence of bone and bone cement debris on counterface roughness in sliding wear tests of ultra-high molecular weight polyethylene on stainless steel. Proc Inst Mech Eng., 1990; 204:65-70.

171. Hall R M, Unsworth A, Wroblewski B M, Siney P, Powell N J. The friction of explanted hip prostheses. Br. J. Rheumatol, 1997; 36: 20-26.

172. Scales J, Kelly P, Goddard D. Friction torque studies of total hip replacements-the use of a simulator. In Lubrication and Wear in Joints, ed. V. Wright. Sector, London, 1969: 88.

173. Weightman B, Simon S, Paul I, Rose R, Radin E. Lubrication mechanism of hip joint replacement prostheses. J. Lub. Tech., 1972; 94:131-135.

174. Auger D D, Dowson D, Fisher J, Jin Z M. Friction and lubrication in cushion form bearings for artificial hip joints. Proc. Inst. Mech. Engrs., 1993; 207H: 25-33.

175. Murakami T, Ohtsuki N, Higaki H. The adaptive multimode lubrication in knee prostheses with compliant layer during walking motion. In Thin Films in Tribology, ed. D. Dowson. Elsevier, Amsterdam, 1993: 673.

176. Hall R M, Unsworth A, Wroblewski B M, Burgess I C. Frictional characterization of explanted charnley hip prostheses. Wear, 1994,175, 159-166.

177. Auger D D, Dowson D, Fisher J. Cushion form bearings for total knee replacement Part 1: design, friction and lubrication. Proc. Inst. Mech. Engrs., l995; 209H: 73-82.

178. Unsworth A, Pearcy M J, White E F T, White G. Soft layer lubrication of artificial hip joints. In Proc. IMechE Int. Conf. Tribology Mech. Engrs, Bury St Edmunds, 1987: 715-724.

179. Amstutz H C, Lodwig W. Wear of polymeric bearing materials: The effects of *in-vivo* implantation J. Biomed. Mater. Res., 1976; 10; 25-31.

180. McKellop H, Clarke I C, Markolf K, Amstutz H. Friction and wear properties of polymer, metal, and ceramic prosthetic joint materials evaluated on a multichannel screening device. J. Biomed. Mater. Res., 1981; 15; 619-653.

181. McKellop H, Clarke I. Wear of artificial joint materials in laboratory tests. Acta Orthop. Stand., 1988; 59: 349-352.

182. Jones W R, Hady W F, Crugnola A. Effect of irradiation on the friction and wear of ultrahigh molecular weight polyethylene. Wear, 1981; 70: 77-92.

183. Kumar P, Oka M, Ikeuchi K, Shimizu K, Yamamuro T, Okumura H, Kotoura Y. Low wear rate of UHMWPE against zirconia ceramic (Y-PSZ) in comparison to alumina ceramic and SUS 316L alloy. J. Biomed. Mater. Res., 1991; 25: 813-828.

184. Caravia L, Dowson D, Fisher J, Corkhill P H, Tighe B J. A comparison of friction in hydrogel and polyurethane materials for cushion form joints. J. Mater. Sci.: Mater: Med., 1993; 4: 515-520.

185. Caravia L, Dowson D, Fisher J. Startup and steady state friction of thin polyurethane layers. Wear, 1993; 160: 191-197.

186. Caravia L, Dowson D, Fisher J, Corkhill P H, Tighe B J. friction of hydogel and polyurethane elastic layers when sliding against each other under a mixed lubrication regime. Wear, 1995; 181: 236-240.

187. Saikko V. Wear and friction properties of prosthetic joint materials evaluated on a reciprocating pin-on-flat apparatus. Wear, 1993; 166:169-178.

188. Wroblewski B M, Siney P D. Charnley low-friction arthroplasty of the hip-long term results. Clin. Orthop. Relat. Res., 1993; 292: 191–201.

189. Hart A J Hester T, Sinclair K, Powell J J, Goodship A E, Pele L, Fersht NL, Skinner J. The association between metal ions from hip resurfacing and reduced T-cell counts. J. Bone Jt. Surg., 2006; 88- B; 449–454.

190. Wang A, Essner A, Polineni V K, Stark C, Dumbleton J H. Lubrication and wear of ultra-high molecular weight polyethylene in total joint replacements. Tribology International, 1998; 31: 17–33.

191. Varano R, Bobyn J D, Medley J B, Yue S. The effect of microstructure on the wear of cobalt-based alloys used in metal-on-metal hip implants. Proc. Inst. Mech. Eng.: Part J: Eng. Med., 2006; 220: 145–159.

192. Essner A, Sutton K, Wang A. Hip simulator wear comparison of metal-on-metal, ceramic-on-ceramic and cross linked UHMWPE bearings. Wear, 2005; 259: 992–995.

193. Katti K S. Biomaterials in total joint replacement. Colloids Surf. B: Biointerfaces, 2004; 39: 133–142.

194. Dowson D. Tribological principles in metal-on-metal hip joint design. Proc. Inst. Mech. Eng.: Part H, 2006; 220: 161–171.

195. Hills B. Boundary lubrication in vivo. Proc. Inst. Mech. Eng.: Part H, 2000; 214: 83–94.

196. Gale L R, Chen Y, Hills B A, Crawford R. Boundary lubrication of joints Characterization of surface-active phospholipids found on retrieved implants. Acta Orthop., 2007; 78: 309–314.

197. Eliaz N. Degradation of Implant Materials. Springer New York, 2012.

198. Swann DA. Role of hyaluronic acid in joint lubrication. Ann. Rheum. Dis., 1974; 3: 318–326.

199. Tadmor R, Chen N, Israelachvilli J. Normal and shear forces between mica and model membrane surfaces with adsorbed hyaluronan. Macromolecules, 2003; 36: 9519–9526.

200. Swann DA, Radin EL. The Molecular basis of articular lubrication. I. Purification and properties of a lubricating fraction from bovine synovial fluid. J. Biol. Chem., 1972; 247: 8069–8073.

201. [201] Schwarz I, Hills B. Surface-active phospholipid as the lubricating component of lubricin. Rheumatology, 1998; 37; 21–26.

202. Wimmer MA, Sprecher C, Hauert R, Täger G, Fischer A. Tribochemical reaction on metal-on- metal hip joint bearings. A comparison between in-vitro and in-vivo results. Wear, 2003; 255: 1007–1014.

203. Pourzal R, Theissmann R, Morlock M, Fischer A. Micro-structural alterations within different areas of articulating surfaces of a metal-on-metal hip resurfacing system. Wear, 2009; 267: 689–694.

204. Pourzal R, Theissmann R, Williams S, Gleising B, Fisher J, Fischer A. Subsurface changes of a MoM hip implant below different contact zones. J. Mech. Behav. Biomed. Mater., 2009; 2: 186–191.

205. Rigney DA. Transfer, mixing and associated chemical and mechanical processes during the sliding of ductile materials. Wear, 2000; 245: 1–9.

206. Maskiewicz VK, Williams Sarah PA, Prates J, Bowsher J G, Clarke I C. Characterization of protein degradation in serum-based lubricants during simulation wear testing of metal-on-metal hip prostheses. J. Biomed. Mat. Res-Part B Appl. Biomater., 2010; 94: 429–440.

207. Jalali-Vahid D, Jin ZM, Dowson D. Effect of start-up conditions on elastohydrodynamics lubrication of metal-on-metal hip implants. Proc. Inst. Mech. Eng.: Part H, 2006; 220: 143–150.

208. Jin Z. Theoretical studies of elastohydrodynamic lubrication of artificial hip joints. Proc. Inst. Mech. Eng.: Part H, 2006; 220: 719–727.

209. Spikes HA. Thin films in elastohydrodynamic lubrication; the contribution of experiment. Proc. Inst. Mech. Eng.: Part J, 1999; 213: 335–352.

210. Velten K, Reinicke R, Friedrich K. Wear volume prediction with artificial neural networks, Tribology International, 2000; 33:731–736.

211. Jones SP, Jansen R, Fusaro R L. Preliminary investigation of neural network techniques to predict tribological properties. Tribol Trans., 1997; 40(2): 312–20.

212. Sakraoui T, Guessasma S, Fenineche N E, Montavon G, Coddet C. Friction and wear behavior prediction of HVOF coatings and electroplated hard chromium using neural computation. Mater Lett., 2004;58: 654–60.

213. Genel K, Kurnaz SC, Durman M. Modeling of tribological properties of alumina fiber reinforced zinc–aluminum composites using artificial neural network. Mater Sci Eng A., 2003; 363: 203–10.

214. Zhang Z, Barkoula N M, Kocsis J, Friedrich K. Artificial neural network predictions on erosive wear of polymers. Wear, 2003; 255: 708–13.

215. Rout A, Satapathy A. Analysis of dry sliding wear behavior of rice husk filled epoxy composites using design of experiment and ANN. Procedia Engineering, International Conference on Modelling Optimization And Computing, 2012; 38: 1218-1232.

216. Canakci A, Varol T, Ozsahin S. Analysis of the effect of a new process control agent technique on the mechanical milling process using a neural network model: Measurement and modeling. Measurement, 2013; 46: 1818-1827.

217. Canakci A, Varol T, Ozsahin S. Prediction of effect of volume fraction, compact pressure and milling time on properties of Al-Al$_2$O$_3$ MMCs using neural networks. Metals Materials International, 2013; 19: 519-526.

218. Varol T, Canakci A, Ozsahin S. Artificial neural network modeling to effect of reinforcement properties on the physical and mechanical properties of Al2024–B4C composites produced by powder metallurgy. Composites: Part B, 2013; 54: 224-233.

219. Gyurova LA, Friedrich K. Artificial neural networks for predicting sliding friction and wear properties of polyphenylene sulfide composites. Tribology International, 2011; 44: 603–609.

220. Altinkok N, Koker R. Use of artificial neural Network for predictions of Physical properties and tensile strengths is particle reinforced aluminium Matrix composites. Journal of Material Science Engineering, 2005; 40: 1767-1770.

221. Rashed F S, Mahmoud T S. Prediction of wear behavior of A356/SiCp MMCs using neural networks. Tribology International, 2009; 42: 642-648.

222. Bronzino JD. The Biomedical Engineering Handbook. New York: CRC Press LLC and Springer-Verlag GmbH & Co. KG, 2000.

223. Black Jonathan. Biological Performance of Materials: Fundamentals of Biocompatibility (4th ed.). New York: CRC Press Taylor and Francis, 2006.

224. Clark GC, Williams D F. The effects of proteins on metallic corrosion. J Biomed Mater Res., 1982; 16:125.

225. Williams RL, Brown S A, Merritt K. Electrochemical studies on the influence of proteins on the corrosion of implant alloys. Biomaterials, 1988; 9:181.

226. Bandyopadhya R, Cahoon J R. Effect of composition on the electrochemical behavior of austenitic stainless steel in Ringer's solution. Corrosion, 1977; 33:204.

227. Gluszek J, Masalki J, Furman P, Nitsch K. Structural and electrochemical examinations of PACVD TiO_2 films in Ringer solution. Biomaterials, 1997; 18:789

228. Hoar TP, Mears DC. Corrosion-Resistant Alloys in Chloride Solutions: Materials for Surgical Implants. Proc R Soc Lond A, 1966; 294:486.

229. Milosev I, Metikos-Hukovic M, Strehblow H H. Passive film on orthopedic TiAlV alloy formed in physiological solution investigated by X-ray photoelectron spectroscopy. Biomaterials, 2000; 21:2103

230. Hsu RW, Yang C, Huang C, Chen Y. Investigation on the corrosion behavior of Ti–6Al–4V implant alloy by electrochemical techniques. Mater Chem Phys 2004; 86: 269-278.

231. Germain MA, Hatton A, Williams S, Matthews J B, Stone M H, Fisher J, Ingham E. Comparison of the cytotoxicity of clinically relevant cobalt-chromium and alumina ceramic wear particles in vitro. Biomaterials, 2003; 24(3): 469- 479.

232. Okazaki Y, Gotoh E. Comparison of metal release from various metallic biomaterials in vitro. Biomaterials, 2005; 26(1):11-21.

233. Masse A, Bosetti M, Buratti C, Visentin O, Bergadano D, Cannas M. Ion release and chromosomal damage from total hip prostheses with metal-on-metal articulation. Journal of Biomedical Materials Research. Part B: Applied Biomaterials, 2003; 67(2): 750-757.

234. Dumbleton JM, Manley J M. Metal-on-metal total hip replacement: What does the literature say? The Journal of Arthroplasty, 2005; 20(2):174-188.

235. Hanawa T. Metal ion release from metal implants. Materials Science and Engineering C, 2004; 24(6-8): 745-752.

236. Fleury C, Petit A, Mwale F, Antoniuou J, Zukor D J, Tabrizian M, Huk O L. Effect of cobalt and chromium ions on human MG-63 osteoblasts in vitro: Morphology, cytotoxicity, and oxidative stress. Biomaterials, 2006; 27(18):3351-3360.

237. Bumgardner Lee M V, Keerthick F S, Smith D H, Kellyle D B, Seth J C, Williams D F. Biocompatibility testing. In. Wnek GE, Browlin GL. Encyclopedia of Biomaterials and Biomedical Engineering. New York: Informa Healthcare; 2008: 169-178.

238. Taguchi G, Konishi S. Taguchi Methods: Orthogonal Arrays and Linear Graphs; Tools for Quality Engineering, American Supplier Institute Inc., Dearborn, MI 1987.

239. Taguchi G. Introduction to Quality Engineering, Asian Productivity Organization, Tokyo 1990.

240. Phadke M S. Quality Engineering using Robost Design, Prentice- Hall, Englewood Cliffs, NJ 1989.

241. Wu Y, Moore W H. Quality Engineering: Product & Process Design Optimization, American Supplier Institute Inc., Dearborn, MI 1986.

242. Logothetis N, Haigh A. A Hierarchical Method for Evaluating Products with Quantitative and Sensory Characteristic. Profession. Statist., 1987; 6:10–16.

243. Logothetis N, Haigh A. Characterizing and Optimizing Multi-response Processes by the Taguchi Method. Qual. Reliab. Eng. Int., 1988; 4:159–169.

244. Shoemaker AC, Kackar R N. A methodology for planning experiments in robust product and process design. Qual. Reliab. Eng. Int., 1988; 4:95–103.

245. Phadke MS, Dehnad K. Optimization of product and process design for quality and cost. Qual. Reliab. Eng. Int., 1988; 4:105–112.

246. Bolboaca SD, Jäntschi L. Design of Experiments: Useful Orthogonal Arrays for Number of Experiments from 4 to 16, Entropy, 2007; 9: 198-232.

247. Poostforush M, Al-Mamun M, Fasihi M. Investigation of Physical and Mechanical Properties of High Density Polyethylene/Wood Flour Composite Foams. Research Journal of Engineering Sciences, 2013; 2: 15-20.

248. Fei NC, Mehat N M, Kamaruddin S. Practical Applications of Taguchi Method for Optimization of Processing Parameters for Plastic Injection Moulding: A Retrospective Review, ISRN Industrial Engineering, 2013: 1-11.

249. Esmizadeh E, Naderi G, Ghoreishy M H R, Bakhshandeh G R. Optimal Parameter Design by Taguchi Method for Mechanical Properties of NBR/PVC Nanocomposites. Iranian Polymer Journal, 2011; 20: 587-596.

250. Sailesh A, Shanjeevi C. Predicting the Best Hardness of Banana-Bamboo-Glass Fiber Reinforced Natural Fiber Composites Using Taguchi Method. International Journal of Engineering Development and Research, 2013; 1:89-92.

251. Vankantia VK, Gantab V. Optimization of Process Parameters in Drilling of GFRP Composite Using Taguchi Method. Journal of Materials Research and Technology, 2014; 3: 35-41.

252. Uysal A, Altan M, Altan E. Effects of Cutting Parameters on Tool Wear in Drilling of Polymer Composite by Taguchi Method. International Journal of Advanced Manufacturing Technology, 2012; 58:915-921.

253. Thong TE, Shahidan A. Optimization on Cutting Parameters (Turning) Using Taguchi Method for Nickel-Based Alloy. Science Engineering Technology National Conference (SETNC), 2013.

254. Fei NC, Mehat N M, Kamaruddin S. Practical Applications of Taguchi Method for Optimization of Processing Parameters for Plastic Injection Moulding: A Retrospective Review, ISRN Industrial Engineering, 2013: 1-11.

255. Basavarajappa S, Chandramohan G, Davim J P. Application of Taguchi techniques to study dry sliding wear behavior of metal matrix composites. Materials and Design, 2007; 28: 1393–1398.

256. Bagci E, Aykut S. A study of Taguchi optimization method for identifying optimum surface roughness in CNC face milling of cobalt-based alloy (stellite 6). The International Journal of Advanced Manufacturing Technology, 2006; 29 (9): 940-947.

257. Banwet DK, Majumdar A. Comparative Analysis of AHP-TOPSIS and GA-TOPSIS Methods for Selection of Raw Materials in Textile Industries. Proceedings of the 2014 International Conference on Industrial Engineering and Operations Management, Bali, Indonesia, 2014; 2071-2080.

258. Levy JK. Multiple criteria decision making and decision support systems for flood risk management. Stochastic Environmental Research and Risk Assessment, 2005; 19: 438-447.

259. Wang M J J, Chang T C. Tool steel materials selection under fuzzy environment. Fuzzy Sets Sys, 1995; 72: 263–70.

260. Tretheway KR, Wood R J K, Puget Y, Roberge P R. Development of a knowledge based system for materials management. Mater Des., 1998; 19: 39–56.

261. Jee D-H, Kang K-J. A method for optimal material selection aided with decision making theory. Mater Des., 2000; 21:199–206.

262. Sapuan SM. A knowledge-based system for materials selection in mechanical engineering design. Mater Des., 2001; 22: 687–95.

263. Bahraminasab M, Jahan A. Material selection for femoral component of total knee replacement using comprehensive VIKOR. Material and Design, 2011; 32: 4471-4477.

264. Ermatita, Hartati S, Wardoyo R, Harjoko A. ELECTRE Methods in Solving Group Decision Support System Bioinformatics on Gene Mutation Detection Simulation. International Journal of Computer Science & Information Technology, 3 2011; 3: 405-2.

265. Rouyendegh BD, Erkan T E. An Application of the Fuzzy ELECTRE Method for Academic Staff Selection. Human Factors and Ergonomics in Manufacturing & Service Industries, 23 2013; 23:107-115.

266. Mazumder P, Decision-Making in Manufacturing Environment Using ELECTRE Methods. Thesis, Jadavpur Unniversity, Kolkata, 2009.

267. Smith RL, Bush R J, Schmoldt D L. The Selection of Bridge Materials Utilizing the Analytical Hierarchy Process, Annual Convention and Exposition, 1997; 4:140-150.

268. Sapuan SM, Kho J Y, Zainudin E S, Leman Z, Ali B A A, Hambali A. Materials Selection for Natural Fiber Reinforced Polymer Composites Using Analytical Hierarchy Process. Indian Journal of Engineering and Materials Sciences, 2011; 18: 255-267.

269. Shanian A, Savadogo O. A methodological concept for material selection of highly sensitive components based on multiple criteria decision analysis. Expert Sys Appl, 2009; 36:1362–70.

270. Athawale VM, Kumar R, Chakraborty S. Decision making for material selection using the UTA method. Int J Adv Manuf Technol. DOI: 10.1007/s00170-011-3293-7.

271. Rathod MK, Kanzaria H V. A methodological concept for phase change material selection based on multiple criteria decision analysis with and without fuzzy environment. Material and Design, 2011; 32: 3578–3585.

272. Chatterjee P, Athawale V M, Chakraborty S. Materials selection using complex proportional assessment and evaluation of mixed data methods. Material and Design, 2011; 32: 851-860.

273. Maniya K, Bhatt M G. A selection of material using a novel type decision-making method: preference selection index method. Material and Design, 2010; 31: 1785-1789.

274. Jahan A, Ismail M Y, Sapuan S M. Material screening and choosing methods – A review. Material and Design, 2010; 31: 696–705.

275. Gervasio H, Simoes da Silva L. A probabilistic decision-making approach for the sustainable assessment of infrastructures. Expert Syst. Appl., 2012; 39: 7121–7131.

276. Jahan A, Bahraminasab M, Multicriteria Decision Analysis in Improving Quality of Design in Femoral Component of Knee Prostheses: Influence of Interface Geometry and Material, Advances in Materials Science and Engineering, 2015, Doi.org/10.1155/2015 /693469.

277. Chen S, Wang X, Zhao X. An attribute recognition model based on entropy weight for evaluating the quality of groundwater sources. Journal of China University Mining & Technology, 2008; 18: 72–75.

278. Zhi-hong Z, Yi Y, Jing-nan S. Entropy method for determination of weight of evaluating indicators in fuzzy evaluation for water quality assessment. Journal of environmental Science. 2006;18: 1020-1023.

279. American society for testing and materials (ASTM). Standard E92, Standard test method for Vickers Hardness of Metallic Materials, West Cons hohocken (PA): Annual book of ASTM standards, ASTM, 2011.

280. Annual book of ASTM standards, ASTM International.

281. International Standard, Biological Evaluation of Medical Devices. Part 1: Evaluation and Testing. ISO 10993-1, 2003.

282. Rout A K, Satapathy A. Study on mechanical and tribo-performance of rice-husk filled glass–epoxy hybrid composites. J Mater Des., 2012; 41: 131–141.

283. Mehat N M, Kamaruddin S. Investigating the Effects of Injection Molding Parameters on the Mechanical Properties of Recycled Plastic Parts Using the Taguchi Method. Materials and Manufacturing Processes. 2011; 26: 202-209.

284. Shipway P H, Kennedy A R, Wilkes A J. Sliding wear behaviour of aluminium-based metal matrix composites produced by a novel liquid route. Wear, 1998; 216: 160-171.

285. Glen S P. Taguchi methods: a hand on approach. NY: Addison-Wesley, 1993.

286. Haykin S. Neural Networks: A Comprehensive Foundation, Prentice Hall, 1999.

287. Ratner B D, Bankman I. Biomedical Engineering Desk Reference, Academic Press, Oxford, 2009.

288. Montero-Ocampo C, Juarez R, Salinas-Rodriguez A. Effect of FCC-HCP phase transformation produced by isothermal aging on the corrosion resistance of a Co-27Cr-5Mo-0.05C alloy. Metall. Mater. Trans., 2002; 33: 2229–2235.

289. Patel B, Inam F, Reece M, Edirisinghe M, Bonfield W, Huang J, Angadji A. A novel route for processing cobalt–chromium–molybdenum orthopaedic alloys. J. R. Soc. Interface, 2014:1-5.

290. Patel B, Favaro G, Inam F, Reece Michael J, Angadji A, Bonfield W, Huang J, Edirisinghe M. Cobalt-based orthopaedic alloys: Relationship between forming route, microstructure and tribological performance. Materials Science and Engineering, C 2012; 32:1222–1229.

291. A.S.T.M. F75 Standard Specification for Cobalt-28 Chromium-6 Molybdenum Alloy Castings and Casting Alloy for Surgical Implants (UNS R30075) 1, ASTM International, Annual Book of Standards, West Consho- hocken, PA 2014.

292. Weston D P, Shipway P H, Harris S J, Cheng M K. Friction and sliding wear behavior of electrodeposited cobalt and cobalt–tungsten alloy coatings for replacement of electrodeposited chromium. Wear, 2009; 267: 934–943.

293. Rosenthal R, Cardoso B R, Bott I S, Paranhos R P R, Carvalho E A. Phase characterization in as-cast F-75 Co–Cr–Mo–C alloy. Journal of material science, 2010; 45:4021–4028.

294. Ahmed R, Lovelock HLDV, Faisal NH, Davies S. Structure-property relationships in a CoCrMo alloy at micro and nano-scales. Tribology International, 2014; 80: 98-114.

295. Balagna C, Spriano S, Faga M G. Characterization of Co–Cr–Mo alloys after a thermal treatment for high wear resistance, Mat. Sci. Eng., 1012; C 32: 1868-1877.

296. Savarimuthu AC, Taber H F, Megat I, Shadley J R, Rybicki E F, Cornell W C, Emery W A, Somerville D A, Nuse J D. Sliding wear behavior of tungsten carbide thermal spray coatings for replacement of chromium electroplate in aircraft applications. Journal of Thermal Spray Technology, 2001; 10: 502–510.

297. Firkins PJ, Tipper J L, Ingham E, Stone M H, Farrar R, Fisher J. A novel low wearing differential hardness, ceramic-on-metal hip joint prosthesis. J. Bio- mechanics. 2001; 34(10): 1291–1298.

298. Doni Z, Alves AC, Toptan F, Gomes JR, Ramalho A, Buciumeanu M, Palaghian L, Silva FS. Dry sliding and tribocorrosion behavior of hot pressed CoCrMo biomedical alloy as compared with the cast CoCrMo and Ti6Al4V alloys. Journal of Materials and Design, 2013; 52: 47–57.

299. Choudhury P, Das S. Effect of nickel aluminides on tribological behaviour of Zn–Al alloy. Mater. Sci. Technol., 2003; 19: 535–537.

300. Yamanoglu R, Karakulak E, Zeren M. Effect of nickel on microstructure and wear behaviour of pure aluminium against steel and alumina counterfaces. International Journal of Cast Metals Research, 2013; 1(1): 1-7.

301. Jeong D H, Gonzales F, Palumbo G, Aust K T, Erb U. The effect of grain size on the wear properties of electrodeposited nanocrystalline nickel coatings. Scripta Materialia 2001; 44: 493–499.

302. Hutchings I M. Tribology: friction and wear of engineering materials, CRC Press, Boca Raton, FL, 1992: 200.

303. Chowdhury M A, Helali MM. The Effect of Frequency of Vibration and Humidity on the Wear rate. Wear, 2007; 262: 198-203.

304. Choudhury P, Das S. Effect of nickel aluminides on tribological behaviour of Zn–Al alloy. Mater. Sci. Technol., 2003; 19: 535–537.

305. Figueiredo-Pina C. G, Yan Y, Neville A, Fisher J. Understanding the differences between the wear of metal-on-metal and ceramic-on-metal total hip replacements. J. Engineering in Medicine, 2008; 363: 285-295.

306. Weston D P, Shipway P H, Harris S J, Cheng M K. Friction and sliding wear behavior of electrodeposited cobalt and cobalt–tungsten alloy coatings for replacement of electrodeposited chromium. Wear, 2009; 267: 934–943.

307. Gispert M P, Serro A P, Colaco R, Saramago B. Friction and wear mechanisms in hip prosthesis: Comparison of joint materials behavior in several lubricants. Wear, 2006; 260: 149–158.

308. Kumagai1 K, Nomura N, Chiba A. Effect of Dissolved Oxygen Content on Pin-on-Disc Wear Behavior of Biomedical Co-Cr-Mo Alloys in a Like-on-Like Configuration in Distilled Water. Materials Transactions, 2007; 48 (6): 1511-1516

309. Capel H, Shipway P H, Harris S J. Sliding wear behavior of electrodeposited cobalt–tungsten and cobalt–tungsten–iron alloys. Wear, 2003; 255: 917–923.

310. Sierros K A, Morris N J, Kukureka S N, Cairns D R. Dry and wet sliding wear of ITO-coated PET components used in flexible optoelectronic applications. Wear, 2009; 267:625–631.

311. Haseeb A, Albers U, Bade K. Friction and wear characteristics of electrodeposited nanocrystalline nickel–tungsten alloy films. Wear, 2008; 264:106–112.

312. Therin M, Meunier A, Christel P. A histomorphometric comparison of the muscular tissue reaction to stainless steel, pure titanium and titanium alloy implant materials. Journal of Materials Science, 1991; 2(1):1-8

313. Gurappa I. Characterization of different materials for corrosion resistance under simulated body fluid conditions. Mater Charact., 2002; 49:73-79.

314. MacDonald D, Mckubre M. Electrochemical impedance techniques in corrosion science: electrochemical corrosion testing. ASTM Spec Tech Publ.1981; 727:110

315. Robert W H, Chun-Chen Y, Ching-An H, Yi-Sui C. Electrochemical corrosion studies on Co–Cr–Mo implant alloy in biological solutions. Materials Chemistry and Physics, 2005; 93: 531–538.

316. Brans JP, Vincke P, Mareschal B. How to select and how to rank projects: the PROMETHEE method. Eur J Oper Res., 1986; 24: 228-38

317. Zeleny M. Multiple criteria decision making, McGraw-Hill, New York. 1982.

318. Maity S R, Chakraborty S. Tool steel material selection using PROMETHEE II method. Int J Adv Manuf Technol, 2015 78:1537–1547.

319. Hwang CL, Yoon K, Multiple attribute decision making: methods and applications, Lecture Notes in Economics and Mathematical Systems. Springer, 1981; 186.

320. Shannon C E, A Mathematical Theory of Communication. Bell System Tech, Journal, 1948; 27:379-423.

321. Satapathy BK, Majumdar A, Tomar BS. Optimal design of fly ash filled composite friction materials using combined Analytical Hierarchy Process and Technique for Order Preference by Similarity to Ideal Solutions approach. Materials and Design, 2010; 31:1937-1944.

List of publications based on the research presented in this thesis

Paper published in International Journals

— **Amit Aherwar**, Amit Singh, Amar Patnaik "Study on mechanical and wear characterization of novel Co30Cr4Mo biomedical alloy with added nickel under dry and wet sliding conditions using Taguchi approach" **Proc IMechE Part L: J Materials: Design and Applications. 2016, DOI: 10.1177/1464420716638112.**

— **Amit Aherwar**, Amit Singh, Amar Patnaik "Current and Future Biocompatibility Aspects of Biomaterials for Hip Prosthesis", **Journal on Bioengineering.** 2016; 3(1): 23-43.

— **Amit Aherwar**, Amit Singh, Amar Patnaik "Cobalt Based Alloy: A Better Choice Biomaterial for Hip Implants", **Trends in Biomaterials and Artificial Organs**. 2016; 30(1):50-55.

Paper published in International Conference

— **Amit Aherwar**, Amit Singh, Amar Patnaik "Physico-mechanical Characterization of Molybdenum Filled Co30Cr Biomedical Metal Matrix Alloy Composite for Hip Joint Replacement", International Conference on Emerging Trends in Mechanical Engineering, Association with M.P. Council of Science & Technology, May 27-28, 2016, Technocrats Institute of Technology (Excellence), Bhopal, India.

*****

Brief Bio-data of the Author

The author, Amit Aherwar born on 05-08-1982 graduated in Mechanical Engineering from Madhav Institute of Technology & Science, Gwalior, Madhya Pradesh, India in the year 2006. Immediately after the completion of B.E he joined MITS, Gwalior as a lecturer in the Department of Mechanical Engineering and worked with from 2006-2008. He finished his Master's in Production Engineering from Madhav Institute of Technology & Science, Gwalior, Madhya Pradesh, India in the year 2010. Soon after completion of his M.Tech programme, he joined as Assistant Professor in Mechanical Engineering Department, Madhav Institute of Technology & Science, Gwalior, Madhya Pradesh, India and worked with from 2010-2011. After that, he joined as Assistant Professor in Mechanical Engineering Department, Anand Engineering College (Sharda Group of Institution), Agra, Uttar Pradesh, India and worked with from 2011-2012.

He has published one research paper in Science Citation Indexed Journals, two research papers in Scopus Journal and presented one research paper in International Conference to his credit. Since 2013, he has been engaged in his Doctoral Research in the area of Development and characterizations of metallic composite materials for wear resistant application at M.N.I.T, Jaipur under the Institute Research Fellowship scheme by the Ministry of Human Resource Development, Government of India.

At present he is working as an Assistant Professor in the Department of Mechanical Engineering, Madhav Institute of Technology & Science, Gwalior, Madhya Pradesh, Autonomous Government Institute, Madhya Pradesh, INDIA.

****